Transcranial Focused Ultrasound for Modulation of Attention Networks in Humans

by

Maria Elizabeth Fini

A Dissertation Presented in Partial Fulfillment
of the Requirements for the Degree
Doctor of Philosophy

Approved October 2020 by the
Graduate Supervisory Committee:

William J.Tyler, Chair
Bradley Greger
Stephen Helms Tillery
Jeffrey Kleim
Marco Santello

ARIZONA STATE UNIVERSITY

December 2020

ABSTRACT

Transcranial focused ultrasound (tFUS) is a unique neurostimulation modality with potential to develop into a highly sophisticated and effective tool. Unlike any other noninvasive neurostimulation technique, tFUS has a high spatial resolution (on the order of millimeters) and can penetrate across the skull, deep into the brain. Sub-thermal tFUS has been shown to induce changes in EEG and fMRI, as well as perception and mood. This study investigates the possibility of using tFUS to modulate brain networks involved in attention and cognitive control.

Three different brain areas linked to saliency, cognitive control, and emotion within the cingulo-opercular network were stimulated with tFUS while subjects performed behavioral paradigms. The first study targeted the dorsal anterior cingulate cortex (dACC), which is associated with performance on cognitive attention tasks, conflict, error, and, emotion. Subjects performed a variant of the Erikson Flanker task in which emotional faces (fear, neutral or scrambled) were displayed in the background as distractors. tFUS significantly reduced the reaction time (RT) delay induced by faces; there were significant differences between tFUS and Sham groups in event related potentials (ERP), event related spectral perturbation (ERSP), conflict and error processing, and heart rate variability (HRV).

The second study used the same behavioral paradigm, but targeted tFUS to the right anterior insula/frontal operculum (aIns/fO). The aIns/fO is implicated in saliency, cognitive control, interoceptive awareness, autonomic function, and emotion. tFUS was found to significantly alter ERP, ERSP, conflict and error processing, and HRV responses.

The third study targeted tFUS to the right inferior frontal gyrus (rIFG), employing the Stop Signal task to study inhibition. tFUS affected ERPs and improved stopping speed.

Using network modeling, causal evidence is presented for rIFG influence on subcortical nodes in stopping.

This work provides preliminarily evidence that tFUS can be used to modulate broader network function through a single node, affecting neurophysiological processing, physiologic responses, and behavioral performance. Additionally it can be used as a tool to elucidate network function. These studies suggest tFUS has the potential to affect cognitive function as a clinical tool, and perhaps even enhance wellbeing and expand conscious awareness.

To the future generations, may they evolve from us as wildly successful progeny. I very humbly intend that with this and future work I can provide something helpful in the human journey towards greater consciousness and bliss, to realize the one-ness of all beings.

ACKNOWLEDGMENTS

It is with a sense of great gratitude that I extend thanks to the following people. To my dissertation committee, Dr. Bradley Greger, Dr. Stephen Helms-Tillery, Dr. Jeffrey Kleim, Dr. Marco Santello, and Dr. William ("Jamie") Tyler, I am grateful that you challenge my intellect and push me to be excellent. I am grateful to Dr. Greger and Dr. Kleim for acting as advocates during my admission to ASU. I must extend a special thanks to Dr. Santello for allowing me to preform my experiments in his laboratory out of the kindness of his heart, with no immediate benefit to himself. Without this I would have been required to decrease the sophistication of my methods. Most of all I am grateful to Dr. Tyler, who saw a spark in me and decided to take a chance by selecting me as a student when my direct background was not in academia. Transitioning from a career in the clinic to one in research was incredibly challenging, but really what my soul needed. I am tremendously fortunate to have such an advisor; he never baulked at my unconventional ideas, but rather encouraged me to explore them.

I am also grateful to have numerous friends and teachers outside of University to whom deserve great thanks. Dr. A. Blaine Williams, your friendship, romance, and support was invaluable in helping me actualize this document. I love you, and thank you. Dr. Jay Sanguinette, thank you for providing valuable scientific advice, inspiration, encouragement, and for being a confidant as well as a friend. Lisa Schremp, who encouraged my development both spiritually and physically through the practice of Ashtanga Yoga. Exposing me to the ancient practices of yoga and spirituality, which helped to ground my being and inspire my curiosity scientifically and beyond.

A wholehearted thanks goes to the Department of Biomedical Engineering, for funding in part my time at ASU and my research.

TABLE OF CONTENTS

Page

APPENDIX Page

LIST OF ACRONYMS

ACC - anterior cingulate cortex

ADHD - attention deficit hyperactive disorder

ANOVA - analysis of variance

CT - computerized tomography

dACC - dorsal anterior cingulate cortex

DCM - dynamic causal model

DLPFC - dorso-lateral prefrontal cortex

EEG - electroencephalography

EOG - electrooculography

ERP - event-related potential

ERSP - event-related spectral perturbation

fMRI - functional magnetic resonance imaging

F-Pp - family-based posterior probability

FUS - focused ultrasound

GLM - general linear model

HIFU - high-intensity focused ultrasound

HR - heart rate (beats per minute)

HRV - heart rate variability

ICA - independent components analysis

IFG - IFG , inferior frontal gyrus

IOG - inferior occipital gyrus

I_{sppa} - spatial peak pulse average intensity

LFP - local field potential

LTS - low threshold spiking

M1 - primary motor cortex

MEG - magnetoencephalography

MFG - middle frontal gyrus

MNI - Montreal Neurologic Institute

MP-RAGE - magnetization prepared - rapid gradient echo

MRI - magnetic resonance imaging

NICE - neuronal intramembrane cavitation excitation

PEB - parametric empirical Bayesian

pNN50 - percent of successive normal R-R intervals exceeding 50 ms

Pre-SMA - pre supplementary motor area

rIFG - right inferior frontal gyrus

rIOG - right inferior occipital gyrus

RF - radio frequency

RM-ANOVA - repeated measures analysis of variance

rMFG - right middle frontal gyrus

RMSSD - root mean square of successive RR interval differences (ms)

R-R - interval between heart beats (ms)

rr_i - relative R-R intervals

ROI - region of interest

RT - reaction time

SD1 - standard deviation taken perpendicular to the identity line on the Poincaré plot of R-R intervals (ms)

SD2 - standard deviation along the identity line on the Poincaré plot of R-R intervals (ms)

SD1/SD2 - ratio of SD1 and SD2

SDNN - standard deviation of the normal R-R intervals (ms)

SEM - standard error of the mean

S1 - primary sensory cortex

SMA - supplementary motor area

SS - successful stop

SSD - stop signal delay

SSRT - stop signal reaction time

STN - subthalamic nucleus

SU - stop that is unsuccessful (failed to inhibit response)

tcMRgHIFU - transcranial MR-guided high-intensity focused ultrasound

tFUS - transcranial focused ultrasound

TMS - transcranial magnetic stimulation

TR - repetition time (ms)

TRD - treatment-resistant depression

TE - echo time (ms)

TRP - transient receptor potential

UNMOD - ultrasonic neuromodulation

US - ultrasound

V1 - primary visual cortex

VAN - ventral attention network

VLPFC - ventro-lateral prefrontal cortex

LIST OF ABBREVIATIONS

Con	-	congruent
Cong.	-	congruency
Emot.	-	emotion
Incon	-	incongruent
Inter.	-	interaction
Mdn	-	median
Neu	-	neutral

PREFACE

This work focuses on developing an approach for modulating brain networks by targeting specific anatomical regions with ultrasound. Although the focus of this text is mainly on anatomy and neurophysiology in the context of well studied cognitive tasks employed in psychology research, this approach was chosen to explore the efficacy of using this neurostimulation technique by comparing its effects to previously studied and conceptualized processes. However, I believe that that ultrasound is capable of much more if used in the proper context.

The anatomical regions selected for targeting were chosen not just for their relevance in the psychology literature, bur for their function in meditation. The purpose of this work is to explore the potential of using ultrasound for psychiatric healing, but the hope is to extend this technique beyond the clinical word. If ultrasound neuromodulation can be used to affect concentration and emotional experience, it has incredible applications to enhance human wellbeing, as well as deepening conscious awareness.

This work was compiled with the hopes that ultimately ultrasound neurostimulation can be used to facilitate higher states of awareness, awakening, and a realization of who we truly are.

CHAPTER 1

INTRODUCTION

Until recently, the only way to modulate neurophysiology for the purpose of enhancing attention and wellbeing, has been dedicated practice, yet the emerging field of neurostimulation has potential to change this. Although numerous brain stimulation modalities exist, transcranial focused ultrasound (tFUS) has been of specific interest for this purpose. Nonthermal tFUS is safe, can be noninvasively focused across the skull, and has been shown to induce changes in EEG and fMRI, as well as perceptual and mood changes. Unlike any other noninvasive neurostimulation technique, tFUS has a high spatial resolution and can penetrate deep into the brain. This work explores the feasibility of using tFUS to target regions of the brain with high anatomical specificity for the purposes of inducing network modulation to affect cognitive and emotional processing, as well as functioning.

Chapter two provides a review on focused ultrasound as a neurostimulation technique. This chapter has already been published in the International Review of Psychiatry (Fini and Tyler, 2017). It is aimed at a clinical audience, and in addition to providing some basic background about tFUS, is meant to highlight the potential of tFUS for use in psychiatry as a tool to investigate, diagnosis, and treat neuropsychiatric disorders.

Chapter three further explores this idea by testing the feasibility of modulating attention networks by stimulating the dorsal anterior cingulate cortex (dACC) with tFUS while subjects performed the flanker task with the addition of fearful and neutral face distractors. The dACC is involved in numerous cognitive functions and thought to be crucial in both executive control and emotional regulation. For this reason, it was targeted to examine the possibility of modulating processing and function. Indeed, the results indicate

that tFUS to the dACC reversed physiologic responses to fear measured through changes in cardiac activity, reduced behavioral slowing, and altered neurophysiologic processing.

Chapter four explores another anatomical target involved in attention and emotion, the right anterior insula/frontal operculum (aIns/fO). The aIns/fO is linked to the dACC through the cingulo-opercular network, and thought to be specifically involved in saliency and perception of, as well as autonomic regulation of fear. The task and measures used were identical to that used in chapter two, but the tFUS target was a deeper and smaller anatomical area. The results did indicate that tFUS to the aIns/fO altered physiologic responses and neurophysiologic processing.

Chapter five explores the application of tFUS to the right inferior frontal gyrus (rIFG) during a response inhibition task (Stop Signal task). A surface, but very specific anatomical target was used. The results demonstrate that tFUS to the rIFG improved stopping performance and altered neurophysiologic processing. Additionally, dynamic causal modeling was employed to explore the feasibility of using tFUS as a tool to causally link anatomical networks. This chapter has been submitted for publication with co-authors (see appendix A).

This body of work demonstrates that in conjunction with subject-specific anatomical targeting and neuronavigation, tFUS can be used to modulate broader network function for the purposes of affecting behavior and perhaps also cognitive and emotional experience. The aim of this work was to lay down the groundwork for the young filed of ultrasound neuromodulation to blossom. tFUS has a profound potential for healing maladaptive neuro-functional patterns seen in psychiatry, but also to help non-psychiatric patients heighten their wellbeing. The potential applications of this tool extend beyond the clinic to enhance concentration, emotional acceptance, and higher states of consciousness.

The following chapter (Chapter 2) is an accepted manuscript of an article published by Taylor & Francis Group © 2017 on behalf of Institute of Psychiatry and Johns Hopkins University in International Review of Psychiatry on 21 Apr 2017, available online: https://www.tandfonline.com/doi/full/10.1080/09540261.2017.1302924

CHAPTER 2

TRANSCRANIAL FOCUSED ULTRASOUND: A NEW TOOL FOR NONINVASIVE NEUROMODULATION

ABSTRACT

Ultrasound (US) is widely known for its utility as a biomedical imaging modality. An abundance of evidence has recently accumulated showing that US is also useful for noninvasively modulating brain circuit activity. Through a series of studies discussed in this short review, it has recently become recognized that transcranial focused ultrasound can exert mechanical (nonthermal) bioeffects on neurons and cells to produce focal changes in the activity of brain circuits. In addition to highlighting scientific breakthroughs and observations that have driven the development of the field of ultrasonic neuromodulation, we also provide a discussion of mechanisms of action underlying the ability of ultrasound to physically stimulate and modulate brain circuit activity. Exemplifying some forward looking tools that can be developed by integrating ultrasonic neuromodulation with other advanced acoustic technologies, we briefly review some innovative acoustic imaging, beam forming, and focusing techniques. Finally, we discuss the future outlook for ultrasonic neuromodulation specifically in the context of applications employing transcranial focused ultrasound for the investigation, diagnosis, and treatment of neuropsychiatric disorders.

INTRODUCTION

Ultrasound (US) is a sound pressure wave that has an acoustic frequency higher than the range of human hearing. Unlike light, magnetic fields, or electrical currents, US can be focused across solid structures and transmitted long distances with minimal power loss in soft biological tissues, which have bulk acoustic properties similar to water (O'Brien, 2007).

Due to these characteristics, its long history of safe use, and other attributes US represents the most widely implemented biomedical imaging modality in the world. The physics governing how sound waves interact with biological tissues, as well as advances in engineering have recently given way to a recent wave of technological breakthroughs demonstrating US and focused ultrasound (FUS) as extremely powerful tools for basic and clinical neuroscience. These breakthroughs cover broad embodiments ranging from clinically performing noninvasive thalamotomies for the treatment of movement disorders to the investigational, precise, focal stimulation of neural circuits (Elias et al., 2016; Naor et al., 2016).

It has long been known that US can produce a variety of thermal and nonthermal effects on cells and tissues depending on several factors including frequency, intensity, duty cycle, and exposure time. The acoustic frequency of the US used in a particular application defines the spatial resolution. In soft tissues, like the brain, the diffraction-limited spatial resolution of 0.5 MHz US is about three millimeters while it is about 15 microns for 100 MHz US. However, power loss due to absorption and scattering of US by tissues becomes greater as acoustic frequency increases. For instance, the optimal gain for transcranial transmission and brain absorption of US is between 0.2 and 0.65 MHz (Hynynen and Clement, 2007; Hynynen and Jolesz, 1998). Higher US frequencies (for example, 2 – 10 MHz) are routinely used in transcranial imaging applications because only nominal acoustic intensities are required for imaging applications. Thus the greater power loss at these higher US imaging frequencies can be tolerated. In other non-imaging applications of transcranial US requiring higher acoustic intensities to be generated in brain tissues, lower US frequencies (< 0.7 MHz) should be used.

High-intensity FUS (HIFU) is often delivered to tissues as a continuous wave having an acoustic intensity exceeding 200 W/cm2. HIFU produces thermal effects on tissues and it is extremely effective at focally and rapidly heating tissues for ablative purposes. Lower intensities of US (0.5 – 100 W/cm2) are less likely to produce thermal effects, but can still induce prominent mechanical bioeffects on cells and tissues especially when delivered in a pulsed mode to further minimize the probability of tissue heating (Dalecki, 2004; Legon et al., 2012a; Legon et al., 2014b). Methods of ablating tissues, like tumors or diseased brain circuits for therapeutic purposes are typically conducted using HIFU at intensities greater than 500 W/cm2. Frequency, intensity, and other ultrasonic parameters influencing the interactions of US with biological tissues are further discussed in the context of brain tissues below.

The idea of using US to modulate biological activity can be traced back to the early part of the 20th Century when Harvey first demonstrated that US could influence the activity of frog and turtle neuromuscular activity (Harvey, 1929). Almost 30 years later, Fry and colleagues first demonstrated that HIFU targeted to the lateral geniculate nucleus of cats can reversibly modulate the amplitudes of light-evoked responses recorded in visual cortex (Fry, 1958a). This and other work by Fry and colleagues during the 1950's culminated with their realization and demonstrations that HIFU could be used to treat human movement disorders, including Parkinson's disease by thermally modulating or ablating diseased deep-brain circuits (Fry, 1956, 1958b). Because at the time transcranial focusing of HIFU was not readily possible, Fry's methods required major craniotomies and were therefore not adopted by the clinical community. With numerous advances in US transducers and focusing methods, electrical engineering, radiologic imaging, and computational modeling over the past 60 years, Fry's original ideas have recently come to fruition. The focal, thermal ablation

of deep-brain circuits can be safely conducted in humans using transcranial MR-guided HIFU (tcMRgHIFU) to treat movement disorders (Elias et al., 2016). This tcMRgHIFU method of focally ablating brain circuits has also demonstrated feasibility as viable neuropsychiatric intervention. Jung and colleagues recently showed that bilateral capsulotomies performed using tcMRgHIFU provided clinical benefits for patients with treatment-resistant obsessive-compulsive disorder without producing psychological or neurological side effects (Jung et al., 2015).

With the recent milestone approval of tcMRgHIFU by the United States Food and Drug Administration for the treatment of essential tremor, it can be expected that additional interventions involving ablative neurosurgery to treat neurological and psychiatric disorders with HIFU will begin to follow. In contrast to the high-intensity applications of FUS, which rely on continuous wave US to focally heat and ablate circuits, low-intensity US was first shown capable of directly stimulating brain circuits through nonthermal mechanisms about a decade ago (Tyler et al., 2008). The remainder of this review focuses on discussing the background and outlook for such nonthermal applications of low-intensity FUS in the rapidly emerging field of ultrasonic neuromodulation (UNMOD; (Naor et al., 2016).

DEVELOPENT OF ULTRASOUND NEUROMODULATION

Since the early observations by Harvey (1929) and Fry and colleagues (1958), several studies have investigated the effects of US on neuronal activity by pre-sonicating neural circuits before electrically stimulating them. Observations made in these studies showed US can differentially effect the amplitudes and durations of compound action potentials and field potentials evoked by electrical stimulation (Bachtold et al., 1998; Mihran et al., 1990; Rinaldi et al., 1991; Tsui et al., 2005). In other words, these studies showed US is capable of

influencing electrically evoked activity, but not that it could directly stimulate neuronal activity or trigger action potentials. Through a series of in vitro studies, Tyler and colleagues provided the first evidence that low-intensity pulsed US could directly stimulate action potentials and synaptic transmission in brain circuits. Using optogenetic probes, whole-cell current-clamp recordings, and optical imaging of ionic transients in hippocampal slice cultures, we found these effects of US on brain activity involved nonthermal mechanisms acting, in part, upon endogenous voltage-gated sodium and calcium channels (Tyler et al., 2008).

Following the initial discovery that low-intensity US could directly stimulate action potentials, synaptic transmission, and brain circuit activity in vitro, we began developing methods for conducting noninvasive, transcranial stimulation of brain circuits using pulsed US. Using these methods we published a series of studies demonstrating in vivo stimulation of motor cortex and hippocampus (Tufail et al., 2010), as well as the rapid attenuation (within seconds) of kainic acid induced electrographic seizure activity in mice (Tufail et al., 2011a). Since then our basic observations have been replicated in numerous experimental models and expanded into new applications and embodiments. For example, other groups have shown the nonthermal (mechanical) bioeffects of FUS can stimulate the activity of intact cortical, thalamic, and hippocampal circuits in rodents (King et al., 2013; Li et al., 2016a; Mehic et al., 2014; Yang et al., 2012), rabbits (Yoo et al., 2011), and sheep (Lee et al., 2016b). Targeting frontal eye fields, transcranial focused ultrasound (tFUS) has been shown to modulate visuomotor behaviors in behaving non-human primates (Deffieux et al., 2013). In addition to these collective observations made by targeting brain circuits with US, it has been shown that FUS can focally and precisely stimulate salamander retinal circuits at temporal resolutions faster than natural photic activation by circumventing the need for

photochemical reactions (Menz et al., 2013). The spatial resolution in these studies was shown to be 90 microns using 43 MHz FUS (Menz et al., 2013). Other embodiments of US for neuromodulation have recently first demonstrated the feasibility of sonogenetics to stimulate and study previously uncharacterized behaviors in *C. elegans* (Ibsen et al., 2015). These observations, on all accounts, have provided evidence that such applications of FUS do not produce heating or tissue damage and can be applied safely for investigational purposes. In most cases the acoustic intensities that have been used in these studies to stimulate brain circuits are below the recommended upper limits (< 190 W/cm2) deemed safe for imaging applications.

The accumulation of safety observations gained through some of the aforementioned studies, other published animal studies, and unpublished preclinical studies supported recent translational investigations of UNMOD using transcranial focused ultrasound (tFUS) in humans. Using a pulsed US waveform having a fundamental acoustic frequency of 0.5 MHz at peak intensities < 50 W/cm^2, Legon and colleagues first demonstrated that tFUS can physiologically and functionally modulate sensory-driven activity of primary sensory cortex (S1) with a lateral spatial resolution of about five millimeters and an axial resolution of about 18 millimeters in healthy human volunteers (Legon et al., 2014b). More specifically Legon and colleagues (2014) first demonstrated functional UNMOD in healthy humans by showing that low-intensity tFUS can focally and specifically suppress somatosensory evoked potentials, as well as alpha-, beta-, and gamma-band EEG activity in response to median nerve stimulation. These neurophysiological changes produced by tFUS targeted to the crown of the postcentral gyrus (S1) and posterior wall of the central sulcus led to a functional enhancement in somatosensory discrimination thresholds as determined through psychophysical investigations. Follow-up work from these

basic observations also showed that tFUS produces an effect on the phase distribution of intrinsic beta EEG activity when targeted to human S1 (Mueller et al., 2014). Expanded studies have more recently shown that 0.35 MHz tFUS targeted to S1 can directly stimulate and evoke somatosensory potentials and thermal/mechanical/pain sensations in the hand and fingers of human volunteers (Lee et al., 2015).

Most recently Lee and colleagues replicated their basic findings to demonstrate that tFUS targeted to primary visual cortex can elicit visual sensations and evoke sensory potentials in humans (Lee et al., 2016a). Although the evidence to date has demonstrated convincingly that UNMOD is safe, appropriate safety precautions should always be taken when modulating brain or neural function with FUS since the full spectrum of safe and effective parameters are still being identified, optimized, and refined. We thus caution the readers to realize strict exposure limits, standard operating procedures, and technical guidelines were imposed in the human studies conducted to date as discussed in more detail elsewhere (Lee et al., 2015; Lee et al., 2016a; Legon et al., 2014b). Presently, UNMOD is being advanced by a growing number of multidisciplinary groups around the world. With these efforts the methods and devices will advance so that UNMOD becomes a more broadly accessible tool for clinical and basic neuroscience over the next few years. Similar to these translational efforts, there are an equally growing number of laboratories investigating the mechanisms of action underlying the ability of low-intensity, pulsed FUS to modulate and stimulate brain activity. With an increased understanding of these mechanisms, we will be able to better target and regulate the activity of brain circuits including deep-brain circuits using tFUS.

MECHANISMS OF ACTION UNDERLYING ULTRASOUND NEUROMODULATION

The ability of pulsed US to stimulate and modulate neuronal activity challenges many of our conventional views regarding basic brain circuit function. It has been grossly underappreciated in neuroscience that the brain is a soft material with physical properties influencing its electrical characteristics and behaviors (Mueller and Tyler, 2014; Tyler, 2012). The brain is a viscoeleastic or non-Newtonian material that displays complex mechanical behaviors across a range of factors (Tyler, 2011, 2012). Considering the physical nature and mechanical properties of the lipids, proteins, and molecules that make up the brain (Tyler, 2012), there are several possible ways that US could influence cells and cellular networks (brain circuits) to activate or modulate neuronal activity (Tyler, 2011).

The most straightforward hypothesis accounting for the mechanisms underlying UNMOD is that the mechanical forces exerted by US act on the fluid mechanical properties of phospholipid membranes and the spring-like properties of membrane bound ion channels to alter neuronal membrane conductance and thereby neuronal activity (Tyler, 2011, 2012). Data in support of this hypothesis has shown that US stimulates brain activity through a nonthermal mechanism that involves the activation of voltage-gated sodium (tetrodotoxin-sensitive) and calcium transients, as well as intact SNARE protein signaling (Tyler et al., 2008). It has been well established that several voltage-gated ion channels including sodium and calcium channels, as well as certain ionotropic neurotransmitter receptors exhibit mechanosensitive properties that render their gating kinetics sensitive to mechanical forces (for review see, (Tyler, 2012). If and how the mechanical forces exerted by US are transduced into changes in ion channel activity has been the source of some debate. Recent

experimental observations and models are beginning to provide further insights into these issues.

Using an artificial bilayer preparation and electrophysiological recordings combined with laser Doppler vibrometry it has been shown that the mechanical forces exerted by US produce changes in the area and capacitance of pure lipid membranes (Prieto et al., 2013). These data demonstrate that US can produce changes in the electromechanical properties of membranes that are not supported by an internal cytoskeleton, embedded with rigid membrane bound proteins, or stabilized by a meshwork of extracellular matrix. The inclusion of these biological elements, which also have specific electrical and mechanical characteristics will influence the deformation actions of US on cell membranes, but how needs to be investigated. Findings from a series of electrophysiological recordings recently provided evidence that the mechanical pressures exerted by FUS can significantly influence the activity of potassium and sodium mechanosensitive ion channels including channels of the two-pore-domain potassium family (K2P) TREK-1, TREK-2, and TRAAK, as well as NaV1.5 channels (Kubanek et al., 2016). Additionally, the influence of FUS-mediated pressure changes on ion channels was used to demonstrate the first functional and practical demonstration of sonogenetics by mis-expressing the pore forming region of the transient receptor potential (TRP) type 4 channel in neurons of *C. elegans* to trigger specific movement behaviors (Ibsen et al., 2015). Collectively, these observations demonstrate that the mechanical pressures and forces exerted by US exert actions on protein ion channels and membranes in a manner that can alter neuronal activity. Undoubtedly there remain numerous unresolved and complicated issues however.

Adding complexity to our ability to fully comprehend the mechanisms underlying UNMOD, FUS has been shown to differentially stimulate and modulate (excite and inhibit)

brain circuit and neural activity across a broad range of acoustic stimulus parameters (frequency, intensity, duty cycle, pulse repetition frequency, and pulse duration), experimental models, and network conditions. For detailed discussions of the US parameters that have been used for UNMOD we refer the reader to several other sources (Naor et al., 2016; Plaksin et al., 2016a; Tufail et al., 2011b). Recently, a unifying framework theorizing how US influences neuronal activity provided a set of baseline models and predictions that help explain many of the experimental UNMOD observations thus far (Krasovitski et al., 2011; Plaksin et al., 2016a). At the core of the biophysical theory is the concept of intramembrane cavitation, which is produced by the effects of positive and negative pressures exerted by US on cells where small membrane regions (bilayer sonophores) experience expansions and contractions (Krasovitski et al., 2011). These bilayer sonophores and membrane deformations produce capacitive displacement currents that can lead to the accumulation of charge over the course of tens of milliseconds until an action potential threshold is reached causing pyramidal neurons to fire (Plaksin et al., 2016a). This basic convention of the theory is referred to as the neuronal intramembrane cavitation excitation (NICE) hypothesis (Plaksin et al., 2016a). When the NICE model was extended to different types of neurons, it was shown that low threshold spiking (LTS) inhibitory cortical interneurons and major types of thalamic neurons, which express T-type voltage-gated calcium channels experience a boost in charge accumulation in between bursts of US making them more likely to be stimulated than pyramidal neurons when low duty-cycle (i.e. 5%) UNMOD waveforms are used (Plaksin et al., 2016a). The NICE model explains the empirical observations in cortex by showing preferential activation of LTS neurons expressing T-type calcium channels when low duty-cycle (i.e. 5%) UNMOD waveforms are used. The preferential activation of these inhibitory interneurons in cortex produces a net

suppression of pyramidal neuron activity, whereas higher duty-cycle UNMOD waveforms (i.e. 50%) lead to the excitation of cortical pyramidal neurons (Plaksin et al., 2016a).

Whether or not the general NICE model and its subsequent refinements will be able to accurately describe ongoing results and observations remains to be determined. Further, additional structural elements like microtubules and extracellular matrix proteins, glia, other neurons, and additional channels that comprise brain circuits will be influenced by US in a manner that also contributes to the effects observed on electrical activity. Therefore, more work is needed to expand these and other models attempting to explain the mechanistic underpinnings of UNMOD. For now, the NICE model and its associated hypotheses indeed provide the most detailed theory of how US can regulate activity and critically it serves as useful framework for generating testable predictions by those interested in using or studying UNMOD.

It is important to realize that the past decade has seen a flurry of activity demonstrating US can stimulate and modulate activity. However, we are just at the beginning of an effort that will require decades in order to unravel how mechanical energy influences the electrical activity of brain circuits. In many cases, the basic observations that US can stimulate brain circuit activity simply do not fit with our conventional models of electrochemical neural activity (Mueller and Tyler, 2014). Therefore the generation of new frameworks, such as the bilayer sonophore and NICE models that elegantly consider how mechanical forces can interact with conventional models of neuronal excitability are required (Krasovitski et al., 2011; Plaksin et al., 2016a). It has taken several decades to understand how electrical currents or pulsed electromagnetic fields influence brain activity and these tools already fit within our existing working models of neuroscience. Despite more than a century of use, we are still grappling with how electrical neuromodulation effects brain

function and behavior. Thus, one can be certain that understanding the biophysical mechanisms of UNMOD poses a particularly difficult challenge that will require research by numerous multidisciplinary groups to solve. Large cross-disciplinary efforts aimed at solving these issues should be justified however since they will reveal some completely novel information about how mechanical forces act to regulate brain activity and plasticity.

INNOVATIVE ACOUSTIC TECHNOLOGIES AND MATERIALS USEFUL FOR ADVANCED ULTRASONIC NEUROMODULATION APPLICATIONS

Other technologies that implement FUS to modulate brain function are related to blood-brain barrier (BBB) disruption for targeted drug, gene, or antibody delivery (McDannold et al., 2015; Meairs, 2015; Rodriguez et al., 2015; Wang et al., 2015). It is imperative to recognize that these specific applications rely on the interaction of intravenously administered microbubbles (contrast agents) that serve as exogenous cavitation bodies in a continuous wave or a high-intensity pulsed FUS field, in order to generate sufficient pressure amplitudes capable of disrupting endothelial tight junctions forming the BBB (Meairs, 2015). It is further important to recognize that UNMOD of brain circuit activity does not require the use of exogenous agents. We see no reason for the intentional production of damage to tissues to deliver a therapeutic agent due to the risk of homeostatic disruption of multiple biological systems from such an event as BBB disruption and thus developed the core UNMOD method such that it did not require such insults. With the advances recently made in demonstrating the basic safety and feasibility of FUS-mediated BBB disruption and drug delivery, there are numerous opportunities for designing and developing biomolecular or synthetic cages and carriers that can release their contents in response to different thermal

and nonthermal effects exerted by FUS. The rapidly advancing field of FUS-mediated drug and gene delivery is one that is poised to deliver impactful results over the next few years.

Recently there have been a number of significant innovations in the fields of physical acoustics, materials engineering, and ultrasonics that can be integrated with basic UNMOD approaches to advance state of the art neuromodulation and brain mapping tools. One of the most logical manners by which these advances can have a near-term impact on brain mapping is through combining recently developed ultrasonic-based imaging methods with neuromodulation applications. For example, new methods enabling functional US imaging have been demonstrated capable of imaging brain activity and functional connectivity at high spatial resolutions in real time (Mace et al., 2011; Osmanski et al., 2014). Other imaging methods have recently combined the physical interactions of light with matter, which under certain conditions can generate sound waves, to develop noninvasive photoacoustic imaging methods also capable of mapping brain activity at high spatial and temporal resolutions (Yang et al., 2007; Yang and Wang, 2008). Besides functional imaging, US can also be used in certain imaging modes as a guidance tool to conduct navigated FUS treatments (Hynynen and Jones, 2016). As UNMOD joins forces with these different US imaging modalities the precision and power of brain mapping and neuromodulation tools employing US will greatly expand.

As mentioned previously, the diffraction limited spatial resolution of tFUS is a function of the acoustic frequency or wavelength of a particular frequency in a tissue. For tFUS used in UNMOD and HIFU applications where US has had to be transmitted across intact human skull bone, the acoustic frequencies have ranged from 0.7 to 0.3 MHz yielding theoretical spatial resolutions of about 2 to 7 millimeters respectively. Quantitative measurements of HIFU-induced thalamic lesions in humans (Elias et al., 2013; Elias et al.,

2016) and functional localization of cortical UNMOD in humans have shown the actual spatial resolution of tFUS to be about 4 to 10 millimeters (Lee et al., 2015; Lee et al., 2016a; Legon et al., 2014b). It was recently shown that when using mice as experimental models, higher US frequencies could be transmitted across their thin skulls with power sufficient to stimulate brain circuits at functional spatial resolution of about 0.3 millimeters for 5 MHz tFUS (Li et al., 2016b).

Some other methods have been developed to improve upon UNMOD spatial resolutions. A particularly interesting method generated a beat frequency of 0.5 MHz by transmitting modulated higher, carrier frequencies such as 2.0 and 1.5 MHz US across rodent skulls to stimulate cortical activity (Mehic et al., 2014). This is an interesting approach to optimizing the spatial targeting of tFUS, which demonstrated feasibility in animals and warrants further investigation in humans to understand the limits for using mixed combinations of high carrier frequencies in UNMOD applications that require US transmission across the skull. Advances in acoustic metamaterials and acoustic hyperlenses have enabled super-resolution acoustic imaging over the past decade by producing sub-diffraction US (Li et al., 2009; Zhang et al., 2009). Whether such advances in acoustic metamaterials (Zhang et al., 2009), hyperlenses (Li et al., 2009), sound bullets (Spadoni and Daraio, 2010), or propagation invariant acoustic field needle beams (Parker and Alonso, 2016) can enable super-resolution UNMOD by tFUS is not yet known, but most certainly worth exploring since such methods could enable totally unprecedented spatial control of both superficial and deep-brain circuit activity in a manner that is noninvasive.

One of the most interesting technical developments in acoustics recently has been the emergence and demonstrations of acoustic holography or holographic US (Melde et al., 2016a). This also brings us to perhaps one of the most fascinating embodiments of

UNMOD, which involves the delivery of holographic US through an acoustic retinal prosthetic device capable of generating multi-focal, patterned neurostimulation of retinal circuits to convey fine spatial visual information (Hertzberg et al., 2010; Omer et al., 2012). Similarly, generating acoustic holograms with tFUS may enable the projection of structured US into brain circuits for the multi-focal, patterned neuromodulation of brain circuit activity. Imagine a situation where one may wish to noninvasively and precisely replicate the flow of somatosensory information throughout the brain. This would require that sparsely distributed regions of both deep and superficial brain circuits (for example, regions of the thalamus, somatosensory cortex, prefrontal cortex, hippocampus, and amygdala) be synchronously and sequentially stimulated and modulated in a precisely timed manner. In other words, FUS would need to produce effects on circuits in many different brain regions at exactly or nearly the exact same time. Such an embodiment of UNMOD seems conceptually possible by projecting dynamically structured acoustic fields or ultrasonic holograms into the brain. Whether or not acoustic holograms and other advanced acoustic technologies will be practically useful for UNMOD remains to be determined. Given the relatively early stage of the UNMOD field combined with the rapid advances being made in acoustic materials/technologies, the coming years will provide fertile ground for developing and advancing ultrasonic tools for noninvasive neuromodulation and brain mapping.

POTENTIAL FOR THE USE OF TRANSCRANIAL FOCUSED ULTRASOUND AND ULTRASOUND NEUROMODULATION IN PSYCHIATRIC MEDICINE

There is a critical need for new neuromodulation-based therapies and diagnostics in neuropsychiatric medicine. Numerous noninvasive and invasive neuromodulation methods have been used in the investigational or clinical treatment of almost every psychiatric

disorder imaginable. For numerous practical and technical reasons, there have been many failures at demonstrating that neuromodulation treatment approaches can provide clinically significant benefits in psychiatry. In fact, electroconvulsive shock therapy remains one of the most effective neuromodulation-based approaches to treating debilitating psychiatric disorders like treatment-resistant depression (TRD). While transcranial magnetic stimulation (TMS) has been shown capable of treating TRD, the outcomes can certainly be improved upon. As discussed below, deep-brain stimulation of various brain targets has been used with mixed results depending on the disorder being treated. Therefore in this section, we outline several aspects discussing how UNMOD and tFUS can become a particularly useful new neuromodulation tool for neuropsychiatry.

It is widely becoming accepted that in order for neuromodulation approaches to be effective treatments of psychiatric disorders, brain regions and circuits should be targeted using functional signatures rather than anatomical landmarks alone. For example, targeting functionally localized prefrontal brain circuits using subject-specific realistic simulations of the electric field distributions generated by TMS pulses would likely improve clinical outcomes when TMS is used for treatment of TRD. This is because subject-specific gyral curvatures and tissue specific anisotropies cause the electric field produced by TMS pulses to be uniquely shaped and distributed throughout cortex in a manner that cannot be easily or accurately predicted without knowing specific anatomical geometries (Opitz et al., 2013a). This highlights one potential advantage of US in that the mechanisms of action underlying UNMOD are less affected by gyral curvature (shape) and mechanical anisotropy than the mechanisms underlying TMS are affected by curvature and electrical anisotropy. In other words, acoustic fields are not as greatly influenced by small differences in tissue shapes as electrical fields. This particular property of tFUS may prove an advantage by minimizing

variability in outcomes arising from tissue/energy interactions. Another advantage of tFUS over TMS is that it is readily compatible with EEG by not producing artifacts or saturating amplifiers. Perhaps the most obvious and biggest advantage of UNMOD over TMS and other noninvasive electrical-based neuromodulation methods is that US can be transmitted across the skull and focused to almost any location in the human brain including deep-brain targets. This advantage immediately opens the potential for exploring deep-brain targets using tFUS as a tool for neuropsychiatric interventions and diagnostics.

Deep-brain stimulation for psychiatric disorders has proven to be a difficult therapeutic platform to advance. This difficulty was most recently displayed when two different randomized clinical trials failed to demonstrate efficacy of DBS for the treatment of TRD (Dougherty et al., 2015), (Bergfeld et al., 2016). These trials targeted the ventral capsule/ventral striatum (Dougherty et al., 2015) and the ventral anterior limb of the internal capsule (Bergfeld et al., 2016) with DBS electrodes to treat TRD. Other clinical trials and studies using DBS targeted to different brain regions including the nucleus accumbens, subgenual cingulate cortex, lateral habenula, inferior thalamic nucleus, and medial forebrain bundles for the treatment of TRD have also been wrought with similar shortcomings or lack appropriate controls to make reliable inferences (Morishita et al., 2014). One of the major problems facing DBS therapies in psychiatry is that emotion and mood tend to be more diffusely localized in the brain making target identification/localization difficult. Therefore, it has been proposed that DBS electrodes should be targeted to brain circuits that have been localized using functional neuroimaging approaches rather than anatomically localized (Keedwell and Linden, 2013; O'Halloran et al., 2016). One issue with this approach is that there may be some amount of functional localization jitter that occurs depending on brain state and network dynamics at any given time neuroimaging may be conducted. In other

words, one may expect the specific location of "sadness" in the brain is likely to vary slightly from day to day depending on several factors. Another issue is that different individuals with the same disorder, clinical manifestation, and severity may have identical functionally identified targets, but the patients may respond to DBS of that target in totally different manners.

The issues raised above highlight the critical need for a noninvasive neuromodulation method capable of reaching deep-brain targets with a high spatial resolution. As discussed above in this review, tFUS seems to fit the bill as it can be focused to deep-brain regions and since the spatial resolution is about the same size as the spatial extent of electric fields generated by standard DBS electrodes. Further, UNMOD is compatible with MRI and has been used to focally stimulate and modulate human BOLD responses at both 3T and 7T (Ai et al., 2016; Lee et al., 2016a). The most logical application of UNMOD for psychiatry is the use of tFUS to interrogate and modulate potential DBS targets during functional neuroimaging experiments combined with measures of behavioral outcomes and neurophysiological assessments. In such an embodiment tFUS could enable exhaustive pre-surgical mapping and surgical planning studies in order to identify the best targets for treating a particular psychiatric disorder in a highly personalized manner. Whether or not such approaches will help improve the clinical outcomes of DBS-based psychiatric therapies or not needs to be thoroughly investigated and our group is engaging in a series of studies to begin evaluating feasibility.

Another application through which UNMOD can provide clinical utility in psychiatric medicine would be in the development of new therapies. Certainly tFUS and UNMOD have been considered as potentially viable treatments for psychiatric disorders, but there have been no clinical or preclinical studies to date to support such a possibility. It does

appear that the field has matured to a point over the past decade where pilot and feasibility studies aimed at treating neuropsychiatric should be planned and conducted. While there is a significant amount of work still required to ensure UNMOD reaches its full potential as a modern tool for psychiatric medicine, the field has finally reached a state where there is a critical mass of laboratories, scientists, companies, and engineers fully engaged in this conducting this work. Therefore, new embodiments of tFUS and UNMOD will begin to emerge in neuropsychiatry soon.

DISCUSSION

Ultrasound represents a fresh method of achieving focal neuromodulation. In particular, tFUS has emerged as a new method of noninvasive neuromodulation over the past decade. The observations made in the field thus far have demonstrated that low-intensity US can reversibly stimulate and modulate intact brain circuits through nonthermal mechanisms of action. More work is required to unravel the optimal UNMOD parameters for modulating and stimulating brain activity. Likewise, understanding the mechanisms of action will require additional multidisciplinary investigations conducted across a variety or experimental preparations and conditions. Continuing to identify the safe parameters for UNMOD applications is also imperative. Despite the efforts that remain ahead, the foundation has been laid and it is anticipated the UNMOD field will continue to grow. If tFUS and UNMOD continue to advance then they will eventually represent a powerful set of next generation tools for neuroscience and medicine.

DISCLOSURE OF INTEREST

WJT is the inventor and co-inventor on issued and pending patents related to methods,

systems, and devices for electrical and ultrasonic neuromodulation.

REFERENCES

Ai, L., Mueller, J.K., Grant, A., Eryaman, Y., and Legon, W. (2016). Transcranial Focused Ultrasound for BOLD fMRI Signal Modulation in Humans. arXiv preprint arXiv:160300415.

Bachtold, M.R., Rinaldi, P.C., Jones, J.P., Reines, F., and Price, L.R. (1998). Focused ultrasound modifications of neural circuit activity in a mammalian brain. Ultrasound in medicine & biology *24*, 557-565.

Bergfeld, I.O., Mantione, M., Hoogendoorn, M.C., and et al. (2016). Deep brain stimulation of the ventral anterior limb of the internal capsule for treatment-resistant depression: A randomized clinical trial. JAMA Psychiatry *73*, 456-464.

Dalecki, D. (2004). Mechanical bioeffects of ultrasound. Annu Rev Biomed Eng *6*, 229-248.

Deffieux, T., Younan, Y., Wattiez, N., Tanter, M., Pouget, P., and Aubry, J.-F. (2013). Low-intensity focused ultrasound modulates monkey visuomotor behavior. Current Biology *23*, 2430-2433.

Dougherty, D.D., Rezai, A.R., Carpenter, L.L., Howland, R.H., Bhati, M.T., O'Reardon, J.P., Eskandar, E.N., Baltuch, G.H., Machado, A.D., Kondziolka, D.*, et al.* (2015). A Randomized Sham-Controleed Trial of Deep Brain Stimulation of the Ventral Capsule/Ventral Striatum for Chronic Treatment-Resistant Depression. Biological Psychiatry *78*, 240-248.

Elias, W.J., Huss, D., Voss, T., Loomba, J., Khaled, M., Zadicario, E., Frysinger, R.C., Sperling, S.A., Wylie, S., Monteith, S.J.*, et al.* (2013). A pilot study of focused ultrasound thalamotomy for essential tremor. N Engl J Med *369*, 640-648.

Elias, W.J., Lipsman, N., Ondo, W.G., Ghanouni, P., Kim, Y.G., Lee, W., Schwartz, M., Hynynen, K., Lozano, A.M., Shah, B.B.*, et al.* (2016). A Randomized Trial of Focused Ultrasound Thalamotomy for Essential Tremor. N Engl J Med *375*, 730-739.

Fry, F. (1958a). Production of reversible changes in the central nervous system by ultrasound. Science *127*, 83-84.

Fry, W.J. (1956). Ultrasound in neurology. Neurology *6*, 693-704.

Fry, W.J. (1958b). Use of intense ultrasound in neurological research. Am J Phys Med *37*, 143-147.

Harvey, E.N. (1929). The effect of high frequency sound waves on heart muscle and other irritable tissues. American Journal of Physiology, 284-290.

Hertzberg, Y., Naor, O., Volovick, A., and Shoham, S. (2010). Towards multifocal ultrasonic neural stimulation: pattern generation algorithms. Journal of neural engineering *7*, 056002.

Hynynen, K., and Clement, G. (2007). Clinical applications of focused ultrasound-the brain. Int J Hyperthermia *23*, 193-202.

Hynynen, K., and Jolesz, F.A. (1998). Demonstration of potential noninvasive ultrasound brain therapy through an intact skull. Ultrasound in medicine & biology *24*, 275-283.

Hynynen, K., and Jones, R.M. (2016). Image-guided ultrasound phased arrays are a disruptive technology for non-invasive therapy. Physics in medicine and biology *61*, R206-248.

Ibsen, S., Tong, A., Schutt, C., Esener, S., and Chalasani, S.H. (2015). Sonogenetics is a non-invasive approach to activating neurons in Caenorhabditis elegans. Nature communications *6*, 8264.

Jung, H.H., Kim, S.J., Roh, D., Chang, J.G., Chang, W.S., Kweon, E.J., Kim, C.H., and Chang, J.W. (2015). Bilateral thermal capsulotomy with MR-guided focused ultrasound for patients with treatment-refractory obsessive-compulsive disorder: a proof-of-concept study. Mol Psychiatry *20*, 1205-1211.

Keedwell, P.A., and Linden, D.E. (2013). Integrative neuroimaging in mood disorders. Current opinion in psychiatry *26*, 27-32.

King, R.L., Brown, J.R., Newsome, W.T., and Pauly, K.B. (2013). Effective parameters for ultrasound-induced in vivo neurostimulation. Ultrasound in medicine & biology *39*, 312-331.

Krasovitski, B., Frenkel, V., Shoham, S., and Kimmel, E. (2011). Intramembrane cavitation as a unifying mechanism for ultrasound-induced bioeffects. Proc Natl Acad Sci U S A *108*, 3258-3263.

Kubanek, J., Shi, J., Marsh, J., Chen, D., Deng, C., and Cui, J. (2016). Ultrasound modulates ion channel currents. Sci Rep *6*.

Lee, W., Kim, H., Jung, Y., Song, I.-U., Chung, Y.A., and Yoo, S.-S. (2015). Image-guided transcranial focused ultrasound stimulates human primary somatosensory cortex. Scientific reports *5*, 8743.

Lee, W., Kim, H.-C., Jung, Y., Chung, Y.A., Song, I.-U., Lee, J.-H., and Yoo, S.-S. (2016a). Transcranial focused ultrasound stimulation of human primary visual cortex. Scientific Reports *6*, 34026.

Lee, W., Lee, S.D., Park, M.Y., Foley, L., Purcell-Estabrook, E., Kim, H., Fischer, K., Maeng, L.-S., and Yoo, S.-S. (2016b). Image-Guided Focused Ultrasound-Mediated Regional Brain Stimulation in Sheep. Ultrasound in medicine & biology *42*, 459-470.

Legon, W., Rowlands, A., Opitz, A., Sato, T.F., and Tyler, W.J. (2012). Pulsed ultrasound differentially stimulates somatosensory circuits in humans as indicated by EEG and FMRI. PLoS ONE *7*, e51177.

Legon, W., Sato, T.F., Opitz, A., Mueller, J., Barbour, A., Williams, A., and Tyler, W.J. (2014). Transcranial focused ultrasound modulates the activity of primary somatosensory cortex in humans. Nat Neurosci *17*, 322-329.

Li, G.-F., Zhao, H.-X., Zhou, H., Yan, F., Wang, J.-Y., Xu, C.-X., Wang, C.-Z., Niu, L.-L., Meng, L., Wu, S.*, et al.* (2016a). Improved Anatomical Specificity of Non-invasive Neuro-stimulation by High Frequency (5 MHz) Ultrasound. Scientific Reports *6*, 24738.

Li, G.F., Zhao, H.X., Zhou, H., Yan, F., Wang, J.Y., Xu, C.X., Wang, C.Z., Niu, L.L., Meng, L., Wu, S.*, et al.* (2016b). Improved Anatomical Specificity of Non-invasive Neuro-stimulation by High Frequency (5 MHz) Ultrasound. Sci Rep *6*.

Li, J., Fok, L., Yin, X., Bartal, G., and Zhang, X. (2009). Experimental demonstration of an acoustic magnifying hyperlens. Nature materials.

Mace, E., Montaldo, G., Cohen, I., Baulac, M., Fink, M., and Tanter, M. (2011). Functional ultrasound imaging of the brain. Nat Methods *8*, 662-664.

McDannold, N., Zhang, Y., Power, C., Arvanitis, C.D., Vykhodtseva, N., and Livingstone, M. (2015). Targeted, noninvasive blockade of cortical neuronal activity. Sci Rep *5*, 16253.

Meairs, S. (2015). Facilitation of Drug Transport across the Blood-Brain Barrier with Ultrasound and Microbubbles. Pharmaceutics *7*, 275-293.

Mehic, E., Xu, J.M., Caler, C.J., Coulson, N.K., Moritz, C.T., and Mourad, P.D. (2014). Increased anatomical specificity of neuromodulation via modulated focused ultrasound. PLoS One *9*, e86939.

Melde, K., Mark, A.G., Qiu, T., and Fischer, P. (2016). Holograms for acoustics. Nature *537*, 518-522.

Menz, M.D., Oralkan, Ö., Khuri-Yakub, P.T., and Baccus, S.A. (2013). Precise neural stimulation in the retina using focused ultrasound. The Journal of Neuroscience *33*, 4550-4560.

Mihran, R.T., Barnes, F.S., and Wachtel, H. (1990). Temporally-specific modification of myelinated axon excitability in vitro following a single ultrasound pulse. Ultrasound in medicine & biology *16*, 297-309.

Morishita, T., Fayad, S.M., Higuchi, M.A., Nestor, K.A., and Foote, K.D. (2014). Deep brain stimulation for treatment-resistant depression: systematic review of clinical outcomes. Neurotherapeutics *11*, 475-484.

Mueller, J., Legon, W., Opitz, A., Sato, T.F., and Tyler, W.J. (2014). Transcranial focused ultrasound modulates intrinsic and evoked EEG dynamics. Brain stimulation *7*, 900-908.

Mueller, J.K., and Tyler, W.J. (2014). A quantitative overview of biophysical forces impinging on neural function. Phys Biol *11*, 051001.

Naor, O., Krupa, S., and Shoham, S. (2016). Ultrasonic neuromodulation. Journal of neural engineering *13*, 031003.

O'Brien, W.D., Jr. (2007). Ultrasound-biophysics mechanisms. Progress in biophysics and molecular biology *93*, 212-255.

O'Halloran, R., Kopell, B.H., Sprooten, E., Goodman, W.K., and Frangou, S. (2016). Multimodal Neuroimaging-Informed Clinical Applications in Neuropsychiatric Disorders. Frontiers in psychiatry *7*, 63.

Omer, N., Yoni, H., Esther, Z., Eitan, K., and Shy, S. (2012). Towards multifocal ultrasonic neural stimulation II: design considerations for an acoustic retinal prosthesis. Journal of neural engineering *9*, 026006.

Opitz, A., Legon, W., Rowlands, A., Bickel, W.K., Paulus, W., and Tyler, W.J. (2013). Physiological observations validate finite element models for estimating subject-specific electric field distributions induced by transcranial magnetic stimulation of the human motor cortex. Neuroimage *81*, 253-264.

Osmanski, B.F., Pezet, S., Ricobaraza, A., Lenkei, Z., and Tanter, M. (2014). Functional ultrasound imaging of intrinsic connectivity in the living rat brain with high spatiotemporal resolution. Nat Commun *5*, 5023.

Parker, K.J., and Alonso, M.A. (2016). Longitudinal iso-phase condition and needle pulses. Opt Express *24*, 28669-28677.

Plaksin, M., Kimmel, E., and Shoham, S. (2016). Cell-Type-Selective Effects of Intramembrane Cavitation as a Unifying Theoretical Framework for Ultrasonic Neuromodulation. eNeuro *3*.

Prieto, M.L., Oralkan, Ö., Khuri-Yakub, B.T., and Maduke, M.C. (2013). Dynamic Response of Model Lipid Membranes to Ultrasonic Radiation Force. PLOS ONE *8*, e77115.

Rinaldi, P.C., Jones, J.P., Reines, F., and Price, L.R. (1991). Modification by focused ultrasound pulses of electrically evoked responses from an in vitro hippocampal preparation. Brain Res *558*, 36-42.

Rodriguez, A., Tatter, S.B., and Debinski, W. (2015). Neurosurgical Techniques for Disruption of the Blood-Brain Barrier for Glioblastoma Treatment. Pharmaceutics *7*, 175-187.

Spadoni, A., and Daraio, C. (2010). Generation and control of sound bullets with a nonlinear acoustic lens. Proc Natl Acad Sci U S A *107*, 7230-7234.

Tsui, P.H., Wang, S.H., and Huang, C.C. (2005). In vitro effects of ultrasound with different energies on the conduction properties of neural tissue. Ultrasonics *43*, 560-565.

Tufail, Y., Matyushov, A., Baldwin, N., Tauchmann, M.L., Georges, J., Yoshihiro, A., Tillery, S.I.H., and Tyler, W.J. (2010). Transcranial pulsed ultrasound stimulates intact brain circuits. Neuron *66*, 681-694.

Tufail, Y., Yoshihiro, A., Pati, S., Li, M.M., and Tyler, W.J. (2011a). Ultrasonic neuromodulation by brain stimulation with transcranial ultrasound. Nature protocols *6*, 1453-1470.

Tufail, Y., Yoshihiro, A., Pati, S., Tauchmann, M.L., and Tyler, W.J. (2011b). Ultrasonic Neuromodulation by Brain Stimulation with Transcranial Ultrasound. Nature protocols *6*, 1453-1470.

Tyler, W.J. (2011). Noninvasive neuromodulation with ultrasound? A continuum mechanics hypothesis. Neuroscientist *17*, 25-36.

Tyler, W.J. (2012). The mechanobiology of brain function. Nat Rev Neurosci *13*, 867-878.

Tyler, W.J., Tufail, Y., Finsterwald, M., Tauchmann, M.L., Olson, E.J., and Majestic, C. (2008). Remote excitation of neuronal circuits using low-intensity, low-frequency ultrasound. PLoS ONE *3*, e3511.

Wang, S., Olumolade, O.O., Sun, T., Samiotaki, G., and Konofagou, E.E. (2015). Noninvasive, neuron-specific gene therapy can be facilitated by focused ultrasound and recombinant adeno-associated virus. Gene therapy *22*, 104-110.

Yang, P.S., Kim, H., Lee, W., Bohlke, M., Park, S., Maher, T.J., and Yoo, S.-S. (2012). Transcranial focused ultrasound to the thalamus is associated with reduced extracellular GABA levels in rats. Neuropsychobiology *65*, 153-160.

Yang, S., Xing, D., Zhou, Q., Xiang, L., and Lao, Y. (2007). Functional imaging of cerebrovascular activities in small animals using high-resolution photoacoustic tomography. Med Phys *34*, 3294-3301.

Yang, X., and Wang, L.V. (2008). Monkey brain cortex imaging by photoacoustic tomography. J Biomed Opt *13*, 044009.

Yoo, S.S., Bystritsky, A., Lee, J.H., Zhang, Y., Fischer, K., Min, B.K., McDannold, N.J., Pascual-Leone, A., and Jolesz, F.A. (2011). Focused ultrasound modulates region-specific brain activity. Neuroimage.

Zhang, S., Yin, L., and Fang, N. (2009). Focusing Ultrasound with an Acoustic Metamaterial Network. Physics Reviews Letters *102*, 194301-194304.

CHAPTER 3

TRANSCRANIAL FOCUSED ULTRASOUND TO THE DORSAL ANTERIOR CINGULATE CORTEX ALTERS CONFLICT AND EMOTIONAL PROCESSING, PHYSIOLOGY, AND PERFORMANCE

ABSTRACT

The dorsal anterior cingulate cortex (dACC) operates as an integrator of bottom up and top down signals and is implicated in both cognitive control and emotion. It is thought to be causally involved in switching between attention networks, and previous work has linked it to cognitive performance, concentration, relaxation, and emotional distraction. This study intended to assess the feasibility of modulating broader attention networks and emotional distraction responses by stimulating the dACC with transcranial focused ultrasound (tFUS). Subjects were divided into two groups, one receiving sham and the other neuronavigation-guided tFUS to the dACC. Subjects performed a modified version of the Erikson flanker paradigm with fear and neutral faces used as background distractors. The results indicate that tFUS to the dACC induced effects that would be expected from relaxed contention, including reduced reaction time slowing from distractor faces, and an increase rather than a decrease in parasympathetic markers of the HRV. This suggests that tFUS altered emotional processing and enhanced sustained attention, perhaps by facilitating reduced attentional engagement with emotional distractors and reduced need for attention switching evidenced by event related potentials (ERPs), reduced alpha suppression, and modulation of delta and theta.

Introduction

Executive attention is widely studied and incredibly important in many life functions for survival, but also plays a key role in emotional wellbeing. There is a growing body of evidence that a few structures forming the cingulo-opercular network are critical to establishing and maintaining executive attention (Sadaghiani and D'Esposito, 2015). The network demonstrates demand-modulated activity in a broad range of cognitive tasks including spatial attention (Eckert et al., 2009), sustained focus (Dosenbach et al., 2007), and meditation (Hölzel et al., 2007). The dorsal anterior cingulated cortex (a major hub in the cingulo-opercular network) is crucial in cognitive behavioral performance as well as emotional regulation (Bush et al., 2000; Posner et al., 2019), and thought to monitor and resolve conflict and action outcome (Botvinick, 2007; Dosenbach et al., 2007).

The dACC is both anatomically and functionally interposed between the default mode network (DMN) and anti-correlated dorsal attention network (DAN) (Fox et al., 2005; Fox et al., 2009). Activation of the DMN is associated with mind wandering and self-referential thoughts, including negative rumination (Andrews-Hanna et al., 2014; Mason et al., 2007); it is inversely correlated with performance (Drummond et al., 2005; Polli et al., 2005), and is suppressed during cognitive tasks (Raichle et al., 2001). The dACC may execute is role in executive control by flexibly coupling with either network (Spreng et al., 2012; Sridharan et al., 2008; Vincent et al., 2008). Additionally, these regions are central to both the dorsal (goal directed behavior) and ventral (saliency) attention systems (Dosenbach et al., 2006), and act as a hub between the two (Eckert et al., 2009; Seeley et al., 2007). It has been suggested that the dACC plays a key role improving recognition and resolving a conscious percept while dealing with distraction (Hampshire et al., 2010; Vaden et al., 2013).

The dACC receives both top down and bottom up input from cortical and subcortical structures and is highly connected to the prefrontal cortex, striatum, hippocampus, and the amygdala (Beckmann et al., 2009; Cassell and Wright, 1986; Rushworth et al., 2007). In addition to its role in deciphering conflict, effortful perception (Wild et al., 2012), and alertness (Coste and Kleinschmidt, 2016), the dACC plays a role in mitigating emotional distraction (Iannaccone et al., 2015; Iordan et al., 2013; Shafer et al., 2012). The dACC demonstrates a clear functional overlap between error processing, pain (emotional suffering), and cognitive control (Albert et al., 2010; Cavanagh and Shackman, 2015; Egner et al., 2007; Foland-Ross et al., 2013; Haas et al., 2006; Kanske et al., 2012; Lane et al., 1998; McRae et al., 2008; Shafer et al., 2012; Shafritz et al., 2006; Wang et al., 2008; Wessel et al., 2012; Whalen et al., 1998; Yang et al., 2014). Activity in the dACC is correlated with emotional awareness (McRae et al., 2008), and changes in the dACC reflect alterations in the broader conscious experience (Aftanas and Golocheikine, 2001). Grey matter thickening is seen in the dACC in both reactively short (Tang et al., 2010), and long-term meditation training; conversely, this anatomical area exhibits cortical thinning in individuals with ADHD (Grant et al., 2013). Chronic pain disorders are known to be correlated with attentional deficits in both humans (Dick and Rashiq, 2007) and animals (Rochais et al., 2016) and linked to the dACC. For example, in patients with chronic low back pain there is a significantly lower engagement of the dACC during cognitive interference (Mao et al., 2014). Emotion can also interfere with attention as a form of distraction as evidenced by attentional biasing towards negative emotions in anxiety disorders (Mogg and Bradley, 2016). Also, shifts in attention and inability to sustain focus and are linked to anxiety and depression (Ólafsson et al., 2011).

There is a clear bidirectional link between emotion and executive function (Inzlicht et al., 2015; Lindström and Bohlin, 2011; Okon-Singer et al., 2015; Sarapas et al., 2017), which has larger implications in human experience and wellbeing. It is hypothesized that the above relationship makes the dACC an extremely promising anatomical target for neuromodulation to improve task performance in during conflict and emotional distraction. We further hypothesize that stimulating this area may also modulate emotional affect and physiological response to fearful faces and increased cognitive load.

Although numerous brain stimulation modalities exist, transcranial focused ultrasound (tFUS) has been of specific interest for its potential to modulate cognition (Fini and Tyler, 2017). Sub-thermal tFUS has been shown to induce changes in EEG (Legon et al., 2014a) and fMRI (Kim et al., 2017; Lee et al., 2016a), as well as perceptual (Lee et al., 2016a; Sanguinetti et al., 2016) and mood changes (Sanguinetti et al., 2020). Unlike any other noninvasive neurostimulation technique, tFUS has a high spatial resolution (on the order of millimeters) and can penetrate deep into the brain (Bystritsky and Korb, 2015).

To test our the above hypothesizes, tFUS was delivered in a trial-by-trial fashion to the dACC while subjects were performing a modified version of the Erickson Flanker task (Eriksen and Eriksen, 1974) in which emotional faces (either fear, neutral, or scrambled) were displayed in the background. The Flanker task is often used as a measure of cognitive control and response to interference. Subjects were asked to report the direction of a middle arrow flanked by two arrows on either side: pointing in the same direction (congruent: > > > > >) or opposite direction (incongruent: < < > < <). The task produces well-defined electroencephalographic (EEG) components and error responses. EEG and heart rate changes were recorded. Performance was measured by reaction times, accuracy, and conflict adaption. In previous studies, EEG frontocentral theta and delta activity can be seen during

conflict processing, and post-error (Debener et al., 2005; Iannaccone et al., 2015). Preceding trials with emotional faces induces response slowing and recruits the cingulo-opercular network (Papazacharias et al., 2015). Although emotion cannot be measured directly, survey was collected data using the Positive and Negative Affect Scale (PANAS) (Crawford and Henry, 2004). If successful in improving performance or mood, neuromodulation has broad implications for reducing the susceptibility to distraction in healthy individuals for use with meditation, as well as treating the clinical symptoms of ADHD, depression, and anxiety.

RESULTS

Subjects were asked to perform a modified version of the Erikson flanker task (Eriksen and Eriksen, 1974) in which emotional faces (fear, neutral, or scrambled) were presented as distractors behind the flanker arrows (Figure 1A). Twenty-eight healthy volunteers were divided into two groups: one receiving sham stimulation (Sham group), and the other receiving active tFUS to the dACC. Sham and stimulation began 28 ms prior to the onset of the faces and distractor arrows. Each experiment session began and ended with 100 simple flanker trials (baseline, post-stimulation) where white arrows were presented on a black background, and both groups received sham (see Methods). In the stimulation group, MRI-guided neuronavigation was used to target tFUS to the dACC during the main trials. A mean stimulation location of $x = 2.9 \pm 0.8$, $y = 22.2 \pm 1.7$, $z = 32.8 \pm 1.6$ (mean $\pm$ SEM) was recorded (Figure 1B-D).

Target-locked ERPs

Each time point in the ERP response at FCz was subjected to permutation testing across groups (Figure 2A, scalp map details can be seen in Figure S1, alone with ERPs at parietal

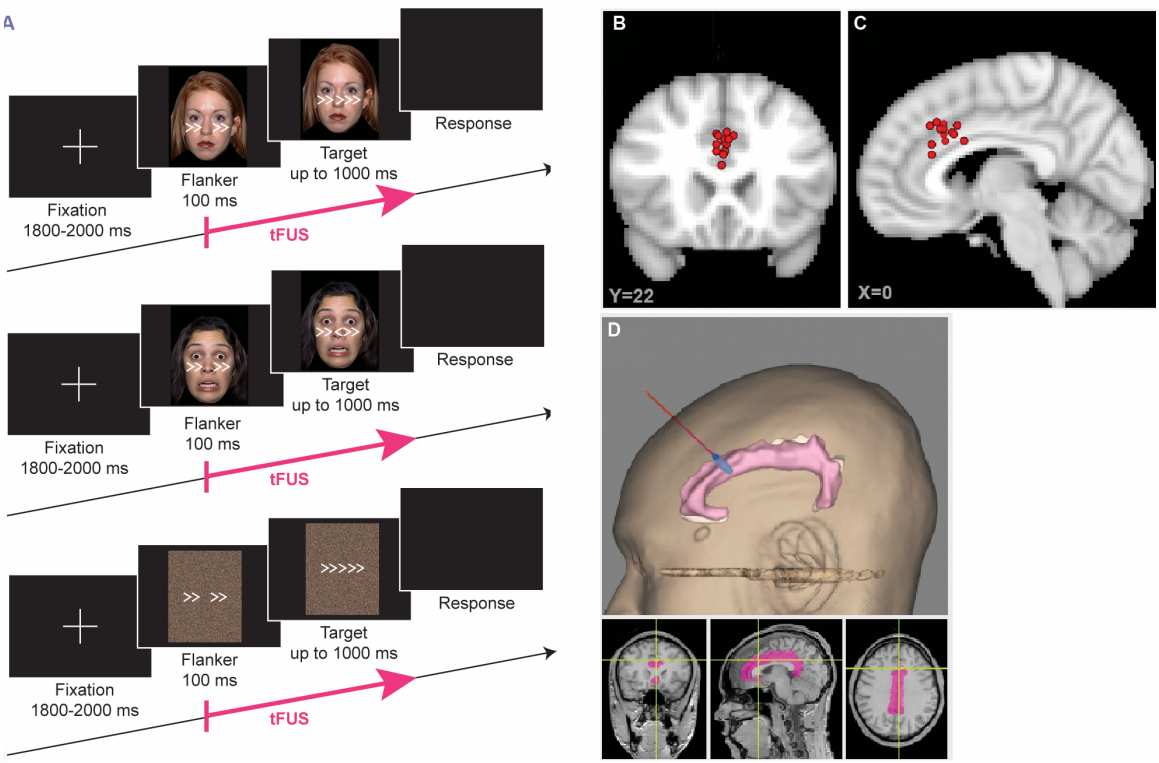

Figure 1: Experimental protocol and stimulation locations
(**A**) All main trials utilized the protocol above. Trials consisted of neutral (top), fearful (middle), or scrambled (bottom) faces. The fearful and neutral faces appeared with equal frequency, while the scrambled trials occurred only 1/50 as an oddball. The stimulation group received online tFUS in all main trials. Stimulation began 28 ms prior to the onset of the distracter flanker arrows and the face image, and lasted 500ms. Both groups were presented with a sham sound during this time period.
(**B-C**) Stimulation locations of all subjects mapped onto the MNI brain in coronal (y = 22) and sagittal (x = 0) planes.
(**D**) An example of neuronavigation in a single subject. Upper panel shows a 3D reconstruction of the subject's head, with the cingulate cortex highlighted in pink, beam trajectory in red, and estimated beam focus in blue. Lower panel shows subject's structural MRI with the cingulate cortex highlighted. Estimated tFUS beam focus center is at the crossing of the green lines.

electrode P4). Results showed that in both the fear and the neutral condition, the distractor elicited D-N1 (first frontocentral negative peak following presentation of distractor face and flanker arrows) shows both a larger negative peak and an earlier onset in the group receiving tFUS to the dACC. Significant differences start as early as 60 ms in the neural condition, and 68 ms in the fear condition. The Sham group shows a longer D-P1 (first frontocentral

positivity) than the tFUS group, which is significant in the neutral congruent trials. Additionally P3 has an earlier onset in the Sham group than tFUS in neutral incongruent trials.

Individual peak-to-peak amplitude and latencies were assessed at FCz using permutation testing and confirmed this result (Table S1, S3). There is greater amplitude a D-N1 in all conditions in the tFUS group (fear congruent: $p = 0.013$, neutral congruent: $p = 0.019$, fear incongruent: $p = 0.017$, neutral incongruent: $p = 0.047$). No other significant differences were found across group for ERP peak-to-peak amplitude (all $p > 0.15$, Table S1).

Similarly peak latency was compared across groups. In both congruent fear and neutral conditions there was an earlier P3 peak in Sham (fear: 476 ± 5 ms, neutral: 476 ± 5 ms) compared with tFUS (fear: 500 ± 4 ms, neutral: 500 ± 4 ms) groups (fear: $p = 0.009$, neutral $p = 0.009$). No other latency effects were found (all $p > 0.08$, Table S3).

Incongruent – congruent difference potential

Congruent potential was subtracted from incongruent potential to create an incongruent – congruent (incon – con) difference potential (Figure 2B). Permutation testing was used to compare each face type across groups and RM-ANOVA was performed within groups [2 congruency conditions (con, incon) × 2 face types (neutral, fear)]. In the neutral condition, there are significant differences across groups in the time range of P3 and the late potential (LP), while the fear condition; there are significant differences across groups in the time ranges of T-N1, P2, P3, and LP. Both groups exhibit a significant congruency effect at N2 (peak more negative in incongruent than congruent), but only in the Sham group is there a

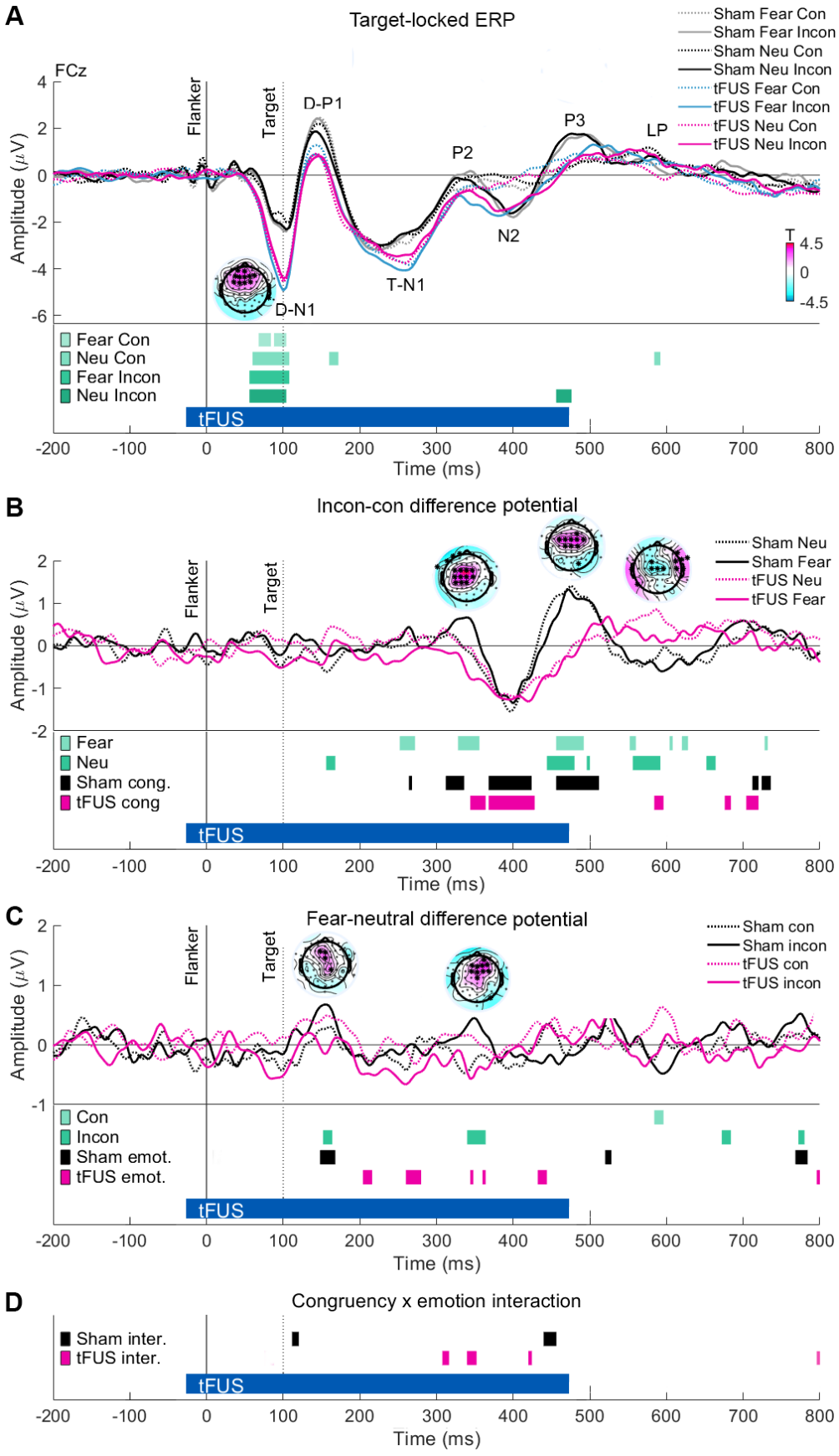
A
Target-locked ERP
FCz
Sham Fear Con
Sham Fear Incon
Sham Neu Con
Sham Neu Incon
tFUS Fear Con
tFUS Fear Incon
tFUS Neu Con
tFUS Neu Incon
Flanker
Target
D-P1
P2
P3
LP
N2
T-N1
D-N1
T
4.5
0
-4.5
Amplitude (μV)
Fear Con
Neu Con
Fear Incon
Neu Incon
tFUS
Time (ms)
B
Incon-con difference potential
Sham Neu
Sham Fear
tFUS Neu
tFUS Fear
Fear
Neu
Sham cong.
tFUS cong
C
Fear-neutral difference potential
Sham con
Sham incon
tFUS con
tFUS incon
Con
Incon
Sham emot.
tFUS emot.
D
Congruency x emotion interaction
Sham inter.
tFUS inter.

Figure 2. Target-locked event-related potentials at FCz
(**A**) ERP at FCz to neutral and fear trials in both congruency conditions. Time 0 ms marks the presentation of the faces and distractor arrows; time 100ms marks the onset of the target arrow. The tFUS stimulation period is marked with a blue bar at the bottom figure (starts 28 ms prior to face presentation and lasts 500 ms). ERP peaks are labeled. Scalp maps represent T values from permutation testing across groups at 96 ms in the fear incongruent condition, scale on bottom right; positive values indicate tFUS more negative than Sham, negative values: tFUS more positive than Sham. Asterisk represents significant electrodes ($*p < 0.05$)
(**B**) Linear subtraction of incongruent from congruent trials to produce an incon – con difference potential. Lower panel displays significant differences across groups for each emotion condition (fear, neutral), and significant congruency effects for each group (RM-ANVOA). Scalp maps represent T values for permutation testing across groups in the fear condition at P2, P3, and LP.
(**C**) Linear subtraction of neutral from fear to create fear - neutral difference potential. Lower panel displays significant differences across groups for each congruency condition (con, incon), as well as significant emotion effects for each group. Scalp T-maps displayed for D-P1 and P2.
(**D**) Congruency × emotion interaction effect for each group. Abbreviations: con: congruent, incon: incongruent. **Related to Figure S1, Table S2, and Table S3.** See also Figure 1.

significant congruency effect at P3. Indeed, there is markedly smaller incon – con frontocentral positivity at P3 for tFUS group compared with Sham. Additionally P3 is slightly faster in sham neutral compared fear trials, and significant congruency × emotion interaction can be seen here. At LP incon – con potential is more positive in the tFUS group than Sham; a significant main effect of congruency is observed in the tFUS group during this time period and significant group difference (primarily on neutral trails). At the earlier P2 peak, the Sham group exhibits a significant effect of congruency. In the fear condition, incongruent P2 is more positive than congruent in the Sham group, but this is not the case the tFUS group, and a significant difference across groups can be seen. Additionally, the tFUS group exhibits a congruency × emotion interaction in this time range between P2 and N2 peaks indicating that N2 onset latency is earlier in the fear condition.

Fear - neutral difference potential

A linear subtraction of neutral from fear trials was performed to produce fear – neutral difference potential (Figure 2C). A significantly more positive frontocentral D-P1 is seen in the Sham group for fear than neutral trials (a significant main effect of emotion is observed here), yet this is not the case for the tFUS group. Indeed on incongruent trials, a significant difference across groups is seen at frontocentral electrodes. The tFUS group does exhibit a significant effect of emotion at T-N1 (enhanced negativity for fear compared with neutral), and there is a significant difference across groups in the incongruent condition at centro-parietal electrodes (Figure S1). Furthermore, there is a significant difference across groups in incongruent trials at P2 across frontocentral electrodes further supporting the finding P2 and therefore N2 onset is earlier in the tFUS than Sham on fear trials.

Within group ERP amplitude

Testing peak-to-peak amplitudes within subjects across all congruency and emotion conditions with nonparametric Friedman's test further support findings described above (Table S2). Results showed D-N1 – D-P1 amplitude was significantly different across conditions in the Sham group ($\chi^2(3) = 7.63$, $p = 0.048$) but not the tFUS group ($\chi^2(3) = 3.74$, $p = 0.29$). However the following D-P1 – TN1 was statically different across conditions not in the Sham group ($\chi^2(3) = 5.06$, $p = 0.089$), but in tFUS group ($\chi^2(3) = 10.85$, $p = 0.013$), with substantial difference across fear and neutral congruent trials ($p = 0.09$), and significant differences between fear congruent and neutral incongruent trials ($p = 0.034$). Both groups exhibited a significant difference between conditions at P2 – N2 (Sham: $\chi^2(3) = 30.43$, $p < 0.001$, tFUS: $\chi^2(3) = 19.06$, $p < 0.001$) and N2 – P3 (Sham: $\chi^2(3) = 31.89$, $p < 0.001$, tFUS:

$\chi^2(3) = 17.03$, $p = 0.001$) where differences were seen between congruency conditions. Post-hoc statistics show at P2 – N2, there are significant differences between congruent and incongruent trials in both groups for neutral trials (Sham: $p = 0.009$, tFUS: $p = 0.003$), but in fear condition, this was only statically significant after Bonferroni correction in the Sham group (Sham: $p < 0.001$, tFUS: $p = 0.059$). Both groups showed a significant difference between neutral congruent and fear incongruent (Sham: $p < 0.001$, tFUS: $p = 0.005$).

Oddball

Analysis of ERP on oddball trials demonstrates that similar to the other trial conditions, there is a larger initial frontal negative deflection in tFUS group compared with sham (Figure S2). Additionally, on incongruent oddball trials, the tFUS group demonstrates both an earlier onset, and a more robust peak at 400ms (N2).

Parietal time-frequency response suggests tFUS to the dACC affects processing at multiple frequency bands

Event-related spectral perturbation (ERSP) data was calculated and compared at parietal (P3/P4) and frontocentral (FCz) across groups with permutation testing and RM-ANOVA, as well as within groups (RM-ANOVA). All data is reflected as dB increase from baseline (200 ms pre-stimulus baseline used). Comparing groups at parietal (ERSP data pooled across P3 and P4) electrodes reveals significant differences in the delta, theta, and beta bands (Figure 3). There were no group differences at the initial event-locked theta peak (4 – 8 Hz). However the Sham group exhibits post trial theta suppression in all conditions but greatest in the fear condition, and a significant main effect of emotion was found here for the Sham

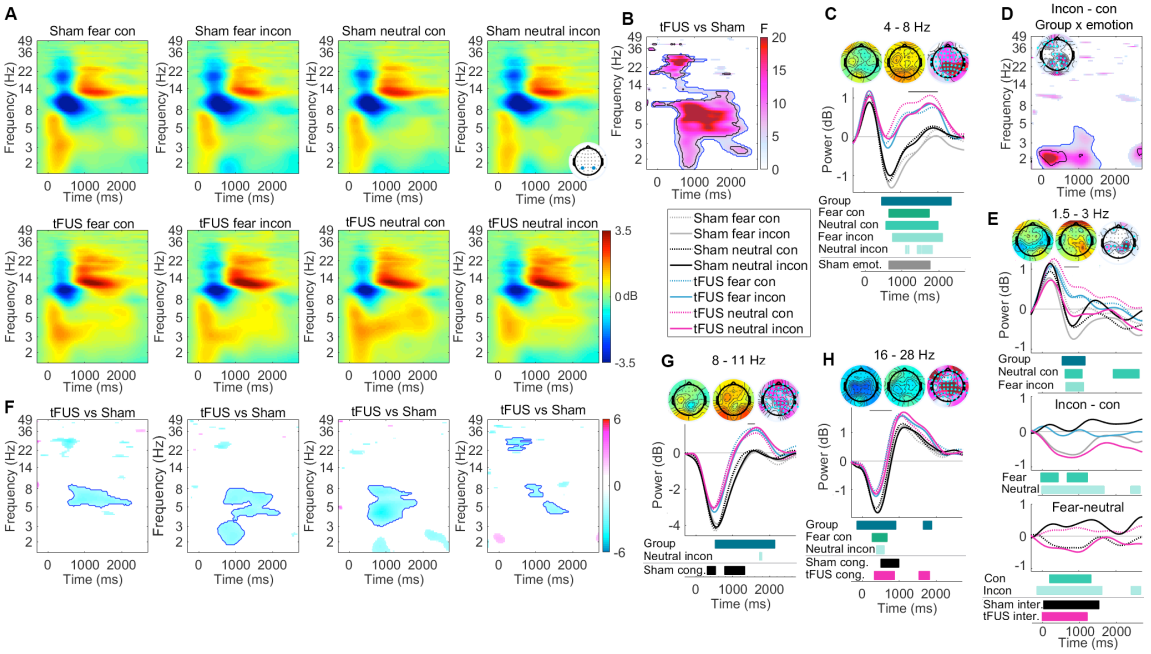

Figure 3. Target-locked time-frequency response at parietal electrodes

(**A**) ERSP data time-locked to target presentation (flanker and faces at 0 ms, target at 100 ms) averaged across P3/P4 (data displayed as dB change from baseline).

(**B**) Results of two-way RM-ANOVA (main effect group). In B, D, and F only significant ($p < 0.05$) statistical data is displayed; blue lines represent threshold-based clustering; black lines represent statistical significance after FDR correction.

(**C**, **G**, **H**) Power over time in various frequency bands. Theta (4-8 Hz) displayed in C, alpha (8-11 Hz) in G, and beta (16-28 Hz) in H. Bars below represent significant differences across groups using RM-ANOVA (Group) and permutation testing for each condition (green: fear con, fear incon, neutral con, neutral incon), as well as main effect of congruency (cong.) and emotion (emot.) for each group (RM-ANOVA within groups). Scalp maps represent power for time period indicated by horizontal bar above data (left sham, middle tFUS, right F values for main effect of group with scale as in B, electrodes significant after FDR correction indicated with cyan dot.

(**D**) Interaction effect of group × emotion for incongruent – congruent contrast power. Scalp map displayed for peak significance (0 - 500 ms, 1.5 - 3 Hz). Scale same as B.

(**E**) Expansion of delta effects displayed in D. Top plot shows power over time and scalp maps as in C, G, and H. Middle plot shows incon – con contrast power for which data is calculated in D. Plot line colors are consistent with legend for C (gray: Sham fear, black: Sham neutral, blue: tFUS fear, magenta: tFUS neutral). Bars below plot represent significant differences across groups (permutation testing) in incon – con contrast data for each emotion condition (fear, neutral). Bottom plot shows fear – neutral contrast power. Bars below represent significant differences across groups for incongruent (dotted lines) and congruent (solid lines) conditions. Under this, significant congruency × emotion interactions are displayed for each group (inter.).

(**F**) Displays T-values from permutation testing across groups for each condition displaced in A.

group (Figure 3C). The tFUS group, in contrast, did not show any theta suppression, but rather a second peak of theta activation in frontal and parietal-occipital electrodes in all conditions peaking between 1000 – 2000 ms post stimulus.

In the alpha range (8 – 11 Hz), the Sham group had larger and longer lasting event-locked alpha suppression than the tFUS group. In the Sham group, this suppression contributed to congruency processing, as there was a significant main effect of contingency. Following the alpha suppression, the tFUS but not the sham group showed post suppression alpha activation largest in parietal and occipital electrodes, but also present in frontocentral electrodes. Permutation testing revealed a significant difference across groups on neutral incongruent trials. This effect was significant over frontal, central, right parietal and occipital electrodes.

In beta band (16 - 28 Hz), both groups exhibited event-locked beta suppression in parietal electrodes, but this was of significantly larger amplitude in the Sham group compared with tFUS in parietal, central, and frontal electrodes. Permutation testing showed significant differences in the fear congruent and neutral incongruent conditions. Both groups exhibited significant congruency effects during this beta suppression.

In the delta band (1.5 – 3 Hz), both the Sham and tFUS groups exhibited significant congruency × emotion interaction effects over the first 1000 ms of the epoch, and there was a significant group × emotion interaction effect at parietal and frontal electrodes in incon-con contrast data. Assessing delta activity along with incon – con contrast power and fear – neutral contrast power unpacks this finding (Figure 3E). The tFUS group showed significantly longer target induced delta activation than the Sham group in neutral congruent and fear incongruent trials. Assessing incon-con contrast showed that in the fear condition, the tFUS group showed no differences in delta between incongruent and congruent trials; in

both conditions delta power increased and then slowing returned to baseline over the trial epoch. However in the Sham group, following initial activation, power quickly returned to baseline on congruent trials and showed a small suppression on incongruent trials, producing a negative incon-con contrast. On neutral trials, following the initial delta activation, both congruent and incongruent Sham, and incongruent tFUS delta returned to baseline around 800 ms post-stimulus, but on neutral congruent trials, delta power remained above baseline for 2000 ms in the tFUS group. Therefore on neutral trials, incon-con power was negative in the tFUS group, and around zero in the Sham group. Indeed comparing both fear and neutral incon – con power across groups yielded significance in both fear and neutral conditions. Furthermore, fear – neutral power was negative in tFUS incongruent and Sham congruent trials, while being slightly positive in tFUS congruent and Sham incongruent trials. Fear – neutral power significantly differed across groups in both congruency conditions.

Frontocentral time-frequency response and congruency effects

ERSP data at frontocentral FCz showed significant differences between groups in the delta, theta alpha, and beta range (Figure 4). In delta range, the tFUS group had an earlier onset of event-locked delta (permutation testing showed significance on neutral congruent trials). Both groups showed small but significant congruency effects in the delta range, this effect is earlier and larger in sham group on neutral trials compared with fear trials (significant difference between groups for incon – con contrast power; significant congruency × emotion interaction in the Sham group). Additionally, the Sham group showed an emotion effect beginning at 1000 ms due to suppression of delta power on fear incongruent trials.

In the theta range, a strong and robust congruency effect was seen in the Sham group consistent with the literature on frontocentral theta and conflict monitoring tasks,

however this effect was more diffuse and of much smaller amplitude in the tFUS group (Figure 4B and C). There was significant main effect of group in incon-con contrast power in the low theta range, most pronounced at central electrodes. Looking at frequency response over time (Figure 4E) demonstrates that incon-con contrast theta power was

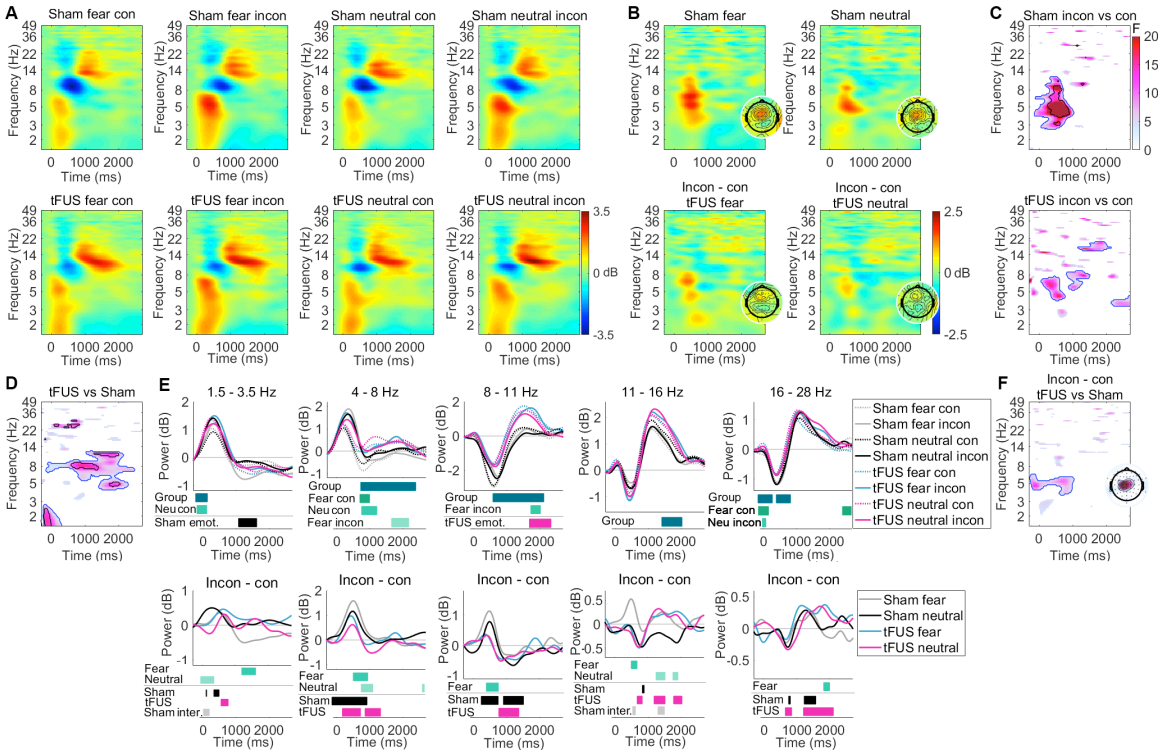

Figure 4. Frontocentral time frequency response with congruency contrasts.
(**A**) ERSP at FCz for each condition (dB power change over baseline).
(**B**) Incon – con contrast power for fear and neutral trials for each group. Inset displays scalp map of power (4 - 8 Hz; 200 - 800ms).
(**C**) Significant main effect of congruency for each for each group (F - values). In C, D, and F, only significant values shows, blue outlines threshold-based clustering; black lines represent FDR correction ($p < 0.05$).
(**D**) Significant main effect of group (RM-ANOVA).
(**E**) Power in various frequency bands (top row); bars below represent significant differences across groups (Group: RM-ANOVA), permutation statistics displayed for each condition (green), and the main effect of emotion within groups (black and magenta). Incon – con contrast power is plotted below for each frequency band. Bars indicate significance across groups for each emotion (green). Additionally, the main effect of congruency for each group (Sham, tFUS), as well as any significant congruency × emotion interaction effects (inter.) are plotted (shades of black and magenta).
(**F**) Statistical differences across groups (RM-ANOVA) for incon – con contrast power. Scalp map of F value peak plotted in inset to the right (4-8 Hz; 0 – 800ms).

significantly smaller and of shorter duration in the tFUS group compared with sham, especially on fear trials. This is due to the fact that the Sham group showed a post-peak theta suppression while the tFUS group did not. Indeed in this time range, there were significant differences in theta power across groups in congruent trials for both face conditions.

In the alpha range, the tFUS group showed significantly less event locked alpha suppression than the Sham group, recovering faster to baseline and exhibiting a post suppression alpha activation, highest in the fear condition. Permutation testing showed a significant main effect of emotion in this time range (~1800 ms). This alpha suppression was related to congruency processing as Sham group showed a congruency effect (earlier and larger peak suppression in congruency compared with incongruent trials producing a positive incon-con power peak). In contrast, the tFUS group showed smaller and faster suppression dynamics, so this effect was blunted; indeed there was a significant difference across groups in the incon – con alpha power in the fear condition.

In the low-beta range (11-16 Hz), there was no difference across groups in target-locked beta power suppression. However the Sham group did show reduced beta suppression in fear incongruent trails than all other trials, and a significant currency × emotion interaction at the low-beta suppression peak. Additionally, incon – con power was significantly larger in Sham than tFUS groups on fear trials. Furthermore the post-suppression low-beta activation was larger and longer in the tFUS group. Liking higher in the beta range (16-28 Hz), there was significantly less target-locked power suppression in tFUS compared with Sham. Both groups showed significant congruency effects during the post-suppression beta recovery and subsequent peak. This peak was significantly longer in incongruent than congruent trials in the tFUS group, and significantly larger incon – con contrast power was observed in the tFUS group compared with Sham in the fear condition.

Frontal time-frequency response to fearful face distractors

Both the Sham and tFUS groups showed significant main effect of emotion (RM-ANOVA) in the low theta range (3.8 – 5.5 Hz) at frontal electrodes (Figure 5), however this effect begins earlier in the tFUS groups. In the 200 – 950 ms time range, the tFUS group showed a significant main effect of emotion, but the Sham group did not (Figure 5A). Comparing fear – neutral contrast power across groups, there was a significant difference between groups at frontal and parietal electrodes. However at a later time window (1000 – 1900 ms), both groups showed a significant effect of emotion with no significant differences across groups. During the stimulus-induced low-theta peak, the tFUS groups showed a lower peak for fear than neutral in both congruency conditions, which was not the case for the Sham group, which showed no difference in congruent trials, and a slightly higher theta peak on fear than neutral trials in the incongruent condition (Figure 5B). Indeed, in this time range there was a significant main effect of group in fear – neutral contrast power, and a significant difference across groups with permutation testing in the incongruent condition. Additionally, a significant main effect of group was seen in the time range of 900 – 2500 ms. Following the initial theta activation, the tFUS group showed continued elevated power, greater in neutral than fear, and especially high in neutral congruent trials. Conversely, in the Sham group power returned to baseline with only a small elevation in power in the neutral condition. Significant differences were seen across groups with permutation statics in neutral congruent trials, and there was a significant congruency × emotion interaction effect in the tFUS group.

Error response in event-related potentials

Baseline-subtracted ERPs were time locked to each subjects' response (button press) to assess response-locked potentials for correct and error responses. Both groups showed no

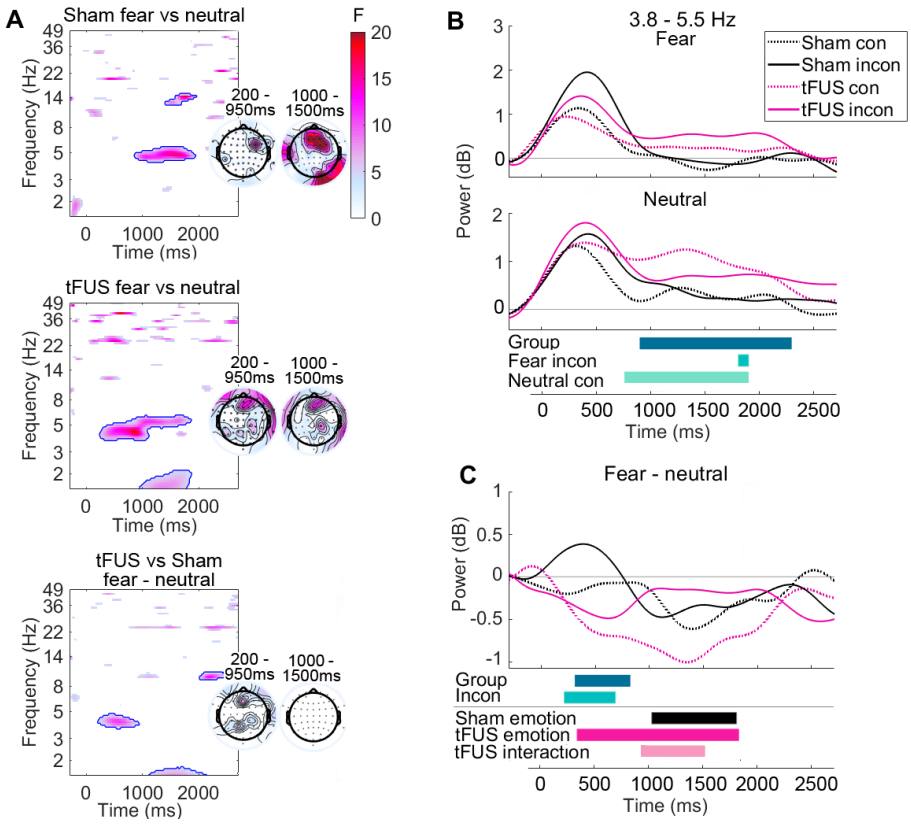

Figure 5. Groups differ in frontal theta during emotional face processing
(**A**) Main effect of emotion (fear vs. neutral, RM-AVOA) for Sham (top), tFUS (middle), and the main effect across groups for fear – neutral contrast power. Scalp maps in inset to the right of each plot represent significant differences across groups for power in the theta band (3.8 – 5.5 Hz) at 200 – 950 ms (left) and 1000 - 1900ms (right).
(**B**) Event locked power in the low-theta band (3.8 – 5.5 Hz) for fear trials (top) and neutral trials (bottom). The main effect of group (Group, RM-ANOVA) and permutation statistics across groups are displayed below plot.
(**C**) Fear – neutral contrast power. The main effect of group (RM-ANOVA) for fear – neutral contrast power (Group) and permutation statistics across groups for incongruent (incon) are displayed below. Additionally, the significant main effect of emotion and congruency × emotion interaction for theta power in B are displayed at the bottom of C (RM-ANOVA). Legend same as in B.

difference across correct and error responses at the pre-response NPe peak, but showed a large frontocentral error-related negativity (ERN) and subsequent frontocentral positivity (Pe, ~200 ms post response) for erroneous responses (Figure 6A and B). There were no differences across groups at NPe or peak ERN, but the ERN negative potential began earlier in the Sham than the tFUS group. Pe peak was significant larger amplitude and longer

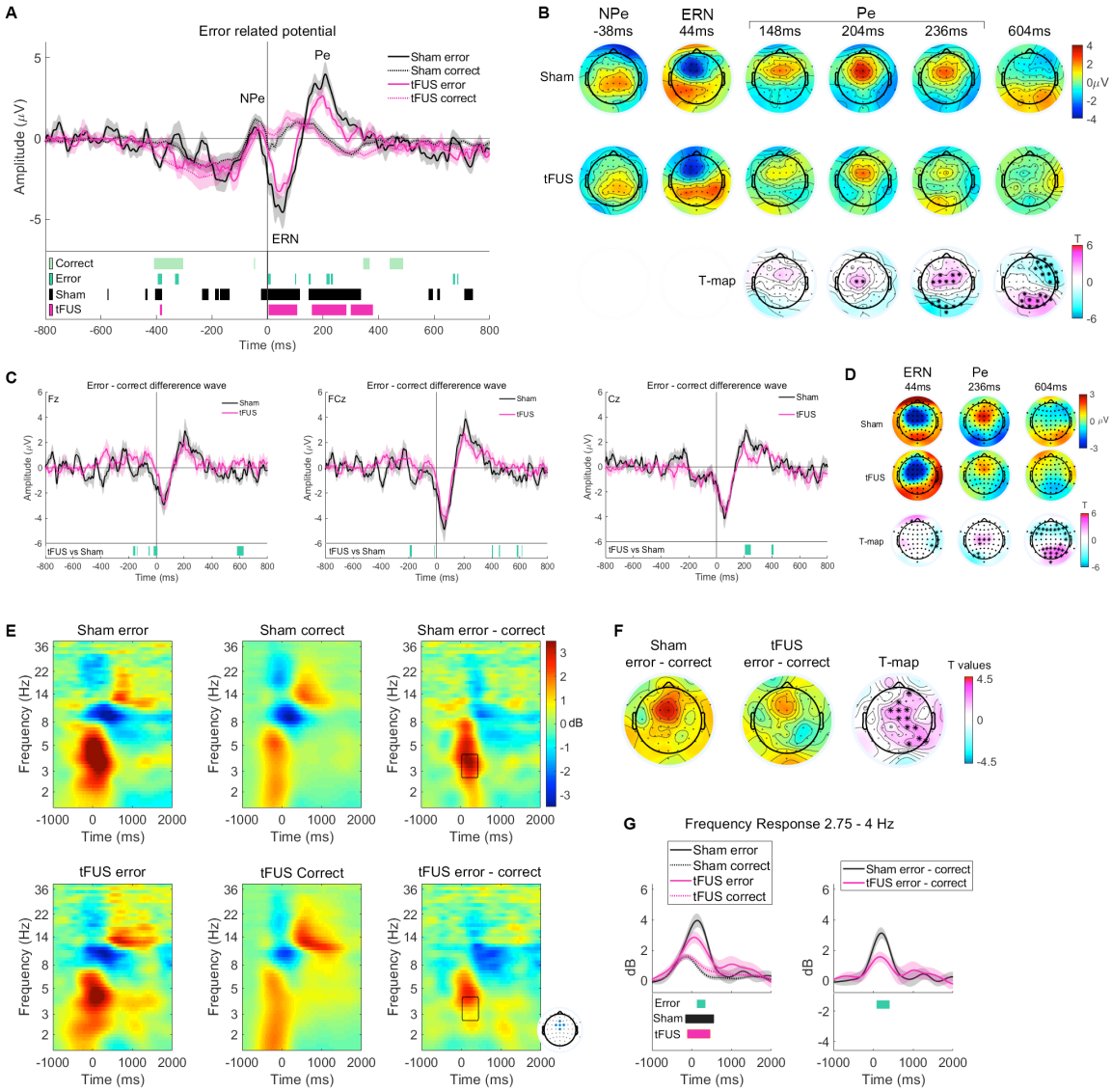

Figure 6. Error Response

(**A**) Response-locked error-related potentials at FCz to correct and incorrect responses. Statistical significance across groups for correct and error trials, as well as error vs. correct for group (Sham, tFUS) (permutation testing) are displayed below plot.

(**B**) Scalp maps correspond to peaks in A for Sham (top) and tFUS (middle). *T* values displayed at the bottom of the figure; asterisk (*) represents significant electrodes.

(**C**) Error – correct difference potential (linear subtraction of correct from error response) for electrodes Fz, FCz, and Cz.

(**D**) Scalp maps correspond to peaks in C and displayed as in B.

(**E**) Error-related time frequency data. ERSP data for erroneous and correct responses, time-locked to the button press (0 ms). Data averaged across electrodes Fz, FCz, Cz, FC1, and FC2. Linear subtractions of correct from error power are also displayed (error – correct). The black boxes highlight region of statistical significance across groups, shown in further detail in F and G; the time (32 – 400 ms) and frequency range (2.75 – 4 Hz).

(**F**) Error – correct contrast power for regions highlighted in E for each group. Scale same as E. Right-most map represents *T* values from permutation testing across groups as in B. (**G**) Frequency response over time in the delta band. Significant differences shown below are results of permutation testing across groups for error responses (Error), and within each group for error vs. correct responses (Sham, tFUS).

duration in the Sham than tFUS group. Additionally there was a significant group difference around 600 ms post-error where a fontal negativity and posterior positivity can be seen in the Sham group but not the tFUS group. Subtracting correct from error potentials produced an error – correct difference wave (Figure 6C and D). Again, no differences were seen at peak ERN, but onset was later in the tFUS group. Additionally a larger Pe was seen in the Sham group (peak group differences in central and occipital electrodes). Finally, around 600ms there was a group difference in frontal and parietal-occipital electrodes.

Error response in time-frequency data

Response-locked ERSP data was calculated for both correct and error responses and pooled at frontocentral electrodes (Figure 6E). Both tFUS and the Sham group showed a larger delta and theta response on error compared with correct trials. Comparing error – correct contrast power across groups showed in the delta range this was significantly reduced in the tFUS group. Comparing the time and frequency range highlighted in figure 6E (2.75 – 4 Hz, 32 – 400 ms) a significant difference was seen across groups in both error ($p < 0.001$), and error-correct power ($p = 0.009$). Scalp maps indicate that the topography of the significant differences is both frontocentral and right parietal. Additionally the tFUS groups show less post-error alpha suppression on correct than error trials.

Heart rate and heart rate variability

In order to assess physiologic changes in response to emotion face distractors and tFUS stimulation, heart rate was measured and several heart rate variability (HRV) metrics were calculated: standard deviation of normal-to-normal heartbeat (SDNN), percent of successive normal R-R intervals exceeding 50 ms (pNN50), short term HRV (SD1, also known as the root mean square of successive R-R interval differences, RMSSD), long term HRV (SD2), and SD1/SD2 ratio (see methods). Three minute time windows were selected for analysis: the first taken towards the end of the baseline trials (while subjects were performing a simple flanker, no faces, no stimulation), and the second being the first three minutes of the main trials (fearful and neutral faces appeared behind flanker distractor arrows, and stimulation group received online tFUS to the dACC, Figure 7). Mixed-measures, two-way RM-ANOVA's [2 groups × 2 time points] show a group × time interaction effect for HR [$F_{HR}(1,24) = 7.74, p = 0.010, \eta_p^2 = 0.24$], as well as all HRV measures: SDNN [$F_{SDNN}(1,24) = 54.23, p < 0.001, \eta_p^2 = 0.69$], pNN50 [$F_{HR}(1,24) = 9.72, p = 0.005, , \eta_p^2 = 0.29$], SD1 [$F_{SD1}(1,24) = 5.80, p = 0.024, \eta_p^2 = 0.19$], SD2 [$F_{SD2}(1,24) = 51.7, p = < 0.001, \eta_p^2 = 0.68$], and SD1/SD2 ratio [$F_{SD1/SD2}(1,24) = 4.31, p = 0.049, \eta_p^2 = 0.15$] (Table S4). Post-hoc analysis shows at the onset of emotional faces the Sham group significantly increased heart rate (↑3 ± 1%, $p = 0.037$, mean ± SEM), while there was a small but not significant decrease in HR seen in the tFUS group (↓2 ± 1%, $p = 0.098$). Additionally, all measures of HRV decreased in Sham group at the onset of faces with significant decreases in SDNN (↓20 ± 4%, $p < 0.001$) and SD2 (↓22 ± 4%, < 0.001). Non-significant decreases were seen in pNN50 (↓9 ± 11%, $p = 0.150$) and SD1 (↓4 ± 6%, $p = 0.37$). Conversely, HRV significantly increased in the group receiving tFUS to the dACC measured in the SDNN (↑24 ± 5%, $p <$

0.001), pNN50 (↑64 ± 18%, p = 0.007), SD2 (↑25 ± 6%, < 0.001), and non-significantly in SD1 (↑21 ± 7%, p = 0.37). The Sham group significantly increased in SD1/SD2 ratio (↑25 ± 9%, 0.039), while the tFUS group showed no change (0 ± 8%, p = 0.51). There were no significant main effects of time (F < 2.91, p > 0.10) or group (F < 1.86, p > 0.19. Unpaired t-test shows no significant differences between groups at baseline (all $T \leq 1.96$, $p \geq 0.062$).

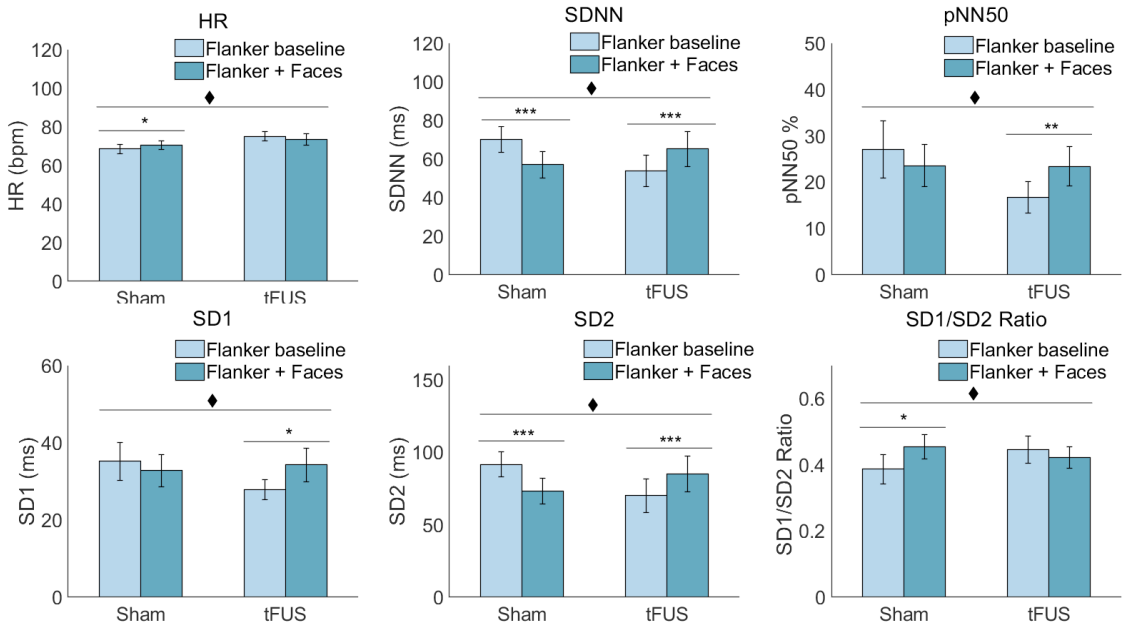

Figure 7. Heart rate and heart rate variability changes with addition of emotional face distractors
HR metrics were calculated from three minute samples recorded at two different time points: baseline (flanker only, no stimulation), and during the first three minutes of the main trials (onset of emotional faces and tFUS). The significant group × time interaction effect (♦p < 0.05), and post-hoc statics are displayed. All post-hoc statistics are Bonferroni-corrected (* p < 0.05, ** p < 0.01, *** p < 0.001). **Related to Table S4.**

Mood Data.

Subjects completed the PANAS mood questionnaire at baseline and immediately following experiment completion. Ratings were summed across positive and negatively valence probes to create PANAS positive and negative scores (Table 1). Score were assessed across group and time using two-way mixed measures RM-ANOVA [2 groups × 2 time points (baseline,

post-experiment)]. PANAS negative scores showed no significant main effect of time, group or interaction effect ($F < 2.52$, $p > 0.12$). For PANAS positive scores however, there was a significant main effect of time [$F_{Positive}(1,26) = 13.99$, $p = 0.001$, $\eta_p^2 = 0.35$] indicating positive PANAS scores decreased post experiment (baseline: 28.9 ± 14, post: 24.2 ±1.7, mean ± SEM). There was no main effect of group [$F_{Positive}(1,26) = 2.49$, $p = 0.19$, $\eta_p^2 = 0.09$] or group × time interaction [$F_{Positive}(1,26) = 0.85$, $p = 0.37$, $\eta_p^2 = 0.03$]. Post-hoc tests revealed that although both groups showed decreased PANAS scores, only the Sham group decreased significantly (Sham: $p = 0.003$, tFUS $p = 0.057$). Both groups showed a decreased score for 'interested' (Sham $p < 0.001$, tFUS $p = 0.002$), but only the Sham group showed significant decreases in scores for 'excited', 'enthusiastic', and 'attentive' ($p = 0.003$, 0.002, 0.007; tFUS p's > 0.21).

	Sham			tFUS		
	Baseline	**Post**	**Baseline vs. post**	**Baseline**	**Post**	**Baseline vs. post**
PANAS positive	31.6 ± 1.9	25.9 ± 2.7	0.003*	26.1 ± 1.9	22.6 ± 2.1	0.057
PANAS negative	13.8 ± 1.1	13.5 ± 1.1	0.64	11.5 ± 0.4	12.1 ± 0.6	0.31

Table 1. Summary of PANAS mood data
PANAS data collected immediately prior to (Baseline) and following completion of experimental session (Post). Statics represent post-hoc paired t-tests performed within groups. All p-values Bonferroni-corrected. All values displayed as mean ± SEM (*$p < 0.05$).

Reaction time: baseline-subtracted reaction time was faster in the tFUS than Sham group on neutral and fear incongruent trials

To rate task performance, a Mann-Whitney U test was performed across groups on baseline-subtracted median RTs (baseline congruent RT was used for congruent trials, and likewise for incongruent trials) (Figure 8). The results indicate that in both the neutral and fear incongruent condition, baseline-subtracted RT was faster in the tFUS group (Mdn = -3 ms,

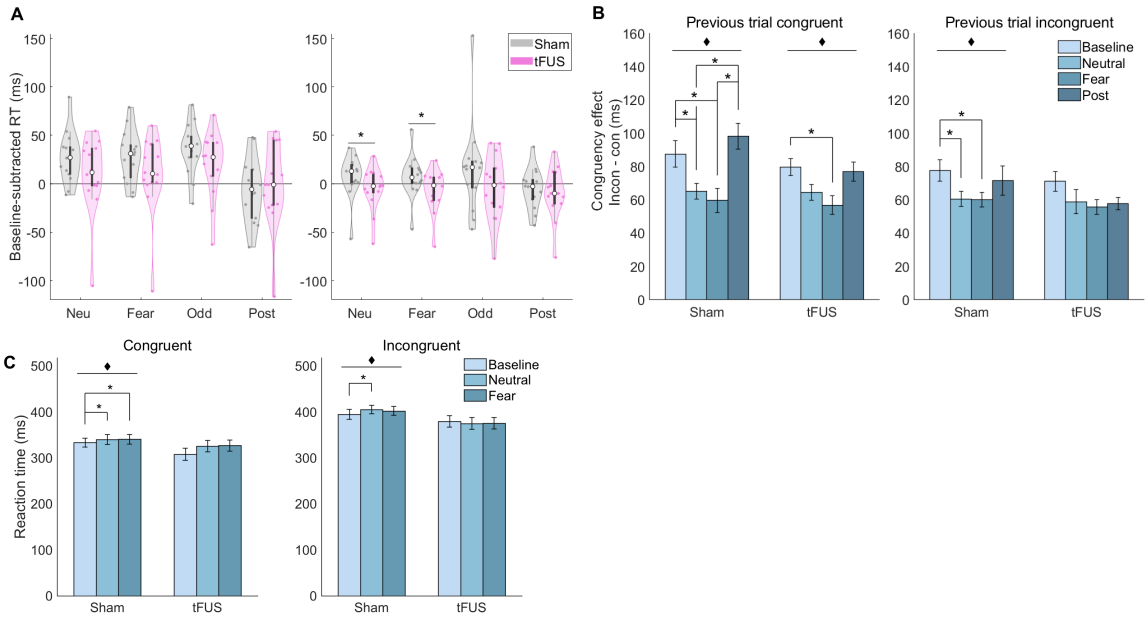

Figure 8. Reaction Time and congruency effect
(**A**) Baseline-subtracted reaction times displayed for both congruent (left) and incongruent (right) trials. Box-plots overlaid on violin plots (white circle at median), statistics represent the results of Mann-Whitney tests across groups $*p < 0.05$.
(**B**) Congruency effect for RT separated by previous trial congruency. Statics represent the results of related-samples Friedman's analysis ($\blacklozenge p < 0.05$) and post-hoc tests ($*p < 0.05$, Bonferroni corrected for multiple comparisons).
(**C**) Uncorrected reaction times compared within group with nonparametric statics as in B.

-3 ms) than the Sham group (Mdn = 13 ms, 7 ms), (fear: U = 48.5, p = 0.021, neutral: U= 54.5, p = 0.044). No Significant difference was found in the neutral, fear, or oddball congruent condition (U ≥ 76.0, $p \geq 0.39$) or oddball and post incongruent condition (U ≥ 74.0, $p \geq 0.285$). Furthermore, more subjects demonstrated faster RTs than baseline in the tFUS group in all conditions except the post congruent (Supplementary Table S5).

Using non-parametric Friedman's test to compare median RTs within groups further supports this finding (Figure 8C). To assess the behavioral effect of emotional face distractors on reaction time, RTs in baseline, neutral and fear trials were compared within group for each congruency condition. In congruent trials, the RT in the Sham group significantly differed across baseline, neutral, and fear RT ($\chi^2(3) = 9.93$, $p = 0.007$), but the

tFUS group does not ($\chi^2(3) = 4.86, p = 0.089$). Post-hoc tests show that in the Sham group both congruent fear ($p = 0.014$) and neutral ($p = 0.032$) were significantly slower than baseline. Similarly, in the incongruent condition the Sham ($\chi^2(3) = 7.00, p = 0.030$), but not the tFUS group ($\chi^2(3) = 1.78, p = 0.41$) showed a significant slowing of RTs with the addition of the faces. Post-hoc tests show that after Bonferroni correction, only the slowing in the neural condition was significant in the Sham group (fear: $p = 0.113$, neutral: $p = 0.042$).

Conflict adaption

Additionally to assess conflict adaption and its interaction with emotion, the congruency effect (also known as the flanker effect: incongruent RT – mean congruent RT) was calculated. RTs were separated by the congruency of the previous trial, and congruency effects were calculated and compared within groups (Figure 8B). On trials following congruent trials, a significant difference in congruency effect between baseline, fear, neutral, and post-stimulation trials is seen in the Sham group ($\chi^2(3) = 19.58, p < 0.001$), and tFUS group ($\chi^2(3) = 11.14, p = 0.011$). Bonferroni-corrected post-hoc statistics show that in the Sham group neutral trials have a significantly smaller congruency effect than baseline ($p = 0.016$) and post-experiment ($p = 0.002$), while in fear congruency effect is significantly smaller than post experiment ($p = 0.010$), and substantially smaller than baseline ($p = 0.062$). In the tFUS group there only a significantly smaller congruency effect on fear compared with baseline ($p = 0.05$).

On trials following incongruent trials however, the Sham group has a significantly smaller congruency effect for trials with distractor faces ($\chi^2(3) = 13.10$, $p = 0.004$) while this

is not the case for the group that received tFUS to the dACC ($\chi^2(3) = 3.62, p = 0.35$). Post-hoc tests show Sham congruency effect is significantly larger at baseline than on trials with fear ($p = 0.016$) or neutral face distractors ($p = 0.041$).

Post-error slowing

To assess post-error slowing, RTs on fear and neutral trials following an error were compared with median RTs in using Wilcox signed rank tests. The Sham group showed significant post-error slowing on fear trails in both flanker conditions (congruent: $Z= 77, p = 0.028$, incongruent: $Z= 78, p = 0.023$). The tFUS group showed post-error slowing in both incongruent conditions (fear: $Z= 66, p = 0.034$, neutral: $Z=77, p = 0.028$). All other conditions were not significantly slower than baseline $Z < 71$, $p > 0.24$).

To assess post-error slowing across groups, median RT was subtracted from post-error RTs. There were no differences across groups in post-error RT ($U \geq 27, p > 0.2$). Additionally, there were no differences in either group in post-error slowing based on current trial distractor face emotions ($Z < 66$, $p > 0.15$).

Accuracy did not differ across groups

Mann-Whitney U tests revealed no significant differences across groups in response accuracy neither at baseline, nor during the experiment *(*$U \geq 68.0, p \geq 0.178$, Table S6).

DISCUSSION

The dACC is highly involved in numerous tasks involved in directing executive control. Previous research has implicated it in attention, cognitive control, conflict, error, reward,

interoceptive awareness, emotion, pain, and relaxation (Critchley et al., 2002b; Critchley et al., 2004; Shackman et al., 2011; Vogt, 2005). Both functional imaging and electrophysiological data have linked activity in the dACC with performance on cognitive attention tasks (Matthews et al., 2007; Weissman et al., 2006), as well as emotional interference (Shafer et al., 2012). Furthermore it is involved in concentration meditation, as well as emotional awareness (McRae et al., 2008). Indeed, attentional lapses (as measured by negative performance on cognitive interference tasks) are correlated with reduced pre-stimulus and evoked activity in the cingulo-opercular network (Kerns et al., 2004; Weissman et al., 2006). Given the central role of the dACC in cognitive control, the aim of this study was to examine the application of tFUS to the dACC and its effect on conflict processing and emotional distraction.

tFUS to the dACC eliminates reaction time slowing in response to emotional face distractors and alters conflict adaption

As was expected based on previous findings (Jasinska et al., 2012; Papazacharias et al., 2015), the group that received Sham showed a significant slowing of RTs from baseline with the addition of neutral and fearful faces as distractors behind the flanker task (Figure 1), yet no significant difference was seen in the tFUS groups (Figure 8C). Additionally comparing baseline-subtracted RTs across groups, the tFUS group was significantly faster in fear and neutral incongruent conditions (Figure 8A). Response slowing induced by emotional faces is known to recruit the cingulo-opercular network (Papazacharias et al., 2015), and these results suggest that this was disrupted by tFUS to the dACC, resulting in a reduced distraction impairment of RT performance.

To study conflict adaption, congruency effect (incongruent-congruent RT) was separated by previous trial congruency and compared within groups. Consistent with previous studies, the Sham group showed significantly reduced congruency effect for trials with emotional distraction in both trials following congruent and incongruent trials (Egner et al., 2007). However the tFUS group only differed from baseline on trials following congruent trials and no difference from baseline on trials following incongruent trials. Previous studies have shown that congruency effect is reduced in negative mood (van Steenbergen et al., 2010). This result suggests that tFUS to the dACC may bias conflict adaption, modulating conflict processing by enhancing sensitization to conflict on trials following incongruent trials.

Event related potentials show enhanced early components and modulated fear processing in tFUS

Individuals receiving tFUS to the dACC showed an earlier onset and larger amplitude early frontocentral negativity and parietal positivity following presentation of the distractor faces and arrows (D-N1, ~ 100 ms). The N1 component is associated with the orienting network, is known to decrease after attention fatigue (Boksem et al., 2005). At D-P1 (the first frontocentral positivity), the sham group shows a greater amplitude peak for fear than neutral distractor trials consistent with the literature (Carlson and Reinke, 2010), yet this is not the case for the tFUS groups, and the two groups differ significantly in fear – neutral potential at frontocentral electrodes. This ERP peak is thought to facilitate spatial attention through involvement of the amygdala, dACC and visual cortex (Carlson et al., 2009; Klumpp et al., 2012), and is sensitive to fear arousal (Dennis and Chen, 2007). Additionally, the Sham group showed no difference across conditions at the following frontocentral negative peak

(T-N1), but the tFUS group shows a significantly pronounced negative potential for fear compared with neutral distractors. It is possible that tFUS to the dACC modulated this emotional appraisal signal, which perhaps had broader implications to reduced distraction effects described above in RT.

There were no significant differences in N2 peak amplitude across groups (Figure 2), yet comparing incon – con contrast is was clear that the tFUS group had an earlier onset of N2 than Sham on fear trials (this has also been observed in mindfulness meditators (Fan et al., 2015)). Additionally the tFUS group had a diminished incon – con response at P3 compared with Sham. Previous research has shown P3 in distractor processing is higher in novices compared to meditators (Cahn and Polich, 2009) and was reduced with mindfulness meditation training (Moore et al., 2012), and that faster RTs in meditators on incongruent trials can be correlated with changes in P3 (Jo et al., 2016). Frontal P3 is presumed to come from the dACC, is evoked by attention-switching (Xie et al.), and is emotion dependent (Albert et al., 2010). This suggests that tFUS perhaps enhanced sustained attention and reduced the need for attention switching.

Time-frequency data is altered across multiple frequency bands with dACC tFUS

The tFUS group had an earlier onset of stimulus-induced frontocentral delta, and a longer sustained delta activation at parietal electrodes than Sham. Both groups show differing congruency × emotion interactions in the delta band at parietal electrodes. In the theta band, there were no differences across groups in target-induced theta peak activation, however the Sham group displayed a post-peak theta suppression, while the tFUS group showed a second theta which was highly significant over the sham group in parietal-occipital electrodes and to a lesser extend frontal electrodes. Additionally differences were seen across groups in the

incon – con contrast power, which was reduced in tFUS subjects in theta band due to sustained activation of theta. Frontocentral theta is known to be present both in cognitive tasks and meditation (Inanaga, 1998), and is thought to originate from the dACC and functionally connects to other regions of the brain for executive control of action updating (Cohen, 2011). It is linked to error monitoring (Cavanagh et al., 2009), conflict adaption (Cohen and Cavanagh, 2011), and theta coherence is modulated by reaction time (Cavanagh et al., 2009). Central delta and frontocentral theta are both associated with N2 and P3 in response inhibition, but thought to indicate separate processes (Harper et al., 2014).

Additionally, subjects receiving tFUS to the dACC showed significantly reduced alpha suppression and subsequent post trial alpha activation at frontal and parietal electrodes. Differences were seen across groups in the incon – con contrast power, in the alpha band due to reduced target-locked alpha suppression on congruent trials in the tFUS group. Alpha is related to tonic alertness and suppression is involved in ignoring emotional distractors, increases with increasing distractor frequency (Murphy et al., 2020). Failure to suppress alpha in visual and sensorimotor areas predicts error and decreased performance in sustained attention (Mazaheri et al., 2009).

It has been proposed that the cingulo-opercular network involving the dACC and insula, maintain tonic alertness through alpha oscillations, alpha is negatively correlated with activity in the dorsal attention network and attention is allocated to this network when necessary by disrupting alpha oscillations (Sadaghiani et al., 2010). Additionally, elevated midfrontal theta and parietal alpha power are associated with increased awareness of conflict (Jiang et al., 2015). The data presented here suggests that tFUS to the dACC modulated task-related alpha suppression, as well and theta congruency processing which could explain the reduced reaction time slowing observed in the tFUS group.

Error responses differ across groups at Pe and in delta band

The tFUS and Sham did not differ in peak ERN amplitude, although the tFUS group did show a slightly delayed ERN onset latency. However the following error-related fontrocentral positivity, Pe, was smaller in amplitude and duration in the tFUS group. Pe represents different aspects of error processing from ERN, and may reflect conscious recognition of an error (Endrass et al., 2007; Overbeek et al., 2005), and have motivational significance.

In addition, significant differences were seen across groups in error responses in the delta range (1.5 – 4 Hz). The tFUS group showed less delta power than the Sham group in frontocentral electrodes on errors as well as in error – correct contrast power, but no differences were seen across groups in the theta range. Delta and theta combined are related to the ERN (Munneke et al., 2015) but may represent separate processes. The delta band is primarily associated with performance monitoring and error detection, while theta band activity may be associated more with motor execution failure (Cohen and Cavanagh, 2011; Yordanova et al., 2004), and correlated with N2 (Cavanagh et al., 2017). Others have shown that response-locked delta-band phase coherence may support general cognitive function (Cavanagh et al., 2009), decision making, and saliency (Knyazev, 2007).

Additionally, the tFUS group shows significant reduction of alpha power post-error compared with correct responses, related to adaption after errors (van Driel et al., 2012), but the Sham group does not. Combined fMRI EEG research and lesion studies suggests that the dACC may not be the generator of N2 but is likely is the generator of the error related ERN (Iannaccone et al., 2015; Stemmer et al., 2004). These findings suggest that tFUS to the

dACC modulated error processes perhaps through delta modulation, potentially effecting awareness or cognitive process related to error recognition.

Heart rate increases and heart rate variability decreases with emotional face distractors in Sham but not tFUS groups

A significant interaction group × time interaction effect was seen for physiologic response to fear and neutral face distractors in heart rate and HRV. The Sham group significantly increased heart rate and decreased SDNN, SD2, and SD1/SD2 ratio, while the dACC tFUS group substantially decreased heart rate, and significantly increased SDNN, pNN50, SD1, and SD2. Previous studies have shown that HRV decreases and HR increases with negative faces and increasing load (Park et al., 2014), exactly as was observed in the Sham group here.

The SDNN, influenced by sympathetic but largely parasympathetic activity, is known to decrease with increased workload (Fallahi et al., 2016) and increase with slow relaxed breathing (Shaffer et al., 2014). SD1 (also called the RMSSD) is associated with short-term HRV and vagal modulation of HRV (Shaffer et al., 2014), whereas SD2 is thought to measure both short and long term HRV and correlated with baroreflex sensitivity (Guzik et al., 2005). SD1/SD2 is associated with autonomic balance. Previous studies have shown that SD1 and SD2 increase with frontocentral theta power during concentration of awareness on the breath in Zen meditation (Kubota et al., 2001). The pNN50, like the SD1 is largely influenced by parasympathetic activity (Shaffer and Ginsberg, 2017).

A Meta-analysis of neuroimaging studies suggests that HRV can provide an index of top-down appraisal of threat, and that cortical substructures including the anterior cingulate influence the body's autonomic response by connections with the insula, and that the perceptual experiences of threat and safety are linked to HRV via the cingulate (Thayer et al.,

2012). The above described results indicate that tFUS to the dACC both inhibited physiologic responses to fearful and neutral distractor faces, but perhaps enhanced states of relaxation and parasympathetic activation. Since lower HRV is associated with an impaired ability to inhibit attention from fearful faces (Park et al., 2012), it is possible that tFUS causally affected reaction times by modulating fear processing.

Conclusions

The dACC is known involved in task switching and error (Nee et al., 2011), but its direct role in conflict processing is debated, and it is now thought not to be the direct generator of N2 (Iannaccone et al., 2015; Nee et al., 2011). This is consistent with the results presented here, in which tFUS to the dACC did modulate conflict processing, but no direct effect on N2 was seen.

The dACC its involvement in cognitive control and emotional distraction, the dACC is known to be active in states of relaxed concentration seen in meditation (Hölzel et al., 2007; Kubota et al., 2001). The results found here indicate that tFUS to the dACC induced hallmark effect that might be expected from relaxed contention, including reduced RT performance reduction in response to fearful face distractors and an increase rather than a decrease in parasympathetic markers of the HRV. This suggests that tFUS altered emotional processing and enhanced sustained attention perhaps by reducing attentional engagement with emotional faces and thereby reducing the need for attention switching evidenced by early ERP components, P3, elevated post-trial theta, reduced alpha suppression, and modulation of delta. These results provide promising evidence that tFUS to a single brain area can be used for broader network modulation with numerous applications in psychiatry and beyond.

METHODS

Participants

The study recruited 28 healthy, right-handed subjects from the university community (ages 19–39). Subjects were randomly assigned to either the sham group (control) or the stimulation group (tFUS). The sham group (n = 14) included 3 women and 11 men, mean age 22.4. The tFUS group (n=14) included 5 women and 9 men (mean age 25.3). All participants reported no history of neurological or psychiatric disorders, no hearing or uncorrected visual impairments, migraines, or medication use, as well as no contraindications for MRI. One subject in each group was removed from EEG and HR analysis due to poor quality data recording.

Behavioral task protocol: modified flanker paradigm with emotional face distractors

Subjects performed a modified version of the Eriksen Flaker task (Eriksen and Eriksen, 1974). After the experimental setup and completion of the mood surveys, subjects began with 32 practice trials, and then performed 100 baseline trials (50 congruent, 50 incongruent). Practice and baseline trials consisted of a simple flanker task with white distractor arrows appearing on a black background for 100 ms, followed by the target arrow. The distractor arrows were either congruent (pointing in the same direction as the target) or incongruent (pointing in opposite direction of the target). Subjects were asked to report the direction of the target arrow via button press with the index (left) or middle (right) finger of their right hand; participants were instructed to respond as quickly as possible without sacrificing accuracy. All main experimental trials utilized the protocol displayed in Figure 1. Each trial began with a fixation cross which was presented for 1800-2500 ms. Both groups were presented with a sham sound meant to imitate the sound of the tFUS pulse that is herd

through bone conduction. This sound began in both groups 28 ms prior to the appearance of the distractor arrows on the screen, and the tFUS stimulation (described below) began at the same time. Both the sound and the stimulation had a duration of 500 ms. Distractor arrows then appeared overlaid on one of three face types: a face exhibiting a neutral expression, one exhibiting a fearful expression, or a scrambled face (colored static). The fearful and neutral faces appeared with equal frequency, while the scrambled trials occurred only 3/50 as an oddball. Trials were presented in four blocks of 105 trials. Trials were pseudo-randomized with equal number of each trial type, and arrow direction. Face images were used from both the NimStim (Tottenham et al., 2009) and MaxPlank (Ebner et al., 2010) (young faces only) datasets. Faces images were edited to have a black background, masked to include just the face, and resized where necessary to ensure consistency in face size as well as position of nose and eyes.

Experimental setup

The task, tFUS stimulation, and all audio and visual information were controlled using PsychoPy software (Peirce, 2007). To ensure accurate notation of timing distractor and target presentation in the EEG file, events were triggered through photodiodes on the presentation computer monitor using Cedrus StimTracker (Cedrus Corporation, San Jose, CA). Likewise, all responses were recorded using a response box. Sham sound and tFUS stimulation were controlled also by the presentation computer via parallel port, and split to record triggers in the EEG system.

Sham

In both the sham and the stimulation group the ultrasound transducer was placed on the head and all ultrasound equipment turned on. For subjects receiving sham the tFUS transducer was disconnected from the RF amplifier. Both groups wore headphones, and at the onset of the tFUS stimulus, a low-volume, high-pitched sound was played to simulate the sound of the tFUS pulses that is herd through bone conduction. The sound file was created by combing a very high frequency tone with a square wave at the pulse repetition frequency. Upon questioning subjects in the tFUS group following the experiment, not perceptual difference was noticed between the sham sound and the tFUS preserved PRF pulse.

MRI acquisition and processing

Structural T1 MRI scans of each subject in the tFUS group were collected prior to experimentation for the purposes of neuronavigation. Images were collected in a Philips Ingenia 3T scanner with a 32-channel head coil, using a 3D MP-RAGE sequence (TR = 2300 ms, TE = 4.5 ms, 1 x 1 x 1.1 mm^3 voxels, field of view 240 x 256 mm^2, 180 sagittal slices). Brainsight neuronavigation system (Rogue industries) was used to plan stimulation targets and guide placement of the transducer beam profile with respect to each individual's anatomy. Montreal Neurologic Institute (MNI) coordinate system (Evans et al., 1994) was warped to each subject's brain, and when planning the tFUS target both MNI coordinates and individual anatomy of the dACC was considered. A mean stimulation location of x = 2.9 ± 0.8, y = 22.2 ± 1.7, z = 32.8 ± 1.6 (mean ± SEM) was recorded (Figure 1).

tFUS stimulation

Participants were blinded to mode of stimulation they received (active vs. sham). Following EEG setup, an infrared optical tracking system (Polars Vicra, NDI Medical, Waterloo, Ontario, Canada) was used to register the subjects' structural MRI scans in virtual space, with their head and the ultrasound transducer in 3D real space. This allowed the transducer to be positioned correctly on the surface of the scalp in order to hit the anatomical target identified prior. A custom built 3D printed housing was made for the transducer to hold the optical tracking unit and silicon spacer (ss-6060, Silicon Solutions, Cuyahoga Falls, OH), which was used to achieve the desired focal depth and couple the transducer to the scalp. Acoustic conductive gel was applied to both the transducer and the scalp. After correct placement of the transducer using the neuronavigation, we recorded the coordinate of the stimulation target. The transducer was held flush to the head with a custom-made, lightweight, elastic mesh cap, which did not interfere with EEG recording.

A broadband, single-focus transducer with a lateral spatial resolution of 4.9 mm^2 and axial spatial resolution of 18 mm^2 was used for this study (Blatek, Inc., State College, PA, USA). Given that tFUS is capable of inducing event related activity (Dallapiazza et al., 2017; Lee et al., 2016a; Lee et al., 2016b), all ultrasound stimulation was be delivered online, in a trial-by-trial manner. Each trial, stimulation began at the onset of the distractor arrows and face image. Each tFUS pulse had a carrier frequency of 0.5 MHz (to optimize signal transmission across the skull (Tufail et al., 2010)), a pulse repetition frequency (PRF) of 1000 Hz, a 24% duty cycle, and duration of 500ms. Stimulation was triggered by the experiment PC, controlled through a two-channel, 2 MHz function generator (BK Precision, Edison, NJ) and driven by a 40 W linear RF amplifier (E&I 240L; Electronics and Innovation, Rochester, NY, USA) as described preciously (Legon et al., 2012b). Water tank

measurements indicated a max pressure of 1.0 MPa and spatial peak pulse average intensity (I_{sppa}) of 20.4 W/cm^2 at the focus.

EEG recording

Electroencephalography (EEG) data was recorded using a 64-channel ActiCap system (BrainVision, Morrisville, NC, USA) with the standard 10-20 electrode layout. Electrode AFz was removed for placement of the ultrasound transducer. Data was recorded using a sampling rate of 5 kHz, resolution of 0.1 V, and band-pass filter of 0.1-100 Hz. The ground was placed at FPz and reference at the left mastoid. EEG electrode locations were recorded with Captrack camera system (BrainVision); fiducials were placed on the left and right tragus, and nasion.

EEG Processing

EEG data was processed using custom scripts in MATLAB R2017b (MathWorks, Natick, MA, USA) with the utilization of EEGLAB v14.1.1 (Delorme and Makeig, 2004). Raw data was first down-sampled to 250 Hz and high-pass filtered at 1 Hz, and notch filtered at 60Hz. Data was then visually inspected for artifacts and bad channels were removed. Additionally any channels with absolute temporal standard deviation greater than five or that exhibited artifacts for greater than 25% of the recording session were removed. All removed channels were then interpolated and all data was re-referenced to the scalp average using individually-recorded electrode locations. Independent Components Analysis was used to remove eye movement, blink, and other glaring artifacts; on average 3.6 ± 0.4 components were removed per subject.

Event related potentials

Data was then epoched around the distractor arrow presentation (target-locked) and 200 ms pre-stimulus baseline was subtracted to create event related potential (ERP) data. A linear subtraction of congruent from incongruent ERP data was performed to assess the incongruent-congruent (incon – con) difference potential. For analysis of response-locked data, ERP data was then time-locked to the button press (response). In order to control for multiple comparisons problems, ERP data was analyzed using nonparametric permutation statistics when comparing across groups and within groups for comparing only two conditions. Statistical *p* values represent the proportion of 1,000 permutations of randomly shuffled data which produce a *t* value greater than that calculated by a standard two-tailed *t*-test (Maris and Oostenveld, 2007) ($p < 0.05$ was considered statically significant). Two-way RM-ANOVA [2 congruency conditions (congruent, incongruent) × 2 face emotions (neutral, fear)] were used to compare within groups.

Additionally for each individual, peak-to-peak amplitude and latency were identified for each the ERP complex, and compared across groups (Table S2 and S4). Additionally nonparametric Friedman's test was used to compare within groups (Table S3).

Error-related potentials

To analyze response-locked ERPs for correct and error responses, baseline-subtracted data was then time-locked to the response (button press). As with target-locked ERPs, each condition was compared across groups using permutation testing. Additionally, error and correct responses were compared within group using permutation testing (paired rather than unpaired t-tests were used).

Time – frequency analysis: Event-related spectral perturbation

Event-related spectral perturbation (ERSP) data for time-frequency analysis was computed on time-locked data using EEGLAB. A 500 ms pre-stimulus baseline was used. Morlet wavelets were used with 3 cycles at the lowest frequency (1.5 Hz), and increasing linearly to 40 cycles at the highest frequency (50 Hz). All results are displayed as decibel power above baseline. Similar to ERPs, permutation testing was used on each time and frequency data point. ERSPs were further quantified across groups with mixed measures RM-ANOVAs [2 groups × 4 trial conditions (fear congruent, fear incongruent, neutral congruent, neutral incongruent)]. On main trials within group analysis was done using RM-ANOVAs [2 congruency conditions (congruent, incongruent) × 2 face emotions (neutral, fear)]. For comparing error with correct responses, permutation statistics were used for across (unpaired) and within (paired) group analysis.

A cluster-based multiple comparisons correction was applied to statistical results by determining clusters of contiguous significant pixels, *F* or *t* values in these clusters were then summed and only clusters greater than 2 standard deviations above the mean were retained. Additionally, false discovery rate (FDR) correction was also applied. Specific frequency band and time windows were selected for analysis as scalp maps and frequency response over time based either on peak responses in the ERSP or the results of group level statistical testing.

For main trails, primary analysis was done only on neutral and fear, congruent and incongruent trials. Linear subtraction of correct from error response, as well as congruent from incongruent target-locked data were used to evaluate error – correct and incongruent – congruent contrasts.

Heart-rate metrics

Heart-rate (HR) data was collected through the EEG electrode removed for the tFUS transducer by placing it below the left clavicle. Raw HR data was initially processed manually in MATLAB to ensure correct identification of heart beats, and then all HR metrics were calculated using HRVTool(Vollmer, 2015). We quantified several HR and HRV (heart rate variability) metrics including average HR, R-R interval, standard deviation of the normal-to-normal heartbeat (SDNN), and percentage of successive normal R-R intervals exceeding 50ms (pNN50). A Poincaré plot (RR_n, RR_{n+1}) was constructed to calculate nonlinear measures SD1 (standard deviation perpendicular to the identity line) and SD2 (standard deviation along the identity line), as well as the SD1/SD2 ratio. SD1 is also known as the root mean square of successive R-R interval differences (RMSSD)

PANAS Mood Ratings

To evaluate mood changed subjects were asked to assess their correct emotional state by completing the Positive Affect and Negative Affect Schedule (PANAS)(Watson et al., 1988). Mood ratings were completed at baseline (prior to stimulation), and again immediately following completion of the experiment. Ratings for positive valence probes ('interested', 'excited', 'strong', 'enthusiastic', 'proud', 'alert', 'inspired', 'determined', 'attentive', 'active') were summed to create a PANAS positive score while negative valence probes ('depressed', 'upset', 'guilty', 'scared', 'hostile', 'irritable', 'ashamed', 'nervous,' 'afraid') were summed to create PANAS negative score. Scores were compared with a mixed-factor RM–ANOVA [2 groups × 2 time points (baseline, post-experiment)]

Behavioral responses

Accuracy and reaction time were measured. Baseline-subtraction was used on RT data to eliminate interference of individual differences. Each subject' s median baseline RT for congruent and incongruent trials was used (baseline consisted of a simple flanker task on a black background, both groups received sham stimulation). Baseline congruent RT was subtracted from congruent trials (neutral, fear, and oddball), and likewise for incongruent. Groups were then compared using Mann-Whitney U test. Additionally, median RT's were compared within group using Friedman's nonparametric test and post-hoc testing with Wilcoxon signed-ranks tests (Bonferroni-corrected).

To access conflict adaption, trials were separated by previous trial congruency (congruent, incongruent), and median congruent RT was subtracted from incongruent to calculated the congruency effect in the RT. These were then compared both across and within group.

Post-error slowing

To assess post-error slowing, RTs on fear and neutral trials following an error were compared with median RTs in both congruency conditions using Wilcox signed-rank tests. To assess post-error slowing across groups, median RT was subtracted from post-error RTs and groups were compared using Mann-Whitney U tests.

Statistical methods

Statistical analyze were conducted using SPSS Statistics Software SPSS 26.0 (IBM Corporation, Armonk, NY). Only correct responses were considered for analysis. Trials with late RTs, RTs greater than 900ms, or that deviated more than three standard deviations from the individual mean, were excluded from analysis to reduce the effect of outliers.

Both parametric (RM-ANOVA), and non-parametric (between groups: permutation testing, Mann-Whitney U test; within groups: Friedman's test and Wilcox signed-ranks tests) tests were employed were appropriate and indicated above. Threshold for statistical significance were set at $p < 0.05$. When necessary normality was confirmed using Kolmogorov- Smirnov tests and Levene's test for homoscedasticity was used to examine all between group data variance (all p's > 0.05). All post-hoc tests were Bonferroni-corrected. All data reported is in the format mean ± SEM unless otherwise specified.

Supplemental materials

See Appendix B for supplemental materials.

CHAPTER 4

TRANSCRANIAL FOCUSED ULTRASOUND TO THE ANTERIOR INSULA / FRONTAL OPERCULUM ALTERS DISTRACTOR PROCESSING IN HUMANS DURING FLANKER TASK PAIRED WITH EMOTIONAL FACES

ABSTRACT

The right anterior insula/frontal operculum (aIns/fO) plays a key role in cognitive and state control as it is involved in attention, emotion, autonomic responses, and integrates saliency. It is also known to be active in mindfulness meditation, and is involved in interoceptive awareness, but also executive control, performance evaluation, and attentional maintenance. This study aimed to assess the feasibility of modulating cognitive control and emotional processing by targeting the aIns/fO with tFUS during a modified version of the Erikson flanker paradigm in which fear and neutral faces were placed behind the flanker task as distractors. Subjects were divided into two groups, one receiving neuro-navigated tFUS to the aIns/fO and the other receiving Sham. The results indicate that modulation of the aIns/fO with tFUS reduced parasympathetic fear responses seen in heart rate variability (HRV), emotional distraction interference on performance, and post-error slowing. Processing differences were measured across groups and demonstrated modulation of event related potentials associated with saliency, emotion, and congruency as well as modulation event-locked delta and beta with tFUS. These frequencies are known to be involved in modulation of physiologic responses though interaction with the amygdala, as well as distractor process through insular-medial frontal regulation during feedback. Overall this study demonstrates that tFUS along with neuronavigation can be used to target specific anatomical areas to induce larger network modulation to effect function and processing.

INTRODUCTION

The right anterior insula and frontal operculum (aIns/fO) likely plays an intriguing role in producing the contents of conscious experience; it is highly involved in both emotional expression and cognitive control, and may play a key role in directing present-center attention and plays a key role in mindfulness meditation (Tang et al., 2015). The functional area of the right aIns/fO spreads from the anterior insular cortex laterally through the inferior frontal operculum, and throughout the pars opercularis (BA44/45) of the right inferior frontal gyrus (rIFG) (Dosenbach et al., 2008). It is part of the cingular-opercular network (Cai et al., 2014; Coste and Kleinschmidt, 2016), and the ventral attention network (Dosenbach et al., 2006).

The aIns/fO is involved in diverse cognitive functions related to attention, is thought to be critical for integrating saliency queues, and orchestrates switching between the default mode (DMN) and executive networks (Eckert et al., 2009; Sridharan et al., 2008). It is thought to integrate emotional salience with afferent homeostatic information from the posterior insula in a bilateral fashion (Craig, 2002; Craig, 2004). The anterior insula is also involved in communicating information about fear stimulus to the amygdala, an important component of controlling physiologic fear expression (Phelps et al., 2001; Shi and Davis, 1999; Williams et al., 2004). It is known to be involved in interoceptive awareness and volitional control of autonomic responses (Critchley et al., 2002b). The aIns/fO is associated with pain and emotion in both first and third person (Jabbi and Keysers, 2008), and is thought to code for negative valence (Corradi-Dell'Acqua et al., 2016). Some authors have proposed this region contributes to the perceptual experience of the body and internal emotional state (Critchley et al., 2004).

Activity in the aIns/fO specifically lateralized to the right is greatly implicated in cognitive control, and is highly connected to the subthalamic nucleus, allowing for broad cortical influence (Aron et al., 2016). The right aIns/fO is linked to attentional performance (Aron et al., 2014), monitoring, and evaluation (Eckert et al., 2009), as well as action conflict (Hampshire et al., 2010), inhibitory control (Cai et al., 2014; Levy and Wagner, 2011), environmental monitoring, response selection (Taylor et al., 2009 ; Zaki et al., 2012), and error processing (Iannaccone et al., 2015 ; Wessel and Aron, 2017; Wessel et al., 2012). It likely plays a key role in attentional maintenance (Dosenbach et al., 2008) through effortful perception (Wild et al., 2012), and in emotional distraction (Shafer et al., 2012).

There is growing optimism in the field of neurostimulation that transcranial focused ultrasound (tFUS) can be used to modulate brain networks for the purpose of enhancing executive functioning and wellbeing (Fini and Tyler, 2017; Sanguinetti et al., 2020). The possibility of modulating executive control in response to cognitive interference and emotional distraction by targeting tFUS at the aIns/fO is explored here. tFUS was delivered in a trial-by-trial manner to the aIns/fO while subjects performed a modified version of the Erickson Flanker (Eriksen and Eriksen, 1974) task in which emotional faces (fear, neutral, or scrambled) were displayed in the background as distractors. The Flanker task has been widely used to study cognitive control and response to interference, and produces well studied evoked electroencephalogram (EEG) activity and error responses. For example, trial-locked frontocentral theta and delta EEG activity can be seen during conflict processing and post-error (Debener et al., 2005; Iannaccone et al., 2015). Others have demonstrated that preceding conflict processing task trials with images of emotional faces induces response slowing and recruits the cingulo-opercular network (Papazacharias et al., 2015).

Behavioral performance was measured by reaction times, accuracy, and conflict adaption. Heart rate data was collected for heart rate variability (HRV) analysis. Mood assessments were collected using the Positive and Negative Affect Scale (PANAS) (Crawford and Henry, 2004).

RESULTS

Twenty-eight healthy participants were divided into two groups: one group receiving sham, and the other receiving active tFUS stimulation to the aIns/fO on each trial. Stimulation mean center coordinates of ($x = 35.4 \pm 13$, $y = 13.5 \pm 1.2$, $z = 1.4 \pm 1.7$, mean $\pm$ SEM, Figure 1, Table S1) were recorded. After performing a brief flanker baseline, the subjects were asked to perform a modified version of the Erikson flanker paradigm in which emotional faces were presented as distractors behind the flanker arrows (see Methods: Figure 9). EEG, heart rate, reaction time, accuracy, and PANAS mood scale were recorded.

Target – locked ERPs

Comparing across tFUS and Sham groups using permutation statistics revealed that event related potentials (ERPs) show an earlier onset, and larger distractor-elicited frontocentral negative (D-N1, 98 $\pm$ 2 ms) in all emotion and congruency conditions (Figure 2A). Significant differences between groups begin as early as 28 ms and last up to 112 ms in the neutral congruent condition at FCz. Comparison of scalp potentials indicates this difference is significant in frontal and right parietal electrodes (see Figure S1 for ERPs at Fz and P4). No differences across groups at the first distractor-elicited positive peak (D-P1, 146 $\pm$ 2 ms) were found. At the first target-elicited negative peak (T-N1, 229 $\pm$ 5 ms), the tFUS group exhibited a significantly greater amplitude peak than the Sham group in both frontal and

parietal electrodes. This effect is significant at FCz in the neutral congruent and incongruent conditions, as well as the fear congruent condition. No significant differences were found at peaks P2 (341 ± 3 ms) or N2 (394 ± 4 ms) at FCz, however N2 is significantly larger in the tFUS group at frontal and right parietal electrodes (Figure S1), although no differences in incongruent – congruent potential are seen.

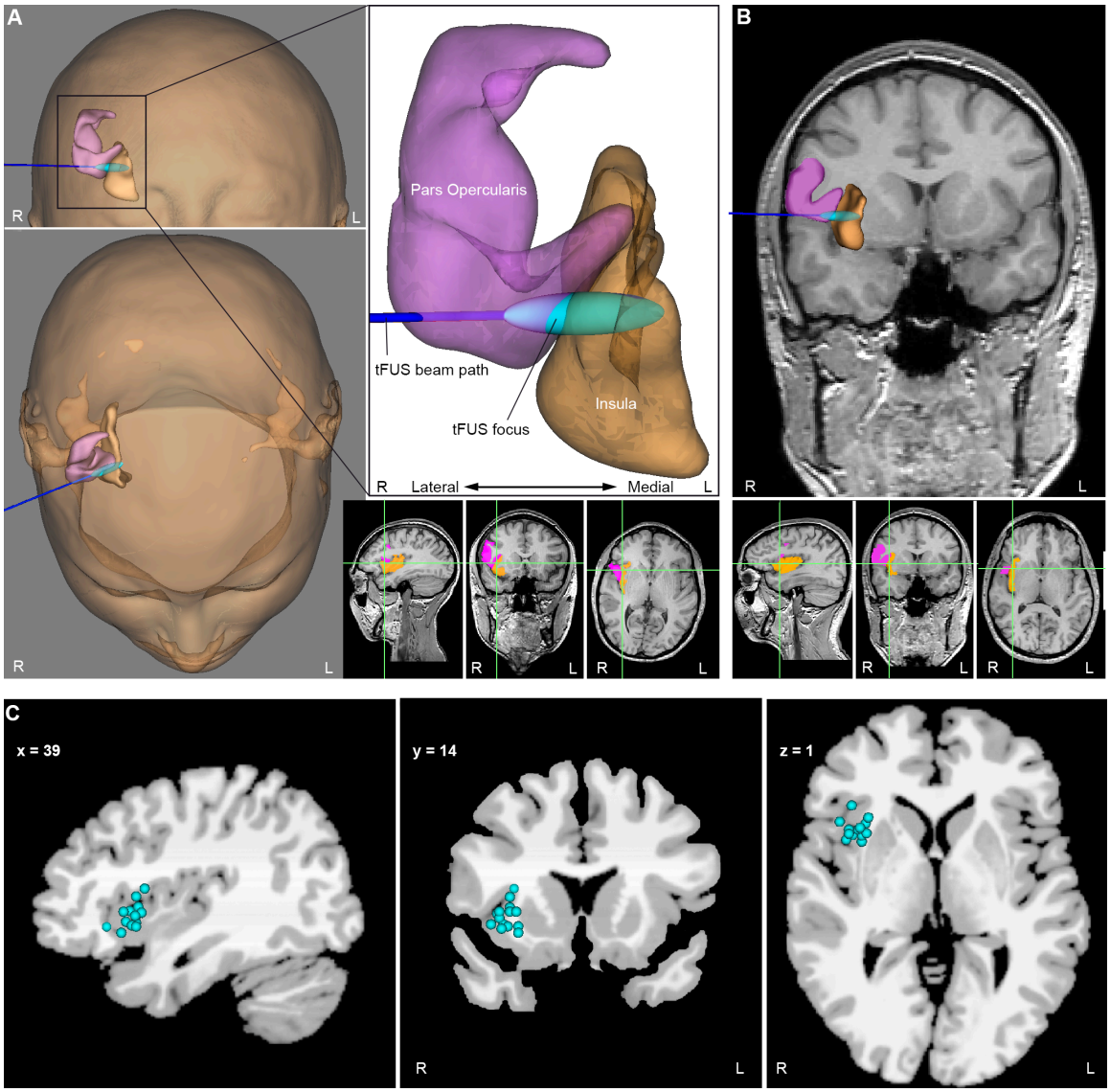

Figure 1. tFUS targets overlap the right anterior insula and frontal operculum
(**A**) 3-D reconstruction of the pars opercularis (pink) and the insula (orange) in a single subject. The tFUS beam path (blue) and focus (cyan ellipsoid) are plotted. Left panel displays 3-D reconstruction of the front and top view of the subject's head; once the tFUS transducer and the subject were registered to the MRI, this representation helped guide

proper placement of the transducer. Lower right panel displays the tFUS focal point on the sagittal, coronal, and transvers MRI slices; the gray matter of the pars opercularis and insula are highlighted.
(**B**) A second subject, upper panel displays 3-D reconstruction of pars opercularis and insula overlaid on the coronal MRI. As in A, stimulation focus overlaps the gray matter of the pars opercularis and anterior insula.
(**C**) Stimulation location foci of all subjects overlaid on average brain. Letters at the bottom of the image designate right (R) and left (L). Slices displayed at MNI coordinates (x = 39, y = 14, z = 1). **Related to Table S1.**

The P3 peak (479 ± 4 ms) showed an earlier onset and larger amplitude in the tFUS group compared with Sham in both congruent conditions. Additionally, in both the neutral and fear incongruent conditions, the tFUS group exhibited a more positive late potential (LP, approximately 520-630ms) than the Sham group following the initial P3 peak. A similar patter in early response activation, T-N1, and N2/P3 is also seen across groups in oddball trials (Figure S2).

Isolating individual subjects' peak-to-peak amplitudes at FCz confirmed this result (Table S2). In all conditions D-N1 is greater amplitude in the tFUS group (fear congruent: p = 0.025, neutral congruent: p = 0.003, fear incongruent: p = 0.001, neutral incongruent: p = 0.009). In the fear and neutral congruent, as well as neutral incongruent conditions, T-N1 – P2 peak-to-peak amplitude is significantly larger in the tFUS (fear congruent: 5.33 ± 0.42 μV, neutral congruent 4.83 ± 0.68 μV, neutral incongruent 5.67 ± 0.58 μV; median ± SEM) than the Sham group (3.39 ± 0.45 μV, 4.83 ± 0.68 μV, 4.23 ± 0.51 μV), (p = 0.007, p = 0.047, p =0.023). Additionally, in both the fear (p = 0.007) and neutral (p =0.003) congruent conditions, the N2 – P2 amplitude was larger in the tFUS group (1.92 ± 0.25 μV, 2.47 ± 0.27 μV) than Sham (0.68 ± 0.39 μV, 0.20 ± 0.27 μV).

No differences were found across groups in peak latency except at N2 in the neutral congruent condition (Table S3). N2 peak latency was earlier in the tFUS group (374 ± 5 ms)

than Sham (402 ± 4 ms, $p = 0.005$). This is related to the earlier onset of P3 in the tFUS group described above. No other differences in latency were found (all $p > 0.10$).

Incongruent – congruent difference potential

Subtracting congruent from incongruent ERPs produced an incon – con difference potential; each face type was compared across groups using permutation testing (Figure 2B). In the fear condition, there was a significant difference across groups in the time range of T-N1, with congruent trials showing a greater amplitude negative peak than incongruent trials in the Sham group, and visa versa in the tFUS group; both groups exhibit a significant main effect of congruency (RM-ANOVA) at this time. Only the Sham group showed a significant main effect of congruency in the time range of P2, but no group differences were found. Similarly, there was a main effect of congruency in both groups in the time range of N2 and P3, but no differences are seen across groups. However in the time range of the LP, there was a significant difference across groups in both the fear and neutral conditions. In the tFUS group LP is more positive in incongruent than congruent conditions, while the Sham group exhibited the opposite effect. This difference is significant for a longer time period in the tFUS group.

Testing peak-to-peak amplitudes using nonparametric Friedman's test within subjects revealed that both groups exhibited a difference between conditions at P2 – N2 (Sham: $\chi^2(3) = 30.43$, $p < 0.001$, tFUS: $\chi^2(3) = 22.29$, $p < 0.001$) and at N2 – P3 (Sham: $\chi^2(3) = 31.89$, $p < 0.001$, tFUS: $\chi^2(3) = 19.11$, $p < 0.001$) resulting from differences between congruent and incongruent trials (see Table S4 for all post-hoc statistics).

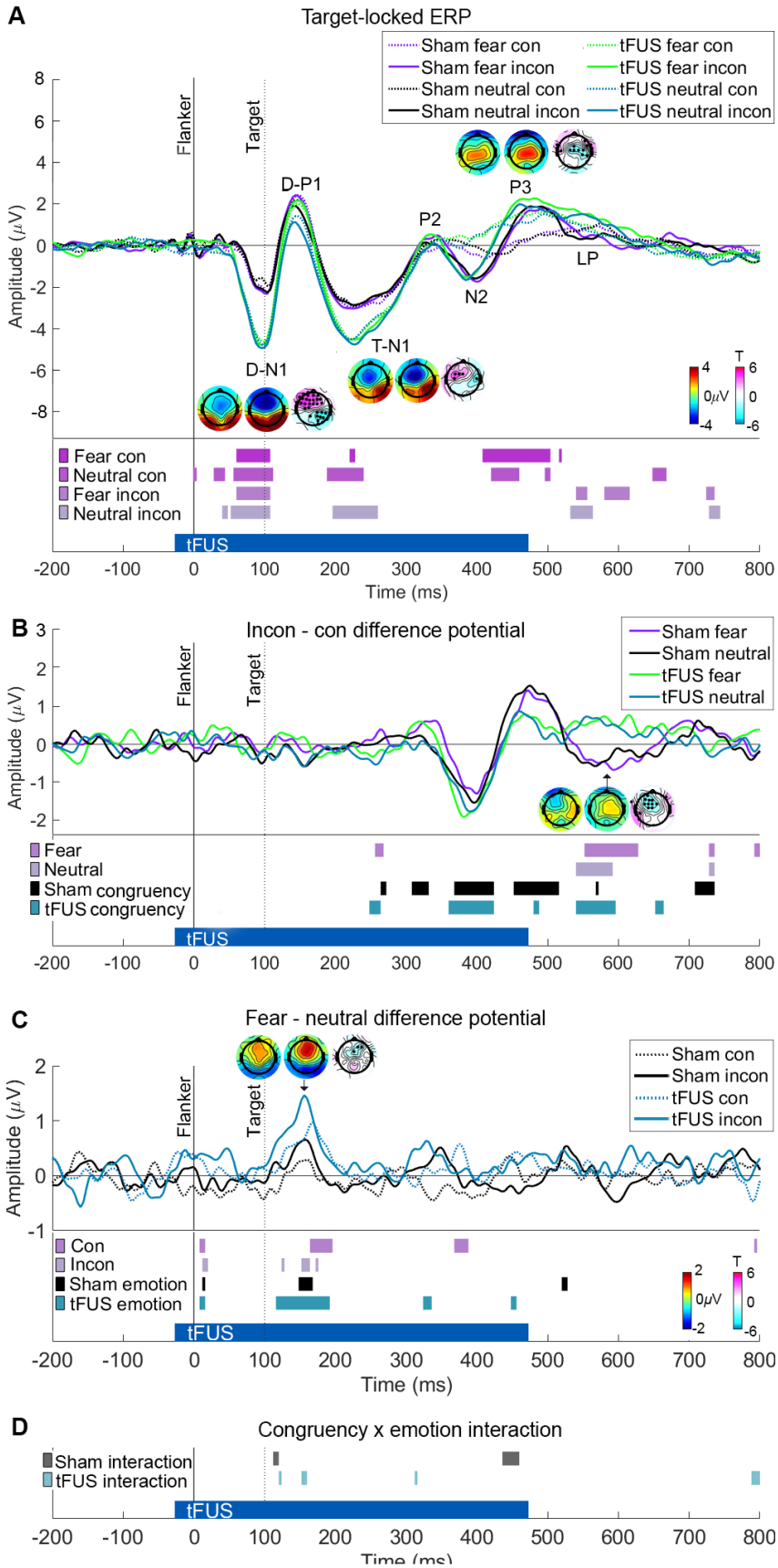
A
Target-locked ERP
Sham fear con
Sham fear incon
Sham neutral con
Sham neutral incon
tFUS fear con
tFUS fear incon
tFUS neutral con
tFUS neutral incon
Flanker
Target
D-P1
P3
P2
LP
N2
T-N1
D-N1
Amplitude (μV)
Fear con
Neutral con
Fear incon
Neutral incon
tFUS
Time (ms)
B
Incon - con difference potential
Sham fear
Sham neutral
tFUS fear
tFUS neutral
Fear
Neutral
Sham congruency
tFUS congruency
C
Fear - neutral difference potential
Sham con
Sham incon
tFUS con
tFUS incon
Con
Incon
Sham emotion
tFUS emotion
D
Congruency x emotion interaction
Sham interaction
tFUS interaction

Figure 2. Target-locked ERPs at FCz compared across groups, two congruency and two emotional distractor conditions
(**A**) ERPs at FCz for each group and all conditions, ERP peaks labeled. Distractor arrows and faces appeared at 0 ms (flanker) and target arrow appeared at 100 ms (target). Scalp potential maps are displayed for the fear congruent condition where there are significant differences across group (left: Sham, middle: tFUS, right: map of T values, significant electrodes marked with a dot). Scale displayed at right of figure. Time points displayed are: D-N1 (96 – 104 ms), T-N1 (220 – 228 ms), and P3 (464 – 472 ms). Significant differences across groups for each condition are displayed in the lower panel (permutation testing, $p < 0.05$). tFUS stimulation period marked with blue bar at the bottom of the panel (tFUS).
(**B**) Subtraction of congruent from incongruent potential to make incon – con difference potential. Lower panel displays significant differences across groups in incon – con potential for each emotion condition (fear, neutral), as well as significant congruency effects for each group (RM-ANVOA, performed on data in A). Scalp map: fear (580 – 596 ms).
(**C**) Subtraction of neutral from fear potential to make fear – neutral difference potential. Lower panel displays significant differences across groups for difference potential in each congruency condition (con, incon), as well as significant main effect of emotion for each group. Scalp maps displayed for D-P1 (152 ms) in the incongruent condition.
(**D**) Congruency × emotion interaction effect. Abbreviations: con: congruent, incon: incongruent. **Related to Figure S1, Table S2, Table S3, Table S4.** See also Figure S2**.**

Fear – neutral difference potential

To access the effect of face emotion on ERPs neutral were subtracted from fear responses to produce a neutral – fear difference potential (Figure 2C). As with the congruency conditions, each condition (congruent, incongruent) was compared across groups. Both groups exhibited a larger D-P1 peak for fear than neutral trials (significant main effect of emotion, RM-ANOVA). This difference is of larger magnitude and duration in the tFUS group than the Sham group in both congruency conditions. At N2 there was a significant difference across groups in the congruent condition; the Sham group exhibited a slightly more negative potential in the fear than neutral condition, although no significant main effect of emotion was found in this time frame.

Comparing peak-to-peak amplitude from individual subjects within each group using Friedman's nonparametric tests further supports this finding (Table S4). There was a

significant difference across conditions in D-N1 – D-P1 amplitude in the tFUS ($\chi^2(3) = 10.54$, $p = 0.014$), but not the Sham group tFUS ($\chi^2(3) = 7.63$, $p = 0.054$). Post-hoc analysis using Wilcox signed-ranks tests showed that fear incongruent (Mdn = 7.22 μV) was significantly larger than neutral incongruent (Mdn = 6.67 μV, $p = 0.032$), and neutral congruent (Mdn = 6.25 μV, $p = 0.032$).

Congruency and emotion ERP interaction

To further access the affect emotion may have on congruency processing, emotion × congruency interaction effect was accessed for each group (Figure 2D). Significant interaction effects where seen for both groups in the time between D-N1 and D-P1. Yet in the time range between N2 and P3 a significant effect was seen only the Sham group. Comparing peak amplitudes from individual subjects with Friedman's nonparametric test supports this finding (Table S4).

Frontocentral event-related spectral perturbation data differs with tFUS in multiple frequency bands

Comparing event-related spectral perturbation (ERSP) data at FCz across groups with RM-ANOVA yields a main effect of group in the delta, theta, and beta bands (Figure 3). In the delta range (1.5 – 3.5 Hz, Figure 3C), it is clear the tFUS group exhibited a larger power response. Permutation testing showed significant differences across groups in the neutral congruent, and fear congruent, and fear incongruent condition. In the theta range (4 – 8 Hz), the event-locked theta peak is of shorter duration in tFUS than Sham. Additionally, in the tFUS group there was a small theta suppression following the initial peak that is not seen in

the Sham group. Both the Sham and tFUS group exhibited a congruency effect during this time frame (higher power in incongruent than congruent trials), with no differences across groups. In the alpha range (8 – 11Hz) there was no difference across groups in power. Both groups exhibit a main effect of congruency (Figure 3D), with congruent trials having a larger and earlier theta suppression than incongruent trials. On neutral trials this effect is larger in the tFUS group than Sham as the tFUS group showed greater alpha suppression. Additionally significance between incongruent and congruent alpha suppression lasts longer in the Sham than tFUS group. Examining the incon – con contrast power during this time frame, there was a significant difference across groups in the neutral condition, and a significant congruency × emotion interaction effect in the tFUS group. There was a greater alpha rebound following the initial suppression in congruent than incongruent trials in both emotional conditions in the Sham group, but in the tFUS group this is only the case for the fear condition, and the opposite is true for neutral trials.

In the low beta range (12 – 22 Hz) the tFUS groups exhibited more event-locked beta suppression than Sham (main effect of group, RM-ANOVA). Permutation statistics confirm there was a significant difference across groups in the neutral and fear congruent conditions, and fear incongruent condition. Additionally, there was higher post-suppression beta activation (~1000ms) in the tFUS group than the Sham group. But groups exhibit more suppression in the incongruent than congruent trials and a significant main effect of congruency. However this effect is greater in the tFUS group than Sham group. Comparing incon – con contrast power across groups, there was a main effect of group, and a significant difference across groups in the fear condition using permutation testing.

In the high beta range (22 – 40 Hz), similar to the lower beta, there was more event-locked beta suppression in the tFUS group than sham with significant differences across

groups in the fear incongruent condition. Comparing incon – con contrast, but groups exhibited some significant effect of congruency, but there are no differences across groups.

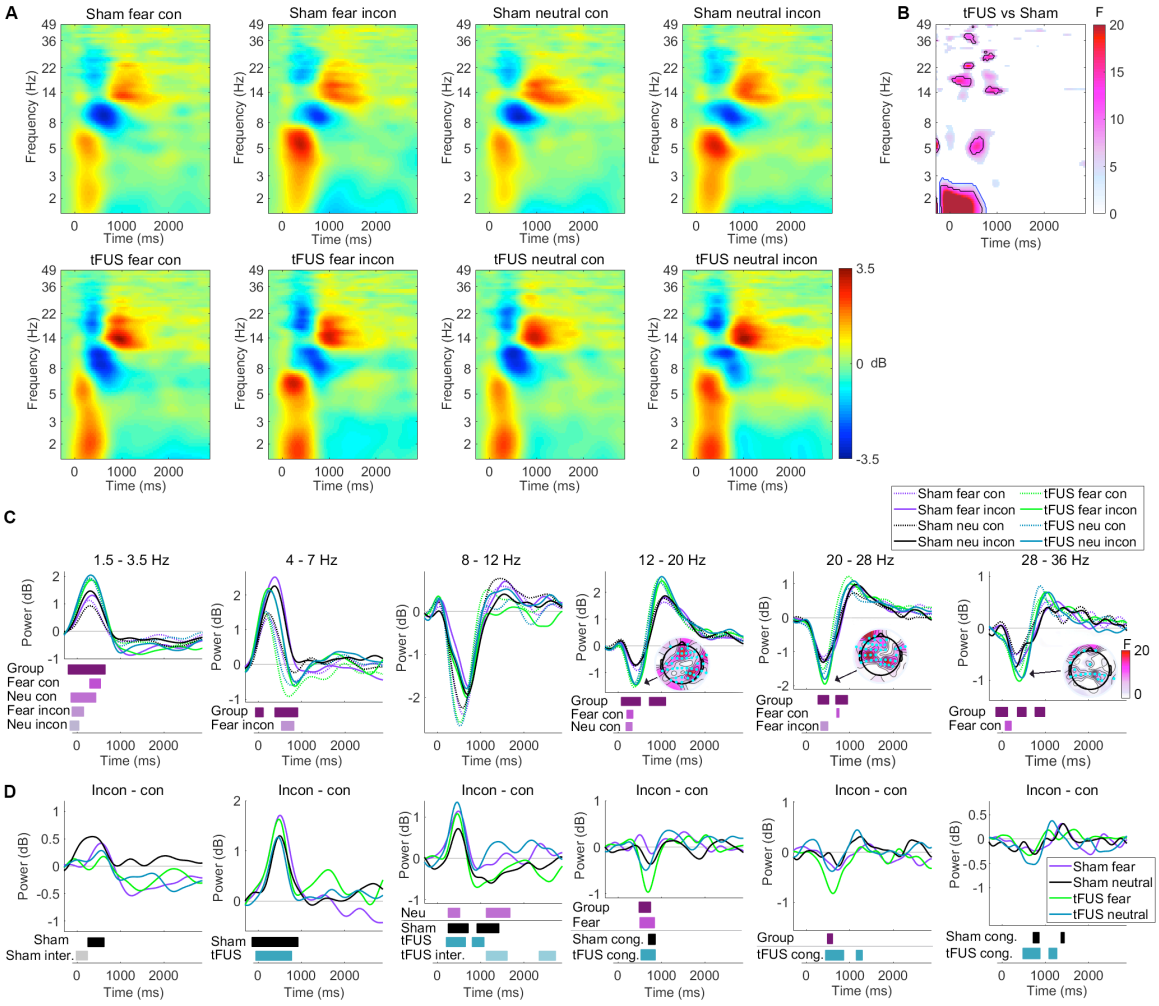

Figure 3. Frontocentral event-related spectral perturbation data
(**A**) ERSP data at FCz for each trial condition (dB power over baseline).
(**B**) Significant main effect of group (F-values, RM-ANOVA, only $p < 0.05$ shown; blue outline: cluster-based threshold outlined; black outline: FDR correction.
(**C**) Power over time in various frequency bands. Lower panel displays significant main effect of group (RM-ANOVA), as well as significant differences in each condition (permutation testing). Scalp maps display significant main effect of group at peak beta suppression (12-20 Hz, 40-360 ms; 20-28 Hz, 100-500 ms; 28-36 Hz, 240-500 ms. Electrodes significant after FDR correction marked with cyan dot.
(**D**) Subtraction of congruent from incongruent power to create incon-con contrast plots for each frequency band in C. Lower panel displays significant differences across groups, as well as main effect of congruency for each group (cong., RM-ANVOA), and congruency × emotion interaction (interaction). **Related to Figure S3 and Figure S4.**

Frontal event-related spectral perturbation data showed earlier and larger beta response in tFUS group

Comparing across groups with RM-ANVOA at frontal electrodes (pooled AF3, AFz, and AF4), it is clear that the tFUS group exhibited both an earlier onset and larger magnitude initial event-locked beta suppression and subsequent beta activation (Figure 4). Permutation testing performed across groups in the beta band (12 – 20 Hz) confirms that there were significant differences across groups at the initial beta suppression in the fear congruent, neutral incongruent, and fear incongruent. At the beta peak activation (peak ~1000 ms) there are significant differences across groups in the fear and neutral congruent, as well as neutral incongruent condition.

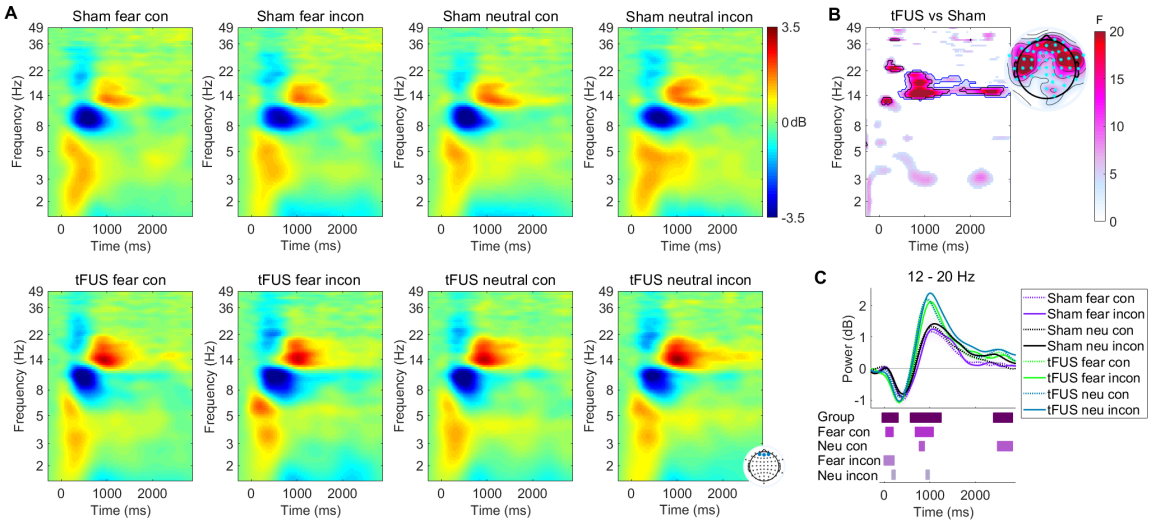

Figure 4. Earlier and larger beta response in tFUS Frontal time-frequency data
(**A**) ERSP data at frontal electrodes (AF3, AFz, AF4) for each condition (Sham top row, tFUS bottom row).
(**B**) Significant main effect of group (RM-ANOVA, $p < 0.05$). Cluster-based threshold outlined in blue, FDR correction in black. Scalp map to the right plots the significance across groups in the low beta range (12-20 Hz, 800-1000 ms); electrodes significant after FDR correction marked with a cyan dot.
(**C**) Power over time in the low beta band (12-20 Hz). Significant differences across groups for each condition, as well as the main effect of (Group, RM-ANOVA), are displayed in lower panel.

Error-related potential

Response-locked ERP data was compared across groups with permutation testing. On error trials, the tFUS group exhibited a larger error-related negativity (40 ms, ERN) at frontal electrodes (Figure 5A inset), and the error – correct potential at frontocentral electrodes (Figure 5B). Comparing each time point of error-locked response at FCz, there was a faster recovery from the ERN peak to the following positive peak in the tFUS group compared with Sham group (Figure 5A). There was also a difference across groups in error (-400 - -50 ms before response) and correct responses 600-300 ms prior to and at the time of response.

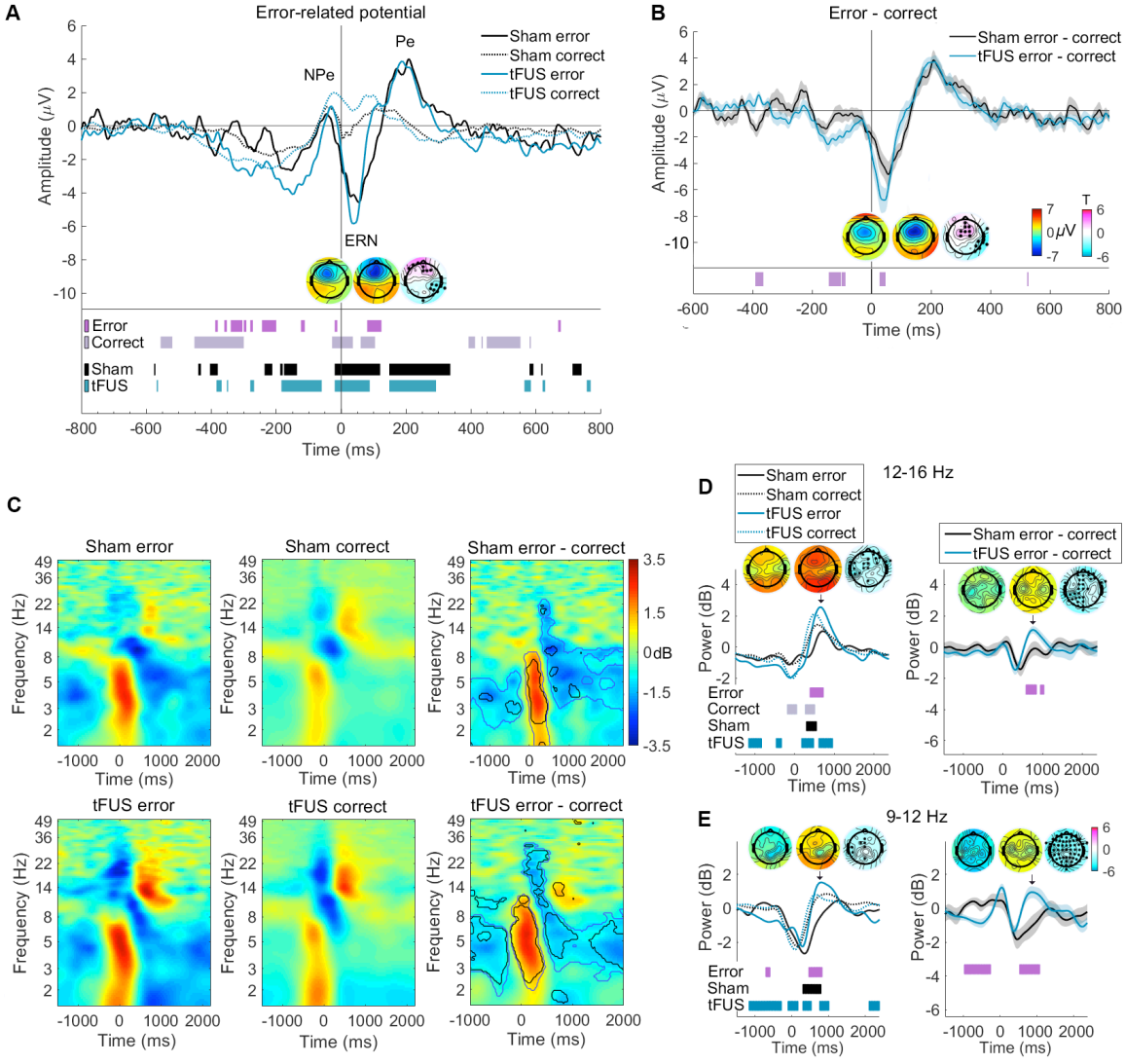

Figure 5. Error Response
(**A**) Response-locked error related potentials for correct and erroneous responses (response, 0 ms) at FCz. Scalp potentials for ERN peak displayed (40 ms; left: Sham, middle: tFUS, right: map of T values from permutation testing with significant electrodes labeled with a black dot, scales displayed in B. Lower panel displays significant differences across groups (error, correct), as well as error vs. correct within groups (Sham, tFUS) (permutation testing $p < 0.05$).
(B) Subtraction of correct from erroneous response-locked potentials in A. Scalp maps displayed error – correct ERN negative peak at 40 ms as in A.
(**C**) ERSP for error (left), correct (middle), and error – correct contrast (right) (dB power over baseline). On error – correct plots, significant differences between correct and error responses are outlined (blue: $p < 0.05$ cluster-based threshold, black: FDR correction).
(**D**) Power in the low-beta band (12 – 16 Hz) for error and correct trials (left, statistics displayed below as in A and error – correct contrast power (right, statics represent permutation testing across groups for error-correct contrast, $p < 0.05$). Scalp maps of post-error low-beta peak power displayed above plot correspond to time point indicated by the arrow, power scale same as that in B for Sham and tFUS scalp maps, scale for t-map (right-most scalp map) displayed in D.
(**E**) Power in the alpha band (12 – 16Hz) for error and correct trials (left) and error – correct contrast power (right). Statistics displayed as in C.

Error related spectral perturbation

Comparing ERSP data across groups at FCz for correct and error responses, both groups exhibit a much larger theta response for error than correct trials (Figure 5B), yet only the tFUS group exhibited a larger response for error than correct trials in the alpha and low beta range (Figure 5B, 5C and 5D). Comparing error – correct contrast power (Figure 5C and 5D), the tFUS group exhibited differences with the Sham group post-response across the whole scalp in the alpha range (9 – 12 Hz), and at frontal, left parietal, and midline electrodes in the low-beta range (12-16 Hz). Examining error and correct responses, it is clear that both groups exhibit a suppression of alpha at the time of response, followed by an alpha recovery (Figure 5D). While there was no difference across groups on correct responses, the tFUS group exhibited significantly higher reactivation of alpha than Sham in frontocentral electrodes. During the post-error recovery of alpha power, the tFUS group showed significantly higher power in error than correct trials, and at the post-recovery peak, higher

power than baseline. Additionally, prior to an erroneous response, the Sham group does not show any differences in alpha power between error and correct trials, but the tFUS group showed significantly less alpha activity on trials where errors were committed, and significantly higher alpha activity at the time of error compared to correct trials (0 ms). There was also a significant group difference in error-correct contrast power beginning 1000 ms prior to response.

In the low-beta range, both groups exhibit and post-response beta activation, yet in front-central electrodes, this activation is significantly greater in the tFUS group than Sham on both correct and error responses (Figure 5C). Additionally, the tFUS group exhibited significantly higher low-beta activation on error than correct response, and visa-versa in the Sham group; with a significant difference across groups in error-correct contrast power at this time. The tFUS group also exhibited significantly lower low-beta activity on error compared with correct trials prior to responding, while no differences were observed in the Sham group.

Heart-rate metrics

To access the effect of emotional face distractors on physiologic response in the case of Sham vs. tFUS stimulation to the aIns/fO, heart-rate metrics were recorded during the final three minutes of the baseline flanker trials (no faces, both groups received sham stimulation), and first three minutes of main trials (faces presented as distractors behind flanker task, and tFUS group received active stimulation on each trial, while the Sham group received sham). Several metrics of heart rate variability (HRV) were calculated and compared (see Methods). Data was analyzed with two-factor, mixed-measures RM-ANOVA ([2 groups (sham, tFUS) × 2 time points (baseline, faces with stimulation)] (Figure 6, Table S5).

The results showed a significant group × time interaction in the standard deviation of the normal-to-normal heartbeat (SDNN) [$F_{SDNN}(1,25) = 5.86$, $p = 0.023$, $\eta_p^2 = 0.19$] and SD2 (long-term HRV, see Methods) [$F_{SD2}(1,25) = 5.87$, $p = 0.023$, $\eta_p^2 = 0.19$]. Post-hoc statics show that in the SDNN, the Sham group showed a significant decrease (-20 ± 4%, mean ± SEM) from baseline to onset of face distractors ($p = 0.001$), while no significant change was seen in the tFUS group (-2 ± 6 %, $p = 0.67$). Similarly, the Sham group showed a significant decrease in SD2 at the onset of faces (-22 ± 4%, $p = 0.001$), while the tFUS group does not (-2 ± 7%, $p = 0.71$). No other significant main effects of group, faces or interaction effects were found for heart rate (HR), mean beat-to-beat interval (RR), SD1 (short-term HRV), or SD1/SD2 ratio ($F \leq 3.42$, $p \geq 0.076$, Figure 6, Table S5). Unpaired t-test showed no significant differences at baseline (all $T \leq 1.62$, $p \geq 0.067$).

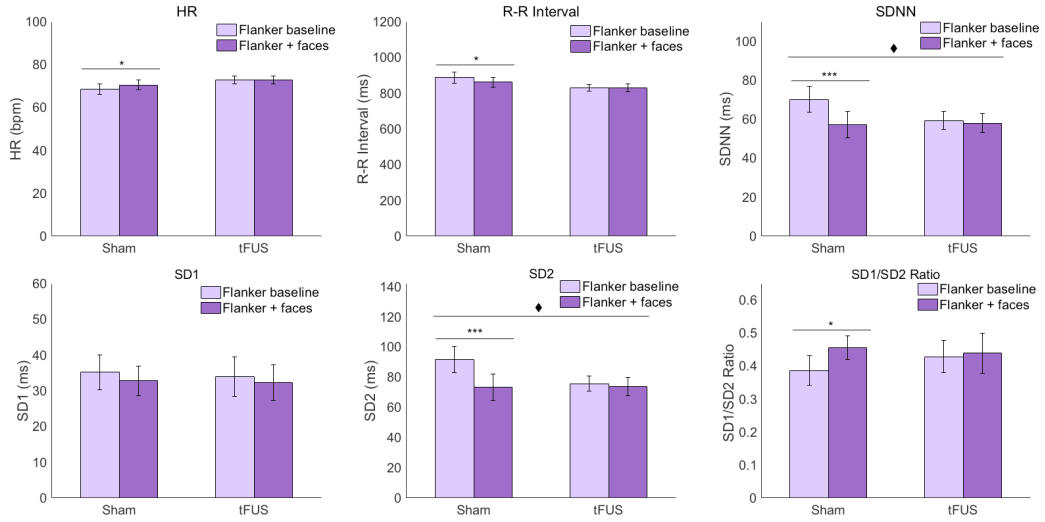

Figure 6. Heart rate and heart rate variability metrics
Comparison of HRV metrics collected in the final three minutes of subjects performing the baseline flanker trials (Baseline: simple flanker, no faces, both groups received sham) and first three minutes of the main trials (Flanker + faces: faces presented as distractors behind flanker arrows, tFUS group received active situation on each trial). Displayed statics represent the results of RM-ANOVA (♦ indicates significant group × time interaction, $p < 0.05$; post-hoc tests Bonferroni-corrected: *$p < 0.05$, **$p < 0.01$, ***$p < 0.001$). **Related to Table S5**.

Baseline-subtracted reaction time does not differ across groups

Mann-Whitney tests indicated no significant differences across groups in baseline-subtracted reaction time (RT) in any trial condition (all $U \geq 21.0$, $p \geq 0.51$ (Table 1).

Baseline-subtracted RT (ms)			Mann-Whitney		
Congruent	**Sham**	**tFUS**	***p***	**U**	**W**
Fear	31 ± 7	19 ± 7	0.57	22.0	32.0
Neutral	27 ± 7	21 ± 6	0.51	21.0	31.0
Oddball	39 ± 7	40 ± 8	0.97	27.0	37.0
Post	-6 ± 9	-7 ± 7	0.65	33.0	43.0
Incongruent					
Fear	7 ± 6	5 ± 6	0.57	22.0	32.0
Neutral	13 ± 6	-3 ± 6	0.51	21.0	31.0
Oddball	17 ± 13	9 ± 8	0.97	27.0	37.0
Post	-3 ± 6	-1 ± 5	0.65	33.0	43.0

Table 1. Baseline-subtracted reaction time does not differ across groups
Group-level statics are displayed on the right (Mann-Whitney U test). RT's displayed as median ± SEM (ms). **Related to Figure 7**, see also Table S6.

Within-group reaction time analysis

Although there was no difference across groups in baseline-subtracted RT, there were differences in within group comparison. Friedman's test showed that in the Sham group, there was a significant difference between RT's in the baseline, fear, neutral, oddball, and post-experiment trials in the congruent condition [$\chi^2(4) = 28.95$, $p < 0.001$] (Figure 7). Post-hoc analysis using Wilcox signed-rank tests showed that for congruent trials, oddball trials (Mdn = 353 ms) were significantly slower than baseline trials (Mdn = 334 ms, $p = 0.002$), and post-stimulation trials (Mdn = 306 ms, $p < 0.001$). In the tFUS group, there was also a significant difference between baseline, fear, neutral, oddball, and post-stimulation trials in congruent condition [$\chi^2(4) = 22.50$, $p < 0.001$]. Post-hoc tests show that in the congruent condition, fear (Mdn = 326ms, $p = 0.049$) and oddball trials (Mdn = 332ms, $p = 0.007$) were

significantly slower than baseline trials (Mdn = 305ms) and post-experiment trials (310 ms; fear: p = 0.015, oddball: p = 0.002). For incongruent trials, the Sham group exhibited a significant differences between conditions [$\chi^2(4) = 10.94$, $p = 0.027$, all post-hocs $p > 0.14$ after Bonferroni-correction], but the tFUS group does not [$\chi^2(4) = 0.91$, $p = 0.82$].

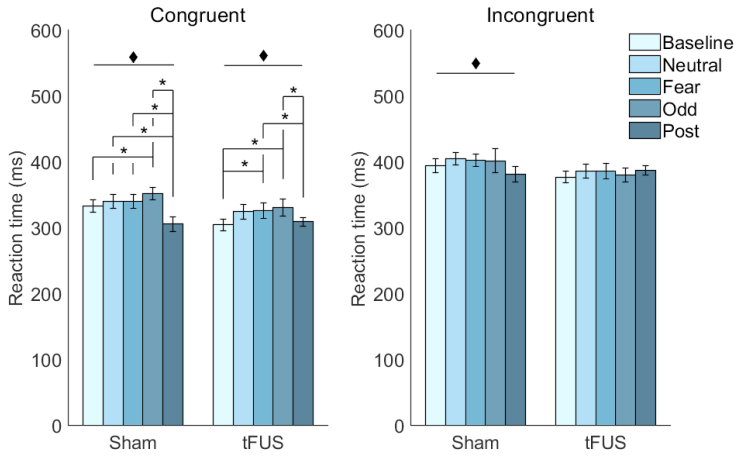

Figure 7. Within-group RT analysis
Median RTs for each trial condition (baseline: simple flanker, no faces, no stimulation), neutral, fear and oddball faces with stimulation, and post-experiment trials: identical to baseline). RTs displayed by group for congruent trials on the left, and incongruent trials on the right. (♦ indicates significant difference across conditions, Friedman's non-parametric test; * $p < 0.05$, Bonferroni-correct post-hoc tests). See also Figure 8, Figure 9.

Conflict adaption: congruency effect in the RT is reduced by face presentation in the Sham but not in the tFUS group on trials following incongruent trials

To assess conflict adaption and its interaction with emotional face distractors and tFUS to the aIns/fO, trials were separated based on congruency of the previous trials (congruent, incongruent). Congruency effect in RT was then calculated by subtracting median congruent from incongruent RT's. There were no differences between groups (Mann-Whitney U test, all $U \geq 82.0$, $p \geq 0.48$).

Additionally, baseline, neutral, fear, and post-stimulation RT's were compared within group (Figure 8). Similar to RTs, for trials following congruent trials, both the Sham group

[$\chi^2(3) = 19.58, p < 0.001$] and the tFUS group [$\chi^2(3) = 11.40, p = 0.010$] exhibited a significant difference across conditions. Post-hoc tests show that in the Sham group, neutral congruency effect (Mdn = 65 ms) was significantly lower than baseline (Mdn = 88 ms, p = 0.016) and post-stimulation trials (Mdn = 99 ms, p = 0.002), while fear (Mdn = 60 ms) was significantly lower than post trials (p = 0.010). In the tFUS group, fear congruency effect (Mdn = 62 ms) was significantly less than post (Mdn = 80 ms, p = 0.032). However for trials following incongruent trials, only in the Sham group was there a significant difference between conditions [Sham: $\chi^2(3) = 13.10, p = 0.004$; tFUS: $\chi^2(3) = 5.57, p = 0.13$]. Post-hoc tests show that in the Sham group, the congruency effect for baseline trials (Mdn = 78) was significantly greater than fear trials (Mdn = 60 ms, p = 0.016) and neutral trials (Mdn = 61 ms, p = 0.041).

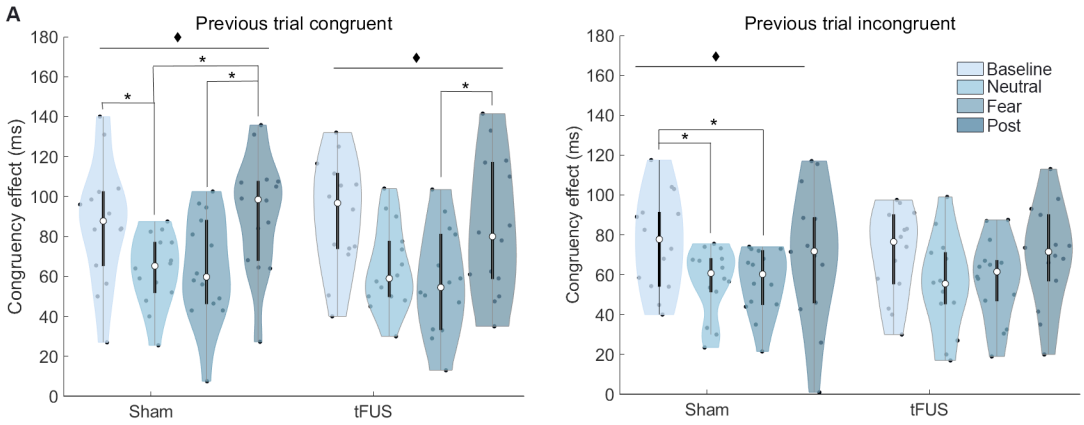

Figure 8. Conflict adaption: congruency effect in reaction time separated by previous trial congruency face trial conditions compared within group
Violin plots display congruency effect by group (median incongruent RT minus congruent RT) for trials in which the previous trial was congruent (left plot) or incongruent (right plot). Trial face types (baseline, neutral, fear, post-stimulation) are compared within group. White dots indicate median, and thick dark-grey bars indicate first and thirds quartiles of the data. (♦ indicates significant difference across conditions, Friedman's non-parametric test; * p < 0.05, Bonferroni-corrected post-hoc tests). See also Figure 7.

Response accuracy does not differ across groups

Mann-Whitney tests indicated no significant differences across groups in any trial condition (all $U \geq 79.0$, $p \geq 0.33$ (Table S6).

Post-error slowing

Mann-Whitney test indicate that in post-error fear congruent trials, RT is significantly slower in the Sham (Mdn = 390) compared with tFUS (Mdn 345 ms, $U = 38.1$, $p = 0.009$, Figure S6). No other conditions were significant across group (all $p > 0.18$). This result was supported by within group testing with Wilcox signed-rank tests which indicated that on post-error congruent trials, median-subtracted RT was slower on neutral (Mdn = 28 ms) than fear (Mdn = 5 ms, $Z = 86$, $p = 0.035$) trials (Figure S7). No other significant within group effects were found ($Z < 36$, $p > 0.18$).

Mood survey: PANAS

For positive PANAS scores mixed-measures, two-way RM-ANOVA ([2 groups (sham, tFUS) × 2 time points (baseline, immediately following experiment completion)] indicated a significant main effect of time [$F_{PANAS}(1,25) = 21.66$, $p < 0.001$, $\eta_p^2 = 0.46$], with positive scores being higher at baseline (mean = 31.0), then immediately following experiment completion (mean = 25.3) (Table S7). Analyzing individual PANAS metrics reveals that this effect is due to interest and motivation, there was a significant decrease in the following categories: 'interested', 'excited', 'strong', 'enthusiastic', and 'attentive', but not in 'proud', 'alert', 'inspired', 'determined', or 'active'. There was no main effect of group ($F_{PANAS}(1,25) =$

0.17, p=0.69, $\eta_p^2 = 0.01$) nor a time × group interaction effect [$F_{PANAS}(1,25) = 0.01$, p =0.95, $\eta_p^2 = 0.00$].

For negative PANAS scores, there was no effect of time [$F_{PANAS}(1,25) = 2.60$, p=0.12, $\eta_p^2 = 0.09$] or main effect of group [$F_{PANAS}(1,25) = 0.16$, p=0.69, $\eta_p^2 = 0.01$], nor was there a significant time × group interaction effect [$F_{PANAS}(1,25) = 4.20$, p =0.051, $\eta_p^2 = 0.14$].

DISCUSSION

The aim of this study was to investigate the feasibility of modulating attentional networks by stimulating a single brain area (the right aIns/fO) with tFUS and to assess the effects on conflict and emotional distractor processing. EEG, HRV, behavioral responses, and mood were assessed. It was hypothesized that since the aIns/fO plays a substantial role in executive control and emotional distraction (Kanske et al., 2011), and has broad structural and functional connections to both executive and autonomic functions, modulating the region may have broader network-level effects on face distractor processing. Indeed, a pronounced response in early ERP components was observed, as well as larger delta and beta activity, and modulation of theta. Differences were also seen in the task-locked alpha and beta bands, as well as in error responses and post-error RTs. Additionally, HRV decreased in response to emotional face distractors in Sham; however, this was not the case for subjects who received tFUS to the aIns/fO.

Enhancement of early ERP components and heightened responses to fearful faces

Early ERP components D-N1 and T-N1 (frontocentral negativity, parietal positivity) are significantly larger at frontocentral and right parietal electrodes in subjects receiving tFUS to

the right aIns/fO, compared with subjects receiving sham. Additionally D-N1 has an earlier onset in the tFUS group. Also, D-P1, frontal positivity, was of greater amplitude in fear compared with neutral trials consistent as with previous studies (Carlson and Reinke, 2010; Eimer, 2000; Righart and de Gelder, 2006), an effect that is notably larger in the tFUS group, especially on incongruent flanker trials.

These early ERP components are associated with perception and exogenous attention selection (Carretié, 2014), emotional processing (Smith et al., 2003), and emotional distraction (Bretherton et al., 2017; Neumann et al., 2011), and have larger amplitudes in fear-sensitive individuals in response to emotional fear arousal (Dennis and Chen, 2007). Interestingly, these ERP effects are not simply modulated through dopaminergic attention networks, as they are not affected by methamphetamine (Bensmann et al., 2018).

Fear face processing is thought to be mediated through involvement of the insula, amygdala, anterior cingulate, and visual cortex. The insula is involved in conscious but not unconscious fear perception while the amygdala is active in both (Critchley et al., 2002a). Insula activity is specifically related to anxiety response, is hyper-reactive to fear faces in social anxiety disorder, and shows reduced connectivity to the prefrontal regions involved in cognitive control (Klumpp et al., 2012). Early frontal positive potentials have been shown to decrease in attentional fatigue (Boksem et al., 2005) and increase with mindfulness meditation training (Moore et al., 2012), which is known to involve in the insula (Tang et al., 2015). It may be that a pronounced frontocentral fear potential in this study resulted from tFUS affecting the insula's regulation of medial prefrontal areas.

At later ERP amplitudes, there was an earlier onset of P3 in congruent neutral and fear trials, and a difference in LPs in incongruent trials, perhaps due to effects related to saliency, in which the aIns/fO is involved (Cuthbert et al., 2000).

Time frequency response showed heightened delta and beta response in aIns/fO tFUS group

In target-locked ERSP time frequency data, the tFUS group showed larger frontocentral delta activity in all conditions and a theta peak that is shorter in duration than the Sham group in the fear incongruent condition. The tFUS group also showed significantly larger frontocentral and parietal beta suppression as well as larger post-suppression beta activation. This effect is especially pronounced in frontal electrodes. Additionally, the frontocentral theta peak was shorter in duration in the aIns/fO tFUS group in the fear incongruent condition. Yet, no differences in congruency effect (incon – con contrast power) were seen in the peak theta range, however there was a significant differences between groups in the lower beta range, the tFUS group showed a larger and longer beta suppression in the fear incongruent condition.

It has been previously demonstrated that larger central delta is distinct from theta contributions, and associated with larger P3 and LP ERP components (Harper et al., 2014, Gilmore, 2010 #6905), which is consistent the findings presented in this study. Task-related delta is related to decision-making, saliency, and produced in the nucleus accumbens during reward (Bernat et al., 2012; Grace, 1995; Knyazev, 2007). Intracortical recordings in the human insular cortex demonstrate that beta amplitude is modulated by the likelihood of performance feedback (Billeke et al., 2020), and delta phase modulated beta power encodes feedback valance. Beta functions to commutate feedback information to the medial prefrontal cortex from the insula. Given this, differences in delta and beta could very likely be mediated through modulation of the aIns/fO with tFUS.

On error responses, the tFUS group showed a larger amplitude and shorter duration frontal/ frontocentral ERN. In response-locked time frequency data, the tFUS group

showed differences compared to Sham in alpha and low beta but not theta. On error trials the tFUS group exhibited an earlier and larger alpha recovery following the response-locked alpha suppression. Error – correct alpha power in this time range is greater in the tFUS over almost all EEG electrodes. The tFUS groups also exhibited more alpha suppression prior to the error as compared with correct trials. Additionally, there was a larger amplitude frontocentral low beta response in tFUS than Sham on both erroneous and correct responses, but was larger on error trials. There was also a group difference in frontal and parietal electrodes for heightened beta in post-error responses in error - correct contrast power.

The ERN is related to cognitive control, attention, and perhaps experience, but not necessarily valence, as it is higher in obsessive compulsive disorder and state worry (Hajcak et al., 2003), but also in meditators (Teper and Inzlicht, 2013). Stronger error-related suppression of alpha as well as parieto-occipital-frontal synchronization is associated with concentration. Attentional lapses have been shown to result in frontal theta as well as posterior alpha suppression, suggesting differential performance monitoring mechanisms. On errors, alpha in parietal electrodes have been linked to phase synchrony with right fronto-inferior electrodes (van Driel et al., 2012). EEG-fMRI research which links the aIns/fO to error processing (Iannaccone et al., 2015). Additionally, it has been suggested that post-error beta in central EEG electrodes can act as a marker for decision making and post-error adjustments (Fischer et al., 2018). Consistent with the beta differences described previously in target-locked ERSP data, this presents a compelling case for successful modulation of performance monitoring primarily through modulation of delta and beta, but also error-related alpha.

Heart rate variability does not increase in response to faces in tFUS group

In addition to electrophysiology, physiological heart rate metrics were also compared across groups. The right insula is known to be involved in cardiac (Abboud et al., 2006) and autonomic (specifically parasympathetic) regulation (de Morree et al., 2016), and has direct neural projections to the amygdala and autonomic regulatory nucleoli of the dorsal medulla (Kapp et al., 1985). HRV provides well-studied metrics of autonomic nervous system activity, known to be sensitive to, anxiety (Gaebler et al., 2013; Thayer et al., 2012), and be involved with distraction by fearful faces (Park et al., 2013; Park et al., 2014). The SDNN (standard deviation of RR intervals) is known to decrease with increased workload (Fallahi et al., 2016). SDNN is influenced by both the sympathetic but largely parasympathetic activity via the rise and fall of the heart rate with slow relaxed breathing (Shaffer et al., 2014). This study showed that in the Sham condition, there was indeed a significant decrease in SDNN with the onset of the face distractors yet no change was seen in the tFUS group. SDNN is known to be lower in patients with right insula stroke (Colivicchi et al., 2004).

Analyzing metrics from the Poincaré plot of R-R intervals (RR_{i+1}, RR_i; see methods), the SD1 (identical to the RMSSD (Ciccone et al., 2017)) which is vagally modulated and though of as short term HRV(Spangler and McGinley, 2020), showed no changes across groups or time. While as with the SDNN, the SD2 significantly decreased in the Sham group at the onset of the face distractors, but no change was seen in the tFUS group. The SD2 is thought to be a long term HRV moving average, but also influenced by short term HRV. SD2 is correlated with baroreflex sensitivity (Guzik et al., 2005), and animal studies have shown that the insula modulates cardiac baroreflex through parasympathetic modulation (Saleh and Connell, 1998). The above findings suggest that tFUS modulated physiology

through right insula, and the physiological suppression of HRV seen in the Sham subjects in response to fearful distractors face is blocked by tFUS to the aIns/fO.

Behavioral metrics

No differences in baseline-subtracted RT or accuracy were observed across groups. However, the Sham group showed a significant RT slow-down with the addition of the fear and neutral face distractors in both congruent and incongruent condition as expected from the literature (Bretherton et al., 2017), whereas this was only the case in the tFUS group in the congruent condition but no significant slowdown from baseline was seen in the tFUS group on incongruent trials.

Similar to reaction time, congruency effect (incon - con RT) showed a significant reduction in the presence of face distractors compared to baseline and post stimulation trials in both group when following a congruent trials. This result was consistent with previous work that demonstrates RT congruency effect decreases with emotionally salient negative distractors (Meng et al., 2019). However on trials following incongruent trials, this was only true for the Sham group. The tFUS group showed no difference in congruency effect with the addition of the faces in the incongruent condition, suggesting that tFUS to the aIns/fO alters salient emotional distraction.

Post-error slowing

Post-error fear congruent trials show a slower RT in the Sham than tFUS group. Additionally, the tFUS group showed significantly less post-error slowing on fear than neutral congruent trials, demonstrating modulation of post-error task processing.

Conclusions

The aIns/fO is involved emotional processing, but also executive control through monitoring task performance evaluation (Eckert et al., 2009) and set attentional maintenance (Dosenbach et al., 2008), perhaps through integrating saliency. It has been proposed that the insula functions in performance feedback through enhanced awareness of autonomic responses resulting from error (Klein et al., 2007). This study provides evidence that modulation of the aIns/fO with tFUS reduces parasympathetic fear response seen in HRV, and functionally reduces emotional distraction interference on performance, as well as response slowing after errors on fear trials. Additionally, ERP differences were measured across groups in components associated with saliency, emotion, and congruency. These effects are likely meditated here through modulation of event-locked delta and beta with tFUS. These frequencies are known to be involved in modulation of physiologic response though interaction with the amygdala, as well as distractor processes in through insular-medial frontal regulation during feedback. Overall this study demonstrates that tFUS along with neuronavigation can be used to target specific anatomical and functional areas to induce larger network modulation and effect function and processing.

METHODS

Participants

Twenty-eight healthy, right-handed adult volunteers with no previous history of neurologic conditions and no current medication use were recruited for this study. All participants had no hearing or uncorrected visual impairments, migraines, or medication use, as well as no contraindications for MRI. Subjects were randomly divided into two groups: one to receive active tFUS to the aIns/fO (6 female, 8 male, mean age 24.1) and the other to receive sham

situation (3 female, 11 male, mean age 22.4). Participants were blinded to the mode of stimulation they received; both groups were told they received active stimulation. One subject was from each group was removed from HRV analysis due to poor recording. One subject in the insula group was removed from mood assessment due to survey incompletion.

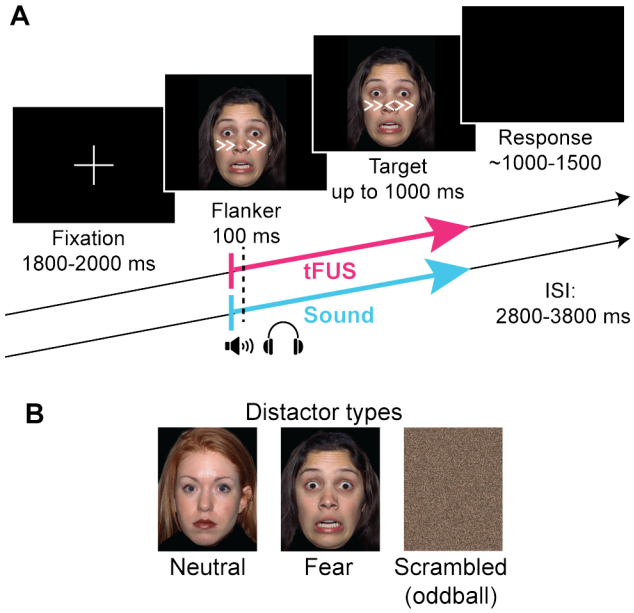

Figure 9. Behavioral task protocol, modified flanker task
(**A**) Each trial began with a fixation cross after which the flanker arrows appeared overlaid on a face image (vertical dotted line), and were displayed for 100 ms. Sham sound and tFUS stimulation began 28 ms prior to the face and distractor arrow presentation, and lasted 500ms. The target arrow appeared on the screen until the subject's response, after which a blank screen appeared. The presentation time of the blank screen was adjusted such that the ISI of tFUS stimulation was never to be less than 2800 ms. The example trial displayed is an incongruent flanker trial, but congruent and incongruent trials were presented with equal probability.
(**B**) Three face types were used as distractor images: neutral expressions, fearful expressions, and scrambled face images. Scrambled faces were presented as an oddball and represented only 6% of trials. **Related to Figure 10.**

Behavioral task protocol: modified flanker paradigm

Subjects performed a modified version of the Eriksen Flaker task (Eriksen and Eriksen, 1974). The experiment began with 32 practice trials, followed by 100 baseline trials (50 congruent, 50 incongruent) of a simple flanker task with white distractor arrows appearing

on a black background for 100 ms, followed by the target arrow. The distractor arrows were either congruent (pointing in the same direction as the middle target arrow: > > > > >) or incongruent (pointing in opposite direction of the target: > > < > >). Subjects were instructed to respond to the direction of the target arrow via button press with their right hand using the index finger for left and the middle for right. Participants were instructed to respond as quickly as possible without sacrificing accuracy.

All main experimental trials utilized the protocol outlined in Figure 9. Trials began with a fixation cross presented for 1800 - 2500 ms. Sham sound began in both groups 28 ms prior to the appearance of the distractor arrows, and the tFUS stimulation (described below) began at the same time. Both the sound and the stimulation had a 500 ms duration. Distractor arrows then appeared overlaid on one of three face types: a face exhibiting a neutral expression, one exhibiting a fearful expression, or a scrambled face (colored static). The fearful and neutral faces appeared with equal frequency, will the scrambled trials occurred only 6% as an oddball. A total of 420 trials were presented in four blocks. Trials were pseudo-randomized with equal number of each trial type, and arrow direction. Trials were controlled such that not more than three consecutive correct responses were pointing in the same direction. Face images were used from both the NimStim (Tottenham et al., 2009) and MaxPlank (young faces only) (Ebner et al., 2010) datasets, were edited to have a black background, masked to include just the face, and resized where necessary to ensure consistency in face size as well as position of nose and eyes. Following the completion of the main trials, subjects completed another 100 trials of post-experiment simple flanker trails (identical to the baseline, simple flanker with black background, no faces, both groups received sham stimulation).

Experimental setup

Trial order was pre-calculated and experimental presentation content was controlled via python and Psychopy (Peirce, 2007). Analogue photodiodes were used to detect the exact time of screen refresh and stimulus presentation (Figure 10A). This signal was digitized by a Cedrus StimTracker box (Cedrus Corporation) and was EEG system via parallel port connection along with information from the subjects' responses, recorded via a button box. tFUS stimulation was controlled via the experiment computer and the timing recorded via parallel-port connection on the EEG.

Sham

All subjects wore headphones for presentation of a low volume sound meant to emulate the sound of the tFUS pulses herd through bone conduction. The sound file was creating by combing a very high frequency tone with a square wave at the pulse repetition frequency. The sound was played simultaneously with the onset of the tFUS pulse. In both groups, the tFUS transducer was placed on the head (Figure 10B)

Stimulation planning and neuronavigation

T1 structural MRI scans were collected on all subjects receiving active tFUS for the purposes of neuronavigation. Images were collected in a Philips Ingenia 3T scanner with a 32-channel head coil, using a 3D MPRAGE sequence (TR = 2300 ms, TE = 4.5 ms, 1 x 1 x 1 mm3 voxels, field of view 240 x 256 mm^2, 180 sagittal slices).

All stimulation targets were planned prior to subject arrival. T1s were processed using Brainsuite by running the cortical extraction sequence and surface volume labeling procedure using the Destrieux atlas (Destrieux et al., 2010). Following this, a 3D mask was

created for both the white and gray matter of each subjects' right *pars opercularis* and anterior insula. These masks were then to assist in planning and visualization of tFUS targets using a Brainsight neuronavigation system (Rogue industries). First, an atlas was created to map the Montreal Neurologic Institute (MNI) coordinate system (Evans et al., 1994) onto each subject's brain by identifying the anterior and posterior commissure, and outer bounds of the cortex. The anatomical mask images were then overlaid on the subject's scan to facilitate anatomical identification in 2D and 3D (Figure 1).

Careful consideration was taken to plot a trajectory target in which the tFUS beam path would overlap with the *pars opercularis* (BA 44) of the rIFG and the tFUS focus would be primarily be within the frontal operculum and anterior insula (BA 13) (Figure 1, Table S1), while the transducer face would be normal to the surface of the scalp and the beam perpendicular. Significant anatomical variation exists in this region, and therefore individual anatomy, rather than MNI coordinates, was prioritized.

An infrared optical tracking system (Polars Vicra, NDI Medical) was used to register the subject's head and tFUS transducer to their MRI using Brainsuite. On the day of the experiment, following EEG setup (described below), glasses with an infrared tracker were placed on the subject in order to register their head in virtual space for neuronavigation. A custom-build housing was 3D-printed for the tFUS transducer to fixate the infrared tracker and to hold acoustically conductive silicone (Silicon Solutions) to couple the transducer to the scalp and adjust the penetration depth of the tFUS focus. Ultrasound conductive gel was liberally applied to the scalp and hair to avoid any air bubbles between the traducer face and the skin. Once the transducer was placed in the appropriate area and stimulation location recorded, the transducer was fixed in place with a lightweight, custom-sewn mesh cap to distribute the weight and avoid interference with EEG recording (Figure 10B). The glasses

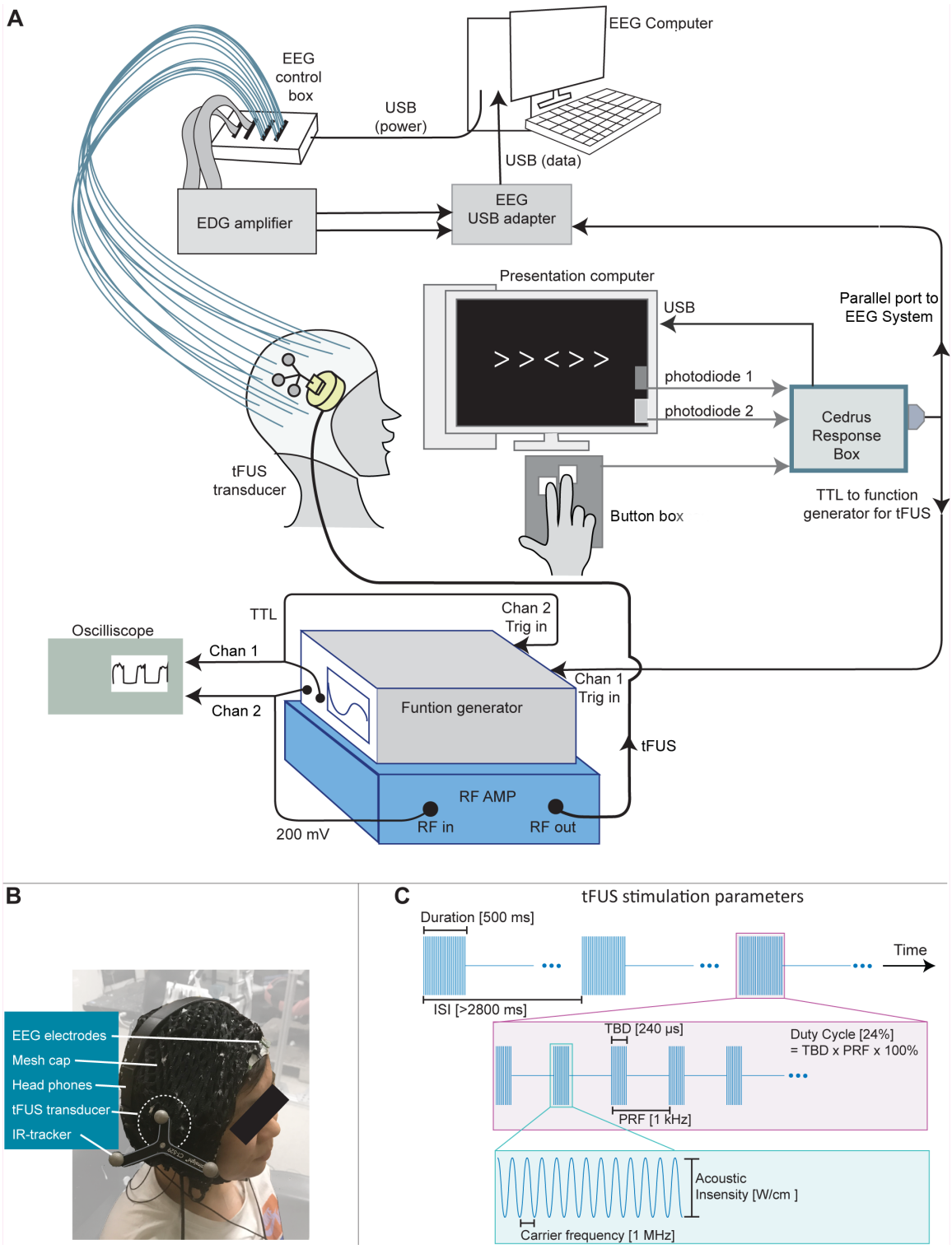

Figure 10. Experimental setup and tFUS parameters

(**A**) Experimental setup for stimulus presentation and recording. The photodiodes are analog sensors, digitized by the Cedrus response box. Participant responses were recorded via a button box and sent to EEG system via parallel port correction with the photodiode

information. Not pictured, headphones from experiment computer, subject tracker, Polaris camera and computer for neuronavigation.
(**B**) Task setup on a single subject. Glasses were used on the subject (not pictured), and the tFUS transducer with attached IR-tracker for neuronavigation. The transducer was held in place with a mesh cap over which the subject wore headphones.
(**C**) tFUS stimulation parameters. Stimulation was repeated at stimulation presentation for each trial in the tFUS group. Acronyms: inter-stimulus interval (ISI), tone burst duration (TBD), pulse repetition frequency (PRF). Abbreviations: Chan- Channel, RF Amp-radio frequency amplifier. See also Figure 1 and Figure 9.

were removed and the transducer remained fixed to the subject's head throughout the experiment. Across all subjects, a mean center coordinates of stimulation were recorded as: x = 35.4 ± 13, y = 13.5 ± 1.2, z = 1.4 ± 1.7 (mean ± SEM, Figure 1, Table S1).

tFUS stimulation parameters

The ultrasound transducer was driven by a 40 W linear RF amplifier (Legon et al., 2012b). The inter-stimulus interval (ISI) between tFUS pulses never exceeded 2800 ms (Figure 9 and Figure 10). Each stimulus period (duration) was 500ms, and consisted of a tone burst duration (TBD) of 24 μs, a pulse repetition frequency (PRF) or 1 kHz, making a duty cycle of 24% (Figure 10C). A broadband, single element transducer (Blatek, Inc.) with carrier frequency of 1 MHz was used to optimize transduction across the skull (Tufail et al., 2010). The transducer had a fixed focal depth of 70 mm, focal depth was adjusted by using various width silicone spacers such that actual focus depth ranged from 40 - 50 mm from the surface of the scalp to the center point of the beam focus. The focal beam profile has a lateral spatial resolution of 4.9 mm^2 and axial spatial resolution of 18 mm^2, identical to that described previously (Legon et al., 2014a; Mueller et al., 2014). Water tank measurements indicated a max pressure of 1.0 MPa and spatial peak pulse average intensity (I_{sppa}) of 20.4 W/cm^2 at the focus, well below the FDA safety limit for imaging fetal tissue, with the spatial-peak pulse-

average intensity (I_{sppa}) ≤ 190 W/cm^2 (Nyborg, 2000), and does not account for power attenuation from the skull.

EEG recording

Electroencephalography (EEG) data was recorded using a 64-channel ActiCap system (BrainVision) with the standard 10-20 electrode layout. Electrode F8 was removed for placement of the ultrasound transducer. Data was recorded using a sampling rate of 5 kHz, resolution of 0.1 V, and band-pass filter of 0.1-100 Hz. The ground was placed at FPz and reference at the left mastoid. Each subject's electrode locations were recorded using a Captrack camera system (BrainVision), with fiducials on the left and right tragus, and nasion.

EEG processing

Custom scripts were used to process EEG data in MATLAB R2017b (MathWorks) with the utilization of EEGLAB v14.1.1 (Delorme and Makeig, 2004). Raw EEG data was down-sampled to 250 Hz and high-pass filtered applied at 1 Hz, and notch filtered at 60Hz. Visual inspection was used to remove glaring artifacts and bad channel. Additionally any channels that exhibited artifacts for more than 25% of the recording session or with absolute temporal standard deviation greater than five were removed. Interpolation was performed over all removed channels. Data was then re-referenced to the scalp average using individually-recorded electrode locations. Blink, eye-movement, and other glaring artifacts were removed with Independent Components Analysis; on average 3.9 ± 0.4 components were removed for each subject. Epoching of the data was then performed around the distractor arrow presentation (target-locked). Trials with late responses or in which reaction

time deviated more than three standard deviations from the individual mean, were excluded from analysis.

Event-related potentials

A pre-stimulus baseline (200 ms) was subtracted to create event related potential (ERP) data. A linear subtraction of congruent from incongruent ERP data was performed to assess the incongruent-congruent difference potential (Figure 2B). Similarly neutral trial responses were subtracted from fearful ones to create a fear – neutral difference potential (Figure 2).

ERP data was compared across groups at each time point for each trial condition using nonparametric permutation to control for multiple comparisons problems. Statistical *p* values represent the proportion of 1,000 permutations of randomly shuffled data which produce a *t* value greater than that calculated by a standard two-tailed, unpaired *t*-test (Maris and Oostenveld, 2007) (statistical significance was considered at $p < 0.05$). Each trial condition, as well as each face type (fear, neutral) in incongruent – congruent contrast data, and each congruency condition (congruent, incongruent) in fear – neutral contrast data were compared across groups.

In addition, a two-way RM-ANOVA [2 congruency conditions (congruent, incongruent) × 2 face types (neutral, fear)] was used to compare within groups. Additionally for each individual, peak-to-peak amplitude and latency were identified for each the ERP complex, and compared across groups (Table S2 and S3). Additionally nonparametric Friedman's test was used to compare within groups (Table S4).

To analyze response-locked ERPs for correct and error responses, baseline-subtracted data was then time-locked to the response (button press). As with target-locked ERPs, each condition was compared across groups using permutation testing. Additionally,

error and correct responses were compared within group using permutation testing (paired rather than unpaired t-tests were used).

Time-frequency analysis: event-related spectral perturbation

Time-frequency analysis was performed by computing event-related spectral perturbation (ERSP) data using EEGLAB. Morlet wavelets were used with 3 cycles at the lowest frequency (1.5 Hz), and increasing linearly to 40 cycles at the highest frequency (50 Hz). A 500 ms pre-stimulus baseline was used, and all results are displayed as decibel power above baseline. Statistics were compared at each time and frequency data point. A cluster-based multiple comparisons correction was applied by determining clusters of contiguous significant pixels, *F* or *t* values in these clusters were then summed and only clusters greater than 2 standard deviations above the mean were retained. Additionally, false discovery rate (FDR) correction for multiple comparisons was also applied. Specific frequency bands and time windows were selected for display as scalp maps and/or power over time. Selection was based either on peak responses in the ERSP or the results of group level statistical testing.

Response-locked data was analyzed with mixed-measures, two-way RM-ANOVA [2 groups × 4 trial conditions (fear congruent, fear incongruent, neutral congruent, neutral incongruent)] (Figure 3 and Figure 4). Similar to ERPs, permutation testing was used to compare all trial conditions across groups, and further quantified within group using RM-ANOVAs [2 congruency conditions (congruent, incongruent) × 2 face types (neutral, fear)] (Figure 3 and 4). Additionally, incongruent – congruent contrast power for each emotion condition (fear, neutral) were compared across groups using permutation testing. Oddball trials were also assessed in a similar way, with RM-ANOVA [2 congruency conditions × trial frequency conditions (neutral, oddball)] compared within groups (Figure S2). In addition, to

disambiguate interaction effects, the results of permutation testing within group across congruent and incongruent conditions are presented for neutral and oddball trials (Figure S2B).

Response-locked correct and error ERSP data were compared both across and within groups using permutation testing (Figure 5). Incongruent – congruent contrast power (linear subtraction of correct from error response) was also compared across groups.

Heart-rate metrics

A single EEG electrode was removed for placement of the tFUS transducer on the head, and was used to record heart-rate (HR) data by placing it below the left clavicle. Raw HR data was first manually processed in MATLAB to ensure correct identification of heart beats peaks. Following this, all HR metrics were calculated using HRVTool (Vollmer, 2015). In add ion to HR, several heart rate variability (HRV) metrics were calculated: R-R interval (time between heart beats), standard deviation of the normal-to-normal heartbeat (SDNN, equation (1)), short term HRV (SD1), long term HRV (SD2), SD1/SD2 ratio, power in the The calculation of SD1 and SD2, which are non-linear measures, can be derived by plotting a Poincaré plot (RR_n, RR_{n+1}) (Karmakar et al., 2009; Vollmer, 2015). SD1 is based on successive differences, and calculated as the standard deviation perpendicular to the identity line, $RR_n = - RR_{n+1}$ (equation (2)). SD2 is the standard deviation along the identity line, $RR_n = RR_{n+1}$ (equation (3)), since it is derived from summation of successive RR intervals it is more representative of long-term HRV. HR and HRV metric were compared with a mixed-measures RM–ANOVA [2 groups (Sham, tFUS) × 2 face/stimulation conditions (baseline flanker, flanker with faces and tFUS stimulation)]. One subject in the Sham group was excluded from heart-rate metric analyses due to recording issues.

$$SDNN = \sqrt{\frac{1}{n-1}\sum_{i=1}^{n}(RR_i - \overline{RR})^2} \quad (1)$$

$$SD1 = \sqrt{1/2} \cdot \sigma(RR_{i+1} - RR_i) \quad (2)$$

$$SD2 = \sqrt{1/2} \cdot \sigma(RR_{i+1} + RR_i) \quad (3)$$

PANAS mood ratings

To evaluate mood changes, subject were asked to complete the Positive Affect and Negative Affect Schedule (PANAS)(Watson et al., 1988) via REDCap. Mood scales were completed at baseline and immediately following experiment completion. PANAS ratings were summed to deduce positive and negative scores. Ratings for positive valence probes ('interested', 'excited', 'strong', 'enthusiastic', 'proud', 'alert', 'inspired', 'determined', 'attentive', 'active') were summed to create a PANAS positive score while negative valence probes ('depressed', 'upset', 'guilty', 'scared', 'hostile', 'irritable', 'ashamed', 'nervous,' 'afraid') were summed to create PANAS negative score. Scores were compared with a mixed-factor RM–ANOVA [2 groups × 2 time points (baseline, post-experiment)]. One subject in the insula group was excluded from PANAS metric analyses due to recording issues.

Behavioral responses

Main trial RT's were baseline-subtracted to removed any individual differences. Each subject' s median baseline RT for congruent and incongruent trials (simple flanker task on black background, both groups received sham stimulation) was used. Baseline congruent RT was subtracted from congruent trials (neutral, fear, and oddball), and likewise for incongruent. Groups were then compared using Mann-Whitney U test. Additionally, median

RT's were compared within group using Friedman's nonparametric test, post-hocs with Wilcoxon signed-ranks test.

To access conflict adaption, trials were separated by previous trial congruency (congruent, incongruent), and median congruent RT was subtracted from incongruent to calculated the congruency effect in the RT. These were then compared both across and within group.

Post-error slowing

To assess post-error slowing, RTs on fear and neutral trials following an error were compared with median RTs in both congruency conditions using Wilcox signed-rank tests. To assess post-error slowing across groups, median RT was subtracted from post-error RTs and groups were compared using Mann-Whitney U tests.

Data analysis and statistical methods

Only correct responses were considered for analysis unless indicated as an error response. Trials with late RTs, RTs that deviated more than three standard deviations from the individual mean or were greater than 900ms, were removed from analysis of behavioral and EEG data.

Statistical analysis was conducted using SPSS Statistics Software SPSS 26.0 (IBM Corporation, Armonk, NY) and EEGLAB v14.1.1. Both parametric (RM-ANOVA), and non-parametric analyze were employed were appropriate and indicated above (between groups: permutation testing, Mann-Whitney U test; within groups: Friedman's test and Wilcox signed-ranks tests). Threshold for statistical significance were set at $p < 0.05$. Bonferroni-correction was used for all post-hoc p-values. FDR correction for multiple

comparisons was applied were indicated. Additionally, a cluster-based multiple comparison correction was employed for time-frequency data in which clusters with cumulative F or T value score than 2 standard deviations from the mean were highlighted. When necessary normality was confirmed using Kolmogorov- Smirnov tests and Levene's test for homoscedasticity was used to examine all between group data variance (all p's > 0.05).

Supplemental materials

See Appendix C for supplemental materials.

CHAPTER 5

TRANSCRANIAL FOCUSED ULTRASOUND ENHANCES BEHAVIORAL AND NEWTORK MECHANISMS UNDERLYING RESPONSE INHIBITION IN HUMANS

ABSTRACT

To prevent erroneous actions, individuals must often inhibit prepared behavioral responses. The right inferior frontal gyrus (rIFG) and its connectivity patterns are prominently implicated as key to behavioral inhibition. However, previous studies have applied neurostimulation methods with low spatial resolution that impede simultaneous network modeling of neural activity. Therefore, direct evidence for inhibitory control in rIFG is lacking, while the accompanying network mechanisms remain unknown. We addressed this gap using a Stop Signal task and transcranial focused ultrasound (tFUS) to pars opercularis in rIFG. tFUS improved stopping performance by enhancing stopping speed. Electroencephalographic dynamic causal modeling indicated inhibition performance increased by tFUS modulating pars opercularis pyramidal neuron connectivity to subcortex. By combining tFUS and network modeling, our results provide causal evidence that response inhibition is implemented along two pathways originating from a direct rIFG to subcortical pathway and a parallel pathway that modulates pre-SMA inhibition onto subcortical nodes.

INTRODUCTION

Behavioral inhibition is necessary to suppress impending actions that become contextually inappropriate (Aron et al., 2014; Baddeley, 1996; Logan and Cowan, 1984). The control over inhibitory capacities is dramatically reduced in pathologies dominated by aberrant impulse control, e.g. ADHD (Bari and Robbins, 2013). The stop-signal task has been widely used as a

paradigm for probing inhibition (Logan and Cowan, 1984). This task involves cueing action execution (Go signal) on every trial. On a percentage of trials, individuals are cued (Stop signal) to attempt inhibiting responses at a delay after a Go. This task allows deriving the stop signal reaction time (SSRT), a latent measure of stopping speed.

The predominant conceptual framework implicates a right-lateralized prefrontal stopping circuit driving inhibition (Aron, Robbins, and Poldrack, 2014; Chambers et al., 2006), with an anatomical locus in the posterior portion of the right inferior frontal gyrus (rIFG), pars opercularis (Aron and Poldrack, 2006). It has been argued this area directly implement motor braking via projections to subcortical nodes (Aron et al., 2014). Supporting evidence is based on demonstrations that rIFG neural activity is larger in successful compared to failed stopping (Aron et al., 2006; Boehler et al., 2010; Li et al., 2006), and both inhibition and SSRTs being altered in individuals with rIFG lesions (Aron et al., 2003) and ADHD (Morein-Zamir et al., 2014). rIFG is considered a core node for response inhibition, nevertheless successful inhibition also engages a broader network that includes pre-supplementary motor area (pre-SMA; Duann et al., 2009), subthalamic nucleus (STN) and striatum (Aron et al., 2007; Mallet et al., 2016).

Although modulation of rIFG activity typically accompanies inhibitory control, several researchers have proposed rIFG's involvement is indirect (Duann et al., 2009; Sharp et al., 2010; Xu et al., 2017). This indirect role involves rIFG registering a stop-signal context, and signaling the context to pre-SMA, which has been argued to explicitly trigger inhibition (Duann et al., 2009; Sharp et al., 2010; Rae et al., 2015). At a network level, this hypothesis has gained support from fMRI connectivity in stop-signal studies wherein pre-SMA alone exhibited modulated connectivity with subcortical structures during successful inhibition (Duann et al., 2009; Rae et al., 2015). However, other connectivity studies have

implicated both rIFG and pre-SMA connectivity to STN and striatal pathways as predicting inhibition speed (Jahfari et al., 2011; Xu et al., 2017). Additionally, primate research implies that direct neural projections to the STN originate in both the rIFG and pre-SMA, with the STN acting as an integrator (Haynes and Haber, 2013). These dual-pathway models leave open the possibility that rIFG can directly trigger inhibition in parallel with pre-SMA (Aron et al., 2016).

In contrast to the above conclusions, an alternative framework posits that neither rIFG or pre-SMA directly implement inhibition, with inhibition emerging from attentional orienting and biased competition processes (Hampshire and Sharp, 2015; Chatham et al., 2012). This proposition is based on findings indicating sectors of rIFG are equivalently active during stop-signal and other putatively non-inhibitory tasks (Erika-Florence et al., 2014; Hampshire et al., 2010; Xu et al., 2017). For example, rIFG activity scales with stimulus probability (Shulman et al., 2009) and regularly during tasks requiring attentional re-orienting (Vossel et al., 2006; Levy and Wagner, 2011). The claim that attentional orienting drives response inhibition is supported primarily by demonstrating rIFG fMRI activity is equivalent during both stop-signal tasks and other tasks with no apparent inhibitory demands (Sharp et al., 2010). In this framework (reviewed in Hampshire and Sharp, 2015), inhibition could occur through rIFG top-down signals that bias attentional processing through increasing synaptic efficacy of sensory cortices (Hampsire, 2015; Feldman and Friston, 2010).

Given the prevalence of findings supporting either a direct or indirect role of rIFG in response inhibition, or the absence of behavioral inhibition processes altogether, delineating between alternative mechanisms has remained inconclusive. For example, an established way to control for attentional demands is comparing neural activity during a

stop-signal and putatively non-inhibitory tasks. However, a notable issue with this comparison is that other tasks may still induce unaccounted for cognitive processes or latent inhibitory demands not directly measurable in behavior (Aron et al., 2014). Given the ambiguity introduced by comparing tasks to parcellate neural activity underlying inhibitory versus other cognitive demands, direct approaches are needed to circumvent these issues.

Neurostimulation during inhibitory tasks offers a potential in-route to identify how rIFG, and particularly pars opercularis, is causally involved in motor braking, while detailing its role in the broader inhibition network. Respectively, several studies have applied transcranial magnetic (TMS; Cai et al., 2012; Obeso et al., 2013; Verbruggen et al., 2010) or direct current (Jacobson et al., 2011) stimulation during inhibition tasks. Some studies found offline TMS applied to either rIFG or pre-SMA impaired or improved inhibition performance (Chambers et al., 2006; Verbruggen et al., 2010), respectively. However, others have shown pre-SMA TMS can either improve inhibition with no effect on rIFG (Obeso, 2013). Limitations of previous human neurostimulation response inhibition studies include either lack of neural activity measurements or limited spatial accuracy (Opitz et al., 2013). For example, TMS applied to rIFG during inhibition tasks most likely engaged ventral premotor areas involved also in action switching (Buch et al., 2010). The implication is that, if rIFG is potentially involved in attentional orienting, inhibitory control, or both, these neurostimulation approaches likely elicited broad effects on these processes. Therefore, it remains to be causally established that rIFG and, more importantly, pars opercularis, engage an explicit motor inhibition mechanism embedded in its connectivity that operates alongside attentional mechanisms (Munkata et al., 2011; Wiecki and Frank, 2013).

Here, we employed MRI-guided, neuronavigated transcranial focused ultrasound stimulation (tFUS) directly to the pars opercularis of the rIFG while humans performed a

stop-signal task. tFUS is a stimulation technique with a millimeter spatial resolution (Fini and Tyler, 2017). Neural activity underlying response inhibition was assessed with EEG event-related potentials (ERPs) and source analysis. Using this approach allowed us to delineate the specific role of pars opercularis, while detailing which ERPs and network functions are directly related to inhibition success and its speed (SSRT). tFUS to pars opercularis significantly improved response inhibition through a targeted effect of shortening SSRT. To determine how tFUS altered biophysical mechanisms generating neural activity underlying inhibitory mechanisms, we built dynamic causal models (DCM) of ERPs using microcircuit models. The main network hypothesis was that an explicit rIFG inhibition mechanism would be embodied in direct rIFG-to-subcortical connectivity weighting that directly reflects tFUS-induced changes in stopping efficiency (SSRT). We confirmed this hypothesis by demonstrating tFUS directly altered rIFG connectivity to a hidden subcortical node. In addition, DCM also indicated that only No-tFUS successful versus failed stopping, rather than successful stopping in general, were differentiated by mechanisms linked to network mechanisms associated with attentional modulation, i.e., recurrent synaptic superficial gain of visual cortex. Importantly, these results support the proposal that rIFG is directly involved in implementing an explicit response inhibition function and stopping efficiency.

RESULTS

Human participants performed a Stop-Signal task with online, trial-by-trial tFUS. Subjects were divided into groups based on receiving one of three stimulation type: (1) active stimulation targeted to right pars opercularis, (2) an active stimulation control site (ipsilateral somatosensory, S1) to account for non-site specific tFUS, and (3) sham stimulation to account for tFUS auditory artifacts. Since tFUS has been demonstrated to illicit immediate

effects on ERPs (Lee et al., 2016), stimulation was applied online (see Methods) either at the onset of the go or stop signal cue, during both Go and Stop trials (Figure 1A). We hypothesized that if rIFG implemented motor inhibition, then tFUS behavioral effects would be limited to alteration of stopping but not going. tFUS in the pars opercularis group improved inhibition, while exerting no effects in control groups. tFUS also altered inhibition related ERPs, which were quantified at electrode and source-localized levels, while also assessing tFUS impact on effective network connectivity assessed using DCM.

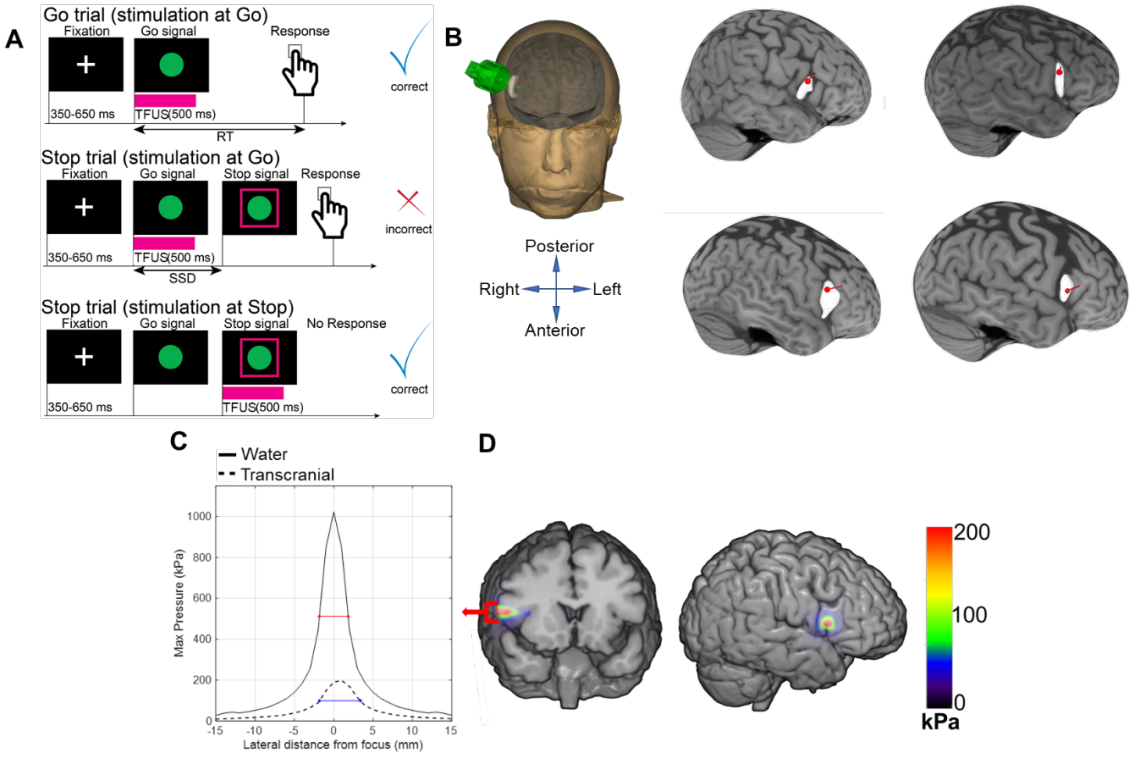

Figure 1. Task protocol and tFUS stimulation
(**A**) Visual layout of Stop-Signal task and corresponding times when tFUS was delivered.
(**B**) The left plot shows the average neuronavigation location of tFUS applied to all MRIs used in the rIFG group. The structural scans on the right show renderings of the targeted tFUS point in pars opercularis in 4 subjects. A mean stimulation location of x = 52 ± 3, y = 15 ± 3, z = 20 ± 5 was recorded across all subjects (MNI coordinates).
(**C**) Lateral maximum pressure profile obtained at 30-mm depth focus in both water and transcranial ultrasound simulation on a CT scan from one patient (solid and dotted lines, respectively). Horizontal red and blue lines denote full-width half maximum of the spatial profile of lateral pressure.
(**D**) Simulated transcranial pressure profile onto T1 MRI plot shown as a color overlay.

Numerical simulation of tFUS to rIFG

To determine intensity and accuracy of tFUS after skull transmission in the rIFG group, we used numerical simulations based on CT and MRI data from 3 preoperative patients and validated the simulation results using a water tank test. At the focus, modeling of transcranial simulations predicted an average maximum intensity of 2.8 W/cm^2. This is in the range of intensity of non-thermal neuromodulation (Legon et al., 2014). Additionally, predicted shifts in peak pressure due to skull transmission was 1.25 mm laterally, relative to a water model simulation, and had a lateral full-width half maximum of 5.1 mm (Figure 1C). These simulations indicate a high spatial precision with >95% of energy limited to pars opercularis (Figure 1D).

Numerical simulation of tFUS to rIFG

To determine intensity and accuracy of tFUS after skull transmission, numerical simulations based on CT and MRI data from three preoperative patients were calculated and validated using a water tank test data. At the focus, modeling of transcranial simulations predicted an average maximum intensity of 2.8 W/cm^2 at rIFG. This is in the range of intensity of non-thermal neuromodulation (Legon et al., 2014). Additionally, predicted shifts in peak pressure due to skull transmission was 1.25 mm laterally, relative to a water model simulation, and had a lateral full-width half maximum of 5.1 mm (Figure 1C). These simulations indicate a high spatial precision with >95% of energy limited to pars opercularis (Figure 1D).

Only tFUS to rIFG alters response inhibition

We first addressed how probability of failing to inhibit responses, P(respond|signal) (Figure 2A), changed across tFUS conditions within and across groups, by fitting a 2-parameter

logistic linear mixed-model to obtain a slope (**β)** of the response inhibition curve across all subjects and tFUS conditions. Modeling indicated a good fit of the logistic curve (mean R^2 = 84%). Analysis of **β** indicated only the rIFG group exhibited a tFUS-altered P(respond|signal). Importantly, behavioral effects of tFUS were not found for either control groups. ANOVA results indicated a significant Group × tFUS interaction ($F(2,50) = 3.8$, $p = 0.034$, $\eta_p^2 = 0.17$), and an overall effect of tFUS condition ($F(2,50) = 11.74$, $p = 0.002$, $\eta_p^2 = 0.29$). Follow-up one-way ANOVAs across tFUS onsets (e.g., coincident with stop signal), but within-groups, showed only the rIFG group exhibited differences across onsets. Follow-up t-tests in this group showed **β** for Stop-tFUS was lower than No-tFUS and Go-tFUS conditions (both $p < 0.01$: mean **β**'s indicating change in probability for approximately 25% change in normalized SSD: No-tFUS = 0.35 (0.12), Stop-tFUS=0.27 (0.08), Go-tFUS=0.35 (0.11)). These results indicate only the rIFG group was affected by tFUS, as predicted, and only during Stop-tFUS.

Figure 2A shows improved inhibition performance during Stop-tFUS for the rIFG group occurred at longer SSDs (65% and 95% SSD). A repeated-measures ANOVA on P(respond|signal) for the rIFG group across all SSD levels and tFUS onsets revealed a significant interaction ($F(6,102) = 8.21$, $p < 0.0001$, $\eta_p^2 = 0.33$). Contrast t-tests between Stop-tFUS and the average of No- and Go-tFUS across all SSDs indicated the interaction resulted from a reduction in P(respond|signal) for Stop-tFUS in the highest two SSDs (all $p < 0.01$; Bonferroni $\alpha = 0.0125$). These results indicate Stop-tFUS induced improvements of inhibition were more pronounced at later SSDs

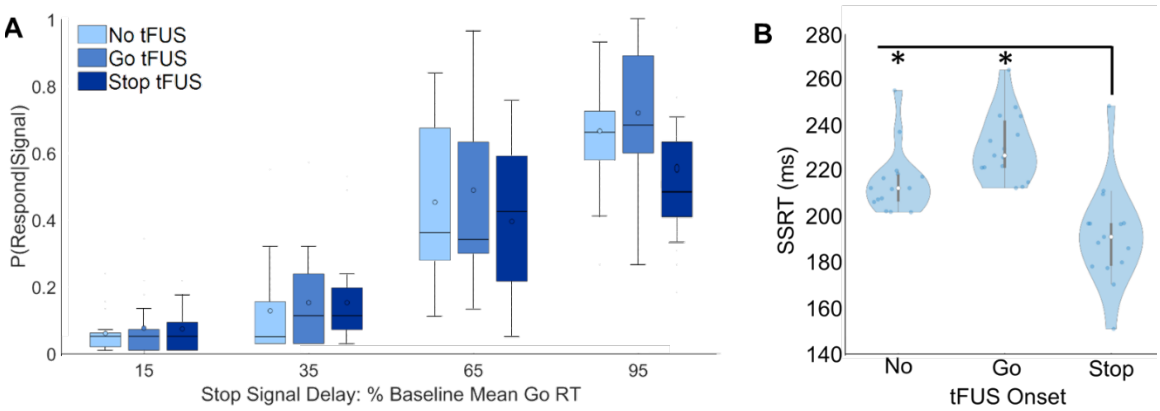

Figure 2. Probability of stopping and SSRT
(**A**) Probability of responding across stop signal delays in the rIFG tFUS group for all tFUS onsets.
(**B**) Violin plots of rIFG group across-subject distribution of stop signal reaction times (SSRT).

Based on the prediction that rIFG implements an inhibitory process and our finding that tFUS improved inhibition in this group, we hypothesized rIFG tFUS changes to P(respond|signal) should result from a shortening of the stopping speed (i.e., SSRT); notably, tFUS did not affect other behavioral variables (e.g., Go RTs, see Supplementary Material). SSRT analysis in a mixed-design ANOVA indicated a significant Group x tFUS interaction ($F(4,100) = 10.2, p < 0.001, \eta_p^2 = 0.21$). Follow-up one-way ANOVAs within-groups indicated only rIFG group SSRTs (Figure 2B) differed between tFUS onsets ($p < 0.05$), with t-tests confirming that SSRTs were indeed shortest and only altered during Stop-tFUS (Figure 2B). This result, along with the above P(respond|signal), indicate rIFG Stop-tFUS altered inhibition by shortening the stop process (SSRT).

Neural components underlying inhibition

In the rest of the results we focus our analysis on the rIFG group because this was the only group exhibiting behavioral effects of tFUS. Furthermore, we only analyze No-tFUS and

Stop-tFUS conditions because Go activity was subtracted from neural data at Stop trials (see Methods).

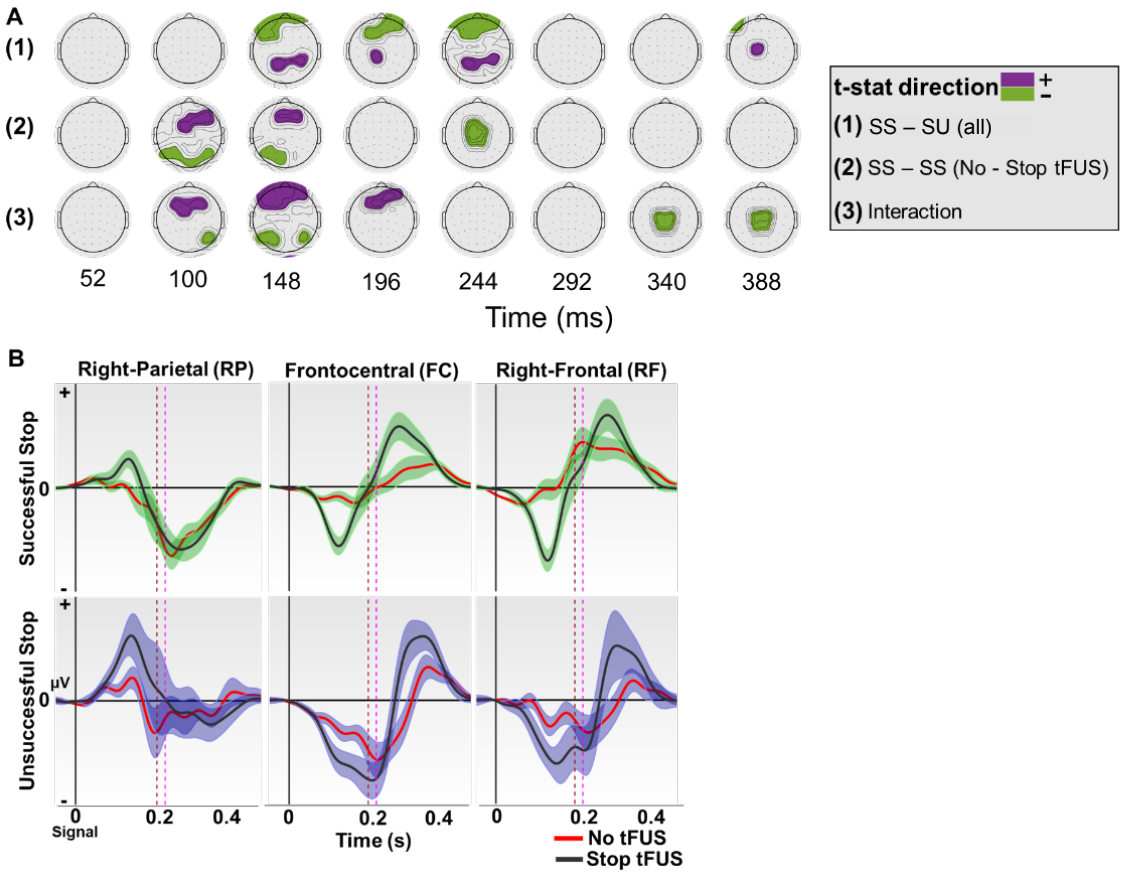

Figure 3. Cluster-based statistics and ERPs
(**A**) Scalp plots of cluster-corrected permutation paired t-tests ($p < 0.01$). Colored contours represent significant clusters. (1). Contrast of all SS and SU trials. (2). Contrast of tFUS conditions SS. (3). Interaction contrast calculated as SS-SU of No-tFUS trials minus SS-SU Stop-tFUS trials.
(**B**) Average ERP time courses of three clusters identified by the permutation testing that were differentiated by statistical contrasts. From left to right, the first cluster (left column) is right-parietal electrodes (CP6, CP4, P6, P8), the second cluster (middle column) is fronto-central electrodes (C1, Cz, C2), and the third cluster (right column) is right-frontal electrodes (F8, F6, F4). The vertical dashed lines represent the stop-signal reaction times for the No-tFUS (magenta) and Stop-tFUS (maroon). Latencies in A and B are expressed relative to stop signal onset (0 ms).

Our first analysis examined sensor-level ERPs across three contrasts using cluster-based permutation t-tests: (1) successful – unsuccessful stopping contrast over both tFUS conditions, (2) successful stopping (No-tFUS) – successful stopping (Stop-tFUS) contrast,

and (3) interaction comparing successful – unsuccessful stopping between the No-tFUS and Stop-tFUS conditions. The cluster-based scalp maps show the progression of clusters time-locked to the stop-signal onset (0 ms, Figure 3A,B).

We identified several ERPs that differentiated successful stopping (SS) and unsuccessful stopping (SU) trials. The first contrast of SS-SU (Figure 3A, row 1) indicated SS trials exhibited a larger ERP centralized over a right-parietal cluster around the time-range typically found for the P100 peak (100-148 ms). The interaction of SS-SU and tFUS showed this effect occurred earlier and during the peak onset (80-100 ms) of Stop-tFUS trials. Consideration of the SS-SS contrast (tFUS effect; Figure 3A-2nd row) indicated the largest effect was attributable to the SS tFUS trials, supporting previous conjectures that inhibition and stopping speed is directly related to larger P100 parietal responses. This result also aligns with previous studies reporting an enhanced P100 during successful stopping (Boehler et al., 2009).

We also examined the N100 in the right-frontal cluster in the 80-120 ms window (Figure 3B). We did not find a difference in the frontal N100 with respect to the overall SS – SU contrast (Figure 3A). This result is in line with several other studies noting a non-significant effect of this contrast (Kenemans, 2015). However, we did find the ERP was substantially larger in SS tFUS trials compared to SS No-tFUS trials indicating a direct contribution to stopping efficacy. This increase for SS tFUS suggests this ERP may stem from rIFG and provide an index of stopping speed, rather than success.

The ERPs most commonly associated with response is the N200/P300 complex. Notably, the N200 often appears in both right-frontal and fronto-central clusters, while the P300 is more aligned with the fronto-central (Huster et al., 2013; Kenemans, 2015). When examining the N200, which typically only appears during SU (Liotti et al., 2010; Wessel et al.,

2015), we found an ERP peaking around 200 ms in both clusters that only appeared in SU trials (Figure 3B). This N200 emerged during both No- and Stop-tFUS (Figure 3, bottom right), with a larger amplitude during SU Stop-tFUS.

Of all possible ERPs, the fronto-central P300 has been regarded as the most robust marker of response inhibition and stopping speed (Wessel and Aron, 2015). Accordingly, we found P300 amplitude differed between SS and SU trials, with SU trials exhibiting a larger amplitude around the peak (290-320 ms) (Figs. 3A-B). However, because P300 peaks occur after the SSRT, this implies it is too temporally protracted to reflect inhibition (Huster et al., 2013). Alternatively, others have indicated the P300 onset latency is related to inhibition because it scales with individuals SSRTs (Wessel and Aron, 2015). Based on this notion, we considered whether the P300 onset was causally related to the SSRT shortening induced by tFUS. We tested the specific prediction that Stop-tFUS SS trials should exhibit an earlier onset that correlates with individual changes in SSRT. Visually, contrasting waveforms of SS trials across tFUS conditions (Figure 3B, upper-middle) supports this intuition that P300 onset (zero-crossing in Figure 3B) shifted earlier in alignment with Stop-tFUS induced SSRT shifts. This was quantitatively supported by a significant, across-subject correlation between the tFUS induced in change P300 onset and SSRT (0.61, $p < 0.05$), providing direct support that P300 latencies reflect the timing of inhibition speed.

Whole-brain source SPM and source-based regression analysis

We also examined source-based activity to localize tFUS-induced changes in evoked activity and generating source location priors for DCM. We hypothesized that, if differential rIFG activation indexed SS versus SU, then conjunction analysis should reveal an overlap between SS – SU and No-tFUS – Stop-tFUS conditions if rIFG activity is related to successful

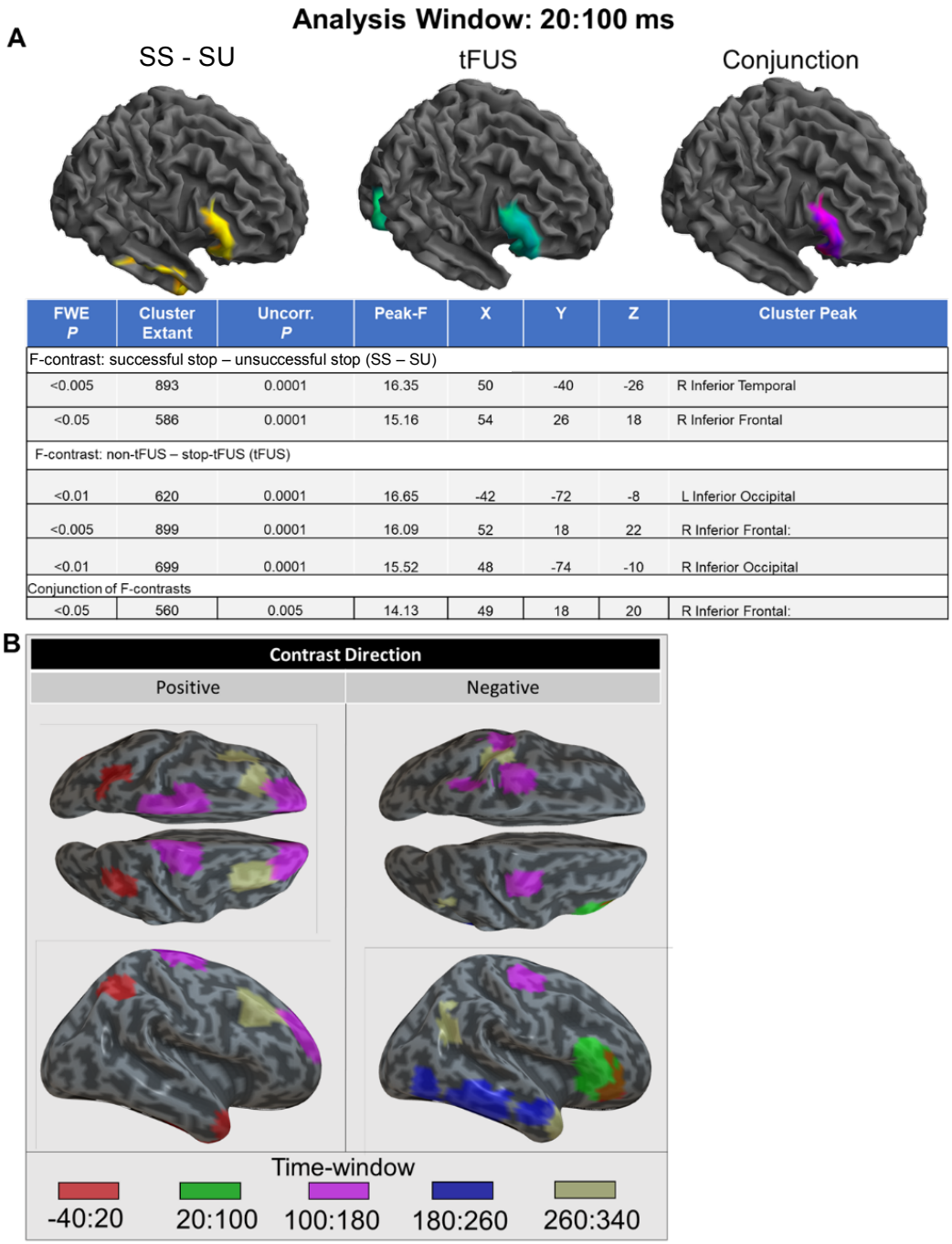

FWE *P*	Cluster Extant	Uncorr. *P*	Peak-F	X	Y	Z	Cluster Peak
F-contrast: successful stop – unsuccessful stop (SS – SU)							
<0.005	893	0.0001	16.35	50	-40	-26	R Inferior Temporal
<0.05	586	0.0001	15.16	54	26	18	R Inferior Frontal
F-contrast: non-tFUS – stop-tFUS (tFUS)							
<0.01	620	0.0001	16.65	-42	-72	-8	L Inferior Occipital
<0.005	899	0.0001	16.09	52	18	22	R Inferior Frontal:
<0.01	699	0.0001	15.52	48	-74	-10	R Inferior Occipital
Conjunction of F-contrasts							
<0.05	560	0.005	14.13	49	18	20	R Inferior Frontal:

Figure 4. Whole Brain SPM

(**A**) Whole-brain SPM F-contrasts of evoked activity in the 20:100 ms window. Figure shows the surface mesh projections of the overall SS – SU (left) tFUS contrast (middle), and conjunction (right). Below the surface meshes is a table listing the statistics.

(**B**) Whole-brain SPM linear regression of activity No-tFUS and Stop-tFUS SS trials against SSRT changes in No-tFUS and Stop-tFUS SS trials.

stopping (Aron et al., 2014). As expected, whole-brain SPMs (Figure 4A) revealed the only area exhibiting an overlap was a pars opercularis-centered rIFG peak during the 20-100 ms time window (results of analysis of other time windows are reported in Supplementary Material).

To understand how tFUS altered stopping efficacy, we compared changes in SSRT between Stop-tFUS and No-tFUS SS trials using whole-brain SPM linear regression. In the regression, positive contrasts indicate Δ SSRT (No-tFUS – tFUS) is associated with larger activity in No-tFUS trials. Negative contrasts indicate tFUS SS trials exhibit larger evoked activity predicted by larger changes in SSRT. The negative contrast in Figure 4B indicates that the first site to exhibit increased tFUS-related predictions is rIFG. This occurred both in the -40:20 and 20:100 time-windows. The positive contrast found in early time windows indicates Stop-tFUS exerted effects on stopping by also decreasing early activity in both bilateral parietal and right temporal sites. We also found pre-SMA was only predictive of SSRT after rIFG, with the pre-SMA modulation peaking at 100:180 ms. These results show that areas typically associated with successful inhibition were predictive of tFUS-induced changes in behavior while occurring before the SSRT itself.

tFUS effects in an inhibition network: Dynamic Causal Modeling

The above tFUS results provide evidence that rIFG activity is causally related to inhibition. Principally, differences in local activation can result from both local and inter-areal connectivity (David et al., 2006). We used Dynamic Causal Modeling (DCM) to quantify network effects. Bayesian model selection established a winning model as a hierarchical network in which rDLPFC and rIFG sat at the top of the hierarchy and pre-SMA being

below these areas. The model also included nodes for right temporal (rTemporal), right inferior occipital gyrus (rIOG), right parietal (rParietal), a hidden subcortical node (Deep) and left motor cortex (M1). These results accord with networks proposed by previous studies implicating both motor inhibition and attentional orienting (Weicki and Frank, 2013; Munkata et al., 2011). The DCM (Figure 5) was fit to individual subject's data to determine how connectivity parameters differentiated (1) No-tFUS baseline SS and SU inhibition differences, and (2) between No-tFUS and Stop-tFUS SS trials and accompanying changes in SSRT. The above approach revealed the models agreeably captured the spatiotemporal properties of the ERP scalp data across both sets of model fits (Figure 5).

The first set of analyses examined what connectivity parameters were altered during No-tFUS successful inhibition. The first comparison examined whether differential rIFG and pre-SMA interactions were related to baseline successful stopping, as suggested by several functional and anatomical studies (Duann et al., 2009; Rae et al., 2015; Swaan et al., 2012; Figure 6A). Model comparisons revealed a winning family included interactions between both areas, but with a moderate posterior probability (0.78). BMA across families revealed both the connection from rIFG to pre-SMA (136%) and pre-SMA to rIFG (193%) were altered during SS trials. Changes in this connection suggest that SS trials were supported by prefrontal interactions. Considering previous data indicating increases in pre-SMA projections (Forstmann et al., 2008) to striatum render increased RTs, this result might reflect an effect of blocking the impetus pre-SMA provides towards responding to the Go signal (Verbruggen and Logan, 2009).

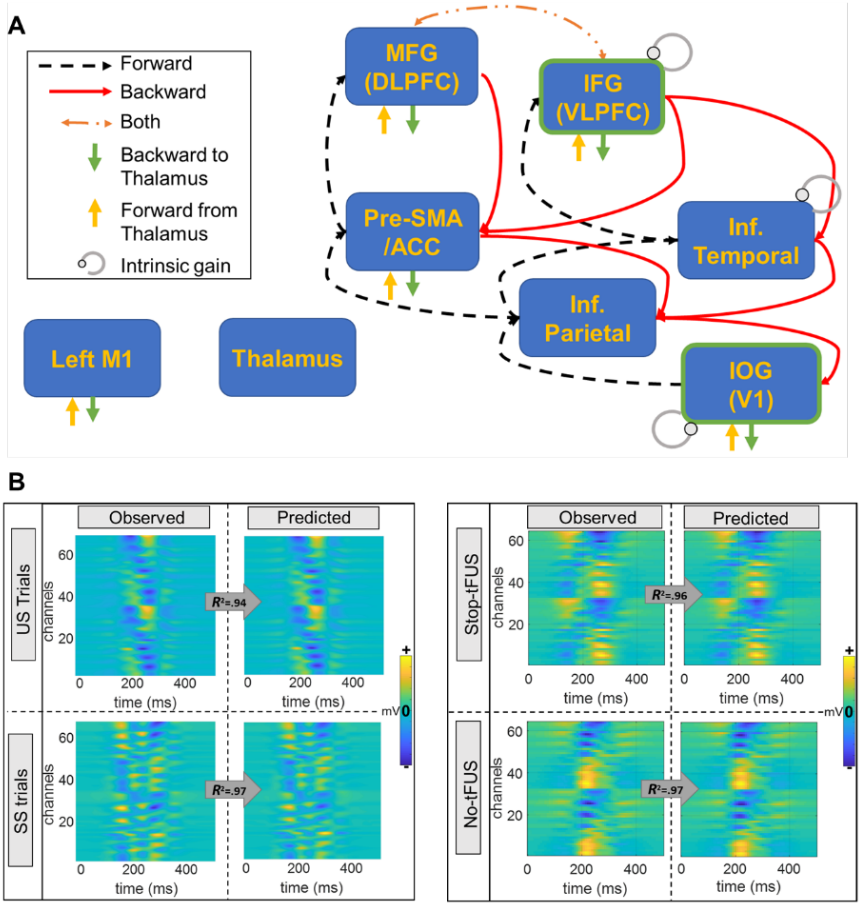

Figure 5. Dynamic causal model structure and fitting
(**A**) Connections used to implement the final dynamic causal model structure. Exogenous inputs entered through rIFG and rIOG represented as a green box. All nodes except Left M1 and Thalamus were all located in the right hemisphere.
(**B**) Left panel shows the mean observed and predicted scalp ERP data derived from the dynamic causal model fit to the No-tFUS SU and SS trials. Right panel shows the mean observed and predicted scalp ERP data derived from the dynamic causal model fit to the No-tFUS SS and Stop-tFUS SS trials. These results show that the final model provided a good fit to the data. Data are plotted relative to stop signal onset (0 ms on x-axis).

The next comparison tested the hypothesis that both pre-SMA and rIFG projections to deep areas are necessary for successful inhibition (Figure 6B). Only a family including changes from rIFG to deep was predictive of successful inhibition. BMA indicated rIFG exhibited a mean reduction in the backwards connection of 65% during successful stopping.

This result agrees with previous fMRI studies (Aron et al., 2006; Jahfari et al., 2011) indicating inhibitory processes are driven by cortical to basal ganglia interactions.

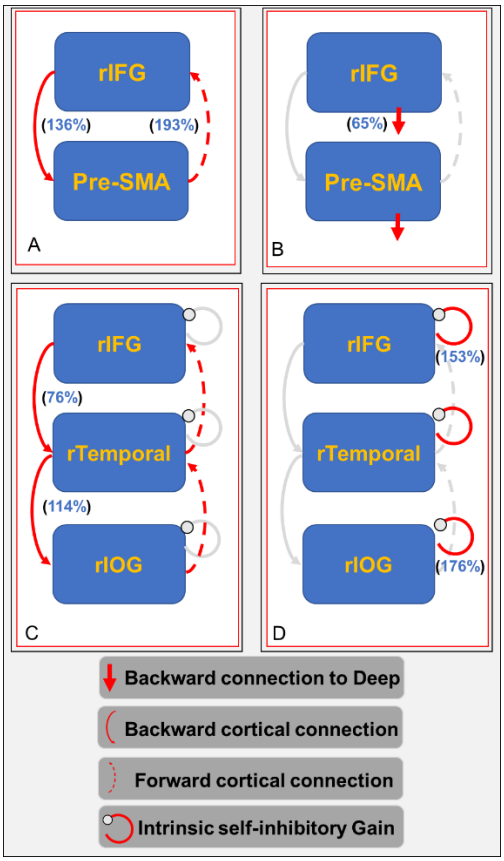

Figure 6. Family-based model comparison for different hypothesized interactions
Plots contain modulatory parameter of connections with strong positive evidence as being different between SU and SS trials. Parameter estimates (>95% posterior probability) are in parentheses next to modulated connection in exponential percentage change. Anything above 100% reflects an increase in SS trials compared to SU (opposite for below 100%).
(**A**) Test of rIFG and pre-SMA interactions.
(**B**) Tests of rIFG and pre-SMA backward projections to deep node.
(**C**) Tests for the ventral pathway connections.
(**D**) Comparison of intrinsic superficial pyramidal cell gains.

Another hypothesis that has been put forth regarding successful inhibition is that it is mainly mediated by attentional orienting in ventral pathways (Hampshire and Sharp, 2015). DCM implementations of attentional process can be cast in terms of hierarchical predictive coding models (Feldman and Friston, 2010). Previous work suggests increased attention in

sensory areas emerges as increased recurrent intrinsic gain (increased disinhibition) of superficial pyramidal cells thought to report prediction errors through forward connections (Auksztulewicz et al., 2015). In DCM, recurrent gains would weight prediction error signals driven changes in top-down (backward) connections (Bastos et al, 2012). We designed the next two comparisons to examine whether SS trials exhibited these network changes. Extrinsic connection analysis in No-tFUS SS indicated a winning family including only changes in top-down backward connections predicted successful inhibition (Pp =1). BMA indicated, however, the inhibitory connection from rIFG to rTemporal was reduced while backward connections from rTemporal to rIOG increased in connectivity (Figure 6C).

The final SS and SU modulation comparison analyzed changes in recurrent gains of rIFG, rTemporal and rIOG (Figure 6D). The winning model (Pp = 0.99) included an increase in gain for both rIOG (176%) and rIFG (153%). Importantly, the increased rIOG gain is predicted by attentional orienting models of response inhibition (Hampshire and Sharp, 2015) and accords with previous DCM studies that have manipulated attentional cueing (Auksztulewicz et al., 2015). Mechanistically, the increased rIOG gain in SS trials results in ascending signal that has a larger effect on decreasing rIFG top-down expectation signals in backward connections.

Stopping efficiency (SSRT) is driven by lower and prefrontal interactions

Another primary goal of understanding inhibitory control is quantifying how the efficiency of stopping, evaluated through the SSRT, is implemented via network pathways. Previous work has employed between-subjects' correlations of SSRT and connectivity parameters to isolate the pathways involved in this process (e.g., Jahfari et al., 2011). Because previous studies using fMRI and a variety of connectivity methods revealed pre-SMA and rIFG to

basal ganglia connections are correlated in different directions with SSRT (Jahfari et al., 2011), we adopted this approach when analyzing the baseline No-tFUS SS versus SU contrast. This correlational analysis indicated both connections were correlated in opposite directions with SSRT. Figure 7 shows that increasing connectivity from rIFG to deep targets predicted shorter SSRTs. The opposite pattern was found for pre-SMA, wherein increasing pre-SMA backward activity predicted longer SSRTs.

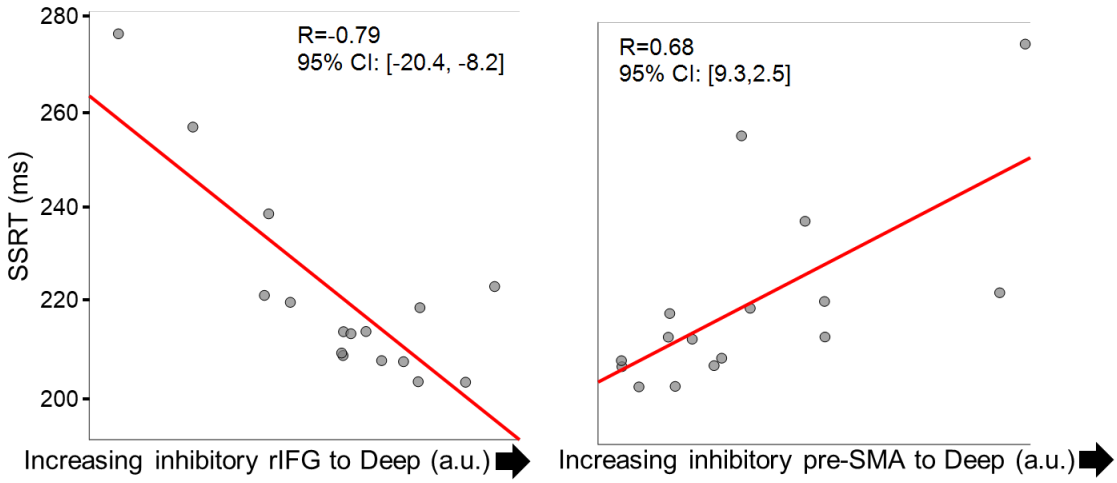

Figure 7. Linear regression of SSRTs from rIFG and pre-SMA
Left and right plots show linear regression fits predicting individual subjects' No-tFUS SSRT from the backward connection to the deep area projecting from rIFG and pre-SMA, respectively. Larger values on the x-axis denote decreasing backward inhibitory connectivity.

tFUS to rIFG causally dissociates inhibitory mechanisms

Building on tFUS's effect of increasing inhibition performance, a primary question was whether the changes in connectivity strength between No-tFUS SS and Stop-tFUS SS trials would reflect stepwise changes in the connections modulated in the SS and SU No-tFUS comparison. This comparison is in line with the idea of failed stop trials resulting partially from less active inhibition mechanisms. By applying tFUS to rIFG, we were able to causally dissociate rIFG's role in implementing inhibitory mechanisms. Below, mean changes

represent the average modulation of connectivity going from No-tFUS SS to Stop-tFUS SS trials. SSRT-based effects represent how changes in SSRT between tFUS conditions predict the change in connectivity between tFUS conditions.

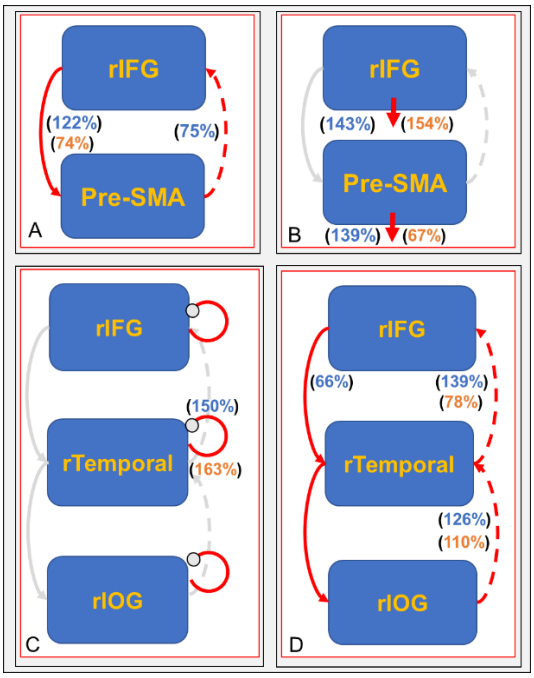

Figure 8. Results of the family-based model comparison for different hypotheses tested when comparing modulation from No-tFUS SS to Stop-tFUS SS trials.
The family-based posterior probability (F-Pp) for the winning model is listed below each model. The outcomes of these plots can be interpreted of as revealing the modulatory parameters connections with very strong, positive evidence of SU and SS trials being different. Parameters estimates with a greater than 95% posterior probability in these families are presented in parentheses next to the modulated connection. The parameters are presented in exponential form of percentage change. Values above 100% equates to a parameter increase in SS trials compared to SU (and the opposite for values below 100%). Parameters in-active in each model are in a gray color.
(**A**) Hypothesis test of rIFG and pre-SMA interactions.
(**B**) Hypothesis tests of rIFG and pre-SMA backward projections to deep node.
(**C**) Comparison of intrinsic superficial pyramidal cell gains.
(**D**) Tests for the ventral pathway connections.

In first analyzing the family of models examining the rIFG and pre-SMA interaction, there was no clear winning family of models for both the mean and SSRT effect (Figure 8A). For the mean, the model with projections from rIFG to pre-SMA (122%) and pre-SMA to

rIFG (75%) was highest in probability (Pp = 0.79). Of these connections, SSRT change was only negatively related to the rIFG to pre-SMA pathway (r^2 = 74%). indicating that an increase in inhibitory connectivity from rIFG to pre-SMA during Stop-tFUS trials predicted a larger change in SSRT. Therefore, changes in SSRT were not related to forward connections between these nodes, but instead were modulated by a top-down inhibitory modulation from rIFG to pre-SMA.

When comparing models testing the role of rIFG or pre-SMA to deep backward connections, family analysis revealed a strong effect of the mean change and SSRT change for both backward connections (Pp > 0.95 both effects). BMA in the winning family indicated both effects were above threshold for both connections. Both rIFG (143%) and pre-SMA (139%) exhibited increased connectivity during tFUS. Concerning changes in tFUS related changes in SSRT, the direction of effects was opposite for rIFG (154%) and pre-SMA (67%): for rIFG, decreased inhibition yielded increased SSRT change, and the opposite for pre-SMA. Together, these results point to differential interactions of both pre-frontal areas with a deep node in responding to tFUS. These results are further in line with the directionally opposite linear correlations of the No-tFUS SSRT to each of these backward connections (Figure 8B).

Finally, we examined ventral pathway parameters for tFUS modulation of top-down, bottom-up, and intrinsic gain changes. Model averaging revealed the rIFG to rTemporal top-down connections (66%) decreased with tFUS, suggesting a direct effect from rIFG tFUS. This decrease in top-down rIFG connection agrees as well with the results found during the SS versus SU comparison, suggesting a causal and overlapping pathway driving inhibition performance. All bottom-up connections increased as well (Figure 8C). With respect to SSRT change (Figure 8D), only the bottom-up connections were related to changes in the

SSRT. However, the forward connectivity relations to SSRT were in opposite directions for modulations of the rIOG to rTemporal (110%) and rTemporal to rIFG (78%). Finally, we found rTemporal recurrent gain increased in mean (150%) and was positively related to changes in SSRT (163%). This relation between the SSRT effect and rTemporal to rIFG forward connection was strong enough such that a leave-one-out cross validation prediction of SSRT change using this connection exhibited a large correlation with actual SSRT change (0.84, $p < 0.01$). These results indicate neural implementation of stopping speed involves processing efficacy of bottom-up, temporal cortex (prediction error) signals.

DISCUSSION

The present study examined whether pars opercularis sector of rIFG is explicitly involved in motor response inhibition. We used a stop-signal task, online tFUS, source-localized EEG, and dynamic causal modeling of ERPs to examine this hypothesis and examine underlying response inhibition network mechanisms. Behaviorally, tFUS applied to pars opercularis and coincident with the stop signal increased the likelihood of successful inhibition. Because tFUS enhancements of inhibition resulted from faster stopping processes (i.e., SSRT), without altering Go RTs, this supports pars opercularis' role as directly triggering action stopping. Examination of scalp ERP analysis indicated tFUS rendered a shift in the fronto-central P300 onset, which has been previously hypothesized as neural marker of stopping speed (Wessel and Aron, 2015). Imperatively, the shifted onsets were directly linked to and correlated with tFUS-induced changes in individuals SSRT. Spatial accuracy of tFUS was supported by whole-brain evoked activity indicating only pars opercularis exhibited a conjunction effect of tFUS with successful compared to failed inhibition (Figure 3). The hypothesis that pars opercularis activity is directly related to stopping efficacy was confirmed

by tFUS-driven activity differences predicting between-subjects SSRT change (Figure 4B). Despite these results, recent work suggested tFUS effects result from auditory artifacts (Sato et al., 2018). Auditory effects, however, cannot explain our findings because control groups exhibited no behavioral effects, and no group exhibited evoked auditory cortex activity (Figure S7). We interpret the above results as indicating tFUS selectively modulated pars opercularis activity, and pars opercularis explicitly implements response inhibition.

Generally, response inhibition involves several processes embedded in connections across a neural network, ranging from sensory cue detection, attention, performance monitoring, and presumably explicit motor inhibition (Munkata et al., 2011; Weicki and Frank, 2013; Wessel and Aron, 2017). Many have proposed that motor inhibition is implemented directly in rIFG connectivity to basal ganglia (STN and striatum), either in parallel or routed through pre-SMA (Aron et al., 2014), or both. In contrast, others have proposed motor inhibition is better understood as an emergent outcome of attentional orienting and biased competition between neural processing of response and inhibition cues (Hampshire and Sharp, 2015). Extant evidence indicates, however, that motor inhibition and attentional processing are likely all involved in different processing stages of inhibitory control tasks (Wessel and Aron, 2017).

Given the evidence for response inhibition as a multi-process phenomenon, a key question is what network connections and biophysical mechanisms support action stopping. A core component of models positing a direct rIFG motor inhibitory process is that its connectivity with subcortical nodes should change with stopping success or efficacy. The present study's DCM analysis of No-tFUS successful and failed inhibition is consistent with the hypothesis that rIFG and pre-SMA subcortical connections are relevant for motor inhibition. DCM results of No-tFUS successful stopping also revealed an anti-correlation of

SSRT to pre-SMA and rIFG deep connection strength (Figure 7). Our findings agree with another fMRI connectivity study (Jahfari et al., 2011) that found successful stopping accompanied increasing pre-SMA to striatum connectivity and predicted longer SSRTs, with the opposite correlation for rIFG to striatum. Pivotal support for rIFG's role is the result that tFUS effects on SSRT were directly related to changes in rIFG and pre-SMA to deep connectivity with a similar anti-correlation pattern as the baseline. We take these results to indicate pars opercularis subcortical connectivity is directly involved in driving motor inhibition through feedback pathways. This indicates a potential mechanistic effect of tFUS, wherein inhibition improved by altering the connectivity of layer V rIFG pyramidal neurons by increasing the excitability of these cells. Notably, this conjecture of an excitatory tFUS effect on pyramidal neurons and our tFUS parameterization are in accordance with the neuronal intramembrane cavitation excitation (NICE) model that has been used recently to explain the acoustical stimulation effects on the biophysics of neuronal firing (see Plaksin et al., 2016).

An unresolved issue regarding the inhibition network is how rIFG and pre-SMA interactions areas relate to inhibition in general (Duann et al., 2009; Swaan et al., 2012). Our DCM optimization indicated rIFG projected to pre-SMA through backwards inhibitory connections and pre-SMA to rIFG via excitatory forward connections. This bidirectional connectivity agrees with previous fMRI stop-signal and DTI studies (Duann et al., 2009; Rae et al., 2015). Functionally, No-tFUS DCM results revealed successful stopping was accompanied by increases in both connections. However, when comparing baseline and tFUS DCMs, our results indicate that only the rIFG to pre-SMA connections in this subset of connections were effectively related to inhibition in terms of the mean gain change in backwards connectivity and its covariation with tFUS induced changes in SSRT (Figure 6A-

B). This result is directly relevant to several studies that have either concluded pre-SMA drives rIFG (Swann et al., 2011) during inhibition or the opposite (Duann et al., 2009). Combining DCM and tFUS indicated the inhibitory effect of rIFG onto pre-SMA is causally responsible for driving inhibition at a cortical level. This raises the question of why the pre-SMA to rIFG connection was only relevant during baseline successful inhibition. An alternative interpretation is found in neuroimaging (Crone et al., 2006), ECoG (Swaan et al., 2012), and TMS studies of proactive inhibition and response switching (Rushworth et al., 2002). These studies have indicated pre-SMA encodes a set of potential actions. During response inhibition, this predicts successful stopping involves pre-SMA signaling the action(stopping)-rule to rIFG. Therefore, the action rule and connectivity conveying it should not differ for successful No-tFUS and Stop-tFUS trials because it should have been similarly communicated under both conditions.

The above results provide causal evidence that pars opercularis and its connectivity are directly involved in motor inhibition. Nonetheless, neuroimaging studies have shown rIFG-related activation predicts attentional orienting and stimulus expectancy processes during response inhibition (Erika-Florence et al., 2014; Hampshire and Sharp, 2015; Xu et al., 2017). Although attention was not manipulated in our study, we derived predicted network mechanisms from predictive coding models of attention (Feldman and Friston, 2010) and DCM-EEG studies directly manipulating attention and stimulus expectancy (Auksztulewicz et al., 2015). Importantly, the microcircuits implemented in the DCM presently used are directly related to predictive coding models and have explicit mechanisms supported by previous DCM studies. For example, these studies have shown increased attention is linked to increased recurrent gain on ascending (forward) sensory (prediction error) signals, while violations of stimulus expectations were linked to decreased top-down

and increased in bottom-up connectivity, respectively (Auksztulewicz et al., 2015; Fardo et al., 2017). Along these lines, our DCM during baseline stopping featured increased rIOG recurrent gain as expected if attention increased the precision afforded to the sensory processing of stop cues (Moran et al., 2013; Figure 7C). Concerning top-down changes, rIFG to rTemporal decreased and rTemporal to rIOG increased (Figure 7D). Successful stopping at baseline therefore may rely on an increased rIOG gain weighted sensory signals that drive top-down changes in rIFG. However, increased connectivity from rTemporal to rIOG seems at odds with this interpretation because it implies a larger reliance on top-down information during successful stopping. This is explained by the finding that optimized inputs to rIOG were negative and therefore inhibitory (rather than excitatory) across subjects. Therefore, increasing rTemporal backward connectivity rendered an enhanced negative rIOG signals.

Although the preceding results seem to accord with attention-based formulations of inhibition, examination of tFUS effects on connectivity indicate inhibition success was generally unrelated to these mechanisms. The only overlap between baseline and tFUS conditions was a decrease in top-down rIFG to rTemporal backwards connectivity. Still, this effect was not directly predictive of a change in SSRT. tFUS effects also involved an increase in bottom-up connectivity that was predictive of SSRT change (Figure 8D) in agreement with expectation violation effects found in other EEG-DCM studies (Auksztulewicz et al., 2015). The most interesting effect was recurrent gains only increased in rTemporal, indicating SSRT changes were not due to increased sensory weighting. We propose that cortically-related SSRT changes were driven by tFUS altering the effects the rIFG to rTemporal connection had on the rTemporal gain. A partial correlation supported this hypothesis by showing covariation of rTemporal gain and SSRT change was rendered null

when accounting for the correlation of rIFG to rTemporal and rTemporal gain. A potential explanation for this result is that rIFG engages in a proactive inhibitory function whereby it biases bottom-up processing of the temporal cortex, which itself may encode the expected probability of stop signal occurring. This interpretation is consistent with fMRI stop-signal studies demonstrating temporal cortex encodes a prediction error of stop-signal probability (Hu et al., 2015; Ide et al., 2013).

In summary, tFUS can induce enhanced response inhibition performance, allowing the underlying mechanisms to be linked to direct and source-resolved electrophysiological neural processes in humans. By pairing tFUS with DCM, we found a network model of response inhibition suggesting pars opercularis explicitly invokes motor inhibition through deep pyramidal connections directly synapsing onto subcortical nodes, as well as pre-SMA and temporal cortex. These results also significantly extend the possible applications by showing tFUS combined with network modeling has the potential to alter and infer the effective connection between biophysical network mechanisms and behavior.

METHODS

Participants

Participants consisted of healthy adult volunteers and were divided into one of three experimental groups. The main experimental group received transcranial focused ultrasound (tFUS) stimulation to the right inferior frontal gyrus (rIFG) (n = 25; 19 males, mean age 24.1, SD 3.2 yrs). A second group was used as cortical site, active control group. These participants received stimulation to the ipsilateral somatosensory cortex (S1) (n = 23; 15 males, mean age 22.4 yrs. SD = 3.3 yrs). A third group received a sham stimulation near the right temple (n = 15; 8 male, mean age 24.2 yrs SD = 2.8 yrs) and was used as control for

possible auditory effects of tFUS over rIFG (sham rIFG). All individuals were right-handed and received financial compensation for participation in the study. Before being enrolled, each subject was screened for neurological disorders and previous history of epilepsy, stroke, or brain injury. Furthermore, a neurologist from the Barrow Neurological Institute (Phoenix, AZ) screened all subjects' T1 scans after structural MRI acquisition, and before participation in the study.

Stop Signal Task and tFUS design

The current study used the conventional Stop Signal Task that involved both 'Go' and 'Stop' trials (Figure 1A). We presented the experiment using Opensesame (Mathôt et al., 2012). Each trial started with a centrally-located fixation cross on the monitor. In both trial types, the fixation cue was replaced by a green 'Go' circle (3° x 3° visual angle), with an exponentially-distributed time interval (mean: 500 ms; standard deviation: 50 ms). Subjects were instructed "to press the up key as soon as they detected the Go circle" (top panel, Figure 1A). In 'Go' trials, the circle vanished when the button was pressed or after 800 ms had passed from the fixation cross stimulus. In 'Stop' trials, the stop was a red square which appeared around the green circle (middle and bottom panel, Figure 1A). If the subject successfully inhibited his/her response with respect to the Stop cue within 800 ms, the red square was extinguished, and the trial was considered a successful inhibition. The time required to inhibit a response following the Stop signal is defined as stop signal reaction time (SSRT) (see below). The timing of the Stop cue relative to Go cue, i.e., the stop signal delay (SSD), was presented at one of four fixed, but subject-specific SSDs. The SSDs were designated by having each subject first perform a practice block of 50 Go trials only to determine their baseline Go reaction time (RT). After this block, the 4 SSD levels were set to

25, 35, 75 and 95% of the mean Go RT. These SSDs were fixed throughout the experimental session. Using a set of fixed SSDs allowed us to calculate the SSRT using routines that are less susceptible to low trial numbers (Matzke et al., 2013; see Data processing). Additionally, we determined the effects of online tFUS at different SSDs to estimate the effects of stimulation on neural and behavioral responses at different stages of a Go process predicted by response inhibition models (Verbruggen and Logan, 2009). All trials were separated by an inter-trial interval of 2000 ms (±300 ms randomly drawn jitter).

tFUS was delivered either simultaneously with (1) the Go signal in both Go and Stop trials, or (2) the Stop signal (Figure 1A). The purpose of delivering tFUS during Go trials was to determine the neural and behavioral effects of tFUS to rIFG independent of a stopping signal. Specifically, this allowed us to assess whether any effects of tFUS on stopping behavior are related merely to alteration of the timing of an underlying Go process. Therefore, we used 5 types of trials. The first two consisted of Go trials with no tFUS or with tFUS locked to the Go cue (No-tFUS and Go-tFUS trials, respectively). The other three trials consisted of Stop trials: No-tFUS trials, Go-tFUS, and tFUS locked to the Stop signal (Stop-tFUS). These three types of Stop trials were examined across the four SSDs.

tFUS delivery for Stop trials was evenly distributed across the 4 SSD levels. The overall probability of a stop trial was set to 35% of all trials (Figure 1B). We chose this level to accommodate the need for large amounts of Stop trials required to examine the effects of tFUS on Stop trials across all SSD levels, while still making Go trials more frequent. Each experimental session consisted of 1200 trials distributed across 12 blocks. Blocks were segmented into stimulation and no-stimulation blocks; the former containing trials with and without stimulation, and the later containing no stimulation. Trial types (Go and Stop trials) were randomly and evenly distributed throughout the experiment. The trial numbers were

chosen to enable the comparison between tFUS and non-stimulation trials across successful and failed inhibition trials, while allowing a reasonable number of trials to be performed without inducing significant fatigue to the participants. The block design, as well as the use of an active-stimulation and sham control groups was chosen to mitigate any possible carry-over effects of the stimulation across trials.

EEG acquisition

EEG was recorded using a 64-channel ActiCap system (BrainVision, Morrisville, NC), with a standard 10–20 layout. Data was recorded at a sampling rate of 5 kHz, with resolution 0.1 μV and bandpass filter of 0.1–100 Hz. Impedances were always kept < 5 kΩ. Online recordings utilized a ground at AFz and left mastoid reference. At the beginning of each session, electrode layouts with respect to each individual's head shape were registered using a CapTrak camera system (BrainVision, Morrisville, NC) with the left and right tragus and nasion as fiducial landmarks. This allowed for later co-registration with each individuals T1 structural MRI scan and for source-localized analysis (see Data Processing).

Structural MRI acquisition (T1) and processing

For purposes of tFUS neuronavigation and co-registering EEG electrode placement, we obtained a structural T1 MRI scan for each participant. T1 volumes were collected using an 3D MP-RAGE sequence (TR = 2300 ms, TE = 4.5 ms, 1 x 1 x 1.1 mm^3 voxels, field of view 240 x 256 mm^2, 180 sagittal slices) in a Philips Ingenia 3T scanner with a 32-channel head coil. Brainsuite (http://brainsuite.org) was used to process T1s using the cortical extraction sequence and a surface label-registration procedure with the BCI-DNI atlas. After

labeling, we checked the locations and created a mask of either pars opercularis (rIFG group) or the centroid of ipsilateral S1 (control group). This volume labeling and mask creation procedure was used for guiding tFUS target identification.

tFUS targeting, setup and parameters

All stimulation targets were planned prior to subject arrival. We used a Brainsight neuronavigation system (Rogue industries) with subjects' T1 scans to guide placement of the transducer beam profile with respect to each individual's neuroanatomy. First, we created a subject-specific mask from the cortical atlas registration and projected it into the Montreal Neurologic Institute (MNI) coordinate system (Evans et al., 1994). When planning the tFUS target, we considered both MNI coordinates and individual anatomy. For example, neuroimaging studies (Boehler et al., 2010) and metanalysis (Chikazoe et al., 2009; Levy and Wagner, 2011) have shown specific activation of the pars opercularis (around x=48, y=16, z=18) for contrasts of successful inhibition versus Go trials and successful versus failed inhibition trials. In the case of the rIFG group, we first identified these MNI coordinates. Notably, the pars opercularis is an anatomical definition and is often referred to as ventro-lateral prefrontal cortex in neuroimaging studies focused on localization of activity that is functionally related to response inhibition and cognitive control (Levy and Wagner, 2011). During target planning, we confirmed the identified MNI coordinates were inside the anatomical region of the pars opercularis, identified from registering atlas maps to individual anatomy. We also performed visually confirmation that the tFUS target was indeed rostral to the inferior precentral sulcus, dorsal to the sylvian fissure, caudal to the ascending rhomulus of the Sylvain fissure, and ventral to the inferior frontal sulcus (Tomaiuolo et al., 1999). Because significant anatomical variation exists in this region, individual anatomy rather than

coordinates were prioritized when planning the tFUS focus. A mean stimulation location of x = 52 ± 3, y = 15 ± 3, z = 20 ± 5 was recorded across all subjects (MNI coordinates).

For the S1 group, stimulation was targeted near x = 43, y = -29, z = 54 and within the right post-central gyrus. Because we used a single element transducer, with a fixed focal depth of 30mm and a 5mm silicon spacer, all stimulation was done at a penetration depth of 25mm and normal the surface of the scalp.

After EEG setup, we used an infrared optical tracking system (Polars Vicra, NDI Medical) to register the subjects' structural MRI scans in virtual space, with their head and the ultrasound transducer in real space. The alignment and cortical registration were accomplished by registering the individual's T1 derived anatomy using the nasion, tip of the nose, philtrum, and left and right periauricular notch and tragus. To visualize the tFUS target in the cortex, we created a custom design in Solidworks that rendered the transducer housing and ellipsoidal beam profile projection into the registered cortex (Figure 1C). A 3D printed housing was made for the transducer to hold the optical tracking unit and silicon spacer (ss-6060 Silicon Solutions, Cuyahoga Falls, OH http://siliconesolutions.com/ss-6060.html). Acoustic conductive gel was applied to both the transducer and the scalp. After correct placement of the transducer using the neuronavigation, we recorded the coordinates of the stimulation target. Figure 1C shows the rendering from one subject's T1 and scalp in the rIFG group, along with the 3D rendering of the transducer housing (green object) and the pars opercularis mask (white anatomical structure). In the auditory rIFG control group, we employed a sham tFUS (similar to Legon et al., 2018) by placing the gel coated transducer perpendicular to the rIFG target. This sham procedure was done to ensure there was still an auditory effect of the ultrasound (from the pulse repetition frequency) without active stimulation.

The tFUS transducer was held flush to the head with a custom-made, lightweight, elastic mesh cap, which did not interfere with EEG recording. To ensure accurate tFUS placement throughout the experimental session, the rotational and cartesian displacement of the beam profile from the cortical target was tracked. The overall accuracy was measured as deviation from the original alignment of the beam with the anatomical target. During the experimental session, we sampled the position of the tFUS transducer during each break. Accuracy was very high, with an average deviation of ±1.5 mm displacement across all subjects and sessions.

The setup and parameters used for tFUS in this experiment were nearly identical to those used by Legon et al. (2014). We used a broadband, single-element focused ultrasound transducer with a center frequency of 0.5 MHz, a fixed focal depth of 30mm, and a lateral spatial resolution of 4.5 mm^2 and axial spatial resolution of 18mm^2 (Blatek, Inc., State College, PA) (Legon et al., 2014). Prior water tank testing through cadaver skull revealed transcranial spatial-peak pulse average intensity (I_{sppa}) of 5.8 W/cm^2, and the optimal frequencies for tFUS transmission while minimizing cranial attenuation are 0.2 - 0.65 MHz (Hayner and Hynynen, 2001; White et al., 2006).

The tFUS waveforms were generated using a two-channel, 2 MHz function generator (BK Precision) (Legon et al, 2014). Channel 1 was triggered by the presentation computer and produced the pulse repetition frequency (PRF) of 1.0 kHz. This was used to trigger channel 2, which produced short burst at the 0.5 MHz acoustic frequency. The result produced a ultrasound waveform with a carrier frequency of 0.5 MHz, PRF of 1.0KHz, and duty cycle 24%. Each stimulation duration was 0.5 s. The transducer power was driven by sending channel 2's output to a 40-W linear RF amplifier (E&I 240L; Electronics and Innovation). The waveforms were triggered in alignment with experimentally-relevant

temporal events (see description below and Figure 1A). It has been previously verified that the resulting waveform does not incur any heating of skin or skull bone (Legon et al., 2014).

Computational simulation of tFUS propagation

We quantified peak pressure amplitude, peak intensity and accuracy of the beam distribution with tFUS target to rIFG using the pseudospectral simulation method in K-wave (Treeby and Cox, 2010). Reference peak pressure planes for the simulations were derived from a water tank test and previous data (Legon et al., 2014). Simulation parameters were first validated by simulating the transducer in water to compare the simulation results with those from the water tank test. The max pressure plane at the 30-mm focus in the water tank was used as a source input pressure for the transducer during the simulation. The transducer was modeled to have a 30-mm radius of curvature. Water simulations used a homogenously medium of water density (1000 kg/m^3) and speed of sound (1482 m/s). We created a computational grid over a 256 x 256 x 256 with 1-mm spacing. The points per wavelength were 6, Courant–Friedrichs–Lewy = 0.1, and simulation time was set to 6 pulses (duration = 250 μs) to ensure simulation stability.

Simulation of ultrasound through water predicted a max pressure of 1.05 MPa and spatial peak pulse average intensity (Isppa) of 22.4 W/cm^2 at the focus. This prediction closely aligns with previous studies and simulations (Legon et al., 2014) of the same transducer. Comparison of simulations and water data indicated a 97% match of pressure/intensity at the focus taken over a 5 mm^3 voxel section in all 3 planes at the focus. The lateral full-width at half maximum of the max pressure at the beam was 4.39 mm in simulation (Figure 1C).

For simulating transcranial ultrasound, we extracted 3-dimensional maps of the skull from a CT (1-mm resolution) and brain from T1 MRI scan (1-mm resolution) from three preoperative patients at Barrow Neurological institute. The MRI and CT were both co-registered and normalized to the MNI space in SPM12. To mimic our approach of targeting used in the experiments, we surface registered the gray matter volume to the BCI-DNI atlas and identified the centroid of pars opercularis. This allowed us to map from world coordinates of the scan to MNI coordinates of the target (Figure 1D). The average stimulation location for these three subjects was x = 48, y = 18, and z = 6. Conversion from Hounsfield units in the CT to sound speed and density were done using the relations described in Aubry et al. (2003). All skull materials were set using these parameters, while other tissues were treated as homogeneous with parameters set to that of water. Attenuation was modeled as a power law with a $\beta = 0.5$ and absorption was also modeled with a $b = 1.08$ (Treeby and Cox, 2010). Results for this simulation are presented in the Results section.

Experimental Behavioral variables

The main variables under consideration were the Go trial reaction time (Go RT), percentage of successfully inhibited responses on Stop trials (successful stopping) per SSD, failed inhibition reaction time, and SSRT. The SSRT was estimated using a hierarchical Bayesian parametric approach (Matzke et al., 2013a) that allows estimation of the distribution of SSRTs while assuming an ex-gaussian distribution of SSRTs. Importantly, we chose this approach as Matzke et al. (2013a) showed that it performs well even when there are only a few trials available per SSD level. This SSRT estimation procedure was run separately per group (rIFG and S1) and trial types (No-tFUS Stop trials, Go-tFUS Stop trials, and Stop-

tFUS Stop trials). As reported in the Results section, combined RTs from Go trials with and without tFUS were used because stimulation did not alter the Go RT.

EEG artifact removal

Continuous EEG data were first down-sampled to 250 Hz, then high-pass filtered (1 Hz) and re-referenced to the scalp average. Any channels that displayed artifacts for more than 25% of the total session were removed before further processing but were later interpolated after artifact rejection. We removed channels that were designated unsuitable for analysis by visual inspection and absolute temporal standard deviation (> 5) across channels. It is important to note that, in each of the stimulation groups, the cortical sites of rIFG and S1 were close to the F8 and CP4 electrodes. Therefore, these electrodes could not be used for EEG recording in their respective groups and were always interpolated after artifact removal. The remaining data processing involved creating epochs from Stop trials locked to stop signal onset (-100 to 500 ms peristimulus) because our analysis focused on this epoch. Individual epochs were then rejected from further analysis if they contained large scalp EMG or rare events (< 8% of all trials). The ERPs baseline corrected by subtracting the activity from -100 ms to the stop signal. Out of the 53 participants, 3 subjects were excluded from analyses due to EEG recording issues (impedance >25 kΩ across channels). The remaining data were bandpass filtered from 1-25 Hz. EOG artifacts related to eye movements and blinks were removed using Independent Components Analysis using eeglab (ICA; Delorme and Makeig, 2004). On average, 3.35 components were removed per participant. Because we later applied a Hanning taper to the edges of the event-related

potentials (ERP) before dynamic causal modeling, we applied the same procedure to the ERPs after cleaning using a Hanning taper.

Behavior analysis

To quantify how the probability of response inhibition changed over levels of SSD, P(respond|signal), and across tFUS conditions within and across groups we fit a 2-parameter logistic model. This was done to analyze P(respond|signal) as a curve. This was achieved using by fitting the 2-parameter linear mixed-effects model with random intercepts and slopes to obtain subject and condition specific model parameters. P(respond|signal), denoted as p, were converted to a negative logit ($\log((1-p)/p)$ before fitting. As our main goal was to estimate the logistic curve slope (β), we ran the mixed-effects model (using LME4 in R) with the full interaction of SSD and stimulation condition (no-tFUS, Go-tFUS, Stop-tFUS). Logistic slopes per subject were estimated by combining fixed and random coefficients. β parameters were analyzed using a mixed-design ANOVA on β with factors of Group (3 levels) and tFUS (3 levels: No, Go, Stop).

Separating neural components of Go-responses and response-inhibition

Our analysis of ERPs was based on the premises of the Independent Horse Race model (Logan and Cowan, 1984) – which posits independent accumulation of Go and Stop activity till one of them reaches threshold. Due to the nature of measuring these processes through EEG and the inhibitory processes, there is overlap of neural processes related to stopping and going during stop trials. Therefore, we removed Go-related activity from both successfully (SS) and unsuccessfully (SU) inhibited Stop trials through subtracting the Go

ERPs from the Stop ERPs. We used the approach employed by Mattia et al. (2012). On a per-subject basis, we found Go-trial ERPs (No-tFUS and tFUS) that had RTs that were latency-matched to SS trials based on each subject's SSRT. These Go trials had to have RTs either equal to or greater than the SSRT. For SU trials, we found latency-matched Go trials with RTs with a different procedure. We first calculated each subject's mean signal-respond RT for each of the two highest SSDs. We then calculated the difference in SSD (ms) and searched for Go RT trials for each SSD that fell within the mean signal-respond RT ± half the difference of the SSD (ms). This was done to prevent overlap of activity from both faster and slower Go RTs and signal-respond RTs. These steps were performed separately for the highest and second highest SSD. This procedure was done separately for SS and SU trials for both tFUS conditions. After correcting the SS and SU stop trial, the corrected ERPs were averaged across the two highest SSDs per subject (corresponding to the 85% and 105% mean Go RT of each subject). These ERPs were used for the remaining analysis.

Analysis of inhibition-related ERP

Our analysis focused on event-related potentials (ERPs) from source-localized analysis and Dynamic Causal Modeling (DCM; David et al., 2006). The primary motivation for these analyses is that previous work has revealed a set of ERPs that often accompany response inhibition following a Stop signal (reviewed in Huster et al., 2013 and Kenemans, 2015). The main ERPs found in inhibitory tasks include a N2/P3 complex that has a fronto-central and radial topography. This component has been hypothesized to be generated mainly by the pre-SMA/SMA in the medial frontal cortex (Huster et al., 2013) and has been considered to reflect a critical signature of reactive stopping elicited by stop signal tasks (Kenemans, 2015; Wessel and Aron, 2017). Furthermore, the P300 of this complex has been proposed to be a

relevant marker of stopping efficiency, given that it predicts the SSRT (Wessel and Aron, 2015) and successful versus failed inhibition (Kok et al., 2003). The ERP associated with stopping in rIFG is typically associated with a negative amplitude difference comparing successful and failed stopping that emerges around 200 ms (N200; Schmajuk et al., 2006). We examined these ERPs and P/N100 responses which are sometimes elicited over sensory areas, depending on whether the stimuli used for Go and Stop signals are in the same sensory modality (Kenemans, 2015). By combining tFUS and EEG, we can examine some of the issues that are addressed by ongoing debate, i.e., which of these potentials are stopping-relevant, and how their activity is generated by a network model through DCM – all without signal interference induced by stimulation.

Scalp space analysis.

To examine the standard ERP effects typically found in the SST, we first examined activity at the sensor level. This was done using permutation-based dependent samples t-tests. Spatiotemporal activity was examined and multiple-comparison corrected for using a cluster-based p-value correction of $p < 0.01$ and 5000 permutations for each contrast considered. The contrasts included comparison of (1) successful stop (SS) – unsuccessful stopp (US) trials over Go-tFUS and Stop-tFUS conditions, a (2) SS (No-tFUS) – SS (Stop-tFUS) contrast, and (3) and interaction contrast comparing SS – SU difference between the No-tFUS and Stop-tFUS conditions. The first contrast is typically used to determine which areas exhibit ERPs (or brain areas) that differentiate successful inhibition (Swaan et al., 2012). The third contrast (interaction) was used to determine how the SS-SU contrast differed between No-tFUS and Stop-tFUS conditions. The second contrast was the main focus of our analysis and was used to determine which scalp ERPs differentiated successful stopping in the No-

tFUS and Stop-tFUS conditions. We anticipated that this contrast would reflect processes that mainly include those responsible for both the success and efficiency of inhibitory processes, e.g., SSRT.

P300 onset and SSRT tFUS effects

Recent work has indicated that the frontocentral P300 onset latency is related to the SSRT (Wessel and Aron, 2015). Therefore, we hypothesized that tFUS altered inhibition through the SSRT and expected a shift in this latency as well. We calculated the shift in P300 onset crossings between tFUS conditions in two steps. First, we took the across-subject mean frontocentral ERP waveform in a time-window of ±50 ms around the zero-crossing. To calculate each subject's zero-crossing time, we calculated the dynamic time warping distance from the template mean ERP to the subject's ERP. Second, this distance was added to the median zero-crossing time to obtain an individual subject crossing for both the No-tFUS- and Stop tFUS-locked conditions.

Source localization

To estimate the activity in source space from the sensor recordings, we used a group inversion with the multiple sparse-priors approach as implemented in SPM12. The individual subject data passed to the inversion routine were mean sensor ERPs per condition. We performed the group inversion only for the rIFG groups and analysis because this was the only group to exhibit behavioral effects from tFUS. In this procedure, the individual's recorded electrode locations and individual T1 were warped to the default MNI anatomical brain and cortical mesh provided in SPM. These meshes were used to calculate the forward solution using a boundary element head model. All conditions were used in the group

inversion routine. Because the multiple sparse-priors approach attempts to fit the sensor data with respect to the lead-field matrix, we performed the inversion over a window starting from the stop signal up to 500 ms. While narrow windows are considered better for time-resolved estimation, we wanted to estimate overall changes in activity using the same window we would employ later for dynamic causal modeling.

Source analysis: Whole-brain contrasts and regression

Based on examination of the sensor level data, we first identified time windows surrounding the ERPs discussed above (N100, N200, and P300). To balance the number of points contributing to the source estimate used for analysis, we used the same window size for estimating the source activity of each ERP. The time windows were centered around the across-subject mean peak activity of each ERP with a window of ±40 ms. These time windows were used to create 3D source image activity interpolated into MNI voxel space for each subject and condition. The resulting images were spatially smoothed (6 mm full-width half maximum) evoked power from 1-25 Hz. We used evoked power because we were concerned with 'activation' and time window, but not the direction of voltage deflection. This choice was driven by the fact that we already established the canonical inhibition related ERPs at the scalp level. These evoked images were analyzed used a flexible factorial design to implement a repeated-measures ANOVA, including all main effects and interactions. The factors included (1) inhibition success (SS or SU trial), and (2) stimulation condition (No-tFUS or Stop tFUS). The resulting statistical parametric maps were analyzed with a threshold set at $p < 0.005$ (peak-level, uncorrected) and cluster-wise FWE $p < 0.05$. For expositional brevity, these SPMs are presented in the supplementary material except for the conjunction F-contrast showing the overlap of the SS-SU and tFUS F-contrasts. This conjunction shown

in the main text both confirms the differential SS-SU effect in rIFG and the spatially precise impact of tFUS.

We also conducted a whole-brain SPM linear regression using the same time windows identified above. We regressed the difference in evoked activity between No-tFUS and Stop-tFUS SS trials against the difference in each subject's SSRT for these conditions. Using this approach, we examined both positive and negative contrasts (t-tests) in each window. This analysis was done to (1) determine prior source locations for the DCM analysis (see below) and (2) identify which areas predicted the change in SSRT due to tFUS. Because a primary goal was determining DCM priors, we used a lenient uncorrected cluster threshold of $P < 0.01$ and a minimum cluster-extant threshold of 20 voxels.

Dynamic Causal Modeling (DCM)

To model the connectivity of the network involved in successful stopping, we used the canonical microcircuit model (Bastos et al., 2012) for all areas except the contralateral motor cortex. For left motor cortex (M1), we used a recently developed version built-off the canonical microcircuit that more closely resembles the agranular structure of M1 (Bhatt et al., 2016). Our sequential model building and analysis focused both on a priori areas of interest that have been well described in response inhibition literature (e.g., Wessel and Aron, 2017) – including rIFG, rpre-SMA, rDLPFC – and those areas that we identified in comparing the effects of Stop tFUS and No-tFUS changes in SSRT on evoked power. Given the typically right-lateralized areas found to be modulated by inhibition, we focused mainly on pathways on the right hemisphere. We used source locations identified in both (1) the regression of change in SSRT and (2) the whole-brain SPM interaction F-contrasts examining locations for which Stop-tFUS and No-tFUS were different for the SS-SU

comparison. The significant source cluster peaks ($P < 0.01$ threshold) revealed by these analysis were labeled using the AAL atlas labeling toolbox, and used to identify source coordinates in MNI space ([x,y,x]: rIFG [48,28,4]; pre-SMA [6, 24, 54]; rDLPFC [30, 28, 40]; rParietal [10,-74,56]; rTemporal [52,-18,-12]; LM1 [-37,-25,-62]; right inferior occipital gyrus (rIOG) [46, -76,10]). These source locations are in general agreement with previous literature in both fMRI, EEG, and MEG studies of SSTs (Aron et al., 2006; Boehler et al., 2010; Rae et al., 2014) and meta-analyses of cortical locations and boundaries (Chikazoe et al., 2009). In building the model, we also included a hidden deep source to model the potential connectivity effects to and from cortical sources. Because the main output of the basal ganglia mediating inhibition and responding is the thalamus, we used a source location [4, -16, -2] identified during a previous fMRI stop signal study (Boehler et al., 2010). This approach of using a deep source node in DCM for EEG has been previously employed by David et al. (2011). In the DCM, we used an equivalent current dipole model and allowed the inversion process to optimize the source locations.

To determine the appropriate model connectivity structure, we first examined the grand mean ERP data in SS No-tFUS trials from a window spanning 0 – 500 ms. Recent work has shown that estimating the model structure from grand means (across subjects) is sufficient and provides a close approximation to fixed-effects selection when using ERP data (Litvak et al., 2015) rather than fitting DCMs across all subjects for each variation in connection structures.

To optimize the model structure, we performed Bayesian model selection using family-wise fixed effects in several iterations. In the first set of iterations, we inverted 48 different models from the grand mean data, and then partitioned it into several families (Penny et al., 2010). These families were based on (1) the structure of the pre-frontal

hierarchy (Figure S1), (2) structure of the lower hierarchy (Figure S1), (3) whether exogenous inputs were supplied to right inferior occipital gyrus (rIOG), rIFG, or both, and (4) whether the cortical nodes projecting to the hidden deep source were of the forward or backward type. Inputs were modeled as a Gaussian bump with a prior onset of 60 ms. With respect to comparison (4), pulling evidence from previous inhibitory control, primate tracing, and tractography studies and reviews, the areas we examined for different connections projecting to the deep node included rIFG, pre-SMA, right dorsolateral prefrontal cortex (rDLPFC) and rIOG. A backward connection from M1 to the deep node was also included based on putative M1 to basal ganglia connections (Nambu et al., 2002). Because the efferent connections from Thalamus output is excitatory and has been found to target deep pyramidal layers (Yamawaki et al., 2014), the above listed areas all received forward connections from the deep source.

In this modeling, we assumed hierarchically connected areas always entailed a backward and forward connection between nodes. Nodes that were lateral in a hierarchy were supplied with both forward and backward nodes (Figure S1). A final note is on the connections between lower areas and prefrontal areas. Rather than optimize all possible connection permutations, we chose to instantiate connections that reflect the cognitive and attentional control-related differences typically postulated to operate in dorsal and ventral pathways (Corbetta and Shulman, 2001). Both streams received forward input from rIOG. The ventral stream included a forward connection from rTemporal cortex to rIFG. The dorsal stream included forward projections from rParietal to both rDLPFC and pre-SMA.

After inversion of each model, we used a fixed-effects Bayesian model selection to perform family inference and calculate the model posterior probability to determine the winning model in each family. The family model probability results from these four different

family comparisons are shown in Figure S2. This analysis indicated that, across families, the winning model had (1) a prefrontal hierarchy with laterally connected rDLPFC and rIFG above pre-SMA, (2) a parallel structure of rParietal and rTemporal cortices without a lateral connection, (3) exogenous inputs to both rIOG and rIFG, and (4) backward cortical to deep connections. A diagram of the final model structure is shown in the DCM results section.

The next step in model building involved determining which connections were modulated by conditions specific changes between No-tFUS SS and SU trials and, primarily, between No-tFUS SS and Stop-tFUS SS trials. For our purposes, this included extrinsic connections between areas and intrinsic gain connections within an area. Instead of testing an expansive set of permutations of condition-specific modulations of extrinsic connections (B matrix in DCM), we a priori opted to use the recently developed Parametric Empirical Bayesian modeling framework for DCM (Friston et al., 2016). As will be explained below, this involves doing Bayesian statistics on full DCMs that will have all condition modulatory parameters of interest entered a hierarchal-general linear model from which hypotheses can be tested. This obviates the need for conventional statistics and model reduction over all extrinsic connections. If a DCM model is referred to as full, this includes condition-driven modulations of all extrinsic connections. Otherwise it includes an explicitly stated set of connections.

After determining a model structure, we inverted this model for each subject's ERPs. This inversion was performed twice, using different combinations of trials to assess different hypotheses. The DCM was first inverted using the No-tFUS SU and SS trial ERPs. The SU trial was set as the baseline. This inversion allowed us to first compare how the network connections were modulated between SU and SS trials in a baseline network without the effects of tFUS. Specifically, we wanted to examine how changes in connectivity (DCM B

matrix) distinguished between unsuccessful and successful inhibition. Analysis of this general linear model (described below) focused on the B matrix which describes how connections changed between conditions. This comparison was done to mirror the standard comparison of SS and SU trials that is typically employed to reveal what inhibitory mechanisms were more potently activated during SS trials (Aron et al, 2014). Furthermore, using this contrast of conditions provides a baseline to ask whether the same connectivity mechanisms were altered when comparing No-tFUS and Stop-tFUS SS trials. Therefore, the second DCM model inversion was applied to the No-tFUS and Stop-tFUS SS trials. The No-tFUS trials were used as a baseline for the fit. Again, this allowed a focus on the connectivity modulation between the two conditions and treated the non-stimulation condition as the baseline network.

To analyze the resultant DCM condition-specific changes and the modulation of connectivity parameters by experiment relevant variables (e.g., SSRT), we tested group-level effects using the Parametric Empirical Bayes (PEB) framework. We give a brief overview of PEB (for in-depth discussion, see Friston et al., 2016) for hypothesis testing and connectivity parameter extraction using a PEB. Building a PEB statistical model involves creating a hierarchical model with, in our case, two levels. The lower level is the subject level, which is the results of DCM fits to individual's ERP data. This first level includes the posterior means and uncertainties for each subject's DCM connectivity parameters. The PEB framework statistically models these parameters using a Bayesian general linear model (GLM) at the group level. As is the case with GLMs (and mixed models), the model attempts to explains the connectivity parameters as between-subject and within-subject variability, while allowing for between-subject differences in connectivity parameters to be treated as random effects. The PEB Bayesian GLM allows using subject-based DCM parameters to be examined using

a linear model with respect to explanatory variables at the between-subject (group) level. Because the PEB framework yields group-level estimates as empirical priors, this approach also allows changing parameters that were estimated at the subject level by allowing them to be estimates distributed around a group mean effect. This process stands in contrast to the typically used "summary statistic" approach, which often involves applying several t-tests or correlations per connection.

For clarity, we built two separate PEB models for the DCMs fit to (1) No-tFUS SU and SS trials, and (2) No-tFUS and Stop-tFUS SS trials. The former PEB model was used to test hypotheses regarding mean changes in connectivity between unsuccessful and successful inhibition at baseline (No-tFUS). The latter PEB model was used to address (1) how the inhibition network connectivity changed on average between tFUS conditions (intercept in GLM), and (2) how individual differences in the change in SSRT between tFUS conditions was embedded in changes in connectivity parameters across subjects (covariate). Therefore, in the first model we only used the mean intercept as the explanatory variable to examine mean changes in connectivity between No-tFUS SU and SS trials. The mean change parameters represent the gain change in connectivity going from SU to SS trials. In the second model, which examined No-tFUS SS and Stop-tFUS SS trials, we used a design matrix of explanatory variables that included an (1) intercept representing mean changes in connectivity (mean tFUS effect), (2) the change in individual subject's SSRT between tFUS conditions, and (3) the tFUS change in individual subject SSRT variability. Before entering the SSRT covariates, they were transformed to a gain change by taking the log-ratio of Stop-tFUS SSRT (mean or variability) over the No-tFUS SSRT (mean or variability). The covariates were then z-scored to have a zero mean and yield standardized PEB model parameters.

When initially estimating each of the two PEBs, we always entered in the full model including all extrinsic and intrinsic connection modulatory parameters. Because our hypotheses centered around changes along prefrontal and deep areas, and ventral pathway interactions, we first compared the PEB model with and without dorsal pathway connection parameters. We show in the results that, across both PEBs, the model without dorsal pathway connection changes yielded a better model with respect to the explanatory variables. This allowed a substantial reduction in connectivity parameters needing to be tested.

Once the group-level GLM parameters were estimated with respect to modulations of extrinsic and intrinsic connectivity, we used this framework to test several hypotheses regarding mean and SSRT driven changes in connectivity parameters. Hypothesis testing proceeds by Bayesian model reduction of the GLM. This involves turning off/on different connectivity parameters and comparing the free energy of reduced models. Comparing models in this manner is similar to performing classical hypothesis testing via model reduction in mixed models by employing likelihood ratio or F-tests.

Hypotheses were tested by designing models with different combinations of parameters on/off. The model space of these hypotheses was defined in a factorial space that focused on 4 factors that could be modulated by mean connectivity changes (PEBs 1 and 2) or connectivity modulation via tFUS induced changes in SSRT (PEB 2). These factor/hypothesis spaces were driven by previous work. The first set of models considered how inhibition is related to pathways the backward connections from rIFG and pre-SMA to the deep (i.e., basal ganglia) nodes. The second factor, driven by work indicating that pre-SMA interacts with rIFG before deep projections (Rae et al., 2009), tested for modulation of their backwards and forwards connections. The third factor was motivated by proposals that differences in inhibition (SS vs. SU) might be mediated changes in attentional orienting,

which predict changes in intrinsic self-inhibitory gain in either rIFG, rIOG, or both. Therefore, this factor examined for modulation of the superficial pyramidal cell gain across the nodes. Finally, to examine how SS versus SU and different tFUS effects on inhibition depend on top-down vs bottom-up processing, our final comparison tested for the inclusion of either backward, forward or both sets of connections along the ventral pathway. Given that each of 4 factors had 3 levels each, plus a null (all zero) model, the first PEB surmounted to testing 3^4+1 (82) models, and PEB model 2 included $2*3^4+1$ (163) models.

Rather than summarize these effects as the free energy for each model, which would surmount to a severe reduction in discerning the probability of a winning model, the hypotheses were grouped into families, and model hypotheses were tested at the family level. After using family model comparison on reduced GLMs, we used Bayesian model averaging (BMA) to obtain GLM model estimates of connectivity parameters having a posterior probability >95%. BMA was performed on all families within a factor, weighting the summarized parameters by the probability of the family. For example, BMA parameters for the second PEB mode that includes the mean SSRT as a predictor, for example, should be interpreted as would a linear regression coefficient; similarly, the mean term would represent the mean change in connectivity. These BMA parameters were reported as the final changes in connectivity and should be considered to have a 95% probability of being non-zero.

Before conducting our main analysis presented, and to reduce the model space, we first considered whether the best PEB model would include ventral and dorsal pathway projections after fitting to individual subjects. Specifically, we asked if describing the baseline difference of no-tFUS SS and SU inhibition involved modulation of either or both the dorsal and ventral pathways. Using the family-based hypothesis comparisons test described above for PEBs, we created factor spaces including the dorsal, ventral, or both pathways. Both sets

of pathways included top-down and bottom-up connections that were grouped together. The dorsal pathway included the rParietal and rDLPFC nodes and the ventral pathway included rIFG and rTemporal. Bayesian model comparison (probability = 1) revealed strong evidence in favor of the model with just ventral pathway connection modulations from SU to SS trials. Based on this result, we excluded dorsal pathway connections from the rest of our DCM analysis to reduce the space of parameters.

SUPPLEMETNAL INFORMATION

See Appendix D for supplemental information

REFERENCES

Aron, A.R., Fletcher, P.C., Bullmore, E.T., Sahakian, B.J., and Robbins, T.W. (2003). Stop-signal inhibition disrupted by damage to right inferior frontal gyrus in humans. Nature neuroscience 6, 115-116.

Aron, A.R., Herz, D.M., Brown, P., Forstmann, B.U., and Zaghloul, K. (2016). Frontosubthalamic Circuits for Control of Action and Cognition. Journal of Neuroscience 36, 11489-11495.

Aron, A.R., and Poldrack, R.A. (2006). Cortical and subcortical contributions to stop signal response inhibition: role of the subthalamic nucleus. Journal of Neuroscience 26, 2424-2433.

Aron, A.R., Robbins, T.W., and Poldrack, R.A. (2014). Inhibition and the right inferior frontal cortex: one decade on. Trends in cognitive sciences 18, 177-185.

Aubry, J.-F., Tanter, M., Pernot, M., Thomas, J.-L., and Fink, M. (2003). Experimental demonstration of noninvasive transskull adaptive focusing based on prior computed tomography scans. The Journal of the Acoustical Society of America 113, 84-93.

Auksztulewicz, R., and Friston, K. (2015). Attentional enhancement of auditory mismatch responses: a DCM/MEG study. Cerebral cortex 25, 4273-4283.

Baddeley, A.D., and Della Sala, S. (1996). Working memory and executive control. Philosophical Transactions of the Royal Society of London Series B: Biological Sciences 351, 1397-1404.

Bari, A., and Robbins, T.W. (2013). Inhibition and impulsivity: behavioral and neural basis of response control. Progress in neurobiology 108, 44-79.

Bastos, A., Usrey, W., Adams, R., Mangun, G., Fries, P., and Friston, K. (2012). 871 Canonical Microcircuits for Predictive Coding. Neuron 76, 695-711.

Bates, D., Mächler, M., Bolker, B., and Walker, S. (2014). Package Lme4: Linear Mixed-Effects Models Using Eigen and S4, Vol 67.

Bhatt, M.B., Bowen, S., Rossiter, H.E., Dupont-Hadwen, J., Moran, R.J., Friston, K.J., and Ward, N.S. (2016). Computational modelling of movement-related beta-oscillatory dynamics in human motor cortex. Neuroimage 133, 224-232.

Boehler, C.N., Appelbaum, L.G., Krebs, R.M., Hopf, J.-M., and Woldorff, M.G. (2010). Pinning down response inhibition in the brain—conjunction analyses of the stop-signal task. Neuroimage 52, 1621-1632.

Boehler, C.N., Münte, T.F., Krebs, R.M., Heinze, H.-J., Schoenfeld, M.A., and Hopf, J.-M. (2009). Sensory MEG responses predict successful and failed inhibition in a stop-signal task. Cerebral Cortex 19, 134-145.

Cai, W., and Leung, H.-C. (2011). Rule-guided executive control of response inhibition: functional topography of the inferior frontal cortex. PloS one 6, e20840.

Chambers, C.D., Bellgrove, M.A., Stokes, M.G., Henderson, T.R., Garavan, H., Robertson, I.H., Morris, A.P., and Mattingley, J.B. (2006). Executive "brake failure" following deactivation of human frontal lobe. Journal of cognitive neuroscience 18, 444-455.

Chambers, C.D., Garavan, H., and Bellgrove, M.A. (2009). Insights into the neural basis of response inhibition from cognitive and clinical neuroscience. Neuroscience & biobehavioral reviews 33, 631-646.

Chatham, C.H., Claus, E.D., Kim, A., Curran, T., Banich, M.T., and Munakata, Y. (2012). Cognitive control reflects context monitoring, not motoric stopping, in response inhibition. PloS one 7, e31546.

Chikazoe, J., Jimura, K., Asari, T., Yamashita, K.-i., Morimoto, H., Hirose, S., Miyashita, Y., and Konishi, S. (2009). Functional dissociation in right inferior frontal cortex during performance of go/no-go task. Cerebral Cortex 19, 146-152.

Corbetta, M., and Shulman, G.L. (2002). Control of goal-directed and stimulus-driven attention in the brain. Nature reviews neuroscience 3, 201-215.

Crone, E.A., Wendelken, C., Donohue, S.E., and Bunge, S.A. (2006). Neural evidence for dissociable components of task-switching. Cerebral cortex 16, 475-486.

David, O., Kiebel, S.J., Harrison, L.M., Mattout, J., Kilner, J.M., and Friston, K.J. (2006). Dynamic causal modeling of evoked responses in EEG and MEG. NeuroImage 30, 1255-1272.

David, O., Maess, B., Eckstein, K., and Friederici, A.D. (2011). Dynamic causal modeling of subcortical connectivity of language. Journal of Neuroscience 31, 2712-2717.

Delorme, A., and Makeig, S. (2004). EEGLAB: an open source toolbox for analysis of single-trial EEG dynamics including independent component analysis. Journal of neuroscience methods 134, 9-21.

Duann, J.-R., Ide, J.S., Luo, X., and Li, C.-s.R. (2009). Functional connectivity delineates distinct roles of the inferior frontal cortex and presupplementary motor area in stop signal inhibition. Journal of Neuroscience 29, 10171-10179.

Erika-Florence, M., Leech, R., and Hampshire, A. (2014). A functional network perspective on response inhibition and attentional control. Nature communications 5, 1-12.

Evans, A.C., Kamber, M., Collins, D., and MacDonald, D. (1994). An MRI-based probabilistic atlas of neuroanatomy. In Magnetic resonance scanning and epilepsy (Springer), pp. 263-274.

Fardo, F., Auksztulewicz, R., Allen, M., Dietz, M.J., Roepstorff, A., and Friston, K.J. (2017). Expectation violation and attention to pain jointly modulate neural gain in somatosensory cortex. Neuroimage 153, 109-121.

Feldman, H., and Friston, K. (2010). Attention, uncertainty, and free-energy. Frontiers in human neuroscience 4, 215.

Fini, M., and Tyler, W.J. (2017). Transcranial focused ultrasound: a new tool for non-invasive neuromodulation. International Review of Psychiatry, 1-10.

Forstmann, B.U., Dutilh, G., Brown, S., Neumann, J., Von Cramon, D.Y., Ridderinkhof, K.R., and Wagenmakers, E.-J. (2008). Striatum and pre-SMA facilitate decision-making under time pressure. Proceedings of the National Academy of Sciences 105, 17538-17542.

Friston, K.J., Litvak, V., Oswal, A., Razi, A., Stephan, K.E., Van Wijk, B.C., Ziegler, G., and Zeidman, P. (2016). Bayesian model reduction and empirical Bayes for group (DCM) studies. Neuroimage 128, 413-431.

Hampshire, A., Chamberlain, S.R., Monti, M.M., Duncan, J., and Owen, A.M. (2010). The role of the right inferior frontal gyrus: inhibition and attentional control. Neuroimage 50, 1313-1319.

Hampshire, A., and Sharp, D.J. (2015). Contrasting network and modular perspectives on inhibitory control. Trends in cognitive sciences 19, 445-452.

Hayner, M., and Hynynen, K. (2001). Numerical analysis of ultrasonic transmission and absorption of oblique plane waves through the human skull. The Journal of the Acoustical Society of America 110, 3319-3330.

Haynes, W.I., and Haber, S.N. (2013). The organization of prefrontal-subthalamic inputs in primates provides an anatomical substrate for both functional specificity and integration: implications for Basal Ganglia models and deep brain stimulation. J Neurosci 33, 4804-4814.

Hu, S., Ide, J.S., Zhang, S., and Chiang-shan, R.L. (2015). Anticipating conflict: neural correlates of a Bayesian belief and its motor consequence. Neuroimage 119, 286-295.

Huster, R.J., Enriquez-Geppert, S., Lavallee, C.F., Falkenstein, M., and Herrmann, C.S. (2013). Electroencephalography of response inhibition tasks: functional networks and cognitive contributions. International Journal of Psychophysiology 87, 217-233.

Ide, J.S., Shenoy, P., Angela, J.Y., and Chiang-Shan, R.L. (2013). Bayesian prediction and evaluation in the anterior cingulate cortex. Journal of Neuroscience 33, 2039-2047.

Jahfari, S., Waldorp, L., van den Wildenberg, W.P., Scholte, H.S., Ridderinkhof, K.R., and Forstmann, B.U. (2011). Effective connectivity reveals important roles for both the hyperdirect (fronto-subthalamic) and the indirect (fronto-striatal-pallidal) fronto-basal ganglia pathways during response inhibition. Journal of Neuroscience 31, 6891-6899.

Kenemans, J.L. (2015). Specific proactive and generic reactive inhibition. Neuroscience & Biobehavioral Reviews 56, 115-126.

Lee, W., Kim, H.-C., Jung, Y., Chung, Y.A., Song, I.-U., Lee, J.-H., and Yoo, S.-S. (2016). Transcranial focused ultrasound stimulation of human primary visual cortex. Scientific Reports 6, 34026.

Legon, W., Bansal, P., Tyshynsky, R., Ai, L., and Mueller, J.K. (2018). Transcranial focused ultrasound neuromodulation of the human primary motor cortex. Scientific reports 8, 1-14.

Legon, W., Sato, T.F., Opitz, A., Mueller, J., Barbour, A., Williams, A., and Tyler, W.J. (2014). Transcranial focused ultrasound modulates the activity of primary somatosensory cortex in humans. Nat Neurosci 17, 322-329.

Levy, B.J., and Wagner, A.D. (2011). Cognitive control and right ventrolateral prefrontal cortex: reflexive reorienting, motor inhibition, and action updating. Ann N Y Acad Sci 1224, 40-62.

Litvak, V., Garrido, M., Zeidman, P., and Friston, K. (2015). Empirical Bayes for group (DCM) studies: a reproducibility study. Frontiers in human neuroscience 9, 670.

Logan, G.D., and Cowan, W.B. (1984). On the ability to inhibit thought and action: A theory of an act of control. Psychological review 91, 295.

Mallet, N., Schmidt, R., Leventhal, D., Chen, F., Amer, N., Boraud, T., and Berke, J.D. (2016). Arkypallidal cells send a stop signal to striatum. Neuron 89, 308-316.

Mathôt, S., Schreij, D., and Theeuwes, J. (2012). OpenSesame: An open-source, graphical experiment builder for the social sciences. Behavior research methods 44, 314-324.

Mattia, M., Spadacenta, S., Pavone, L., Quarato, P., Esposito, V., Sparano, A., Sebastiano, F., Di Gennaro, G., Morace, R., and Cantore, G. (2012). Stop-event-related potentials from intracranial electrodes reveal a key role of premotor and motor cortices in stopping ongoing movements. Frontiers in neuroengineering 5, 12.

Matzke, D., Love, J., Wiecki, T.V., Brown, S.D., Logan, G.D., and Wagenmakers, E.-J. (2013). Release the BEESTS: Bayesian estimation of ex-Gaussian stop-signal reaction time distributions. Frontiers in Psychology 4, 918.

Moran, R.J., Campo, P., Symmonds, M., Stephan, K.E., Dolan, R.J., and Friston, K.J. (2013). Free energy, precision and learning: the role of cholinergic neuromodulation. Journal of Neuroscience 33, 8227-8236.

Morein-Zamir, S., Dodds, C., van Hartevelt, T.J., Schwarzkopf, W., Sahakian, B., Müller, U., and Robbins, T. (2014). Hypoactivation in right inferior frontal cortex is specifically associated with motor response inhibition in adult ADHD. Human brain mapping 35, 5141-5152.

Munakata, Y., Herd, S.A., Chatham, C.H., Depue, B.E., Banich, M.T., and O'Reilly, R.C. (2011). A unified framework for inhibitory control. Trends in cognitive sciences 15, 453-459.

Obeso, I., Robles, N., Muñoz-Marrón, E., and Redolar-Ripoll, D. (2013). Dissociating the role of the pre-SMA in response inhibition and switching: a combined online and offline TMS approach. Frontiers in human neuroscience 7, 150.

Opitz, A., Legon, W., Rowlands, A., Bickel, W.K., Paulus, W., and Tyler, W.J. (2013). Physiological observations validate finite element models for estimating subject-specific electric field distributions induced by transcranial magnetic stimulation of the human motor cortex. Neuroimage 81, 253-264.

Penny, W.D., Stephan, K.E., Daunizeau, J., Rosa, M.J., Friston, K.J., Schofield, T.M., and Leff, A.P. (2010). Comparing families of dynamic causal models. PLoS Comput Biol 6, e1000709.

Plaksin, M., Kimmel, E., and Shoham, S. (2016). Cell-Type-Selective Effects of Intramembrane Cavitation as a Unifying Theoretical Framework for Ultrasonic Neuromodulation. eneuro 3, ENEURO. 0136-0115.2016.

Rademacher, J., Morosan, P., Schormann, T., Schleicher, A., Werner, C., Freund, H.-J., and Zilles, K. (2001). Probabilistic mapping and volume measurement of human primary auditory cortex. Neuroimage 13, 669-683.

Rae, C.L., Hughes, L.E., Anderson, M.C., and Rowe, J.B. (2015). The prefrontal cortex achieves inhibitory control by facilitating subcortical motor pathway connectivity. Journal of neuroscience 35, 786-794.

Ray Li, C.-s., Huang, C., Constable, R.T., and Sinha, R. (2006). Imaging Response Inhibition in a Stop-Signal Task: Neural Correlates Independent of Signal Monitoring and Post-Response Processing. The Journal of Neuroscience 26, 186-192.

Sato, T., Shapiro, M.G., and Tsao, D.Y. (2018). Ultrasonic neuromodulation causes widespread cortical activation via an indirect auditory mechanism. Neuron 98, 1031-1041. e1035.

Schmajuk, M., Liotti, M., Busse, L., and Woldorff, M.G. (2006). Electrophysiological activity underlying inhibitory control processes in normal adults. Neuropsychologia 44, 384-395.

Sharp, D., Bonnelle, V., De Boissezon, X., Beckmann, C., James, S., Patel, M., and Mehta, M.A. (2010). Distinct frontal systems for response inhibition, attentional capture, and error processing. Proceedings of the National Academy of Sciences 107, 6106-6111.

Shulman, G.L., Astafiev, S.V., Franke, D., Pope, D.L., Snyder, A.Z., McAvoy, M.P., and Corbetta, M. (2009). Interaction of stimulus-driven reorienting and expectation in ventral and dorsal frontoparietal and basal ganglia-cortical networks. Journal of Neuroscience 29, 4392-4407.

Swann, N.C., Cai, W., Conner, C.R., Pieters, T.A., Claffey, M.P., George, J.S., Aron, A.R., and Tandon, N. (2012). Roles for the pre-supplementary motor area and the right inferior frontal gyrus in stopping action: Electrophysiological responses and functional and structural connectivity. NeuroImage 59, 2860-2870.

Tomaiuolo, F., MacDonald, J., Caramanos, Z., Posner, G., Chiavaras, M., Evans, A.C., and Petrides, M. (1999). Morphology, morphometry and probability mapping of the pars opercularis of the inferior frontal gyrus: an in vivo MRI analysis. European Journal of Neuroscience 11, 3033-3046.

Treeby, B.E., and Cox, B.T. (2010). k-Wave: MATLAB toolbox for the simulation and reconstruction of photoacoustic wave fields. BIOMEDO 15, 021314.

Verbruggen, F., Aron, A.R., Stevens, M.A., and Chambers, C.D. (2010). Theta burst stimulation dissociates attention and action updating in human inferior frontal cortex. Proceedings of the National Academy of Sciences 107, 13966-13971.

Verbruggen, F., and Logan, G.D. (2009). Models of response inhibition in the stop-signal and stop-change paradigms. Neuroscience & Biobehavioral Reviews 33, 647-661.

Vossel, S., Thiel, C.M., and Fink, G.R. (2006). Cue validity modulates the neural correlates of covert endogenous orienting of attention in parietal and frontal cortex. Neuroimage 32, 1257-1264.

Wessel, J.R., and Aron, A.R. (2015). It's not too late: The onset of the frontocentral P3 indexes successful response inhibition in the stop-signal paradigm. Psychophysiology 52, 472-480.

Wessel, J.R., and Aron, A.R. (2017). On the globality of motor suppression: unexpected events and their influence on behavior and cognition. Neuron 93, 259-280.

White, P.J., Clement, G.T., and Hynynen, K. (2006). Local frequency dependence in transcranial ultrasound transmission. Physics in medicine and biology 51, 2293-2305.

Wiecki, T.V., and Frank, M.J. (2013). A computational model of inhibitory control in frontal cortex and basal ganglia. Psychological Review 120, 329.

Xu, K.Z., Anderson, B.A., Emeric, E.E., Sali, A.W., Stuphorn, V., Yantis, S., and Courtney, S.M. (2017). Neural basis of cognitive control over movement inhibition: human fMRI and primate electrophysiology evidence. Neuron 96, 1447-1458. e1446.

Yamawaki, N., Borges, K., Suter, B.A., Harris, K.D., and Shepherd, G.M. (2014). A genuine layer 4 in motor cortex with prototypical synaptic circuit connectivity. Elife 3, e05422

CHAPTER 6

SUMMARY AND CONCLUSIONS

The field of ultrasound neurostimulation is still in its infancy but is rapidly developing. Chapter 1 of this document explores the efficacy and applications of tFUS for the purposes of treating neuropsychiatric maladaptive patterns by describing ultrasound as a neurostimulation modality for clinical applications, and summarizing the initial work that has been done on ultrasound neuromodulation for a clinical audience. It can be concluded that low-intensity ultrasound can modulate intact brain circuits using nonthermal vibratory mechanisms. Although the elective parameter space is yet unexplored, and the mechanism(s) of action are not fully understood, the modality is safe, and its capacity of modulating the brain in a focused manner is clear.

One of the most critical elements to mental health and well-being is related to the interaction of attention and emotion. There is a growing body of evidence that a few structures forming the cingulo-opercular network are critical to establishing and maintaining executive attention (Sadaghiani and D'Esposito, 2015) while also being involved in emotional processing. This includes the dorsal anterior cingulate (dACC) and anterior insula along with the basal ganglia (Posner, 2011). Functional imaging shows that the cingulo-opercular network demonstrates demand-modulated activity in a broad range of cognitive tasks across sensory modalities, including word recognition, spatial attention (Eckert et al., 2009), sustained focus (Dosenbach et al., 2007), meditation (Hölzel et al., 2007), and may causally act for network switching between the DMN and DAN. For this reason the dACC and the anterior insula were targeted with tFUS to observe the resultant effects on cognitive control and emotional processing.

Chapter 2 targets the dACC with tFUS while subjects performed a modified version of the Erikson flanker task with fear and neutral faces in the background as distractors. The results indicate that tFUS to the dACC induced physiologic and behavioral effects that might be expected from the relaxed concentration and emotional acceptance seen in meditation. Compared with Sham, the tFUS group demonstrated reduced reaction time slowing in response to fearful and neutral faces, and faster reaction times than Sham on incongruent trials. Additionally, an increase rather than a decrease in HRV was observed at the onset of face distractors and stimulation, inferring that stimulation to the dACC causally induced parasympathetic activity. tFUS enhanced early ERP components and altered ERP components associated with emotion, reaction time, and congruency (incon - con P3 but not N2). In time-frequency data, tFUS elevated post-trial theta, reduced alpha suppression, and modulated error-related delta. These results suggest that tFUS altered emotional processing and enhanced sustained attention by modulation of network connections in the theta, alpha, and delta band. Perhaps by effectively reducing attentional engagement with emotional distraction and reducing the need for attention switching evidenced by early ERP components, theta and alpha.

Chapter 3 employed the same behavioral task and recording modalities using in chapter 2 but applied tFUS to the anatomical overlap between the anterior insula and frontal operculum of the right inferior gyrus (aIns/fO). Evidence from this chapter demonstrates that tFUS modulated the aIns/fO by effectively reducing parasympathetic fear response in HRV, reducing response slowing after errors on fear trials, and functionally reducing emotional distraction interference on RT performance. Although RTs were not faster than Sham, unlike the Sham group, the tFUS group did not show slowed RTs from baseline with addition of emotional faces (on incongruent trials only). tFUS to the aIns/fO resulted in

enhanced early ERP amplitudes in frontal and parietal electrodes, and in early ERPs components known to code for emotional face valence, as well as showing an enhanced P3. These effects may likely be meditated by modulation of event-locked delta and beta with tFUS as they are known to be involved in saliency and modulation of physiologic responses though and distractor processing via interaction with the amygdala, and regulation of the medial frontal cortex. Overall this study demonstrates that tFUS along with neuronavigation can be used to target specific anatomical and functional areas to induce larger network modulation and effect function and processing.

The dACC and aIns/fO are function interposed between the default mode network (DMN) and anti-correlated dorsal attention network (DAN) (Fox et al., 2005; Fox et al., 2009). They are though to flexibility couple to each in their role in executive control (Spreng et al., 2012; Sridharan et al., 2008; Vincent et al., 2008). Additionally, these regions are central to both the dorsal (goal directed behavior) and ventral (saliency) attention systems (Dosenbach et al., 2006). The success of these results are likely due to the selection of function targets, but could undoubtedly be enhanced by refined target and parameter identification and/or the addition of neurofeedback.

Chapter 4 targeted the pars opercularis of the rIFG less for the intension of modulating performance, but more to explore the efficacy of utilizing tFUS as a tool to deduce casual involvement of certain brain areas in function and draw conclusions regarding functional connectivity. Specificity, the chapter examined whether pars opercularis of the rIFG is explicitly involved in motor response inhibition. The stop-signal task was used in conjunction with online tFUS. Neuronavigation was highly specified to individual anatomy. Data processing involved source-localized EEG, and dynamic causal modeling of ERPs.

Results showed that tFUS applied in a trial-by-trial manner enhanced successful inhibition and resulted in faster stopping (measured through SSRT). Additionally ERP analysis indicated tFUS rendered a shift in the fronto-central P300 onset, which was directly correlated with improved SSRT. Although changes in this ERP component are associated with faster SSRTs (Wessel and Aron, 2015), it remains unclear weather tFUS acting on the pars opercularis had causal effects on behavior via ERP modulation or was simply a marker of a different mechanism. To examine underlying response inhibition network mechanism and tFUS's modulation thereof, dynamic causal models were employed to explore the rIFG's function in stopping. Results indicate that the rIFG to pre-SMA connections in were effectively related to inhibition in terms of the mean gain change in backwards connectivity and its variation with tFUS induced changes. By pairing tFUS with DCM, network model of response inhibition was created, suggesting that motor inhibition is explicitly invoked by the pars opercularis through deep pyramidal connections by direct synaptic connection onto the pre-SMA, temporal cortex, and sub-cortex. These results indicate tFUS combined with network modeling has the potential inform known regarding existing network connections, as well as effective targets for tFUS modulation for affecting biophysical network mechanisms and behavior.

This work demonstrates that tFUS can be applied to specific anatomical areas for modulation of processing and performance in the clinic or lab by using neuronavigation to highlight individual anatomical targets and application of tFUS with EEG. These results provide promising evidence that tFUS to a single brain area can be used for broader network modulation. Much work is still to be done to fully characterize and realize the potential of ultrasound as a modulation tool for medicine and beyond, but this work begins to lay the groundwork for its future development by demonstrating the efficacy of modulating

functional networks, attentional processing, emotional physiology, and behavior performance.

FUTURE DIRECTIONS

In this study, tFUS was targeted at anatomical areas of interest by first collecting structural MRIs, developing region of interest identification based on individual anatomy and assumptions about neuro-functional connections baseline on the literatures. Although this body of work does demonstrate efficacy to this technique, there is certainly room for improvement when it comes to the sophistication of functional accuracy since subject structural, as well as functional anatomy varies widely. This could be done by collecting functional data on each subject with fMRI or Magnetoencephalography (MEG) and using this information to inform target identification.

The biggest benefits from the use of ultrasound will likely come from enhancing the human native capability of regulation. For example, tFUS could be combined with either fMRI or EEG, such that the tFUS pulse could be used to further enhance the effects of neurofeedback. The easy integration of tFUS with EEG demonstrated in this work, can make this process accessible to both researchers and clinicians, and can be done in real-time.

The studies presented here used a single focus tFUS transducer with no power feedback information. Although the results presented above do indicate that tFUS successful modulated functional networks, this hardware setup provided no ability to steer the ultrasound beam or account for diffraction from the skull. Neither did this setup provide confirmation or feedback regarding power input into the brain. Although copious amounts of ultrasound gel and silicone were used to couple the transducer to the head and create the desired focal depth, there was no way to know if a bubble might form or if the transducer

lifted from the surface of the scalp slightly. Additionally, the only focal plane available was the one normal to the surface of the skill. As ultrasound develops as a neurostimulation field, multi-lens focusable transducers which incorporate skull correction and individualistic beam correction based on k-wave simulations will become more common, as this has already been demonstrated in thalamic mapping and ablation (Dallapiazza et al., 2017; Elias et al., 2013). Additionally, the incorporation of power feedback information via the imaging capabilities of ultrasound will provide improved confirmation of stimulation power transfer across the skull and into the brain. It is also possible to combine tFUS with ultrasound thermography and measure tFUS stimulation locational accuracy in the fMRI scanner by inducing a very small temperature change (Dallapiazza et al., 2017), although this would no longer be considered 'non-thermal' low intensity ultrasound.

In the future it may be possible to combine tFUS with meta-materials or optics to interact with the brain through dynamic acoustic-optical holography for stimulation and recording. It is well known that using multiple transducer elements and using wave addition and subtraction does allow for some beam steering, it is possible that advances in material science may ameliorate this capability further. It has been demonstrated that 3D-printed lenses can be used to create complex holographic focal shapes with ultrasound (Melde et al., 2016b). Perhaps the advancement of materials with light-tunable material properties will allow for the creation of dynamic and interactive holographic ultrasound (Ketner et al., 2007; Kumar et al., 2009).

Additionally, it may be possible to pair functional imaging with ultrasound stimulation. It has been theorized that this can be done non-invasively using electrophysiological imaging (He, 2016), while ultrasound functional imaging has been demonstrated invasively in animals (Gesnik et al., 2017; Kim et al., 2017) and humans

(Imbault et al., 2017). Combining ultrasound with infrared optics allows for photo-acoustic functional imaging of tissues (Sivasubramanian et al., 2018) and may also be applicable to neuroimaging.

Finally, it should be noted that the parameter space for possible temporal patters of tFUS stimulation is broad and largely unexplored. There are some limitations when trying to cross the skull, for which carrier frequencies around 500 kHz are ideal, however the pulse repetition frequency, and temporal duration can be modulated wildly as long as remaining within the FDA safety limits for imaging. In this study a PRF of 1000Hz and stimulation duration of 500ms was employed in all studies. However the field is only in its infancy in terms of understanding the possible inhibitor, excitatory, or neurochemical effects of different parameters.

REFERENCES

Abboud, H., Berroir, S., Labreuche, J., Orjuela, K., and Amarenco, P. (2006). Insular involvement in brain infarction increases risk for cardiac arrhythmia and death. Annals of Neurology *59*, 691-699.

Aftanas, L.I., and Golocheikine, S.A. (2001). Human anterior and frontal midline theta and lower alpha reflect emotionally positive state and internalized attention: high-resolution EEG investigation of meditation. Neuroscience Letters *310*, 57-60.

Ai, L., Mueller, J.K., Grant, A., Eryaman, Y., and Legon, W. (2016). Transcranial Focused Ultrasound for BOLD fMRI Signal Modulation in Humans. arXiv preprint arXiv:160300415.

Albert, J., Lopez-Martin, S., and Carretie, L. (2010). Emotional context modulates response inhibition: neural and behavioral data. Neuroimage *49*, 914-921.

Andrews-Hanna, J.R., Smallwood, J., and Spreng, R.N. (2014). The default network and self-generated thought: component processes, dynamic control, and clinical relevance. Ann N Y Acad Sci *1316*, 29-52.

Aron, A.R., Fletcher, P.C., Bullmore, E.T., Sahakian, B.J., and Robbins, T.W. (2003). Stop-signal inhibition disrupted by damage to right inferior frontal gyrus in humans. Nature neuroscience *6*, 115-116.

Aron, A.R., Herz, D.M., Brown, P., Forstmann, B.U., and Zaghloul, K. (2016a). Frontosubthalamic Circuits for Control of Action and Cognition. The Journal of Neuroscience *36*, 11489-11495.

Aron, A.R., Herz, D.M., Brown, P., Forstmann, B.U., and Zaghloul, K. (2016b). Frontosubthalamic Circuits for Control of Action and Cognition. Journal of Neuroscience *36*, 11489-11495.

Aron, A.R., and Poldrack, R.A. (2006). Cortical and subcortical contributions to stop signal response inhibition: role of the subthalamic nucleus. Journal of Neuroscience *26*, 2424-2433.

Aron, A.R., Robbins, T.W., and Poldrack, R.A. (2014). Inhibition and the right inferior frontal cortex: one decade on. Trends in cognitive sciences *18*, 177-185.

Aubry, J.-F., Tanter, M., Pernot, M., Thomas, J.-L., and Fink, M. (2003). Experimental demonstration of noninvasive transskull adaptive focusing based on prior computed tomography scans. The Journal of the Acoustical Society of America *113*, 84-93.

Auksztulewicz, R., and Friston, K. (2015). Attentional enhancement of auditory mismatch responses: a DCM/MEG study. Cerebral cortex *25*, 4273-4283.

Bachtold, M.R., Rinaldi, P.C., Jones, J.P., Reines, F., and Price, L.R. (1998). Focused ultrasound modifications of neural circuit activity in a mammalian brain. Ultrasound in medicine & biology *24*, 557-565.

Baddeley, A.D., and Della Sala, S. (1996). Working memory and executive control. Philosophical Transactions of the Royal Society of London Series B: Biological Sciences *351*, 1397-1404.

Bari, A., and Robbins, T.W. (2013). Inhibition and impulsivity: behavioral and neural basis of response control. Progress in neurobiology *108*, 44-79.

Bastos, A., Usrey, W., Adams, R., Mangun, G., Fries, P., and Friston, K. (2012). 871 Canonical Microcircuits for Predictive Coding. Neuron *76*, 695-711.

Bates, D., Mächler, M., Bolker, B., and Walker, S. (2014). Package Lme4: Linear Mixed-Effects Models Using Eigen and S4, Vol 67.

Beckmann, M., Johansen-Berg, H., and Rushworth, M.F. (2009). Connectivity-based parcellation of human cingulate cortex and its relation to functional specialization. Journal of Neuroscience *29*, 1175-1190.

Bensmann, W., Roessner, V., Stock, A.K., and Beste, C. (2018). Catecholaminergic Modulation of Conflict Control Depends on the Source of Conflicts. Int J Neuropsychopharmacol *21*, 901-909.

Bergfeld, I.O., Mantione, M., Hoogendoorn, M.C., and et al. (2016). Deep brain stimulation of the ventral anterior limb of the internal capsule for treatment-resistant depression: A randomized clinical trial. JAMA Psychiatry *73*, 456-464.

Bernat, E., Nelson, L., and Baskin-Sommers, A. (2012). Time-frequency Theta and Delta measures index separable components of feedback processing. International Journal of Psychophysiology *3*, 341.

Bhatt, M.B., Bowen, S., Rossiter, H.E., Dupont-Hadwen, J., Moran, R.J., Friston, K.J., and Ward, N.S. (2016). Computational modelling of movement-related beta-oscillatory dynamics in human motor cortex. Neuroimage *133*, 224-232.

Billeke, P., Ossandon, T., Perrone-Bertolotti, M., Kahane, P., Bastin, J., Jerbi, K., Lachaux, J.-P., and Fuentealba, P. (2020). Human anterior insula encodes performance feedback and relays prediction error to the medial prefrontal cortex. Cerebral Cortex *30*, 4011-4025.

Bissett, P.G., and Logan, G.D. (2014). Selective stopping? Maybe not. Journal of Experimental Psychology: General *143*, 455.

Boehler, C.N., Appelbaum, L.G., Krebs, R.M., Hopf, J.-M., and Woldorff, M.G. (2010). Pinning down response inhibition in the brain—conjunction analyses of the stop-signal task. Neuroimage *52*, 1621-1632.

Boehler, C.N., Münte, T.F., Krebs, R.M., Heinze, H.-J., Schoenfeld, M.A., and Hopf, J.-M. (2009). Sensory MEG responses predict successful and failed inhibition in a stop-signal task. Cerebral Cortex *19*, 134-145.

Boksem, M.A., Meijman, T.F., and Lorist, M.M. (2005). Effects of mental fatigue on attention: an ERP study. Brain Res Cogn Brain Res *25*, 107-116.

Botvinick, M.M. (2007). Conflict monitoring and decision making: reconciling two perspectives on anterior cingulate function. Cognitive, Affective, & Behavioral Neuroscience *7*, 356-366.

Bretherton, P.M., Eysenck, M.W., Richards, A., and Holmes, A. (2017). Target and distractor processing and the influence of load on the allocation of attention to task-irrelevant threat. Neuropsychologia.

Bush, G., Luu, P., and Posner, M.I. (2000). Cognitive and emotional influences in anterior cingulate cortex. Trends in cognitive sciences *4*, 215-222.

Bystritsky, A., and Korb, A.S. (2015). A Review of Low-Intensity Transcranial Focused Ultrasound for Clinical Applications. Current Behavioral Neuroscience Reports *2*, 60-66.

Cahn, B.R., and Polich, J. (2009). Meditation (Vipassana) and the P3a event-related brain potential. Int J Psychophysiol *72*, 51-60.

Cai, W., and Leung, H.-C. (2011). Rule-guided executive control of response inhibition: functional topography of the inferior frontal cortex. PloS one *6*, e20840.

Cai, W., Ryali, S., Chen, T., Li, C.S.R., and Menon, V. (2014). Dissociable Roles of Right Inferior Frontal Cortex and Anterior Insula in Inhibitory Control: Evidence from Intrinsic and Task-Related Functional Parcellation, Connectivity, and Response Profile Analyses across Multiple Datasets. Journal of Neuroscience *34*, 14652-14667.

Carlson, J.M., and Reinke, K.S. (2010). Spatial attention-related modulation of the N170 by backward masked fearful faces. Brain and Cognition *73*, 20-27.

Carlson, J.M., Reinke, K.S., and Habib, R. (2009). A left amygdala mediated network for rapid orienting to masked fearful faces. Neuropsychologia *47*, 1386-1389.

Carretié, L. (2014). Exogenous (automatic) attention to emotional stimuli: a review. Cognitive, Affective, & Behavioral Neuroscience *14*, 1228-1258.

Cassell, M., and Wright, D. (1986). Topography of projections from the medial prefrontal cortex to the amygdala in the rat. Brain research bulletin *17*, 321-333.

Cavanagh, J.F., Cohen, M.X., and Allen, J.J. (2009). Prelude to and resolution of an error: EEG phase synchrony reveals cognitive control dynamics during action monitoring. J Neurosci *29*, 98-105.

Cavanagh, J.F., Meyer, A., and Hajcak, G. (2017). Error-Specific Cognitive Control Alterations in Generalized Anxiety Disorder. Biological Psychiatry: Cognitive Neuroscience and Neuroimaging *2*, 413-420.

Cavanagh, J.F., and Shackman, A.J. (2015). Frontal midline theta reflects anxiety and cognitive control: Meta-analytic evidence. Journal of Physiology-Paris *109*, 3-15.

Chambers, C.D., Bellgrove, M.A., Stokes, M.G., Henderson, T.R., Garavan, H., Robertson, I.H., Morris, A.P., and Mattingley, J.B. (2006). Executive "brake failure" following deactivation of human frontal lobe. Journal of cognitive neuroscience *18*, 444-455.

Chambers, C.D., Garavan, H., and Bellgrove, M.A. (2009). Insights into the neural basis of response inhibition from cognitive and clinical neuroscience. Neuroscience & biobehavioral reviews *33*, 631-646.

Chatham, C.H., Claus, E.D., Kim, A., Curran, T., Banich, M.T., and Munakata, Y. (2012). Cognitive control reflects context monitoring, not motoric stopping, in response inhibition. PloS one *7*, e31546.

Chikazoe, J., Jimura, K., Asari, T., Yamashita, K.-i., Morimoto, H., Hirose, S., Miyashita, Y., and Konishi, S. (2009). Functional dissociation in right inferior frontal cortex during performance of go/no-go task. Cerebral Cortex *19*, 146-152.

Ciccone, A.B., Siedlik, J.A., Wecht, J.M., Deckert, J.A., Nguyen, N.D., and Weir, J.P. (2017). Reminder: RMSSD and SD1 are identical heart rate variability metrics. Muscle & Nerve *56*, 674-678.

Cohen, M., and Cavanagh, J.F. (2011). Single-Trial Regression Elucidates the Role of Prefrontal Theta Oscillations in Response Conflict. Frontiers in Psychology *2*.

Cohen, M.X. (2011). Error-related medial frontal theta activity predicts cingulate-related structural connectivity. NeuroImage *55*, 1373-1383.

Colivicchi, F., Bassi, A., Santini, M., and Caltagirone, C. (2004). Cardiac Autonomic Derangement and Arrhythmias in Right-Sided Stroke With Insular Involvement. Stroke *35*, 2094-2098.

Corbetta, M., and Shulman, G.L. (2002). Control of goal-directed and stimulus-driven attention in the brain. Nature reviews neuroscience *3*, 201-215.

Coste, C.P., and Kleinschmidt, A. (2016). Cingulo-opercular network activity maintains alertness. Neuroimage *128*, 264-272.

Craig, A.D. (2002). How do you feel? Interoception: the sense of the physiological condition of the body. Nature reviews neuroscience *3*, 655.

Craig, A.D. (2004). Human feelings: why are some more aware than others? Trends in Cognitive Sciences *8*, 239-241.

Crawford, J.R., and Henry, J.D. (2004). The Positive and Negative Affect Schedule (PANAS): Construct validity, measurement properties and normative data in a large non - clinical sample. British journal of clinical psychology *43*, 245-265.

Critchley, H.D., Mathias, C.J., and Dolan, R.J. (2002a). Fear Conditioning in Humans: The Influence of Awareness and Autonomic Arousal on Functional Neuroanatomy. Neuron *33*, 653-663.

Critchley, H.D., Melmed, R.N., Featherstone, E., Mathias, C.J., and Dolan, R.J. (2002b). Volitional control of autonomic arousal: a functional magnetic resonance study. Neuroimage *16*, 909-919.

Critchley, H.D., Wiens, S., Rotshtein, P., and Dolan, R.J. (2004). Neural systems supporting interoceptive awareness. Nature neuroscience *7*, 189.

Crone, E.A., Wendelken, C., Donohue, S.E., and Bunge, S.A. (2006). Neural evidence for dissociable components of task-switching. Cerebral cortex *16*, 475-486.

Cuthbert, B.N., Schupp, H.T., Bradley, M.M., Birbaumer, N., and Lang, P.J. (2000). Brain potentials in affective picture processing: covariation with autonomic arousal and affective report. Biological Psychology *52*, 95-111.

Dalecki, D. (2004). Mechanical bioeffects of ultrasound. Annu Rev Biomed Eng *6*, 229-248.

Dallapiazza, R.F., Timbie, K.F., Holmberg, S., Gatesman, J., Lopes, M.B., Price, R.J., Miller, G.W., and Elias, W.J. (2017). Noninvasive neuromodulation and thalamic mapping with low-intensity focused ultrasound. Journal of neurosurgery, 1-10.

David, O., Kiebel, S.J., Harrison, L.M., Mattout, J., Kilner, J.M., and Friston, K.J. (2006). Dynamic causal modeling of evoked responses in EEG and MEG. NeuroImage *30*, 1255-1272.

David, O., Maess, B., Eckstein, K., and Friederici, A.D. (2011). Dynamic causal modeling of subcortical connectivity of language. Journal of Neuroscience *31*, 2712-2717.

de Morree, H.M., Rutten, G.-J., Szabó, B.M., Sitskoorn, M.M., and Kop, W.J. (2016). Effects of Insula Resection on Autonomic Nervous System Activity. Journal of Neurosurgical Anesthesiology *28*, 153-158.

Debener, S., Ullsperger, M., Siegel, M., Fiehler, K., Von Cramon, D.Y., and Engel, A.K. (2005). Trial-by-trial coupling of concurrent electroencephalogram and functional magnetic resonance imaging identifies the dynamics of performance monitoring. Journal of Neuroscience *25*, 11730-11737.

Deffieux, T., Younan, Y., Wattiez, N., Tanter, M., Pouget, P., and Aubry, J.-F. (2013). Low-intensity focused ultrasound modulates monkey visuomotor behavior. Current Biology *23*, 2430-2433.

Delorme, A., and Makeig, S. (2004). EEGLAB: an open source toolbox for analysis of single-trial EEG dynamics including independent component analysis. Journal of neuroscience methods *134*, 9-21.

Dennis, T.A., and Chen, C.-C. (2007). Neurophysiological mechanisms in the emotional modulation of attention: The interplay between threat sensitivity and attentional control. Biological Psychology *76*, 1-10.

Destrieux, C., Fischl, B., Dale, A., and Halgren, E. (2010). Automatic parcellation of human cortical gyri and sulci using standard anatomical nomenclature. Neuroimage *53*, 1-15.

Dick, B.D., and Rashiq, S. (2007). Disruption of attention and working memory traces in individuals with chronic pain. Anesthesia & Analgesia *104*, 1223-1229.

Dosenbach, N.U., Fair, D.A., Cohen, A.L., Schlaggar, B.L., and Petersen, S.E. (2008). A dual-networks architecture of top-down control. Trends in cognitive sciences *12*, 99-105.

Dosenbach, N.U., Fair, D.A., Miezin, F.M., Cohen, A.L., Wenger, K.K., Dosenbach, R.A., Fox, M.D., Snyder, A.Z., Vincent, J.L., Raichle, M.E.*, et al.* (2007). Distinct brain networks for adaptive and stable task control in humans. Proc Natl Acad Sci U S A *104*, 11073-11078.

Dosenbach, N.U., Visscher, K.M., Palmer, E.D., Miezin, F.M., Wenger, K.K., Kang, H.C., Burgund, E.D., Grimes, A.L., Schlaggar, B.L., and Petersen, S.E. (2006). A core system for the implementation of task sets. Neuron *50*, 799-812.

Dougherty, D.D., Rezai, A.R., Carpenter, L.L., Howland, R.H., Bhati, M.T., O'Reardon, J.P., Eskandar, E.N., Baltuch, G.H., Machado, A.D., Kondziolka, D.*, et al.* (2015). A Randomized Sham-Controleed Trial of Deep Brain Stimulation of the Ventral Capsule/Ventral Striatum for Chronic Treatment-Resistant Depression. Biological Psychiatry *78*, 240-248.

Drummond, S.P., Bischoff-Grethe, A., Dinges, D.F., Ayalon, L., Mednick, S.C., and Meloy, M. (2005). The neural basis of the psychomotor vigilance task. Sleep *28*, 1059-1068.

Duann, J.-R., Ide, J.S., Luo, X., and Li, C.-s.R. (2009). Functional connectivity delineates distinct roles of the inferior frontal cortex and presupplementary motor area in stop signal inhibition. Journal of Neuroscience *29*, 10171-10179.

Ebner, N.C., Riediger, M., and Lindenberger, U. (2010). FACES--a database of facial expressions in young, middle-aged, and older women and men: development and validation. Behav Res Methods *42*, 351-362.

Eckert, M.A., Menon, V., Walczak, A., Ahlstrom, J., Denslow, S., Horwitz, A., and Dubno, J.R. (2009). At the heart of the ventral attention system: the right anterior insula. Human brain mapping *30*, 2530-2541.

Egner, T., Etkin, A., Gale, S., and Hirsch, J. (2007). Dissociable neural systems resolve conflict from emotional versus nonemotional distracters. Cerebral cortex *18*, 1475-1484.

Eimer, M. (2000). Attentional modulations of event-related brain potentials sensitive to faces. Cognitive Neuropsychology *17*, 103-116.

Elias, W.J., Huss, D., Voss, T., Loomba, J., Khaled, M., Zadicario, E., Frysinger, R.C., Sperling, S.A., Wylie, S., Monteith, S.J.*, et al.* (2013). A pilot study of focused ultrasound thalamotomy for essential tremor. N Engl J Med *369*, 640-648.

Elias, W.J., Lipsman, N., Ondo, W.G., Ghanouni, P., Kim, Y.G., Lee, W., Schwartz, M., Hynynen, K., Lozano, A.M., Shah, B.B.*, et al.* (2016). A Randomized Trial of Focused Ultrasound Thalamotomy for Essential Tremor. N Engl J Med *375*, 730-739.

Endrass, T., Reuter, B., and Kathmann, N. (2007). ERP correlates of conscious error recognition: aware and unaware errors in an antisaccade task. Eur J Neurosci *26*, 1714-1720.

Erika-Florence, M., Leech, R., and Hampshire, A. (2014). A functional network perspective on response inhibition and attentional control. Nature communications *5*, 1-12.

Eriksen, B.A., and Eriksen, C.W. (1974). Effects of noise letters upon the identification of a target letter in a nonsearch task. Perception & psychophysics *16*, 143-149.

Evans, A.C., Kamber, M., Collins, D., and MacDonald, D. (1994). An MRI-based probabilistic atlas of neuroanatomy. In Magnetic resonance scanning and epilepsy (Springer), pp. 263-274.

Fallahi, M., Motamedzade, M., Heidarimoghadam, R., Soltanian, A.R., and Miyake, S. (2016). Effects of mental workload on physiological and subjective responses during traffic density monitoring: A field study. Applied Ergonomics *52*, 95-103.

Fan, Y., Tang, Y.Y., Tang, R., and Posner, M.I. (2015). Time course of conflict processing modulated by brief meditation training. Front Psychol *6*, 911.

Fardo, F., Auksztulewicz, R., Allen, M., Dietz, M.J., Roepstorff, A., and Friston, K.J. (2017). Expectation violation and attention to pain jointly modulate neural gain in somatosensory cortex. Neuroimage *153*, 109-121.

Feldman, H., and Friston, K. (2010). Attention, uncertainty, and free-energy. Frontiers in human neuroscience *4*, 215.

Fini, M., and Tyler, W.J. (2017). Transcranial focused ultrasound: a new tool for non-invasive neuromodulation. International Review of Psychiatry, 1-10.

Fischer, A.G., Nigbur, R., Klein, T.A., Danielmeier, C., and Ullsperger, M. (2018). Cortical beta power reflects decision dynamics and uncovers multiple facets of post-error adaptation. Nature Communications *9*.

Foland-Ross, L.C., Hamilton, J.P., Joormann, J., Berman, M.G., Jonides, J., and Gotlib, I.H. (2013). The neural basis of difficulties disengaging from negative irrelevant material in major depression. Psychological science *24*, 334-344.

Forstmann, B.U., Dutilh, G., Brown, S., Neumann, J., Von Cramon, D.Y., Ridderinkhof, K.R., and Wagenmakers, E.-J. (2008). Striatum and pre-SMA facilitate decision-making under time pressure. Proceedings of the National Academy of Sciences *105*, 17538-17542.

Fox, M.D., Snyder, A.Z., Vincent, J.L., Corbetta, M., Van Essen, D.C., and Raichle, M.E. (2005). The human brain is intrinsically organized into dynamic, anticorrelated functional networks. Proceedings of the National Academy of Sciences *102*, 9673-9678.

Fox, M.D., Zhang, D., Snyder, A.Z., and Raichle, M.E. (2009). The global signal and observed anticorrelated resting state brain networks. Journal of neurophysiology *101*, 3270-3283.

Friston, K.J., Litvak, V., Oswal, A., Razi, A., Stephan, K.E., Van Wijk, B.C., Ziegler, G., and Zeidman, P. (2016). Bayesian model reduction and empirical Bayes for group (DCM) studies. Neuroimage *128*, 413-431.

Fry, F. (1958a). Production of reversible changes in the central nervous system by ultrasound. Science *127*, 83-84.

Fry, W.J. (1956). Ultrasound in neurology. Neurology *6*, 693-704.

Fry, W.J. (1958b). Use of intense ultrasound in neurological research. Am J Phys Med *37*, 143-147.

Gaebler, M., Daniels, J.K., Lamke, J.-P., Fydrich, T., and Walter, H. (2013). Heart rate variability and its neural correlates during emotional face processing in social anxiety disorder. Biological Psychology *94*, 319-330.

Gelman, A., and Hill, J. (2007). Data analysis using regression and multilevelhierarchical models, Vol 1 (Cambridge University Press New York, NY, USA).

Gesnik, M., Blaize, K., Deffieux, T., Gennisson, J.-L., Sahel, J.-A., Fink, M., Picaud, S., and Tanter, M. (2017). 3D functional ultrasound imaging of the cerebral visual system in rodents. NeuroImage *149*, 267-274.

Grace, A.A. (1995). The tonic/phasic model of dopamine system regulation: its relevance for understanding how stimulant abuse can alter basal ganglia function. Drug and Alcohol Dependence *37*, 111-129.

Grant, J.A., Duerden, E.G., Courtemanche, J., Cherkasova, M., Duncan, G.H., and Rainville, P. (2013). Cortical thickness, mental absorption and meditative practice: possible implications for disorders of attention. Biol Psychol *92*, 275-281.

Guo, H., Hamilton, M., Offutt, S.J., Gloeckner, C.D., Li, T., Kim, Y., Legon, W., Alford, J.K., and Lim, H.H. (2018). Ultrasound Produces Extensive Brain Activation via a Cochlear Pathway. Neuron *98*, 1020-1030.e1024.

Guzik, P., Piskorski, J., Krauze, T., Bychowiec, B., Wesseling, K., Schneider, R., Girgus, P., Wykrtowicz, A., and Wysocki, H. (2005). Numerical descriptors of Poincaré plots analysis of RR intervals are related to baroreflex sensitivity and hemodynamic parameters in healthy people. Folia Cardiol *12*, 56-59.

Haas, B.W., Omura, K., Constable, R.T., and Canli, T. (2006). Interference produced by emotional conflict associated with anterior cingulate activation. Cognitive, Affective, & Behavioral Neuroscience *6*, 152-156.

Hajcak, G., McDonald, N., and Simons, R.F. (2003). Anxiety and error-related brain activity. Biological Psychology *64*, 77-90.

Hampshire, A., Chamberlain, S.R., Monti, M.M., Duncan, J., and Owen, A.M. (2010). The role of the right inferior frontal gyrus: inhibition and attentional control. Neuroimage *50*, 1313-1319.

Hampshire, A., and Sharp, D.J. (2015). Contrasting network and modular perspectives on inhibitory control. Trends in cognitive sciences *19*, 445-452.

Harper, J., Malone, S.M., and Bernat, E.M. (2014). Theta and delta band activity explain N2 and P3 ERP component activity in a go/no-go task. Clinical Neurophysiology *125*, 124-132.

Harvey, E.N. (1929). The effect of high frequency sound waves on heart muscle and other irritable tissues. American Journal of Physiology, 284-290.

Hayner, M., and Hynynen, K. (2001). Numerical analysis of ultrasonic transmission and absorption of oblique plane waves through the human skull. The Journal of the Acoustical Society of America *110*, 3319-3330.

Haynes, W.I., and Haber, S.N. (2013). The organization of prefrontal-subthalamic inputs in primates provides an anatomical substrate for both functional specificity and integration: implications for Basal Ganglia models and deep brain stimulation. J Neurosci *33*, 4804-4814.

He, B. (2016). Focused Ultrasound Help Realize High Spatiotemporal Brain Imaging?-A Concept on Acousto-Electrophysiological Neuroimaging. IEEE transactions on bio-medical engineering *63*, 2654-2656.

Hertzberg, Y., Naor, O., Volovick, A., and Shoham, S. (2010). Towards multifocal ultrasonic neural stimulation: pattern generation algorithms. Journal of neural engineering *7*, 056002.

Hölzel, B.K., Ott, U., Hempel, H., Hackl, A., Wolf, K., Stark, R., and Vaitl, D. (2007). Differential engagement of anterior cingulate and adjacent medial frontal cortex in adept meditators and non-meditators. Neuroscience Letters *421*, 16-21.

Hu, S., Ide, J.S., Zhang, S., and Chiang-shan, R.L. (2015). Anticipating conflict: neural correlates of a Bayesian belief and its motor consequence. Neuroimage *119*, 286-295.

Huster, R.J., Enriquez-Geppert, S., Lavallee, C.F., Falkenstein, M., and Herrmann, C.S. (2013). Electroencephalography of response inhibition tasks: functional networks and cognitive contributions. International Journal of Psychophysiology *87*, 217-233.

Hynynen, K., and Clement, G. (2007). Clinical applications of focused ultrasound-the brain. Int J Hyperthermia *23*, 193-202.

Hynynen, K., and Jolesz, F.A. (1998). Demonstration of potential noninvasive ultrasound brain therapy through an intact skull. Ultrasound in medicine & biology *24*, 275-283.

Hynynen, K., and Jones, R.M. (2016). Image-guided ultrasound phased arrays are a disruptive technology for non-invasive therapy. Physics in medicine and biology *61*, R206-248.

Iannaccone, R., Hauser, T.U., Staempfli, P., Walitza, S., Brandeis, D., and Brem, S. (2015). Conflict monitoring and error processing: New insights from simultaneous EEG–fMRI. NeuroImage *105*, 395-407.

Ibsen, S., Tong, A., Schutt, C., Esener, S., and Chalasani, S.H. (2015). Sonogenetics is a non-invasive approach to activating neurons in Caenorhabditis elegans. Nature communications U6 - ctx_ver=Z3988-2004&ctx_enc=info%3Aofi%2Fenc%3AUTF-8&rfr_id=info%3Asid%2Fsummonserialssolutionscom&rft_val_fmt=info%3Aofi%2Ffmt%3Akev%3Amtx%3Ajournal&rftgenre=article&rftatitle=Sonogenetics+is+a+non-invasive+approach+to+activating+neurons+in+Caenorhabditis+elegans&rftjtitle=Nature+communications&rftau=Ibsen%2C+Stuart&rftau=Tong%2C+Ada&rftau=Schutt%2C+Carolyn&rftau=Esener%2C+Sadik&rftdate=2015&rfteissn=2041-1723&rftvolume=6&rftspage=8264&rft_id=info%3Apmid%2F26372413&rftexternalDocID=26372413&paramdict=en-US U7 - Journal Article *6*, 8264.

Ide, J.S., Shenoy, P., Angela, J.Y., and Chiang-Shan, R.L. (2013). Bayesian prediction and evaluation in the anterior cingulate cortex. Journal of Neuroscience *33*, 2039-2047.

Imbault, M., Chauvet, D., Gennisson, J.-L., Capelle, L., and Tanter, M. (2017). Intraoperative Functional Ultrasound Imaging of Human Brain Activity. Scientific Reports *7*, 7304.

Inanaga, K. (1998). Frontal midline theta rhythm and mental activity. Psychiatry and clinical neurosciences *52*, 555-566.

Inzlicht, M., Bartholow, B.D., and Hirsh, J.B. (2015). Emotional foundations of cognitive control. Trends in Cognitive Sciences *19*, 126-132.

Iordan, A.D., Dolcos, S., and Dolcos, F. (2013). Neural signatures of the response to emotional distraction: a review of evidence from brain imaging investigations. Front Hum Neurosci *7*.

Jabbi, M., and Keysers, C. (2008). Inferior frontal gyrus activity triggers anterior insula response to emotional facial expressions. Emotion *8*, 775-780.

Jahfari, S., Waldorp, L., van den Wildenberg, W.P., Scholte, H.S., Ridderinkhof, K.R., and Forstmann, B.U. (2011). Effective connectivity reveals important roles for both the hyperdirect (fronto-subthalamic) and the indirect (fronto-striatal-pallidal) fronto-basal ganglia pathways during response inhibition. Journal of Neuroscience *31*, 6891-6899.

Jasinska, A.J., Ho, S.S., Taylor, S.F., Burmeister, M., Villafuerte, S., and Polk, T.A. (2012). Influence of Threat and Serotonin Transporter Genotype on Interference Effects. Front Psychol *3*.

Jiang, J., Zhang, Q., and Van Gaal, S. (2015). EEG neural oscillatory dynamics reveal semantic and response conflict at difference levels of conflict awareness. Scientific Reports *5*.

Jo, H.G., Schmidt, S., Inacker, E., Markowiak, M., and Hinterberger, T. (2016). Meditation and attention: A controleed study on long-term meditators in behavioral performance and event-related potentials of attentional control. Int J Psychophysiol *99*, 33-39.

Jung, H.H., Kim, S.J., Roh, D., Chang, J.G., Chang, W.S., Kweon, E.J., Kim, C.H., and Chang, J.W. (2015). Bilateral thermal capsulotomy with MR-guided focused ultrasound for patients with treatment-refractory obsessive-compulsive disorder: a proof-of-concept study. Mol Psychiatry *20*, 1205-1211.

Kanske, P., Heissler, J., Schönfelder, S., Bongers, A., and Wessa, M. (2011). How to Regulate Emotion? Neural Networks for Reappraisal and Distraction. Cerebral Cortex *21*, 1379-1388.

Kanske, P., Heissler, J., Schönfelder, S., and Wessa, M. (2012). Neural correlates of emotion regulation deficits in remitted depression: the influence of regulation strategy, habitual regulation use, and emotional valence. Neuroimage *61*, 686-693.

Kapp, B.S., Schwaber, J.S., and Driscoll, P.A. (1985). The organization of insular cortex projections to the amygdaloid central nucleus and autonomic regulatory nuclei of the dorsal medulla. Brain Research *360*, 355-360.

Karmakar, C.K., Khandoker, A.H., Gubbi, J., and Palaniswami, M. (2009). Complex correlation measure: a novel descriptor for Poincaré plot. Biomedical engineering online *8*, 17.

Keedwell, P.A., and Linden, D.E. (2013). Integrative neuroimaging in mood disorders. Current opinion in psychiatry *26*, 27-32.

Kenemans, J.L. (2015). Specific proactive and generic reactive inhibition. Neuroscience & Biobehavioral Reviews *56*, 115-126.

Kerns, J.G., Cohen, J.D., MacDonald, A.W., Cho, R.Y., Stenger, V.A., and Carter, C.S. (2004). Anterior cingulate conflict monitoring and adjustments in control. Science *303*, 1023-1026.

Ketner, A.M., Kumar, R., Davies, T.S., Elder, P.W., and Raghavan, S.R. (2007). A simple class of photorheological fluids: surfactant solutions with viscosity tunable by light. Journal of the American Chemical Society *129*, 1553-1559.

Kim, E., Anguluan, E., and Kim, J.G. (2017). Monitoring cerebral hemodynamic change during transcranial ultrasound stimulation using optical intrinsic signal imaging. Scientific Reports *7*, 13148.

King, R.L., Brown, J.R., Newsome, W.T., and Pauly, K.B. (2013). Effective parameters for ultrasound-induced in vivo neurostimulation. Ultrasound in medicine & biology *39*, 312-331.

Klein, T.A., Endrass, T., Kathmann, N., Neumann, J., von Cramon, D.Y., and Ullsperger, M. (2007). Neural correlates of error awareness. NeuroImage *34*, 1774-1781.

Klumpp, H., Angstadt, M., and Phan, K.L. (2012). Insula reactivity and connectivity to anterior cingulate cortex when processing threat in generalized social anxiety disorder. Biological Psychology *89*, 273-276.

Knyazev, G.G. (2007). Motivation, emotion, and their inhibitory control mirrored in brain oscillations. Neuroscience & Biobehavioral Reviews *31*, 377-395.

Krasovitski, B., Frenkel, V., Shoham, S., and Kimmel, E. (2011). Intramembrane cavitation as a unifying mechanism for ultrasound-induced bioeffects. Proc Natl Acad Sci U S A *108*, 3258-3263.

Kubanek, J., Shi, J., Marsh, J., Chen, D., Deng, C., and Cui, J. (2016). Ultrasound modulates ion channel currents. Sci Rep *6*.

Kubota, Y., Sato, W., Toichi, M., Murai, T., Okada, T., Hayashi, A., and Sengoku, A. (2001). Frontal midline theta rhythm is correlated with cardiac autonomic activities during the performance of an attention demanding meditation procedure. Cognitive brain research *11*, 281-287.

Kumar, R., Ketner, A.M., and Raghavan, S.R. (2009). Nonaqueous photorheological fluids based on light-responsive reverse wormlike micelles. Langmuir *26*, 5405-5411.

Lacouture, Y., and Cousineau, D. (2008). How to use MATLAB to fit the ex-Gaussian and other probability functions to a distribution of response times. Tutorials in quantitative methods for psychology *4*, 35-45.

Lane, R.D., Reiman, E.M., Axelrod, B., Yun, L.-S., Holmes, A., and Schwartz, G.E. (1998). Neural correlates of levels of emotional awareness: Evidence of an interaction between emotion and attention in the anterior cingulate cortex. Journal of Cognitive Neuroscience *10*, 525-535.

Lee, W., Kim, H., Jung, Y., Song, I.-U., Chung, Y.A., and Yoo, S.-S. (2015). Image-guided transcranial focused ultrasound stimulates human primary somatosensory cortex. Scientific reports *5*, 8743.

Lee, W., Kim, H.-C., Jung, Y., Chung, Y.A., Song, I.-U., Lee, J.-H., and Yoo, S.-S. (2016a). Transcranial focused ultrasound stimulation of human primary visual cortex. Scientific Reports *6*, 34026.

Lee, W., Lee, S.D., Park, M.Y., Foley, L., Purcell-Estabrook, E., Kim, H., Fischer, K., Maeng, L.-S., and Yoo, S.-S. (2016b). Image-Guided Focused Ultrasound-Mediated Regional Brain Stimulation in Sheep. Ultrasound in medicine & biology *42*, 459-470.

Legon, W., Bansal, P., Tyshynsky, R., Ai, L., and Mueller, J.K. (2018). Transcranial focused ultrasound neuromodulation of the human primary motor cortex. Scientific reports *8*, 1-14.

Legon, W., Rowlands, A., Opitz, A., Sato, T.F., and Tyler, W.J. (2012a). Pulsed ultrasound differentially stimulates somatosensory circuits in humans as indicated by EEG and FMRI. PLoS ONE *7*, e51177.

Legon, W., Rowlands, A., Opitz, A., Sato, T.F., and Tyler, W.J. (2012b). Pulsed Ultrasound Differentially Stimulates Somatosensory Circuits in Humans as Indicated by EEG and fMRI. PLoS ONE *7*, 1-14.

Legon, W., Sato, T.F., Opitz, A., Mueller, J., Barbour, A., Williams, A., and Tyler, W.J. (2014a). Transcranial focused ultrasound modulates the activity of primary somatosensory cortex in humans. Nat Neurosci *17*, 322-329.

Legon, W., Sato, T.F., Opitz, A., Mueller, J., Barbour, A., Williams, A., and Tyler, W.J. (2014b). Transcranial focused ultrasound modulates the activity of primary somatosensory cortex in humans. Nat Neurosci *17*, 322-329.

Levy, B.J., and Wagner, A.D. (2011). Cognitive control and right ventrolateral prefrontal cortex: reflexive reorienting, motor inhibition, and action updating. Ann N Y Acad Sci *1224*, 40-62.

Li, G.-F., Zhao, H.-X., Zhou, H., Yan, F., Wang, J.-Y., Xu, C.-X., Wang, C.-Z., Niu, L.-L., Meng, L., Wu, S.*, et al.* (2016a). Improved Anatomical Specificity of Non-invasive Neuro-stimulation by High Frequency (5 MHz) Ultrasound. Scientific Reports *6*, 24738.

Li, G.F., Zhao, H.X., Zhou, H., Yan, F., Wang, J.Y., Xu, C.X., Wang, C.Z., Niu, L.L., Meng, L., Wu, S.*, et al.* (2016b). Improved Anatomical Specificity of Non-invasive Neuro-stimulation by High Frequency (5 MHz) Ultrasound. Sci Rep *6*.

Li, J., Fok, L., Yin, X., Bartal, G., and Zhang, X. (2009). Experimental demonstration of an acoustic magnifying hyperlens. Nature materials.

Lindström, B.R., and Bohlin, G. (2011). Emotion processing facilitates working memory performance. Cognition & Emotion *25*, 1196-1204.

Litvak, V., Garrido, M., Zeidman, P., and Friston, K. (2015). Empirical Bayes for group (DCM) studies: a reproducibility study. Frontiers in human neuroscience *9*, 670.

Logan, G.D., and Cowan, W.B. (1984). On the ability to inhibit thought and action: A theory of an act of control. Psychological review *91*, 295.

Mace, E., Montaldo, G., Cohen, I., Baulac, M., Fink, M., and Tanter, M. (2011). Functional ultrasound imaging of the brain. Nat Methods *8*, 662-664.

Mallet, N., Schmidt, R., Leventhal, D., Chen, F., Amer, N., Boraud, T., and Berke, J.D. (2016). Arkypallidal cells send a stop signal to striatum. Neuron *89*, 308-316.

Mao, C.P., Zhang, Q.L., Bao, F.X., Liao, X., Yang, X.L., and Zhang, M. (2014). Decreased activation of cingulo-frontal-parietal cognitive/attention network during an attention-demanding task in patients with chronic low back pain. Neuroradiology *56*, 903-912.

Maris, E., and Oostenveld, R. (2007). Nonparametric statistical testing of EEG- and MEG-data. J Neurosci Methods *164*, 177-190.

Mason, M.F., Norton, M.I., Van Horn, J.D., Wegner, D.M., Grafton, S.T., and Macrae, C.N. (2007). Wandering minds: the default network and stimulus-independent thought. science *315*, 393-395.

Mathôt, S., Schreij, D., and Theeuwes, J. (2012). OpenSesame: An open-source, graphical experiment builder for the social sciences. Behavior research methods *44*, 314-324.

Matthews, S.C., Simmons, A.N., Strigo, I., Jang, K., Stein, M.B., and Paulus, M.P. (2007). Heritability of anterior cingulate response to conflict: an fMRI study in female twins. NeuroImage *38*, 223-227.

Mattia, M., Spadacenta, S., Pavone, L., Quarato, P., Esposito, V., Sparano, A., Sebastiano, F., Di Gennaro, G., Morace, R., and Cantore, G. (2012). Stop-event-related potentials from intracranial electrodes reveal a key role of premotor and motor cortices in stopping ongoing movements. Frontiers in neuroengineering *5*, 12.

Matzke, D., Love, J., Wiecki, T.V., Brown, S.D., Logan, G.D., and Wagenmakers, E.-J. (2013). Release the BEESTS: Bayesian estimation of ex-Gaussian stop-signal reaction time distributions. Frontiers in Psychology *4*, 918.

Mayka, M.A., Corcos, D.M., Leurgans, S.E., and Vaillancourt, D.E. (2006). Three-dimensional locations and boundaries of motor and premotor cortices as defined by functional brain imaging: A meta-analysis. Neuroimage *31*, 1453-1474.

Mazaheri, A., Nieuwenhuis, I.L.C., van Dijk, H., and Jensen, O. (2009). Prestimulus alpha and mu activity predicts failure to inhibit motor responses. Human Brain Mapping *30*, 1791-1800.

McDannold, N., Zhang, Y., Power, C., Arvanitis, C.D., Vykhodtseva, N., and Livingstone, M. (2015). Targeted, noninvasive blockade of cortical neuronal activity. Sci Rep *5*, 16253.

McRae, K., Reiman, E.M., Fort, C.L., Chen, K., and Lane, R.D. (2008). Association between trait emotional awareness and dorsal anterior cingulate activity during emotion is arousal-dependent. NeuroImage *41*, 648-655.

Meairs, S. (2015). Facilitation of Drug Transport across the Blood-Brain Barrier with Ultrasound and Microbubbles. Pharmaceutics *7*, 275-293.

Mehic, E., Xu, J.M., Caler, C.J., Coulson, N.K., Moritz, C.T., and Mourad, P.D. (2014). Increased anatomical specificity of neuromodulation via modulated focused ultrasound. PLoS One *9*, e86939.

Melde, K., Mark, A.G., Qiu, T., and Fischer, P. (2016a). Holograms for acoustics. Nature *537*, 518-522.

Melde, K., Mark, A.G., Qiu, T., and Fischer, P. (2016b). Holograms for acoustics. Nature *537*, 518-522.

Meng, X., Gao, S., Liu, W., Zhang, L., Suo, T., and Li, H. (2019). The Childhood Maltreatment Modulates the Impact of Negative Emotional Stimuli on Conflict Resolution. Frontiers in Psychology *10*.

Menz, M.D., Oralkan, Ö., Khuri-Yakub, P.T., and Baccus, S.A. (2013). Precise neural stimulation in the retina using focused ultrasound. The Journal of Neuroscience *33*, 4550-4560.

Mihran, R.T., Barnes, F.S., and Wachtel, H. (1990). Temporally-specific modification of myelinated axon excitability in vitro following a single ultrasound pulse. Ultrasound in medicine & biology *16*, 297-309.

Mogg, K., and Bradley, B.P. (2016). Anxiety and attention to threat: Cognitive mechanisms and treatment with attention bias modification. Behaviour Research and Therapy *87*, 76-108.

Moore, A., Gruber, T., Derose, J., and Malinowski, P. (2012). Regular, brief mindfulness meditation practice improves electrophysiological markers of attentional control. Frontiers in human neuroscience *6*.

Moran, R.J., Campo, P., Symmonds, M., Stephan, K.E., Dolan, R.J., and Friston, K.J. (2013). Free energy, precision and learning: the role of cholinergic neuromodulation. Journal of Neuroscience *33*, 8227-8236.

Morein‐Zamir, S., Dodds, C., van Hartevelt, T.J., Schwarzkopf, W., Sahakian, B., Müller, U., and Robbins, T. (2014). Hypoactivation in right inferior frontal cortex is specifically associated with motor response inhibition in adult ADHD. Human brain mapping *35*, 5141-5152.

Morishita, T., Fayad, S.M., Higuchi, M.A., Nestor, K.A., and Foote, K.D. (2014). Deep brain stimulation for treatment-resistant depression: systematic review of clinical outcomes. Neurotherapeutics *11*, 475-484.

Mueller, J., Legon, W., Opitz, A., Sato, T.F., and Tyler, W.J. (2014). Transcranial focused ultrasound modulates intrinsic and evoked EEG dynamics. Brain stimulation *7*, 900-908.

Mueller, J.K., and Tyler, W.J. (2014). A quantitative overview of biophysical forces impinging on neural function. Phys Biol *11*, 051001.

Munakata, Y., Herd, S.A., Chatham, C.H., Depue, B.E., Banich, M.T., and O'Reilly, R.C. (2011). A unified framework for inhibitory control. Trends in cognitive sciences *15*, 453-459.

Munneke, G.-J., Nap, T.S., Schippers, E.E., and Cohen, M.X. (2015). A statistical comparison of EEG time- and time–frequency domain representations of error processing. Brain Research *1618*, 222-230.

Murphy, J., Devue, C., Corballis, P.M., and Grimshaw, G.M. (2020). Proactive Control of Emotional Distraction: Evidence From EEG Alpha Suppression. Frontiers in Human Neuroscience *14*.

Naor, O., Krupa, S., and Shoham, S. (2016). Ultrasonic neuromodulation. Journal of neural engineering *13*, 031003.

Nee, D.E., Kastner, S., and Brown, J.W. (2011). Functional heterogeneity of conflict, error, task-switching, and unexpectedness effects within medial prefrontal cortex. Neuroimage *54*, 528-540.

Neumann, M.F., Mohamed, T.N., and Schweinberger, S.R. (2011). Face and object encoding under perceptual load: ERP evidence. NeuroImage *54*, 3021-3027.

Nyborg, W.L. (2000). Biological effects of ultrasound: development of safety guidelines. Part I: personal histories. Ultrasound in medicine & biology *26*, 911-964.

O'Brien, W.D., Jr. (2007). Ultrasound-biophysics mechanisms. Progress in biophysics and molecular biology *93*, 212-255.

O'Halloran, R., Kopell, B.H., Sprooten, E., Goodman, W.K., and Frangou, S. (2016). Multimodal Neuroimaging-Informed Clinical Applications in Neuropsychiatric Disorders. Frontiers in psychiatry *7*, 63.

Obeso, I., Robles, N., Muñoz-Marrón, E., and Redolar-Ripoll, D. (2013). Dissociating the role of the pre-SMA in response inhibition and switching: a combined online and offline TMS approach. Frontiers in human neuroscience *7*, 150.

Okon-Singer, H., Hendler, T., Pessoa, L., and Shackman, A.J. (2015). The neurobiology of emotion–cognition interactions: fundamental questions and strategies for future research. Frontiers in Human Neuroscience *9*.

Ólafsson, R.P., Smári, J., Guðmundsdóttir, F., Ólafsdóttir, G., Harðardóttir, H.L., and Einarsson, S.M. (2011). Self reported attentional control with the Attentional Control Scale:

Factor structure and relationship with symptoms of anxiety and depression. Journal of Anxiety Disorders *25*, 777-782.

Omer, N., Yoni, H., Esther, Z., Eitan, K., and Shy, S. (2012). Towards multifocal ultrasonic neural stimulation II: design considerations for an acoustic retinal prosthesis. Journal of neural engineering *9*, 026006.

Opitz, A., Legon, W., Rowlands, A., Bickel, W.K., Paulus, W., and Tyler, W.J. (2013a). Physiological observations validate finite element models for estimating subject-specific electric field distributions induced by transcranial magnetic stimulation of the human motor cortex. Neuroimage *81*, 253-264.

Opitz, A., Legon, W., Rowlands, A., Bickel, W.K., Paulus, W., and Tyler, W.J. (2013b). Physiological observations validate finite element models for estimating subject-specific electric field distributions induced by transcranial magnetic stimulation of the human motor cortex. Neuroimage *81*, 253-264.

Osmanski, B.F., Pezet, S., Ricobaraza, A., Lenkei, Z., and Tanter, M. (2014). Functional ultrasound imaging of intrinsic connectivity in the living rat brain with high spatiotemporal resolution. Nat Commun *5*, 5023.

Overbeek, T.J.M., Nieuwenhuis, S., and Ridderinkhof, K.R. (2005). Dissociable Components of Error Processing. Journal of Psychophysiology *19*, 319-329.

Papazacharias, A., Taurisano, P., Fazio, L., Gelao, B., Di Giorgio, A., Lo Bianco, L., Quarto, T., Mancini, M., Porcelli, A., Romano, R.*, et al.* (2015). Aversive emotional interference impacts behavior and prefronto-striatal activity during increasing attentional control. Front Behav Neurosci *9*, 97.

Park, G., Van Bavel, J.J., Vasey, M.W., and Thayer, J.F. (2012). Cardiac vagal tone predicts inhibited attention to fearful faces. Emotion *12*, 1292.

Park, G., Van Bavel, J.J., Vasey, M.W., and Thayer, J.F. (2013). Cardiac vagal tone predicts attentional engagement to and disengagement from fearful faces. Emotion *13*, 645-656.

Park, G., Vasey, M.W., Van Bavel, J.J., and Thayer, J.F. (2014). When tonic cardiac vagal tone predicts changes in phasic vagal tone: the role of fear and perceptual load. Psychophysiology *51*, 419-426.

Parker, K.J., and Alonso, M.A. (2016). Longitudinal iso-phase condition and needle pulses. Opt Express *24*, 28669-28677.

Peirce, J.W. (2007). PsychoPy—psychophysics software in Python. Journal of neuroscience methods *162*, 8-13.

Penny, W.D. (2012). Comparing dynamic causal models using AIC, BIC and free energy. Neuroimage *59*, 319-330.

Penny, W.D., Stephan, K.E., Daunizeau, J., Rosa, M.J., Friston, K.J., Schofield, T.M., and Leff, A.P. (2010). Comparing families of dynamic causal models. PLoS Comput Biol *6*, e1000709.

Phelps, E.A., O'Connor, K.J., Gatenby, J.C., Gore, J.C., Grillon, C., and Davis, M. (2001). Activation of the left amygdala to a cognitive representation of fear. Nature neuroscience *4*, 437-441.

Plaksin, M., Kimmel, E., and Shoham, S. (2016a). Cell-Type-Selective Effects of Intramembrane Cavitation as a Unifying Theoretical Framework for Ultrasonic Neuromodulation. eNeuro *3*.

Plaksin, M., Kimmel, E., and Shoham, S. (2016b). Cell-Type-Selective Effects of Intramembrane Cavitation as a Unifying Theoretical Framework for Ultrasonic Neuromodulation. eneuro *3*, ENEURO. 0136-0115.2016.

Polli, F.E., Barton, J.J.S., Cain, M.S., Thakkar, K.N., Rauch, S.L., and Manoach, D.S. (2005). Rostral and dorsal anterior cingulate cortex make dissociable contributions during antisaccade error commission. Proceedings of the National Academy of Sciences *102*, 15700-15705.

Posner, M.I. (2011). Attention in a social world (Oxford University Press).

Posner, M.I., Rothbart, M.K., and Ghassemzadeh, H. (2019). Restoring Attention Networks. Yale J Biol Med *92*, 139-143.

Prieto, M.L., Oralkan, Ö., Khuri-Yakub, B.T., and Maduke, M.C. (2013). Dynamic Response of Model Lipid Membranes to Ultrasonic Radiation Force. PLOS ONE *8*, e77115.

Rademacher, J., Morosan, P., Schormann, T., Schleicher, A., Werner, C., Freund, H.-J., and Zilles, K. (2001). Probabilistic mapping and volume measurement of human primary auditory cortex. Neuroimage *13*, 669-683.

Rae, C.L., Hughes, L.E., Anderson, M.C., and Rowe, J.B. (2015). The prefrontal cortex achieves inhibitory control by facilitating subcortical motor pathway connectivity. Journal of neuroscience *35*, 786-794.

Raichle, M.E., MacLeod, A.M., Snyder, A.Z., Powers, W.J., Gusnard, D.A., and Shulman, G.L. (2001). A default mode of brain function. Proceedings of the National Academy of Sciences *98*, 676-682.

Ray Li, C.-s., Huang, C., Constable, R.T., and Sinha, R. (2006). Imaging Response Inhibition in a Stop-Signal Task: Neural Correlates Independent of Signal Monitoring and Post-Response Processing. The Journal of Neuroscience *26*, 186-192.

Righart, R., and de Gelder, B. (2006). Context Influences Early Perceptual Analysis of Faces—An Electrophysiological Study. Cerebral Cortex *16*, 1249-1257.

Rinaldi, P.C., Jones, J.P., Reines, F., and Price, L.R. (1991). Modification by focused ultrasound pulses of electrically evoked responses from an in vitro hippocampal preparation. Brain Res *558*, 36-42.

Rochais, C., Fureix, C., Lesimple, C., and Hausberger, M. (2016). Lower attention to daily environment: a novel cue for detecting chronic horses' back pain? Scientific reports *6*.

Rodriguez, A., Tatter, S.B., and Debinski, W. (2015). Neurosurgical Techniques for Disruption of the Blood-Brain Barrier for Glioblastoma Treatment. Pharmaceutics *7*, 175-187.

Rushworth, M., Behrens, T., Rudebeck, P., and Walton, M. (2007). Contrasting roles for cingulate and orbitofrontal cortex in decisions and social behaviour. Trends in cognitive sciences *11*, 168-176.

Sadaghiani, S., and D'Esposito, M. (2015). Functional Characterization of the Cingulo-Opercular Network in the Maintenance of Tonic Alertness. Cerebral Cortex *25*, 2763-2773.

Sadaghiani, S., Scheeringa, R., Lehongre, K., Morillon, B., Giraud, A.L., and Kleinschmidt, A. (2010). Intrinsic Connectivity Networks, Alpha Oscillations, and Tonic Alertness: A Simultaneous Electroencephalography/Functional Magnetic Resonance Imaging Study. Journal of Neuroscience *30*, 10243-10250.

Saleh, T.M., and Connell, B.J. (1998). Role of the insular cortex in the modulation of baroreflex sensitivity. American Journal of Physiology-Regulatory, Integrative and Comparative Physiology *274*, R1417-R1424.

Sanguinetti, J., Smith, E., Goldstein, M., Tyler, W., Hameroff, S., and JJB, A. (2016). Transcranial ultrasound (TUS) effects on mood, vigor, and non-attachment. Psychophysiology *53*.

Sanguinetti, J.L., Hameroff, S., Smith, E.E., Sato, T., Daft, C.M.W., Tyler, W.J., and Allen, J.J.B. (2020). Transcranial Focused Ultrasound to the Right Prefrontal Cortex Improves Mood and Alters Functional Connectivity in Humans. Frontiers in Human Neuroscience *14*.

Sarapas, C., Weinberg, A., Langenecker, S.A., and Shankman, S.A. (2017). Relationships among attention networks and physiological responding to threat. Brain and Cognition *111*, 63-72.

Sato, T., Shapiro, M.G., and Tsao, D.Y. (2018). Ultrasonic neuromodulation causes widespread cortical activation via an indirect auditory mechanism. Neuron *98*, 1031-1041. e1035.

Schmajuk, M., Liotti, M., Busse, L., and Woldorff, M.G. (2006). Electrophysiological activity underlying inhibitory control processes in normal adults. Neuropsychologia *44*, 384-395.

Schmittmann, V.D., Jahfari, S., Borsboom, D., Savi, A.O., and Waldorp, L.J. (2015). Making Large-Scale Networks from fMRI Data. PLOS ONE *10*, e0129074.

Seeley, W.W., Menon, V., Schatzberg, A.F., Keller, J., Glover, G.H., Kenna, H., Reiss, A.L., and Greicius, M.D. (2007). Dissociable intrinsic connectivity networks for salience processing and executive control. Journal of Neuroscience *27*, 2349-2356.

Shackman, A.J., Salomons, T.V., Slagter, H.A., Fox, A.S., Winter, J.J., and Davidson, R.J. (2011). The Integration of Negative Affect, Pain, and Cognitive Control in the Cingulate Cortex. Nature reviews Neuroscience *12*, 154-167.

Shafer, A.T., Matveychuk, D., Penney, T., O'Hare, A.J., Stokes, J., and Dolcos, F. (2012). Processing of emotional distraction is both automatic and modulated by attention: evidence from an event-related fMRI investigation. Journal of cognitive neuroscience *24*, 1233-1252.

Shaffer, F., and Ginsberg, J.P. (2017). An Overview of Heart Rate Variability Metrics and Norms. Front Public Health *5*, 258.

Shaffer, F., McCraty, R., and Zerr, C.L. (2014). A healthy heart is not a metronome: an integrative review of the heart's anatomy and heart rate variability. Frontiers in Psychology *5*.

Shafritz, K.M., Collins, S.H., and Blumberg, H.P. (2006). The interaction of emotional and cognitive neural systems in emotionally guided response inhibition. Neuroimage *31*, 468-475.

Sharp, D., Bonnelle, V., De Boissezon, X., Beckmann, C., James, S., Patel, M., and Mehta, M.A. (2010). Distinct frontal systems for response inhibition, attentional capture, and error processing. Proceedings of the National Academy of Sciences *107*, 6106-6111.

Shi, C., and Davis, M. (1999). Pain pathways involved in fear conditioning measured with fear-potentiated startle: lesion studies. Journal of Neuroscience *19*, 420-430.

Shulman, G.L., Astafiev, S.V., Franke, D., Pope, D.L., Snyder, A.Z., McAvoy, M.P., and Corbetta, M. (2009). Interaction of stimulus-driven reorienting and expectation in ventral and dorsal frontoparietal and basal ganglia-cortical networks. Journal of Neuroscience *29*, 4392-4407.

Sivasubramanian, K., Periyasamy, V., Dienzo, R.A., and Pramanik, M. (2018). Hand-held, clinical dual mode ultrasound - photoacoustic imaging of rat urinary bladder and its applications. Journal of Biophotonics *11*, e201700317.

Smith, N.K., Cacioppo, J.T., Larsen, J.T., and Chartrand, T.L. (2003). May I have your attention, please: Electrocortical responses to positive and negative stimuli. Neuropsychologia *41*, 171-183.

Spadoni, A., and Daraio, C. (2010). Generation and control of sound bullets with a nonlinear acoustic lens. Proc Natl Acad Sci U S A *107*, 7230-7234.

Spangler, D.P., and McGinley, J.J. (2020). Vagal Flexibility Mediates the Association Between Resting Vagal Activity and Cognitive Performance Stability Across Varying Socioemotional Demands. Frontiers in Psychology *11*.

Spreng, R.N., Sepulcre, J., Turner, G.R., Stevens, W.D., and Schacter, D.L. (2012). Intrinsic Architecture Underlying the Relations among the Default, Dorsal Attention, and Frontoparietal Control Networks of the Human Brain. Journal of Cognitive Neuroscience *25*, 74-86.

Sridharan, D., Levitin, D.J., and Menon, V. (2008). A critical role for the right fronto-insular cortex in switching between central-executive and default-mode networks. Proc Natl Acad Sci U S A *105*, 12569-12574.

Stemmer, B., Segalowitz, S.J., Witzke, W., and Schönle, P.W. (2004). Error detection in patients with lesions to the medial prefrontal cortex: an ERP study. Neuropsychologia *42*, 118-130.

Swann, N.C., Cai, W., Conner, C.R., Pieters, T.A., Claffey, M.P., George, J.S., Aron, A.R., and Tandon, N. (2012). Roles for the pre-supplementary motor area and the right inferior frontal gyrus in stopping action: Electrophysiological responses and functional and structural connectivity. NeuroImage *59*, 2860-2870.

Tang, Y.-Y., Lu, Q., Feng, H., Tang, R., and Posner, M.I. (2015). Short-term meditation increases blood flow in anterior cingulate cortex and insula. Frontiers in Psychology *6*.

Tang, Y.Y., Lu, Q., Geng, X., Stein, E.A., Yang, Y., and Posner, M.I. (2010). Short-term meditation induces white matter changes in the anterior cingulate. Proc Natl Acad Sci U S A *107*, 15649-15652.

Taylor, K.S., Seminowicz, D.A., and Davis, K.D. (2009). Two systems of resting state connectivity between the insula and cingulate cortex. Human brain mapping *30*, 2731-2745.

Teper, R., and Inzlicht, M. (2013). Meditation, mindfulness and executive control: the importance of emotional acceptance and brain-based performance monitoring. Social cognitive and affective neuroscience *8*, 85-92.

Thayer, J.F., Ahs, F., Fredrikson, M., Sollers, J.J., 3rd, and Wager, T.D. (2012). A meta-analysis of heart rate variability and neuroimaging studies: implications for heart rate variability as a marker of stress and health. Neurosci Biobehav Rev *36*, 747-756.

Tomaiuolo, F., MacDonald, J., Caramanos, Z., Posner, G., Chiavaras, M., Evans, A.C., and Petrides, M. (1999). Morphology, morphometry and probability mapping of the pars opercularis of the inferior frontal gyrus: an in vivo MRI analysis. European Journal of Neuroscience *11*, 3033-3046.

Tottenham, N., Tanaka, J.W., Leon, A.C., McCarry, T., Nurse, M., Hare, T.A., Marcus, D.J., Westerlund, A., Casey, B.J., and Nelson, C. (2009). The NimStim set of facial expressions: judgments from untrained research participants. Psychiatry Res *168*, 242-249.

Treeby, B.E., and Cox, B.T. (2010). k-Wave: MATLAB toolbox for the simulation and reconstruction of photoacoustic wave fields. BIOMEDO *15*, 021314.

Tsui, P.H., Wang, S.H., and Huang, C.C. (2005). In vitro effects of ultrasound with different energies on the conduction properties of neural tissue. Ultrasonics *43*, 560-565.

Tufail, Y., Matyushov, A., Baldwin, N., Tauchmann, M.L., Georges, J., Yoshihiro, A., Tillery, S.I.H., and Tyler, W.J. (2010). Transcranial pulsed ultrasound stimulates intact brain circuits. Neuron *66*, 681-694.

Tufail, Y., Yoshihiro, A., Pati, S., Li, M.M., and Tyler, W.J. (2011a). Ultrasonic neuromodulation by brain stimulation with transcranial ultrasound. Nature protocols *6*, 1453-1470.

Tufail, Y., Yoshihiro, A., Pati, S., Tauchmann, M.L., and Tyler, W.J. (2011b). Ultrasonic Neuromodulation by Brain Stimulation with Transcranial Ultrasound. Nature protocols *6*, 1453-1470.

Tyler, W.J. (2011). Noninvasive neuromodulation with ultrasound? A continuum mechanics hypothesis. Neuroscientist *17*, 25-36.

Tyler, W.J. (2012). The mechanobiology of brain function. Nat Rev Neurosci *13*, 867-878.

Tyler, W.J., Tufail, Y., Finsterwald, M., Tauchmann, M.L., Olson, E.J., and Majestic, C. (2008). Remote excitation of neuronal circuits using low-intensity, low-frequency ultrasound. PLoS ONE *3*, e3511.

Vaden, K.I., Jr., Kuchinsky, S.E., Cute, S.L., Ahlstrom, J.B., Dubno, J.R., and Eckert, M.A. (2013). The cingulo-opercular network provides word-recognition benefit. J Neurosci *33*, 18979-18986.

van Driel, J., Ridderinkhof, K.R., and Cohen, M.X. (2012). Not All Errors Are Alike: Theta and Alpha EEG Dynamics Relate to Differences in Error-Processing Dynamics. Journal of Neuroscience *32*, 16795-16806.

van Steenbergen, H., Band, G.P., and Hommel, B. (2010). In the mood for adaptation: how affect regulates conflict-driven control. Psychol Sci *21*, 1629-1634.

Verbruggen, F., Aron, A.R., Stevens, M.A., and Chambers, C.D. (2010). Theta burst stimulation dissociates attention and action updating in human inferior frontal cortex. Proceedings of the National Academy of Sciences *107*, 13966-13971.

Verbruggen, F., and Logan, G.D. (2008). Response inhibition in the stop-signal paradigm. Trends in cognitive sciences *12*, 418-424.

Verbruggen, F., and Logan, G.D. (2009). Models of response inhibition in the stop-signal and stop-change paradigms. Neuroscience & Biobehavioral Reviews *33*, 647-661.

Vincent, J.L., Kahn, I., Snyder, A.Z., Raichle, M.E., and Buckner, R.L. (2008). Evidence for a frontoparietal control system revealed by intrinsic functional connectivity. Journal of neurophysiology *100*, 3328-3342.

Vogt, B.A. (2005). Pain and emotion interactions in subregions of the cingulate gyrus. Nature reviews Neuroscience *6*, 533.

Vollmer, M. (2015). A robust, simple and reliable measure of heart rate variability using relative RR intervals. Paper presented at: 2015 Computing in Cardiology Conference (CinC) (IEEE).

Vossel, S., Thiel, C.M., and Fink, G.R. (2006). Cue validity modulates the neural correlates of covert endogenous orienting of attention in parietal and frontal cortex. Neuroimage *32*, 1257-1264.

Wang, L., LaBar, K.S., Smoski, M., Rosenthal, M.Z., Dolcos, F., Lynch, T.R., Krishnan, R.R., and McCarthy, G. (2008). Prefrontal mechanisms for executive control over emotional distraction are altered in major depression. Psychiatry Research: Neuroimaging *163*, 143-155.

Wang, S., Olumolade, O.O., Sun, T., Samiotaki, G., and Konofagou, E.E. (2015). Noninvasive, neuron-specific gene therapy can be facilitated by focused ultrasound and recombinant adeno-associated virus. Gene therapy *22*, 104-110.

Watson, D., Clark, L.A., and Tellegen, A. (1988). Development and validation of brief measures of positive and negative affect: the PANAS scales. Journal of personality and social psychology *54*, 1063.

Weissman, D.H., Roberts, K.C., Visscher, K.M., and Woldorff, M.G. (2006). The neural bases of momentary lapses in attention. Nat Neurosci *9*, 971-978.

Wessel, J.R., and Aron, A.R. (2015). It's not too late: The onset of the frontocentral P3 indexes successful response inhibition in the stop - signal paradigm. Psychophysiology *52*, 472-480.

Wessel, J.R., and Aron, A.R. (2017). On the globality of motor suppression: unexpected events and their influence on behavior and cognition. Neuron *93*, 259-280.

Wessel, J.R., Danielmeier, C., Morton, J.B., and Ullsperger, M. (2012). Surprise and error: common neuronal architecture for the processing of errors and novelty. Journal of Neuroscience *32*, 7528-7537.

Whalen, P.J., Bush, G., McNally, R.J., Wilhelm, S., McInerney, S.C., Jenike, M.A., and Rauch, S.L. (1998). The emotional counting Stroop paradigm: a functional magnetic resonance imaging probe of the anterior cingulate affective division. Biological psychiatry *44*, 1219-1228.

White, P.J., Clement, G.T., and Hynynen, K. (2006). Local frequency dependence in transcranial ultrasound transmission. Physics in medicine and biology *51*, 2293-2305.

Wiecki, T.V., and Frank, M.J. (2013). A computational model of inhibitory control in frontal cortex and basal ganglia. Psychological Review *120*, 329.

Wild, C.J., Yusuf, A., Wilson, D.E., Peelle, J.E., Davis, M.H., and Johnsrude, I.S. (2012). Effortful listening: the processing of degraded speech depends critically on attention. Journal of Neuroscience *32*, 14010-14021.

Williams, L.M., Brown, K.J., Das, P., Boucsein, W., Sokolov, E.N., Brammer, M.J., Olivieri, G., Peduto, A., and Gordon, E. (2004). The dynamics of cortico-amygdala and autonomic activity over the experimental time course of fear perception. Cognitive Brain Research *21*, 114-123.

Xie, L., Ren, M., Cao, B., and Li, F. (2017). Distinct brain responses to different inhibitions: Evidence from a modified Flanker Task. Sci Rep *7*, 6657.

Xu, K.Z., Anderson, B.A., Emeric, E.E., Sali, A.W., Stuphorn, V., Yantis, S., and Courtney, S.M. (2017). Neural basis of cognitive control over movement inhibition: human fMRI and primate electrophysiology evidence. Neuron *96*, 1447-1458. e1446.

Yamawaki, N., Borges, K., Suter, B.A., Harris, K.D., and Shepherd, G.M. (2014). A genuine layer 4 in motor cortex with prototypical synaptic circuit connectivity. Elife *3*, e05422.

Yang, P.S., Kim, H., Lee, W., Bohlke, M., Park, S., Maher, T.J., and Yoo, S.-S. (2012). Transcranial focused ultrasound to the thalamus is associated with reduced extracellular GABA levels in rats. Neuropsychobiology *65*, 153-160.

Yang, S., Luo, W., Zhu, X., Broster, L.S., Chen, T., Li, J., and Luo, Y. (2014). Emotional content modulates response inhibition and perceptual processing. Psychophysiology *51*, 1139-1146.

Yang, S., Xing, D., Zhou, Q., Xiang, L., and Lao, Y. (2007). Functional imaging of cerebrovascular activities in small animals using high-resolution photoacoustic tomography. Med Phys *34*, 3294-3301.

Yang, X., and Wang, L.V. (2008). Monkey brain cortex imaging by photoacoustic tomography. J Biomed Opt *13*, 044009.

Yoo, S.S., Bystritsky, A., Lee, J.H., Zhang, Y., Fischer, K., Min, B.K., McDannold, N.J., Pascual-Leone, A., and Jolesz, F.A. (2011). Focused ultrasound modulates region-specific brain activity. Neuroimage.

Yordanova, J., Falkenstein, M., Hohnsbein, J., and Kolev, V. (2004). Parallel systems of error processing in the brain. NeuroImage *22*, 590-602.

Zaki, J., Davis, J.I., and Ochsner, K.N. (2012). Overlapping activity in anterior insula during interoception and emotional experience. NeuroImage *62*, 493-499.

Zhang, S., Yin, L., and Fang, N. (2009). Focusing Ultrasound with an Acoustic Metamaterial Network. Physics Reviews Letters *102*, 194301-194304.

APPENDIX A

CO-AUTHOR PERMISSIONS

CHAPTER 2

Chapter 2 of this document is a reprint of an accepted manuscript of an article published by Taylor & Francis Group © 2017 on behalf of Institute of Psychiatry and Johns Hopkins University in International Review of Psychiatry on 21 Apr 2017, available online: https://www.tandfonline.com/doi/full/10.1080/09540261.2017.1302924 (Fini and Tyler, 2017). The article was coauthored with Dr. William "Jamie" Tyler. Dr. Tyler as well as the publisher have given their permission for use of material in this document.

CHAPTER 5

Chapter 5 of this document was co-authored with Dr. Justin M. Fine, Archana Mysore, Dr. William "Jamie" Tyler, and Dr. Marco Santello. All co-authors have granted their permission for the reproduction of this material. The chapter was prepared for publication, but not yet accepted.

APPENDIX B

SUPPLEMENTARY MATERIALS FOR CHAPTER 3

Supplemental Information

Transcranial focused ultrasound to the dorsal anterior cingulate cortex alters conflict and emotional processing, physiology, and performance

Supplemental Figures

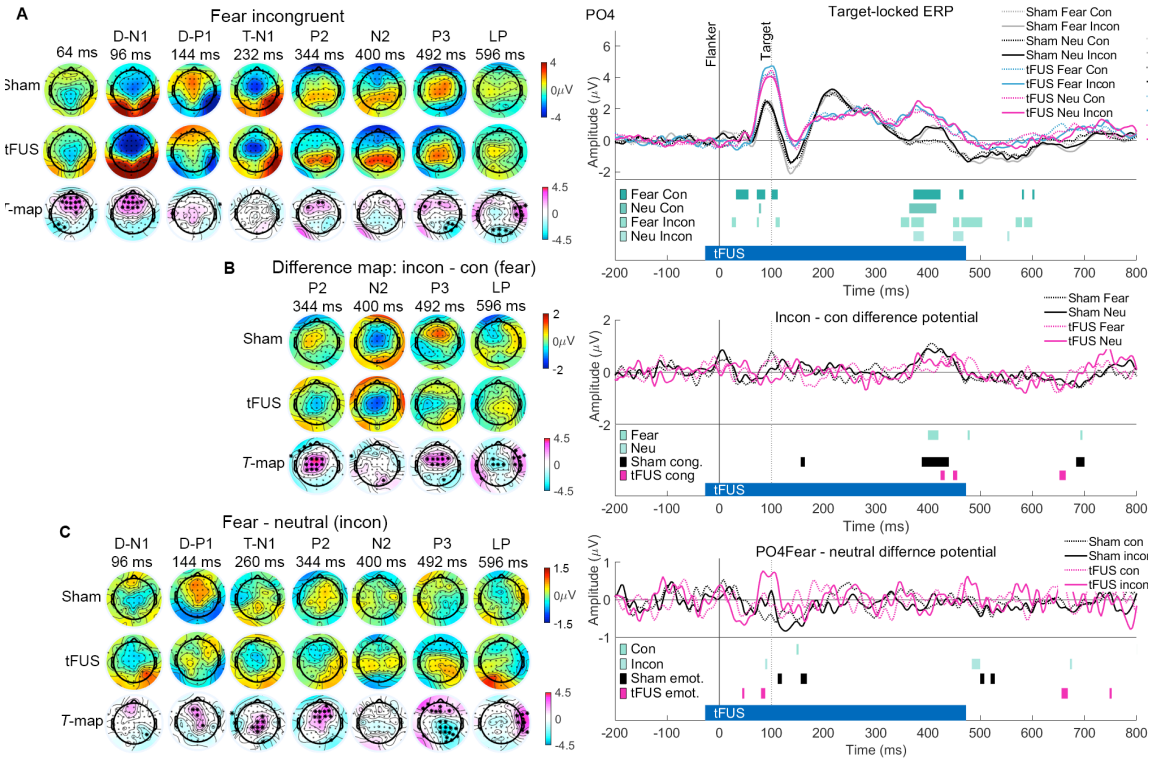

Figure S1. Scalp potentials and ERPs at P4
(A) Scalp-potential voltage topography maps of target locked ERPs displayed in Figure 2. Faces and flanker distractor arrows appeared at 0 ms, and target arrow appeared at 100 ms. tFUS stimulation began 28 ms prior to the faces, and lasted until 472 ms. T value maps plotted below (permutation testing, significant electrodes marked with *; magenta indicates Sham more positive than tFUS, cyan Sham more negative than tFUS.
(B) Incongruent minus congruent potential (fear condition) for later ERP peaks in A.
(C) Fear – neutral potential (incongruent condition).
Right-hand panel displays ERP at PO4 with incon – con and fear – neutral difference potential. Green bars represent permutation testing across groups, magenta and black bars represent main effect of congruency (cong.) or emotion (emot.) within groups (RM-ANOVA). Related to Figure 2, Table S1, Table S2 and Table S3.

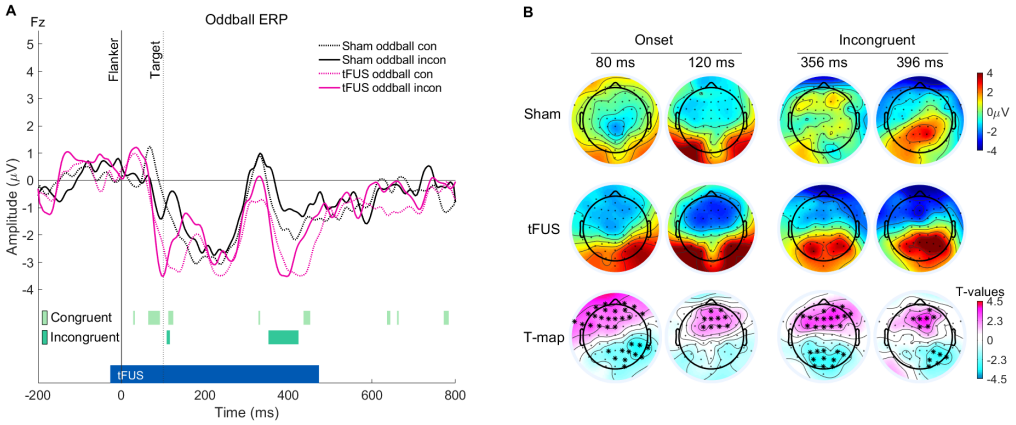

Figure 2. Oddball event related potentials.
(A) ERP to the oddball trials at Fz, 0ms represents onset of oddball/scrambled image and distractor flanker arrows, 100 ms marks onset of target arrow. Bars on the bottom of the figure represent the results of Sham vs. tFUS permutation testing ($p < 0.05$).
(B) Scalp maps correspond to significant regions in A. Oddball onset displays the results of pooled incongruent and congruent trials. *T* values displayed at the bottom of the figure; * represents electrodes $p < 0.05$ (permutation testing).

Supplemental Tables

	Fear congruent			Neutral congruent		
SEP complex	Sham	tFUS	*p*	Sham	tFUS	*p*
D N1	-2.95 ± 0.62	-4.59 ± 0.77	0.013*	-3.26 ± 0.50	-4.61 ± 0.60	0.019*
D N1 - D P1	5.73 ± 0.97	6.26 ± 0.94	0.86	5.09 ± 1.03	6.36 ± 0.88	0.64
D P1 - T N1	-6.45 ± 1.19	-5.04 ± 1.16	0.67	-6.60 ± 1.12	-4.50 ± 1.12	0.64
T N1 - P2	3.01 ± 0.48	3.36 ± 0.72	0.47	4.22 ± 0.45	3.20 ± 0.79	0.93
P2 - N2	0.10 ± 0.47	0.20± 0.43	0.77	0.04 ± 0.47	0.84 ± 0.43	0.65
N2 - P3	0.76 ± 0.42	0.94 ± 0.61	0.52	0.25 ± 0.51	1.35 ± 0.62	0.39
	Fear incongruent			Neutral incongruent		
SEP complex	Sham	tFUS	*p*	Sham	tFUS	*p*
D N1	-2.73 ± 0.61	-4.84 ± 0.82	0.017*	-2.84 ± 0.75	-4.99 ± 0.63	0.047*
D N1 - D P1	5.53 ± 1.07	6.28 ± 0.98	0.83	4.76 ± 0.99	5.56 ± 0.99	0.72
D P1 - T N1	-6.35 ± 1.30	-5.75 ± 1.18	0.66	-5.78 ± 1.08	-5.28 ± 1.08	0.78
T N1 - P2	4.94 ± 0.52	3.48 ± 0.69	0.69	4.12 ± 0.55	3.31 ± 0.56	0.84
P2 - N2	-2.63 ± 0.54	-1.06 ± 0.71	0.067	-2.29 ± 0.43	-1.14 ± 0.68	0.29
N2 - P3	4.01 ± 0.78	3.57 ± 0.71	0.15	4.01 ± 0.71	2.72 ± 0.62	0.16

Table S1. ERP peak-to-peak amplitude at FCz comparing Sham and tFUS groups
Amplitude displayed as median ± SEM (μV) and represent peak-to-through (ERP complex) amplitude values from individual subjects' ERP peaks. *p*- values represent the results of permutation testing across groups (* $p < 0.05$). Related to Figure 2 and Table S2. See also Table S3.

Sham								
			Post – hoc statics					
ERP complex	χ^2	p	Neutral con vs incon	Fear con vs incon	Con fear vs neu	Incon fear vs neu	Fear con vs neu incon	Neu con vs fear incon
D-N1	1.11	0.48	-	-	-	-	-	-
D-N1 - D-P1	7.63	0.048*	1	1	0.20	0.41	0.20	0.41
D-P1 - T-N1	5.06	0.089	-	-	-	-	-	-
T-N1 - P2	13.46	0.010*	1	0.005*	0.64	0.34	0.47	0.24
P2 - N2	30.43	< 0.001*	0.023*	< 0.001*	1	1	0.005*	< 0.001*
N2 - P3	31.89	< 0.001*	0.009*	< 0.001*	1	0.57	0.09	< 0.001*

tFUS								
			Post – hoc statistics					
ERP complex	χ^2	p	Neutral con vs incon	Fear con vs incon	Con fear vs neu	Incon fear vs neu	Fear con vs neu incon	Neu con vs fear incon
D-N1	4.20	0.24	-	-	-	-	-	-
D-N1 - D-P1	3.74	0.29	-	-	-	-	-	-
D-P1 - T-N1	10.85	0.013*	1	1	0.09	0.20	0.037*	0.41
T-N1 - P2	0.79	0.85	-	-	-	-	-	-
P2 - N2	19.06	< 0.001*	0.003*	0.059	1	1	0.037*	0.005*
N2 - P3	17.03	0.001*	0.29	0.009*	1	0.41	1	0.001*

Table S2. ERP peak-to-peak amplitude at FCz compared within each group using non-parametric Friedman's test

Statistics from non-parametric Friedman's test performed across neutral congruent, fear congruent, neutral incongruent and fear incongruent trials, with three degrees of freedom for all tests, both groups n = 14. Post-hoc statics listed for each trial pair, all post-hoc *p*-values are Bonferroni-corrected. (*$p < 0.05$). Abbreviations: Related to Figure 2 and Table S1. See also Table S3.

	Fear congruent			Neutral congruent		
SEP peak	Sham	tFUS	*p*	Sham	tFUS	*p*
D N1	108 ± 3	104 ± 1	0.75	104 ± 3	100 ± 2	0.87
D P1	148 ± 3	136 ± 3	0.14	144 ± 4	144 ± 4	0.80
T N1	228 ± 8	244 ± 9	0.72	220 ± 8	244 ± 9	0.31
P2	340 ± 4	332 ± 4	0.83	340 ± 4	332 ± 4	0.77
N2	404 ± 5	400 ± 6	0.11	400 ± 4	400 ± 6	0.38
P3	476 ± 5	500 ± 4	0.009*	476 ± 5	500 ± 4	0.009*
	Fear incongruent			Neutral incongruent		
SEP peak	Sham	tFUS	*p*	Sham	tFUS	*p*
D N1	96 ± 3	100 ± 1	0.23	100 ± 3	100 ± 1	0.83
D P1	144 ± 4	140 ± 3	0.67	144 ± 4	144 ± 3	0.90
T N1	228 ± 8	244 ± 8	0.95	220 ± 7	248 ± 8	0.10
P2	340 ± 5	328 ± 3	0.32	340 ± 7	332 ± 4	0.22
N2	408 ± 9	400 ± 5	0.95	400 ± 8	400 ± 5	0.84
P3	488 ± 5	500 ± 4	0.077	488 ± 5	500 ± 4	0.095*

Table S3. ERP peak latency at FCz comparing Sham and tFUS groups
Latencies are displayed as median ± SEM (ms). *p*- values represent the results of permutation testing across groups (* $p < 0.05$). Related to Figure 2. See also Table S1 and Table S2.

	Interaction stimulation × time			Post-hoc statics			
				Sham		tFUS	
	F(1,24)	*p*	η_p^2	% Change	*p*	% Change	*p*
HR (bpm)	7.74	0.010*	0.24	↑ 3 ± 1	0.037*	↓ 2 ± 1	0.098
SDNN (ms)	54.23	< 0.001*	0.69	↓ 20 ± 4	< 0.001*	↑ 24 ± 5	< 0.001*
pNN50 (%)	9.72	0.005*	0.29	↓ 9 ± 11	0.15	↑ 64 ± 18	0.007*
HRV triang.	16.67	< 0.001*	0.41	↓ 9 ± 5	0.12	↑ 34 ± 8	< 0.001*
SD1 (ms)	5.8	0.024*	0.19	↓ 4 ± 6	0.37	↑ 21 ± 7	0.020*
SD2 (ms)	51.7	< 0.001*	0.68	↓ 22 ± 4	< 0.001*	↑ 25 ± 6	< 0.001*
SD1/SD2	4.31	0.049*	0.15	↑ 25 ± 9	0.039*	0 ± 8	0.51

Table S4 Heart rate and heart rate variability changes differ across groups with emotional faces distractors and tFUS
Mixed-measures RM-ANOVA on heart rate and HRV metrics collected during the final three minutes of baseline trials (simple flanker no faces, no stimulation), and the first three minutes of the main trail period (flanker arrows were displayed with emotional distractor faces in the background and the stimulation group received online tFUS on each trial). Related to Figure 7

	Mann-Whitney		H+: Sham > tFUS	H+: Sham < tFUS	Median		Number of subjects RT< baseline		Number of subjects RT > baseline	
Congruent	*p*	U	BF_{+0}	BF_{-0}	Sham	tFUS	Sham	tFUS	Sham	tFUS
Neutral	0.33	76.0	1.02	0.22▽	27	12	1 (0)	3 (1)	11 (10)	9 (6)
Fear	0.33	76.5	0.96	0.19▽	31	11	2 (0)	5 (1)	12 (8)	8 (6)
Oddball	0.33	76.0	0.88	0.17▽	39	28	1 (0)	3 (1)	12 (6)	11 (6)
Post	0.60	110.0	0.21▽	0.44	-6	-1	8 (4)	8 (2)	5 (3)	6 (3)
Incongruent										
Neutral	0.021*	48.5	5.93❖	0.13▽	13	-3	3 (1)	8 (3)	11 (4)	5 (1)
Fear	0.044*	54.5	4.08❖	0.17▽	7	-2	2 (1)	9 (2)	11 (6)	5 (2)
Oddball	0.29	74.0	0.91	0.19▽	17	-2	4 (1)	7 (1)	9 (4)	6 (1)
Post	0.70	89.0	0.52	0.25▽	-3	-10	8 (5)	10 (2)	6 (1)	4 (3)

Table S5. Reaction time group level statistic for baseline-subtracted median RT and change from baseline

Bayesian statistics calculated for the alternative hypothesis that the Sham group is slower than the tFUS group (BF+0), and visa versa (BF-0). Number of subjects with a reaction time faster than their baseline for each trial condition listed in far right column. Number of subjects changing RT from baseline in response to face distractors and stimulation. Number in parenthesis represents number of subjects with significant change from baseline (p <0.05, Mann-Whitney U test).

* p <0.05, Mann-Whitney U test

❖ statistical significance of the alternative hypothesis over the null, Bayesian (BF_{10} > 3)

▽ statistical evidence for the null hypothesis (BF_{10} < 0.3). Related to Figure 8.

	Mann-Whitney		Wilcoxon	H+: Sham > *tFUS*	H+: Sham < *tFUS*		
Congruent	*p*	U	W	BF_{+0}	BF_{-0}	Sham	tFUS
Baseline	0.33	119.5	224.0	$0.25^{\triangledown}$	0.83	99.0 ± 0.22	100.0 ± 26.46
Neutral	1.00	83.5	188.0	0.34	0.38	98.5 ± 0.10	98.0 ± 26.33
Fear	0.18	68.0	173.0	1.66	$0.16^{\triangledown}$	99.0 ± 0.04	98.0 ± 26.46
Oddball	0.51	74.0	179.0	1.31	$0.24^{\triangledown}$	100.0 ± 0.07	100.0 ± 26.73
Post	0.29	83.5	188.0	1.28	$0.18^{\triangledown}$	99.0 ± 0.05	98.0 ± 26.46
Incongruent							
Baseline	0.64	109.0	214.0	$0.29^{\triangledown}$	0.43	95.0 ± 0.11	98.0 ± 25.39
Neutral	0.60	86.0	191.0	0.83	$0.20^{\triangledown}$	92.0 ± 0.05	91.5 ± 24.59
Fear	0.51	83.5	188.0	0.63	$0.22^{\triangledown}$	91.0 ± 0.06	89.0 ± 24.32
Oddball	0.38	78.0	183.0	1.07	$0.22^{\triangledown}$	100.0 ± 0.06	95.0 ± 26.73
Post	0.30	75.5	180.5	0.86	$0.21^{\triangledown}$	93.0 ± 0.06	88.0 ± 24.86

Table S6. Response accuracy

Table displays group level statistics for accuracy. Group median and SEM listed in right hand column. Statistical evidence for the null hypothesis ($^{\triangledown}BF_{10} < 0.3$). See also Table S5.

APPENDIX C

SUPPLEMENTARY MATERIALS FOR CHAPTER 4

Supplemental Information

Transcranial focused ultrasound to the anterior insula/ frontal operculum alters distractor processing during flanker task paired with emotional faces

Supplemental Figures

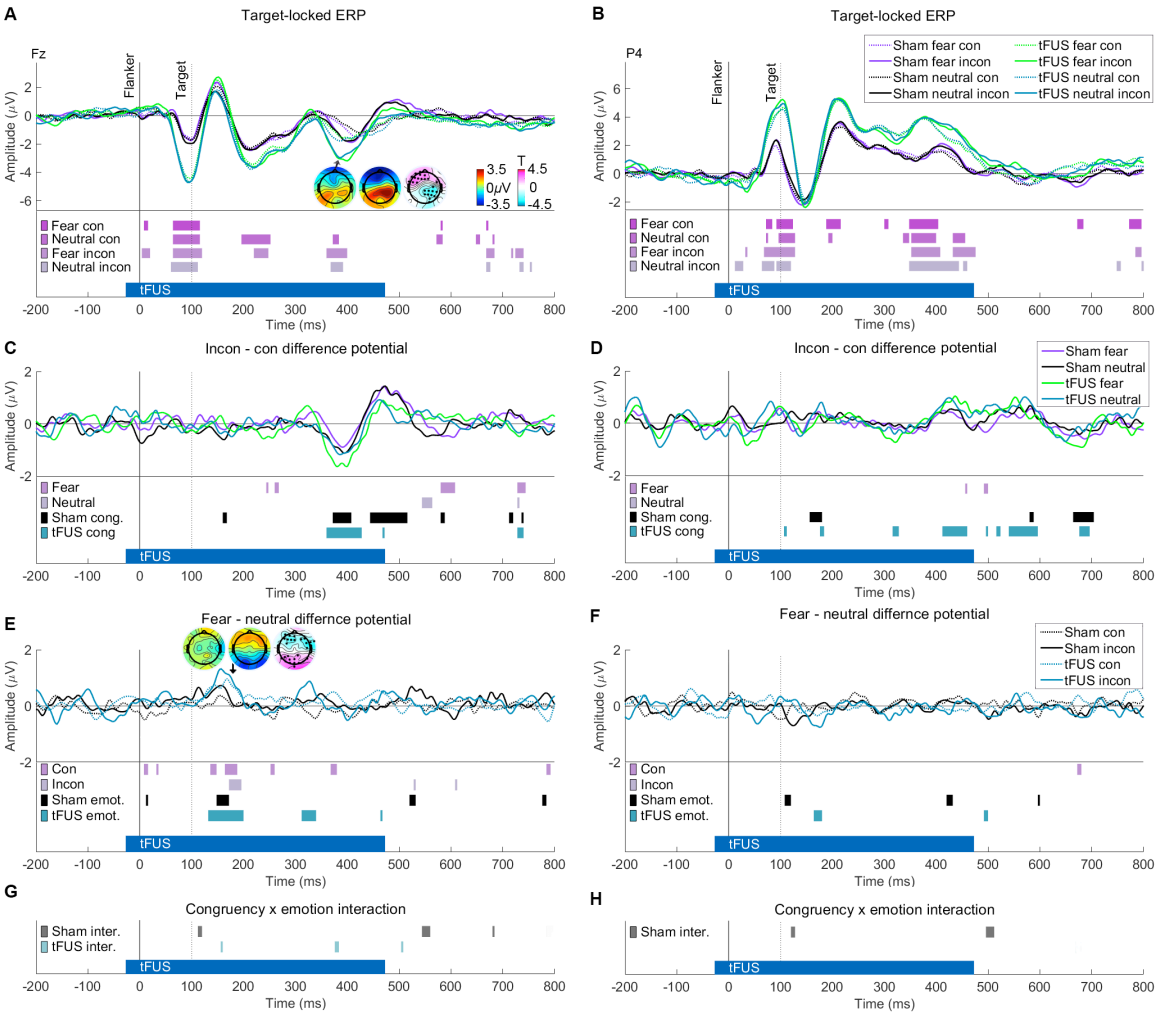

Figure S1 Target-locked ERP for frontal and parietal electrodes
(A-B) Displays ERPs at Fz (A) and P4 (B) for each group, emotion, and congruency condition. Significant differences across groups for condition are displayed in the lower panel (permutation testing, $p < 0.05$). tFUS and Sham sound stimulation period marked with blue bar at the bottom of the panel (tFUS). In A, scalp maps show potential for Sham (left), tFUS (middle), and the results of permutation testing across groups (right) for the fear incongruenct condition, significant electrodes marked with a black dot.
(C-D) Subtraction of congruent from incongruent ERPs to make a difference potential for Fz (C) and P4 (D). Lower panel displays significant differences across groups for fear and neutral conditions. Below this, main effect of congruency (RM-ANOVA) is displayed for each group (Sham, tFUS).

(E-F) Subtraction of neutral from fear ERPs to produce difference potential at Fz (E) and P4 (F). Lower panel displays significant differences across groups for each congruency condition (con, incon), as well as significant main effect of emotion for each group
(G-H) Congruency × emotion interaction effect for each group at Fz (G) and P4 (H).
Abbreviations: con: congruent, incon: incongruent. Related to Figure 2.

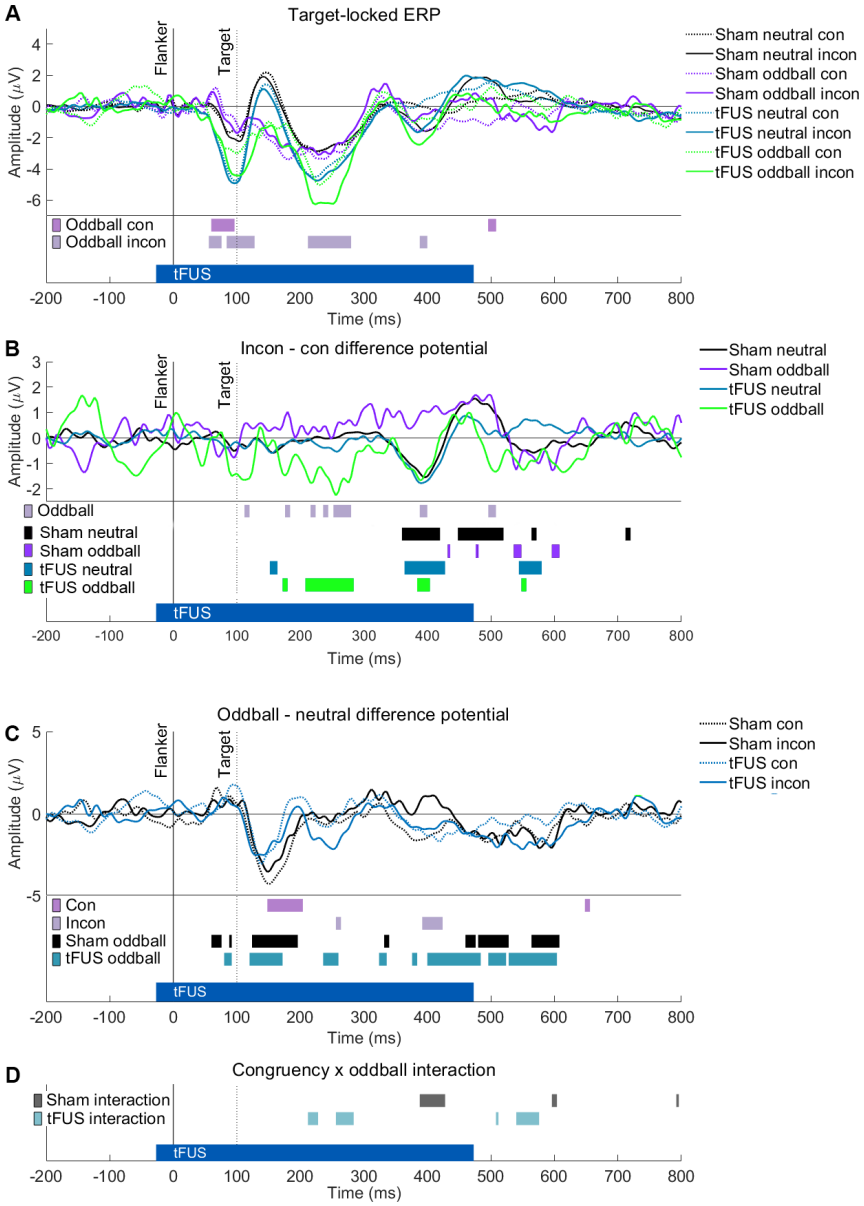

Figure S2 Target-locked ERP for oddball trial response at FCz
(A) Displays ERPs at FCz for each group for neutral and oddball trials (scrambled images, 6% of trials). Both congruent and incongruent trial responses are displayed. Neutral trial data is duplicated from Figure 2 for comparison purposes. Significant differences across groups for each oddball condition (oddball con, oddball incon) are displayed in the lower panel

(permutation testing, $p < 0.05$). tFUS and Sham sound stimulation period marked with blue bar at the bottom of the panel (tFUS).
(B) Subtraction of congruent from incongruent potential to make a difference potential. Lower panel displays significant differences across groups for the oddball condition. Below this, permutation testing across congruent and incongruent trials for each condition are displayed for each group (Sham neutral, Sham oddball, tFUS neutral, tFUS oddball).
(C) Subtraction of neutral from fear potential to make difference potential. Lower panel displays significant differences across groups for each congruency condition (con, incon), as well as significant main effect of oddball for each group (RM-ANOVA).
(D) Congruency × oddball interaction effect for each group (RM-ANOVA).
Abbreviations: con: congruent, incon: incongruent. See also Figure 2.

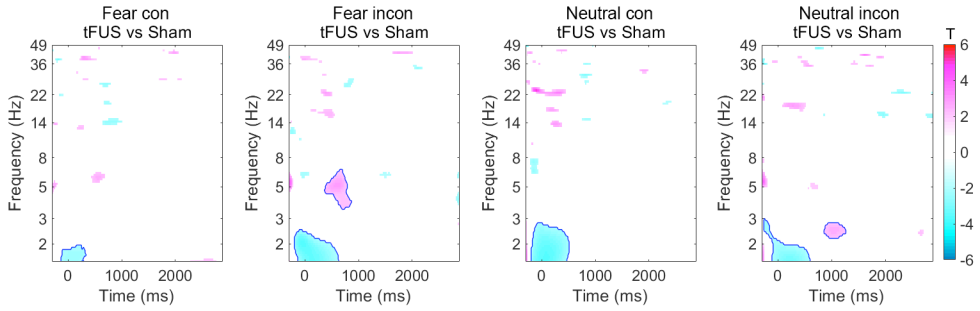

Figure S3. Group comparison of ERSP data at FCz
Displays t-values from permutation testing across groups for each trial condition, only $p < 0.05$ displayed. Positive t values indicate power in the Sham group > tFUS, negative indicate Sham < tFUS. Blue outline indicates areas that survive cluster-based thresholding. Related to Figure 3 and Figure S4. See also Figure S5.

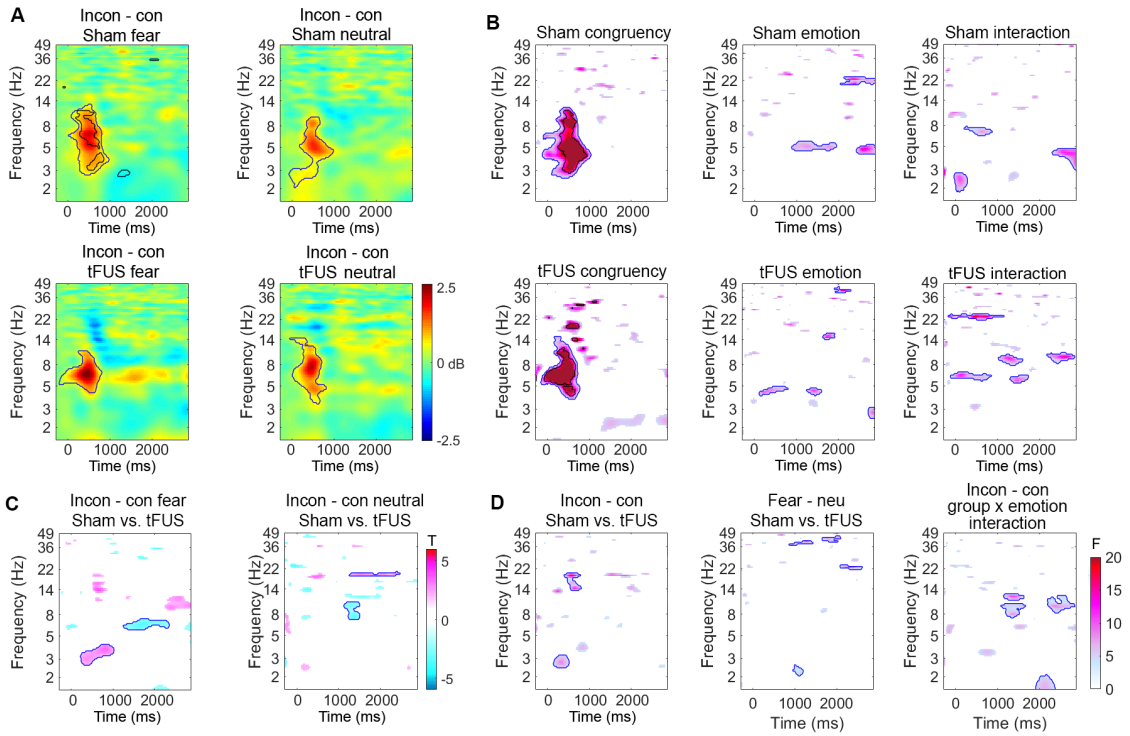

Figure S4. Congruency, emotion, and congruent x emotion interaction ERSP data at FCz, compared across and within groups

(A) Incongruent - congruent contrast power for each emotion condition for each group. Data displayed as dB power over baseline. Permutation statistics (incon vs con) are represented by blue line encircles ($p < 0.05$, cluster-based thresholding), and black line (FDR correction).

(B) F-values from RM-ANOVA performed within groups. Left column the main effect of congruency (incon, con), middle the main effect of face emotion (fear, neutral), and right the congruency × emotion interaction effect. Only $p < 0.05$ displayed; blue line: cluster-based thresholding, black line: FDR correction.

(C) Permutation testing performed across groups for incongruent - congruent contrast data displayed in A, and separated by face emotion (fear, neutral).

(D) Group comparisons: left plot displays F-values from the main effect of group for the incon-con contrast power displayed in A (RM-ANOVA). Middle displays the main effect of group for fear - neutral contrast power. Right-most plot displays the group × emotion interaction effect for incon - con contrast power. Related to Figure 3 and Figure S3. See also Figure S5.

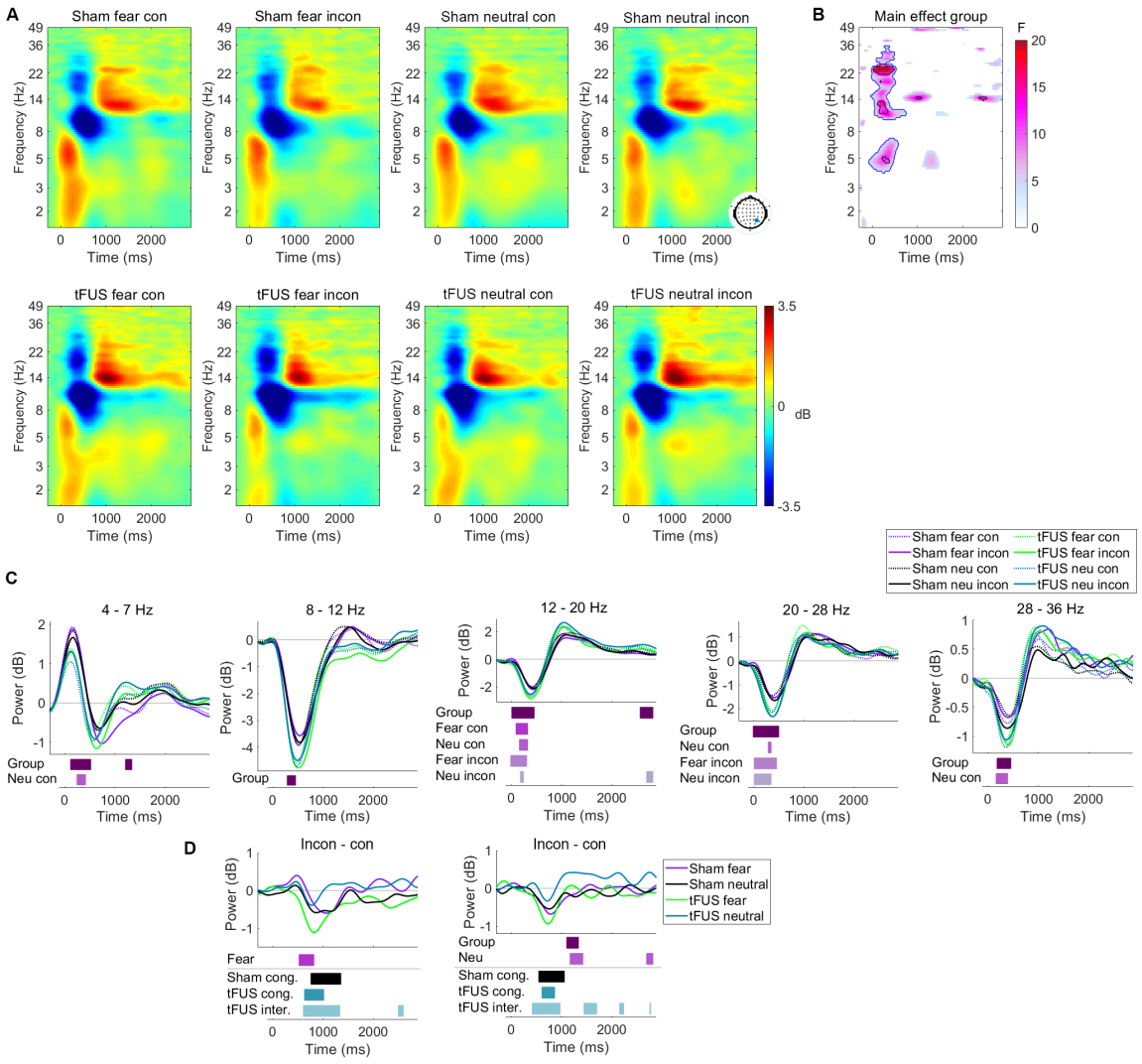

Figure S5. ERSP data at P4

(A) ERSP data at P4 for each group and condition (dB power over baseline).

(B) Main effect of group (RM-ANOVA) of ERSP data displayed in A (F-values). Only $p < 0.05$ displayed; blue line: cluster-based thresholding, black line: FDR correction.

(C) Power over time in various frequency bands. Lower panel displays significant main effect of group (RM-ANOVA), as well as significant differences in each condition (permutation testing).

(D) Incongruent – congruent contrast power for 8-12 Hz (left) and 12-20 Hz (right) frequency bands. Lower panel displays significant main effect of group (RM-ANOVA), and significant differences across groups in each condition (permutation testing). Additionally, significant main effect of congruency (cong.) and congruency × emotion interaction (inter.) are displayed below for each group (within groups: RM-ANOVA).

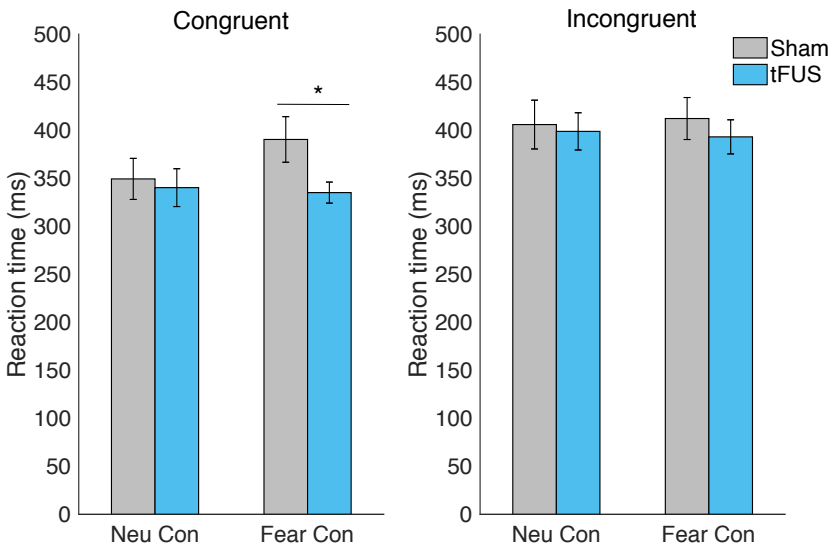

Figure S6. Post-error reaction times compared across groups
Significant differences across groups marked with (*p <0.05).

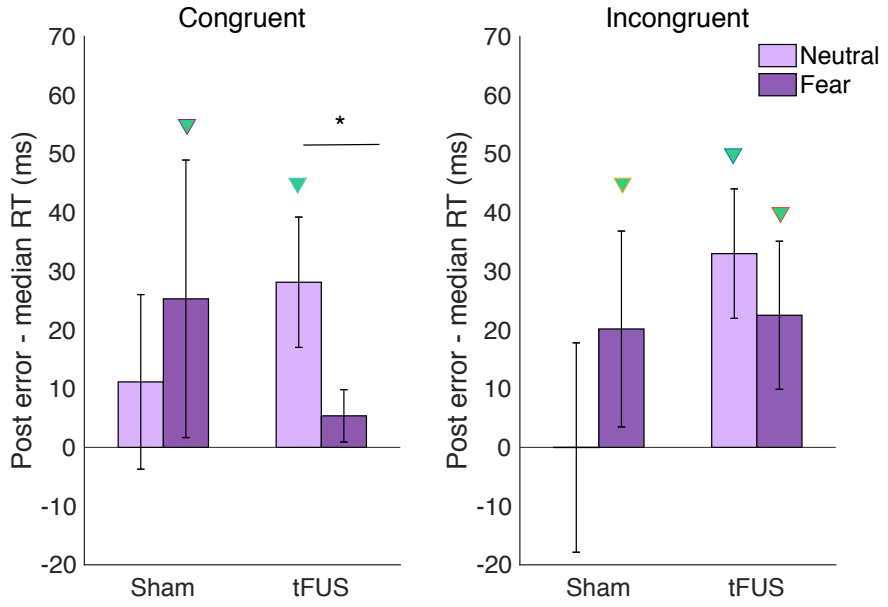

Figure S7. Post-error slowing
Post-error slowing was calculated by subtracting each subjects' median RT for that condition from their post-error trial RT. Green triangles indicate the post-error RTs are significantly slower than median RTs. Significance within group across emotions indicated with asterisk (*p < 0.05). Note in both congruent and incongruent post-error trials, the sham group exhibited significant slowing for fear but not neutral trials. In the tFUS group all post-error conditions are significantly slower than regular trials, except the fear congruent condition.

And there was a significant difference between post-error delay in neural and fear congruent trials in the tFUS groups.

Supplemental Tables

Subject	x	y	z
1	26	16	-7
2	38	11	-3
3	41	9	2
4	40	12	0
5	33	7	14
6	36	13	-4
7	44	17	-3
8	35	10	5
9	32	17	3
10	39	25	-5
11	31	11	-4
12	35	11	10
13	35	14	3
14	31	16	8
Mean	35.4	13.5	1.4
SEM	1.3	1.2	1.7

Table S1. Stimulation locations for each subject
MNI coordinates of tFUS focus center point for each subject. Related to Figure 1.

	Fear congruent			Neutral congruent		
ERP complex	Sham	tFUS	*p*	Sham	tFUS	*p*
D-N1	-3.28 ± 0.55	-5.28 ± 0.62	0.025*	-3.19 ± 0.45	-5.61 ± 0.61	0.003*
D-N1 - D-P1	5.49 ± 0.90	7.07 ± 0.62	0.36	4.96 ± 0.94	6.25 ± 0.62	0.31
D-P1 - T-N1	-5.73 ± 1.14	-7.79 ± 0.55	0.75	-6.57 ± 1.07	-6.89 ± 0.60	0.96
T-N1 - P2	3.39 ± 0.45	5.33 ± 0.42	0.007*	4.48 ± 0.42	4.83 ± 0.68	0.047*
P2 - N2	0.05 ± 0.56	-0.68 ± 0.33	0.44	-0.40 ± 0.55	-0.85 ± 0.29	0.19
N2 - P3	0.68 ± 0.39	1.92 ± 0.25	0.007	0.20 ± 0.47	2.47 ± 0.27	0.003*
	Fear incongruent			Neutral incongruent		
ERP complex	Sham	tFUS	*p*	Sham	tFUS	*p*
D-N1	-2.66 ± 0.55	-5.96 ± 0.68	0.001*	-2.75 ± 0.70	-6.17 ± 0.60	0.009*
D-N1 - D-P1	5.40 ± 1.00	7.22 ± 0.64	0.21	4.90 ± 0.92	6.67 ± 0.61	0.27
D-P1 - T-N1	-6.09 ± 1.24	-7.28 ± 0.67	0.69	-5.35 ± 1.02	-6.63 ± 0.65	0.52
T-N1 - P2	5.02 ± 0.49	5.68 ± 0.55	0.057	4.23 ± 0.51	5.67 ± 0.58	0.023*
P2 - N2	-2.95 ± 0.52	-2.97 ± 0.37	0.56	-2.43 ± 0.44	-2.70 ± 0.36	0.86
N2 - P3	3.97 ± 0.73	4.34 ± 0.68	0.90	4.06 ± 0.65	4.78 ± 0.50	0.43

Table S2. ERP peak-to-peak amplitude at FCz comparing Sham and tFUS groups
Amplitude displayed as median ± SEM (μV) and represent peak-to-through (ERP complex) amplitude values from individual subjects' ERP peaks. *p*- values represent the results of permutation testing across groups (* $p < 0.05$). Related to Figure 2 and Table S4.

	Fear congruent			Neutral congruent		
ERP peak	Sham	tFUS	*p*	Sham	FUS	*p*
Distractor-N1	104 ± 3	98 ± 2	0.57	102 ± 4	98 ± 2	0.92
Distractor-P1	146 ± 4	148 ± 2	0.43	144 ± 4	148 ± 2	0.36
Target-N1	228 ± 7	222 ± 7	0.65	220 ± 7	222 ± 6	0.95
P2	340 ± 4	344 ± 5	0.10	340 ± 4	340 ± 5	0.75
N2	404 ± 4	396 ± 6	0.10	402 ± 4	374 ± 5	0.005*
P3	476 ± 5	484 ± 6	0.97	476 ± 5	484 ± 8	0.82
	Fear incongruent			Neutral incongruent		
ERP peak	Sham	tFUS	*p*	Sham	tFUS	*p*
Distractor-N1	96 ± 3	94 ± 2	0.82	100 ± 3	92 ± 2	0.19
Distractor-P1	142 ± 3	144 ± 2	0.51	140 ± 3	140 ± 2	0.66
Target-N1	224 ± 8	234 ± 5	0.76	220 ± 6	226 ± 5	0.24
P2	342 ± 5	338 ± 5	0.62	340 ± 6	338 ± 4	0.43
N2	406 ± 8	384 ± 5	0.33	400 ± 7	388 ± 5	0.43
P3	486 ± 5	482 ± 6	0.27	486 ± 5	478 ± 6	0.36

Table S3. ERP peak latency at FCz comparing Sham and tFUS groups
Latencies are displayed as median ± SEM (ms). *p*- values represent the results of permutation testing across groups (* $p < 0.05$). Related to Figure 2.

Sham								
			Post – hoc statics					
ERP complex	χ^2	p	Neutral con vs. incon	Fear con vs. incon	Con fear vs. neu	Incon fear vs. neu	Fear con vs. neu incon	Neu con vs. fear incon
D-N1	1.11	0.77	-	-	-	-	-	-
D-N1 - D-P1	7.63	0.054	-	-	-	-	-	-
D-P1 - T-N1	5.06	0.17	-	-	-	-	-	-
T-N1 - P2	13.46	0.004*	1	0.002*	0.64	0.34	0.47	0.24
P2 - N2	30.43	< 0.001*	0.013	< 0.001*	1	1	0.005*	< 0.001*
N2 - P3	31.89	< 0.001*	0.003*	< 0.001*	1	0.86	0.05	< 0.001*
tFUS								
			Post – hoc statistics					
ERP complex	χ^2	p	Neutral con vs. incon	Fear con vs. incon	Con fear vs. neutral	Incon fear vs. neutral	Fear con vs. neu incon	Neu con vs. fear incon
D-N1	10.37	0.016*	0.11	0.24	1	1	0.032*	0.644
D-N1 - D-P1	10.54	0.014*	1	0.86	1	0.032*	1	0.032*
D-P1 - T-N1	9.69	0.021*	1	1	0.17	0.17	0.24	0.11
T-N1 - P2	0.60	0.90	-	-	-	-	-	-
P2 - N2	22.29	< 0.001*	0.12	< 0.001*	1	1	0.008*	0.008*
N2 - P3	19.11	< 0.001*	0.008*	0.020*	1	1	0.005*	0.032*

Table S4. ERP peak-to-peak amplitude at FCz compared within each group using non-parametric Friedman's test

Statistics from non-parametric Friedman's test performed across neutral congruent, fear congruent, neutral incongruent and fear incongruent trials, with three degrees of freedom for all tests, both groups n = 14. Post-hoc statics listed for each trial pair, all post-hoc p-values are Bonferroni-corrected. (*$p < 0.05$). Abbreviations: Related to Figure 2 and Table S2. See also Table S3.

	Main effect faces			Main effect group			Interaction group × faces			Post-hoc			
										Sham		tFUS	
	F(1,25)	p	η_p^2	F(1,25)	p	η_p^2	F(1,25)	p	η_p^2	% Change	p	% Change	p
HR (bpm)	2.35	0.14	0.09	1.31	0.26	0.05	2.36	0.14	0.09	↑ 3 ± 1%	0.043*	0 ± 2%	1.00
R-R (ms)	2.74	0.11	0.10	1.63	0.21	0.06	2.91	0.10	0.10	↓ 3 ± 1%	0.028*	0 ± 2%	0.97
SDNN (ms)	9.12	0.006*	0.27	0.42	0.52	0.02	5.86	0.023*	0.19	↓20 ± 4%	0.001*	↓ 2 ± 6%	0.67
SD1 (ms)	1.53	0.23	0.06	0.02	0.89	0.00	0.05	0.82	0.00	↓ 4 ± 6%	0.32	↓ 3 ± 5%	0.48
SD2 (ms)	8.68	0.007*	0.26	0.64	0.43	0.03	5.87	0.023*	0.19	↓22 ± 4%	0.001*	↓ 2 ± 7%	0.71
SD1/SD2	3.42	0.076	0.12	0.04	0.84	0.00	1.82	0.19	0.07	↑26 ± 9%	0.031*	↑ 3 ± 6%	0.72
LF (ms^2)	9.83	0.004*	0.28	0.58	0.45	0.02	0.74	0.40	0.03	↓ 6 ± 4%	0.13	↓ 11 ± 4%	0.008*
HF (ms^2)	9.83	0.004*	0.28	0.58	0.45	0.02	0.74	0.40	0.03	↑ 8 ± 5%	0.13	↑ 12 ± 4%	0.008*
LF/HR	6.41	0.018*	0.20	0.93	0.34	0.04	0.67	0.42	0.03	↓ 8 ± 8%	0.245	↓ 18 ± 7%	0.023*

Table S5. Heart rate metrics compared across groups and time with presentation of emotion face distractors and tFUS stimulation

Mixed-measures RM-ANOVA on heart rate and HRV metrics collected during the final three minutes of baseline (simple flanker no faces, no stimulation), and the first three minutes of the main trail period (flanker arrows were displayed with emotional distractor faces in the background and the stimulation group received online tFUS on each trial). Related to Figure 6.

	Accuracy (% correct)		Mann-Whitney		
Congruent	Sham	tFUS	p	U	W
Baseline	99.86 ± 0.14%	100.00 ± 0.00%	0.77	91.0	196.0
Fear	98.36 ± 0.60%	97.71 ± 0.67%	0.60	109.5	214.5
Neutral	98.07 ± 0.45%	96.43 ± 1.22%	0.84	102.5	207.5
Oddball	99.21 ± 0.79%	96.29 ± 1.77%	0.33	119.5	224.5
Post	99.57 ± 0.23%	98.97 ± 0.75%	0.95	99.5	204.5
Incongruent					
Baseline	100.00 ± 0.00%	99.31 ± 0.31%	0.21	126.0	231.0
Fear	90.86 ± 1.58%	85.00 ± 2.62%	0.11	133.0	238.0
Neutral	90.70 ± 1.69%	85.71 ± 2.05%	0.09	135.0	240.0
Oddball	93.32 ± 2.96%	95.71 ± 1.83%	0.70	89.0	194.0
Post	99.40 ± 0.26%	99.22 ± 0.78%	0.40	79.0	184.0

Table S6. Response accuracy does not differ across groups

Group level statics (non-parametric Mann-Whitney tests) are listed on the right. Test statics performed on number of trials incorrect. See also Table 1.

PANAS Positive	Sham	tFUS
Baseline	31.6 ± 1.8	30.4 ± 2.0
Post	25.9 ± 2.6	24.8 ± 2.2
PANAS Negative		
Baseline	13.8 ± 1.0	13.0 ± 0.8
Post	13.5 ± 1.1	15.4 ± 1.2

Table S7. PANS scores
PANAS Scores for each group (mean ± SEM).

APPENDIX D

SUPPLEMENTARY MATERIALS FOR CHAPTER 5

Supplemental Information

Transcranial focused ultrasound enhances behavioral and network mechanisms underlying response inhibition in humans

S1. Dynamic causal modeling structure optimization
Below the structures used for building and optimizing the dynamic causal model based on the no-tFUS successful stopping event related potentials are displayed. The process is described in in full in the Methods section. Figure S1 shows the tested structures and possible connections. Figure S2 shows comparisons for these models using Bayesian models, model comparisons for which nodes receiving thalamic input, and tests for the type of connection projecting from cortical to deep areas (forward, backward, or both).

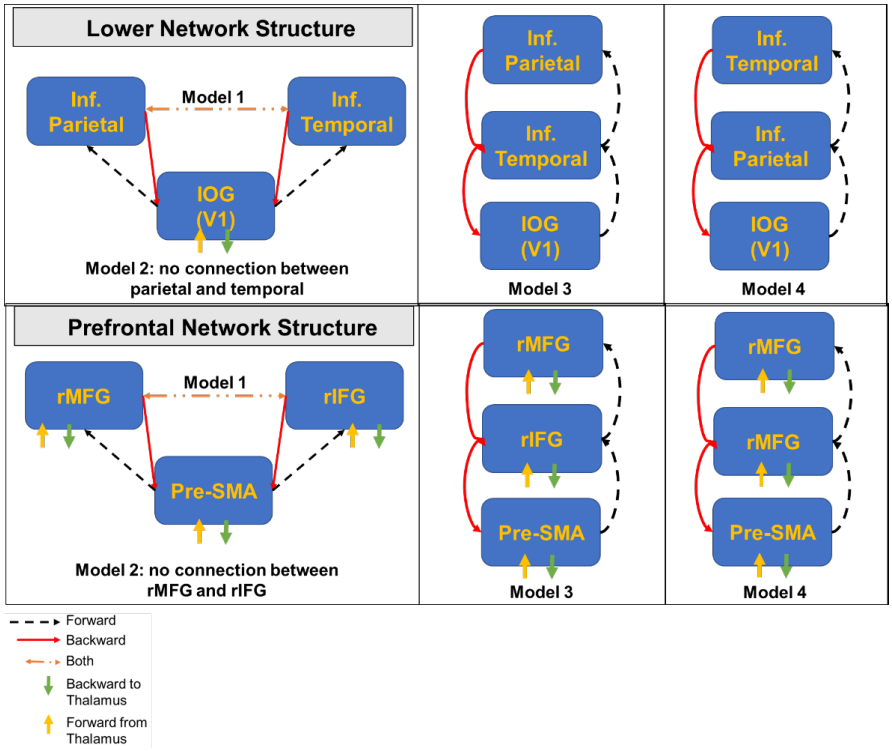

Figure S1. Differences in dynamic causal model spaces that were compared for the lower network structure and prefrontal network structure
Lower network displayed on top, and prefrontal on bottom panel. The legend on the bottom shows how different connections are coded in these putative model spaces.

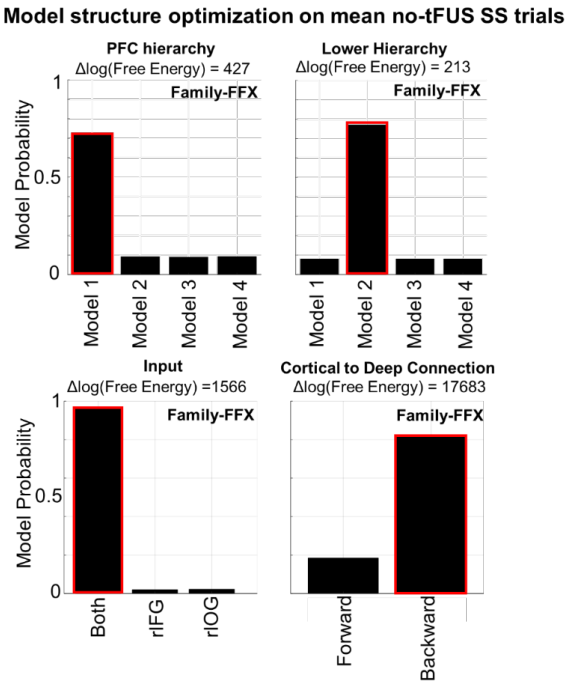

Figure S2. Model probabilities for the different model tests.
Each of these tests was examined on the mean ERP data for No-tFUS SS trials using family-wise fixed effect Bayesian model selection. Above each plot shows the model component being optimized. For example, the first bar plot shows the different prefrontal hierarchy arrangements. Above each plot is the difference in log-free energy between the best family and the 2nd best. The log difference of free energies approximates a log-Bayes factor (Penny, 2012). It is considered positive evidence in favor of a model if this value is > 5. Evidence in favor of the winning models (bars enclosed in red) was very strong. The plots on the right show the different structural arrangements used to examine the prefrontal and lower-level hierarchical structure.

S2. Go Reaction Times

We addressed whether tFUS (real or sham) exerted any effects on simply responding to the Go signal. We analyzed this by extracting the ex-gaussian-based mean RT using a maximum likelihood approach (Lacouture and Cousineau, 2008). The means were calculated separately for all subjects, and then analyzed using a 3 × 2 mixed-design ANOVA with factors of the 3 groups, and tFUS state: No-tFUS and Go-tFUS trials. This analysis allowed us to assess if "going", independent of "stopping", was altered by potential tFUS auditory artifacts, stimulation to unrelated areas (S1 group), or whether tFUS to rIFG also influenced Go RT processes independent of a stopping context signal. Table 1 shows the per group mean difference of the RT between No-tFUS and Go-tFUS per group. Across groups, there was a consistent negative difference indicating that RTs during tFUS may have been slightly shorter. These differences in means seemed marginally larger for the rIFG group. However, the ANOVA did not reveal any significant effect of tFUS, group, or their interaction (all $p >$ 0.05). These results suggest that neither tFUS (rIFG and S1 groups) nor auditory factors alone (sham rIFG group) altered Go RTs independent of a stop signal.

Time-Window (ms)	Regression Direction	Region	Peak MNI Coordinates (x,y,z)	Z-value	Extent (Voxels)
-20:40	Positive	R Supramarginal	56, -40, 16	2.05	316
		L Supramarginal	-56, -50, 18	1.94	123
		R Inferior Temporal	40, -4, -40	1.92	45
	Negative	R Inferior Frontal	40, 30, 10	1.94	55
20:100	Negative	R Inferior Frontal	56, 28, 12	2.64	455
100:180	Positive	R Superior Frontal	26, 50, 18	3.18	568
		R Paracentral Lobule	6, -20, 68	2.98	389
		L Paracentral Lobule	-6, -20, 68	2.94	563
		L Superior Frontal	22, 52, 28	2.74	574
	Negative	L Supramarginal	-60, -28, 38	1.76	52
180:260	Negative	R Inferior Occipital	46, -82, -6	4.12	41
		R Inferior Temporal	58, -40, -24	3.62	552
		L Inferior Temporal	-58, -38, -18	3.55	342
		R Middle Temporal	62, -2, -24	3.16	22
260:340	Positive	L inferior Frontal	-46, 14, 32	4.25	39
		L Middle Frontal	-30, 22, 34	2.84	236
		R Middle Frontal	26, 14, 42	2.61	442
	Negative	R Angular	44, -62, 38	3.62	62
		L Postcentral	-42, -34, 52	2.91	92
		R Middle Temporal	50, 8, -30	2.81	73

Table S1. Regression of ΔSSRT and SS (No-tFUS) – SS (Stop-tFUS)
Significant regions of regression for the change in tFUS induced SSRT.

S3. Signal-respond RTs and context independence

Calculating a measure of stopping latency (SSRT) based on the independent race- model (Logan and Cowan, 1984; Bissett and Logan, 2014) assumes that signal-respond RTs are Go processes resulting from a censoring of the Go RT distribution. Testing this assumption predicts that (a) mean signal-respond RT should be faster than mean Go RT, and (b) during fixed-SSD paradigms like the one employed here, signal-respond RT should increase with longer SSDs because there are more failed inhibitory responses. Before testing (a) and (b), we wanted to discern whether our tFUS manipulation exerted any effects on the signal-respond RTs. Based on the context-independence assumption of the race model that signal-respond RTs are Go processes escaping inhibition, and (2) if the tFUS-driven changes in inhibition (P(respond|signal) (Figure 3) are due to changes in inhibition, we should expect no differences in signal-respond RTs between conditions or groups. We used a mixed-design ANOVA to examine the subject level signal-respond RT means with Group (3 levels) and

tFUS (3 levels: no-tFUS, Go-tFUS, Stop-tFUS). We found no significant interactions or effects. Importantly, follow-up t-tests revealed no differences across tFUS conditions within the rIFG group (mean signal-respond RT: no-tFUS: 375 ±18 ms; Go-tFUS: 368 ±13 ms; Stop tFUS: 353 ±13 ms). This supports the conclusion that tFUS did not alter the mean of Go processes that escaped inhibition.

Given the lack of difference in mean signal-respond RTs (across all SSDs) across tFUS conditions, we collapsed these RT means across tFUS conditions and compared them to each subject's mean Go RT with a mixed-design ANOVA. There was no interaction or Group differences ($p > 0.05$). As expected, the mean signal-respond RT (all groups: 365 ±15) was significantly shorter ($F(1,50) = 89.77$, $p < 0.0001$) than the mean Go RT (all groups: 436 ±22). Next, we examined whether the signal-respond RT increased with increasing SSD by regressing all subjects' signal-respond RTs (collapsed across tFUS conditions) onto their SSDs to obtain a single-slope parameter. This revealed a significant regression slope of 0.44 ($p < 0.001$), indicating signal-respond RTs did increase with increasing SSD.

Having confirmed that tFUS did not alter signal-respond RTs or the Go RTs, we sought to test the context-independence assumption of the race model. This has been done in several ways (see Bissett and Logan, 2014 for a non-parametric approach). The standard approach for examining this assumption is comparing predicted signal-respond RTs from fitting the independent race model to the observed signal-respond RTs (Verbruggen and Logan, 2009). The independence assumption is typically assessed by showing that observed signal-respond RTs and those predicted by the independent race model are not different. Because we used a parametric (ex-gaussian) based approach to estimate the SSRT (Matzke et al, 2013), we verified these derived fits by using a posterior predictive model comparison to the observed data. The models were used to simulate 500 predictive distributions of signal-respond RTs to estimate the absolute goodness of fit (Gelman & Hill, 2007) to each individual subject's signal-respond RT. This approach generates *p*-values that test for the difference in the predicted and observed signal-respond RTs at each SSD level. The typical metric for assuming goodness of fit is that the *p*-value is close to 0.5, while being below and above 0.05 and 0.95, respectively, is considered a poorly predictive model. As pointed out by Matzke et al. (2013), these estimates are most stable for SSDs in which several signal-respond RTs are observed. Therefore, we analyzed each subject's p-values averaged across the two highest SSDs.

The mixed-design ANOVA across groups and tFUS conditions did not reveal any effects or interaction on the *p*-values. This result also agrees with the analysis showing no differences in signal-respond RTs between tFUS conditions, indicating the Bayesian procedure for estimating SSRT provided accurate predictions of signal-respond RTs. For all participants, the *p*-values were in the range of 0.1 to 0.9 with a mean of 0.48 and standard deviation of 0.2.

S4. SSRT Variability was not altered by tFUS.

One possible driver of increased response inhibition performance in the rIFG tFUS group is reduced within-subject SSRT variability. Therefore, as tFUS did not alter mean or variance of Go RTs, if it reduced SSRT variability, this would increase the likelihood of successful inhibition. Using the same statistical approach for the mean SSRT in the main text, we found no significant effects of SSRT variability between any of the conditions (all $p > 0.05$).

S5. SS (No-tFUS) – SS (Stop-tFUS) whole-brain regression table

Table S1 lists the peak coordinates of clusters of the difference in evoked activity of No-tFUS and Stop-tFUS SS with the between-subjects changes in SSRT. These coordinates were used to identify which areas exhibited differential activation with respect to the speed of stopping across subjects. Coordinates for relevant regions of interest were used as prior locations in subsequent dynamic causal modeling in the main text.

Time-Window (ms)	t-contrast Direction	Region	Peak MNI Coordinates (x,y,z)	Z-value	Extent (Voxels)
20:100	tFUS > No-tFUS	Right Inferior Frontal	44, 28, 5	2.8	979
100:180	tFUS > No-tFUS	L pre-SMA	-10, -10, 50	2.7	1108
		R pre-SMA	6, 22, 50	2.67	1069
		R DLPFC	30, 28 40	2.91	850
180:260	tFUS > No-tFUS	Right Inferior Occipital	50, -70, 8	2.62	47
260:340	tFUS > No-tFUS	Left Superior Occipital	-18, -82, 34	2.34	594
		Right Cuneus	18, -70, 32	2.31	259
		Anterior Cingulate	8, 6, 24	2.01	253
	tFUS < No-tFUS	Left Postcentral	-18, -38, 68	2.02	578
		Right Postcentral	26, -24, 70	1.99	362

Table S2. SS (No-tFUS) – SS (Stop-locked tFUS) model location: F-contrast.

Here we show brain areas that exhibited differential evoked activation according to (1) successful compared to unsuccessful stopping (SS – SU F-contrast), and (2) which areas were modulated by tFUS (tFUS F-contrast). We computed these whole-brain SPM contrasts using a flexible factorial model to implement a repeated-measures ANOVA. We examined these contrasts over three time windows that covered the time from stop-signal onset till after the range of subject SSRTs. The main result from all of these analyses is that the only brain area exhibiting overlap between a significant SS-SU and tFUS contrast was a right inferior frontal gyrus cluster centered on pars opercularis, during the 20:100 ms time window. This result supports the accuracy of our tFUS manipulation and its effects on inhibition performance. Uncorrected voxel: $p < 0.005$ and cluster uncorrected: $p < 0.05$. Related to Figures S3-5.

S6. Whole-brain SPM analysis

We performed a whole-brain SPM analysis for (1) positive t-contrast for SS (No-tFUS) – SS (Stop-tFUS) trials to examine where activity was larger for tFUS compared to No-tFUS trials, (2) SS – SU main effects, and (3) tFUS main effect. In all of the analysis below, we used a cluster-forming voxel threshold of $p< 0.005$.

In the stop-signal locked window (-40:20 ms), we found differences in left supramarginal gyrus. In the N100 window (20:100 ms), the contrast was significant, as anticipated, in rIFG. This result supports our scalp ERP measures and previous results indicating that an N100 occurs in the rIFG that is predictive of stop success. In the N200 window (100:180 ms), we found increased source activity in tFUS trials in bilateral clusters

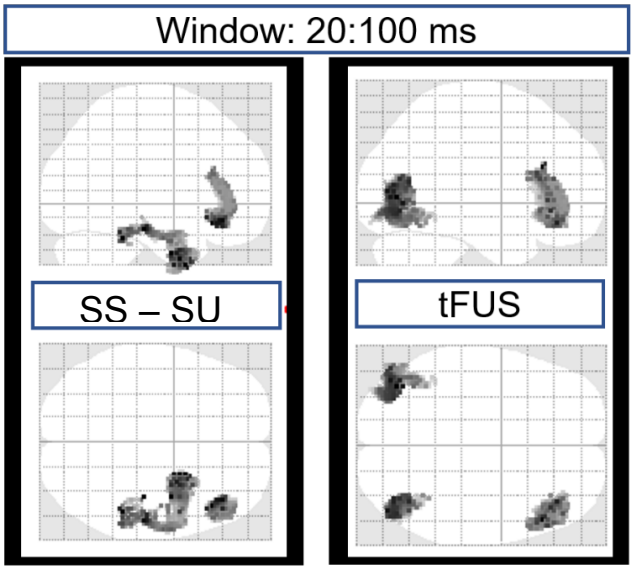

FWE *P*	Cluster Extant	Uncorr. *P*	Peak-F	X	Y	Z	Cluster Peak
F-contrast: successful stop – unsuccessful stop (SS – SU)							
<0.005	893	0.0001	16.35	50	-40	-26	R Inferior Temporal
<0.05	586	0.0001	15.16	54	26	18	R Inferior Frontal
F-contrast: non-tFUS – stop-tFUS (tFUS)							
<0.01	620	0.0001	16.65	-42	-72	-8	L Inferior Occipital
<0.005	899	0.0001	16.09	52	18	22	R Inferior Frontal:
<0.01	699	0.0001	15.52	48	-74	-10	R Inferior Occipital

Figure S3. SPM F-contrasts of source evoked power during the 20:100 ms post stop signal window. F-contrasts and their cluster corrected statistics are shown for the contrast and the contrast of SS trials during non-tFUS and stop-tFUS.

with locations indicative of pre-SMA (Mayka et al., 2006). Consideration of the fourth time window (180:260 ms), which overlapped with the SSRT, revealed that only the right inferior occipital area produced a larger response in tFUS trials. In the last window (260:340 ms), we found clusters of activity larger in tFUS trials for left superior occipital, right cuneus, and anterior cingulate. Because this window always occurred after the SSRT for both No-tFUS and tFUS conditions, it is likely these changes in activity represent a component of performance monitoring rather than inhibition per se. Examination of the contrast for larger No-tFUS SS trial activity revealed this contrast was only significant in the latest time-window (260:340 ms). This contrast indicated source ERP activity was larger in No-tFUS trials in bilateral postcentral gyrus clusters. An important result from these contrasts is the primary areas in which activity was larger during tFUS trials. We found that both rIFG and pre-SMA activity coincided with increased tFUS-related stopping. Interestingly, this analysis confirmed that rIFG differences occurred before those in pre-SMA. However, a temporal precedent of change in ERP does not necessitate that stopping-related changes occurred in rIFG before pre-SMA. The source cluster MNI locations and cluster sizes are presented in Table S2.

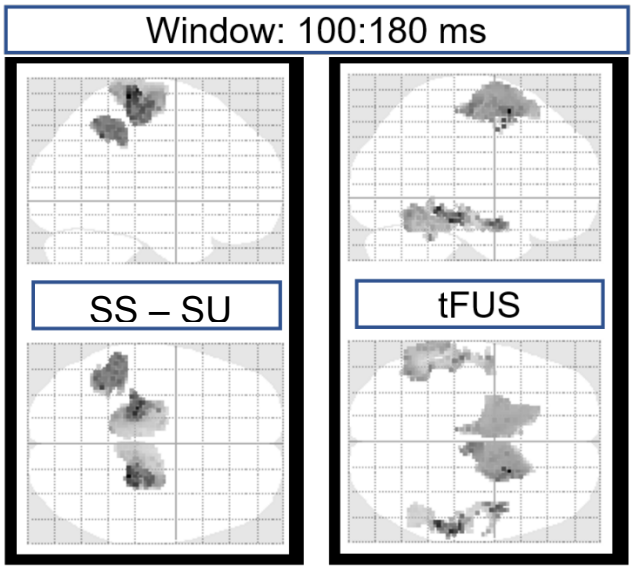

FWE *P*	Cluster Extant	Uncorr. *P*	Peak-F	X	Y	Z	Cluster Peak
F-contrast: successful stop – unsuccessful stop (SS – SU)							
<0.0	F-contrast: successful stop – unsuccessful stop (SS – SU)				-34	68	R Postcentral
<0.0005	1279	<0.0001	21.85	-22	-28	72	L Pre/Postcentral
<0.05	479	<0.005	19.23	-36	-52	42	L Inferior Parietal
F-contrast: non-tFUS – stop-tFUS (tFUS)							
<0.0001	1337	<0.0001	18.41	22	8	56	R pre-SMA
=0.2	343	<0.01	16.15	52	18	22	R Middle Temporal
<0.05	590	<0.001	13.18	48	-74	-10	L Middle Temporal
<0.001	1113	<0.0001	11.99	-6	-28	56	L Precentral

Figure S4. SPM F-contrasts of source evoked power during the 100:180 ms post stop signal window. F-contrasts and their cluster corrected statistics are shown for the SS-SU contrast and the contrast of SS trials during non-tFUS and stop-tFUS.

Interaction t-contrasts

The most common contrast in analyzing stop-signal neural data involves comparing successful to unsuccessful stop activation (SS – SU) as we did for the above whole-brain analysis. The rationale is based on the assumption that areas directly related to stopping/inhibition are more 'potently' active in successful trials, and that failed stop trials (US) also reflect go activity according to the independent race model of Logan and Cowan (1984). This choice of contrast also stems from the fact that typical stop-signal tasks do not offer a second set of SS trials for comparison (which our experiment does). Therefore, this raises the following question: Did tFUS yield changes in stopping by merely altering what would have been SU Stop-tFUS trials? If tFUS merely raised the overall level of activity across all stop trials, (i.e., SS and SU), then we should expect no interactions. We examined the whole-brain SPM interaction across the 4 time windows used in the previous analysis. In

each window, we examined the t-contrast interaction that compared for a bigger SS-SU difference in either Stop-tFUS or No-tFUS trials. We only found these effects for the 100:180 ms and 180:260 ms window. The interaction t-contrast SPMs and corresponding tables are shown in Figures S6-7.

We note that we only found significant contrasts in the latter two time windows, i.e., 100-180 and 180-260 ms from the Go signal. In both contrasts, the SS-SU difference was larger in the Stop-tFUS conditions. Generally, these results agree with that of the main text examining just the SS-SS contrast and other studies (Aron and Poldrack, 2006; Boehler et al., 2010). However, as Boehler et al. (2010) point out, this contrast is conservative which lends itself to identifying areas primarily involved in successful stopping. It is also unlikely that this conservative contrast can identify areas involved in the broader stopping network. It is therefore not surprising that we did not find difference in parietal cortices, for example. Importantly, though, these results demonstrating mainly activation differences in inferior frontal and occipital cortices is almost identical to that found in Boehler et al. (2010). This indicates that our results generally agree with previous studies using the SS – SU contrast.

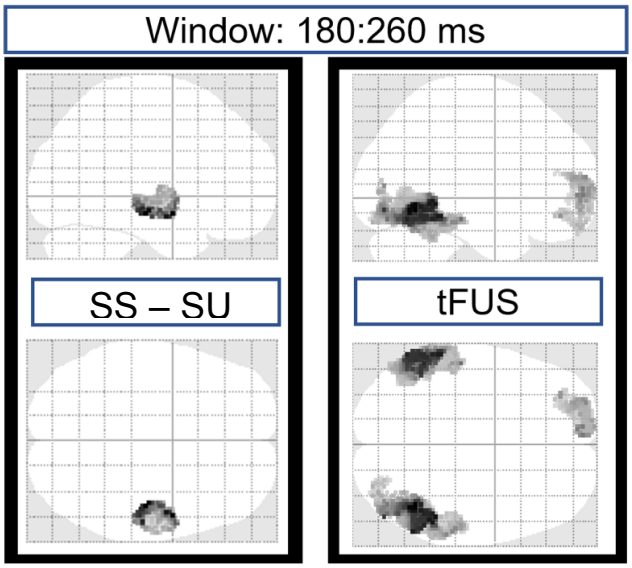

FWE *P*	Cluster Extant	Uncorr. *P*	Peak-F	X	Y	Z	Cluster Peak
F-contrast: successful stop – unsuccessful stop (SS – SU)							
<0.05	497	<0.005	16.83	46	-20	-14	R Middle Temporal
F-contrast: non-tFUS – stop-tFUS (tFUS)							
<0.0001	1702	<0.00001	19.64	42	-58	-10	R Inferior Temporal
<0.001	1270	<0.0001	17.92	-58	-40	-14	L Middle Temporal
<0.05	584	<0.005	13.49	-4	60	0	L Medial Superior Frontal

Figure S5. SPM F-contrasts of source evoked power during the 180:260 ms post stop signal window. F-contrasts and their cluster corrected statistics are shown for the SS-SU contrast and the contrast of SS trials during non-tFUS and stop-tFUS.

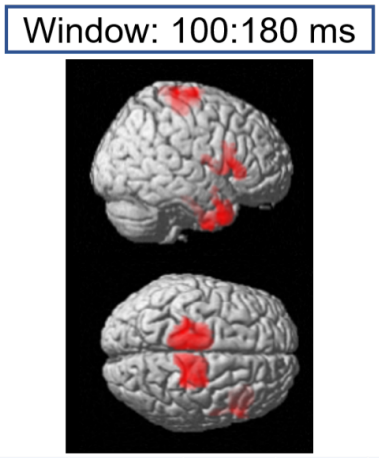

FWE *P*	Cluster Extent	Uncorr. *P*	Peak-T	X	Y	Z	Cluster Peak
F-contrast: Interaction SS-SU (stop-tFUS) > SS-SU (non-tFUS)							
<0.001	1364	<0.0001	4.42	52	-18	-12	L Postcentral
<0.005	1153	<0.00001	4.41	42	-90	4	R Middle Occipital
<0.005	988	<0.00001	4.30	32	-4	38	R Inferior Temporal
<0.05	670	<0.005	3.70	44	14	10	R Frontal Operculum /Inferior Frontal /Pars Opercularis

Figure S6. SPM interaction t-contrasts of source evoked power during the 100:180 ms post stop signal window. The t-contrast tested for areas in which the SS-SU contrast was higher during stop-tFUS compared to non-tFUS. The cluster corrected statistics are shown are shown below the plot.

S7. ROI Interaction analysis

In the main text we presented a time-based source analysis of the main ROIs of interest, including Right IFG, Right pre-SMA, Right DLPFC, Left M1, and Right Inferior Temporal cortices. In the main text's analysis, we compared SS trials across tFUS conditions. To address the change in time-course activation at the ROI level, we computed the interaction of SS-SU (no-tFUS) and SS-SU (Stop-tFUS) trials using the same MNI locations as used for analyses reported in the main text (Figure S6).

Only three of these ROIs are different before the minimum SSRT across tFUS conditions (185 ms). These include pars opercularis, Right Inferior Occipital, and Right inferior temporal ROIs. This result is mostly in line fMRI (Boehler et al., 2010; Li et al., 2006) and EEG/MEG (Boehler et al., 2009; Wessel and Aron, 2015) studies, although previous work has also identified right temporal cortex (Rae et al., 2015; Xu et al., 2017). Nevertheless, previous findings of differential temporal cortex activity have been based on comparing SS to Go trials rather than the SS – SU (and interaction) comparison we used here. Given the DCM and SSRT regression results indicating changes in temporal cortex activity – as well as the temporal cortex's role in visual signal in both the top-down and bottom-up processing directions – these results suggest the success of stopping may rely on information transfer of node between sensory and prefrontal ventral areas, e.g., rIFG. Finally, an interesting result is the lack of difference in r pre-SMA before SSRT. Notably, there was differential activation but only after SSRT. This result speaks to the broader debate of whether pre-SMA or rIFG lead to stopping in a serial process fashion (Aron et al., 2016;

Obeso et al., 2013). For example, some studies have suggested that information for stopping passes through pre-SMA onto rIFG and vice versa in other accounts. These serial accounts, though, forego three factors. First, visual information regarding stop contexts are passed up both the ventral and dorsal pathways which inherently project separately to rIFG and r pre-SMA, respectively. Second, the prefrontal cortex is likely arranged hierarchically with both areas connected with basal ganglia structures, such as the STN and striatum. The third comparison is based on considering the current EEG-DCM (main test) results to those from other fMRI-DCM and other connectivity results (Schmittmann et al., 2015) on inhibition. Specifically, the previous bilinear DCM models used in fMRI accounts of response inhibition are unlikely to capture the fast-timescale processes that underlies stopping processes. Along this same line, though, when considering connectivity as a property of inhibition processes, caution should also be used in interpreting temporal precedence of control between brain areas based solely on activation. Thus, the above results indicate that the set of expected ROIs were differentially modulated by tFUS during SS stopping.

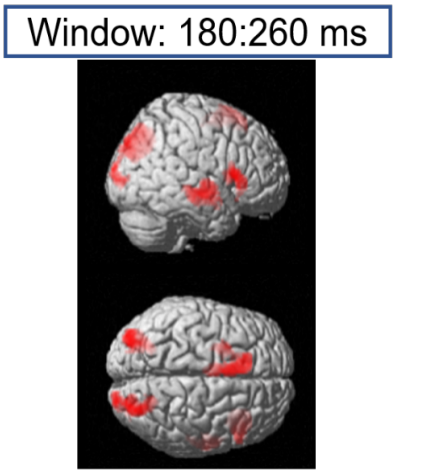

FWE *P*	Cluster Extent	Uncorr. *P*	Peak-T	X	Y	Z	Cluster Peak
F-contrast: Interaction SS-SU (stop-tFUS) > SS-SU (non-tFUS)							
<0.01	706	<0.001	4.21	52	-18	-12	R Middle Temporal
<0.005	984	<0.00001	3.90	42	-90	4	R Middle Occipital
<0.05	567	<0.0001	3.73	46	16	4	R Inferior Frontal Gyrus / Pars Opercularis
<0.005	822	<0.001	3.61	-2	14	64	pre-SMA/SMA
<0.005	780	<0.005	3.25	-34	-68	28	L Middle Occipital

Figure S7. SPM interaction t-contrasts of source evoked power during the 180:260 ms post stop signal window. The t-contrast tested for areas in which the SS-SU contrast was higher during stop-tFUS compared to non-tFUS. The cluster corrected statistics are shown are shown below the plot.

S8. Assessment of possible auditory effects of tFUS

Recent work examining the effects of tFUS on cortical activity has employed animal models to consider the possibility that tFUS may alter activity in auditory pathways. Using a single-element transducer and optical imaging on a mouse model, Guo et al. (2018) showed that,

regardless of the transducer placement and target, tFUS caused activation of the auditory pathway. They suggested that this activity may spread cortically and induce artifactual effects of tFUS in cortical areas not directly targeted by tFUS. It remains unknown how auditory pathway activation via tFUS would yield our behavioral and neural effects. Nevertheless, it is critically important to quantify the extent to which auditory pathway activation might have affected our results. To address this question, we analyzed source-localized evoked results across the rIFG group, as well as S1 and sham rIFG control groups. Because our goal was to determine whether tFUS altered the evoked activity with respect to No-tFUS, we compared the time courses of source power for stop-locked data by using a source-based ROI of right auditory cortex. We used the source location of x = 46, y = -14, z = 8 for right auditory cortex, which was obtained from Rademacher et al. (2001). These locations were used to extract the eigenvariate time-course after source localization in a sphere with radius of 8 mm to be conservative. These source-time courses were converted to a pseudo activation using the (exp(SOURCE)+exp(-SOURCE))/2 transform. We used this procedure to ensure we could properly detect differences regardless of the ERP activity sign (Figure S9).

If the behavioral results in the rIFG group were merely the result of changes in auditory pathway activity, we should at least see a difference when contrasting the SS-SU trials for No-tFUS and Stop-tFUS conditions in the rIFG group, or at least across groups. Paired samples t-tests did not reveal any significant differences (after false discovery rate correction of $p < 0.05$) when comparing the time courses of the No-tFUS and Stop-tFUS conditions (Figure S9). Therefore, given the spatiotemporal fidelity of EEG, we conclude that our results were not contaminated by tFUS artifacts activating the auditory pathway (Rademacher, et al., 2001).

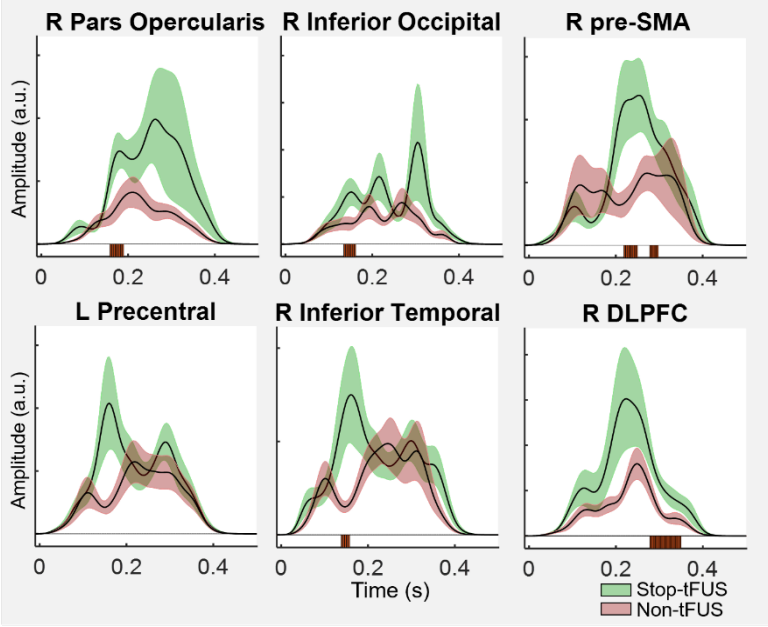

Figure S8. Source-base evoked power time-series for different regions-of-interest
Each ROI was extracted with a radius of 6 mm. Related to Figure 6. See also Figure S9.

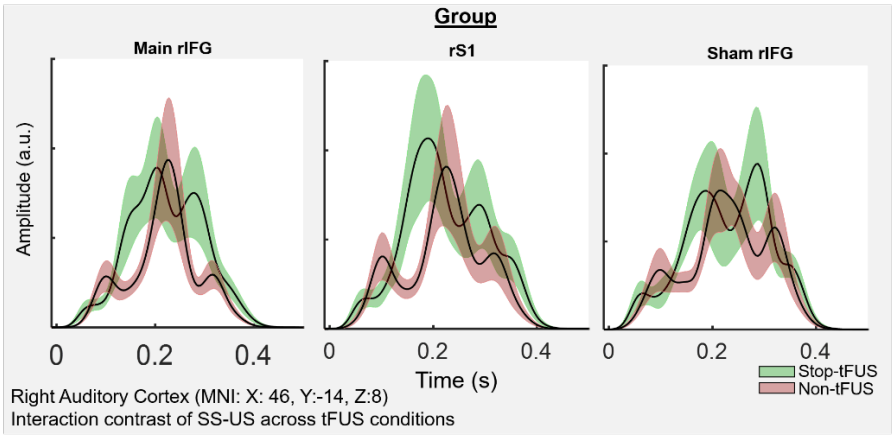

Figure S9. Group source-evoked power time series from right auditory cortex
Each ROI was extracted with a radius of 6 mm. Related to Figure 6. See also Figure S9.

Overall, these results suggest that, although tFUS may exert an auditory pathway effects measurable in mouse single neurons and LFPs, (1) this activity may not be measurable at the macroscopic level, and (2) support the notion that changes in auditory cortical activity cannot account for our tFUS-related neural and behavioral effects. Additionally, we note that Guo et al. (2018) found that the auditory pathway activation was accompanied by startle-like reflexes. Our behavioral results (Figure 2) are not compatible with a startle release reflex. If that were the case, tFUS auditory-related startle activity would likely predict shorter RTs during Go trials and failed inhibition Stop trials. The effects of tFUS on our behavioral responses are not compatible with the involvement of startle reflexes, as we found no tFUS effects on the Go RTs. Therefore, we conclude that the effects of tFUS on stopping behavior, nor processing by the cortical and subcortical nodes of the inhibition network, were not induced by artifactual activation of the auditory pathway.

S9. DCM family model hypothesis spaces and results
Below we show the resultant family model posterior probabilities for the family comparisons over the 4 factors (3 levels each) for both parametric empirical Bayesian (PEB) GLMs (Figure S10-11). PEB GLM model 1 examined the changes in mean connectivity from No-tFUS SU to SS trials. Changes in mean connectivity represent the gain on connectivity to represent the No-tFUS SS trials. PEB GLM model 2 examined the effects of tFUS-induced changes in mean connectivity and changes in connectivity that accompanied change in SSRT across subjects. Figures S8 and S9 show the changes in connections and family model probabilities for PEB model 1. Figure S12 shows the results of tests of the exact same factor space displayed as bar plots to represent the family probability of each model separately for the tFUS-induced mean and SSRT change in successful inhibition connectivity.

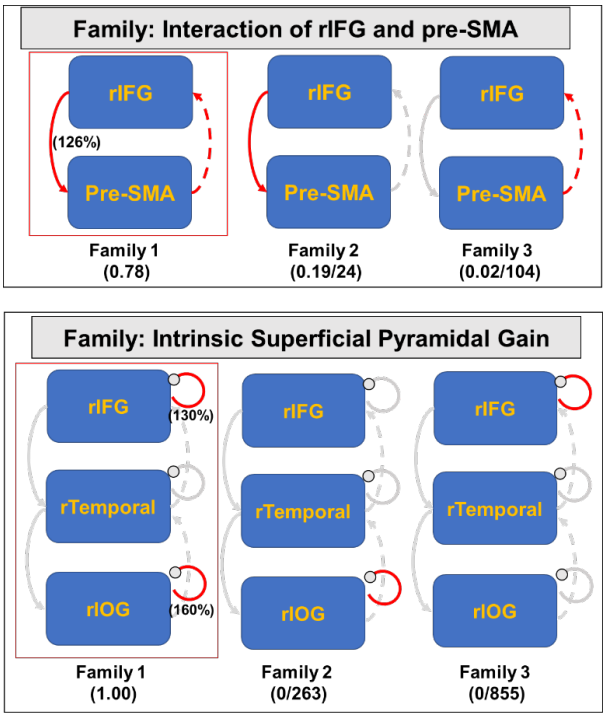

Figure S10. Hypothesis space and results of the Family based PEB Bayesian model comparison for different hypotheses.
Family-based posterior probability (F-Pp) and the log-Bayes factor with respect to the winning model are listed below each model and were computed as the difference in free energy between families (F-Pp/log-Bayes). The winning model family is enclosed in a red box. The outcomes of these plots can be interpreted of as revealing the modulatory parameters connections with very strong, positive evidence being different between SU and SS trials. Parameters estimates with a greater than 95% posterior probability in these families are presented in parentheses next to the modulated connection. The parameters are presented in exponential form of percentage gain. Values above 100% equates to a parameter increase in SS trials compared to SU (and the opposite for values below 100%). Parameters in-active in each model are in a gray color. The top Panel shows the hypothesis test of rIFG and pre-SMA interactions. The bottom panel shows the hypothesis test of intrinsic gains modulation.

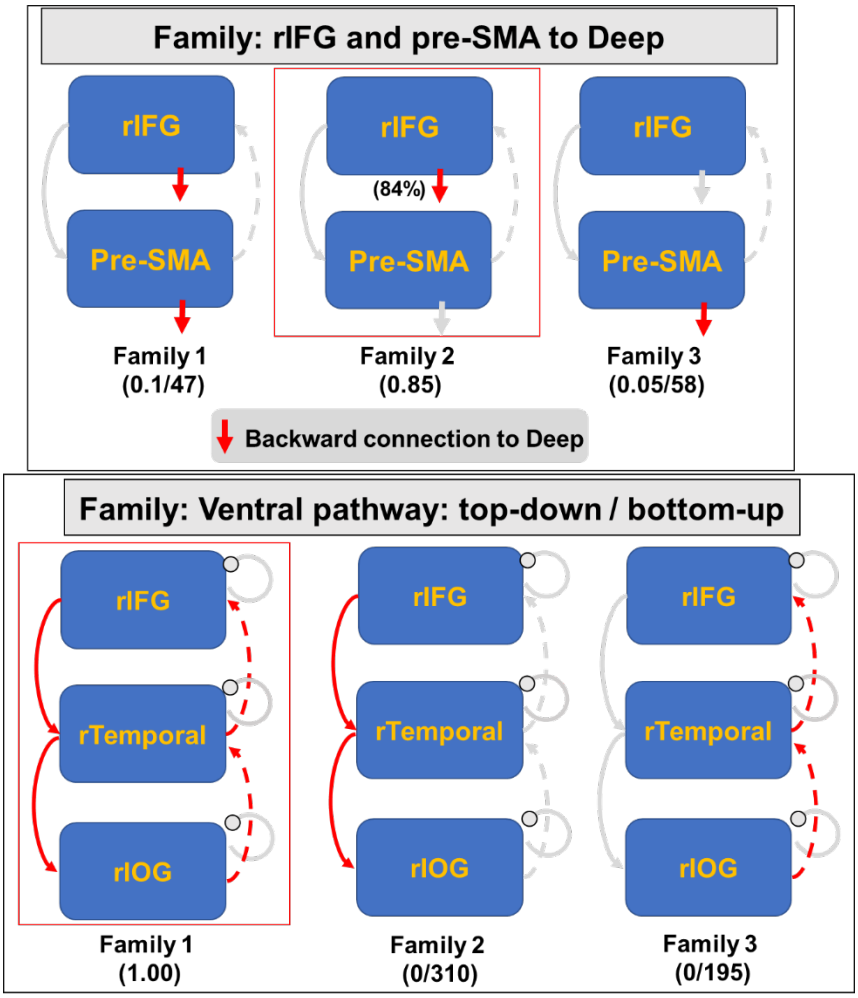

Figure S11. Hypothesis space and results of the Family based PEB Bayesian model Comparison for 3 different families comparing hypothetical different interactions between rIFG and the deep node, pre-SMA and the deep node, or both interacting with the deep pathway. The plot is in the same format as Figure S8. Both of these nodes had backward, inhibitory connections with the deep pathway. The top panel compares families comparing the rIFG and pre-SMA to deep backwards connection. The bottom panel compares families testing for differences in top-down v bottom-up connections along the ventral pathway.

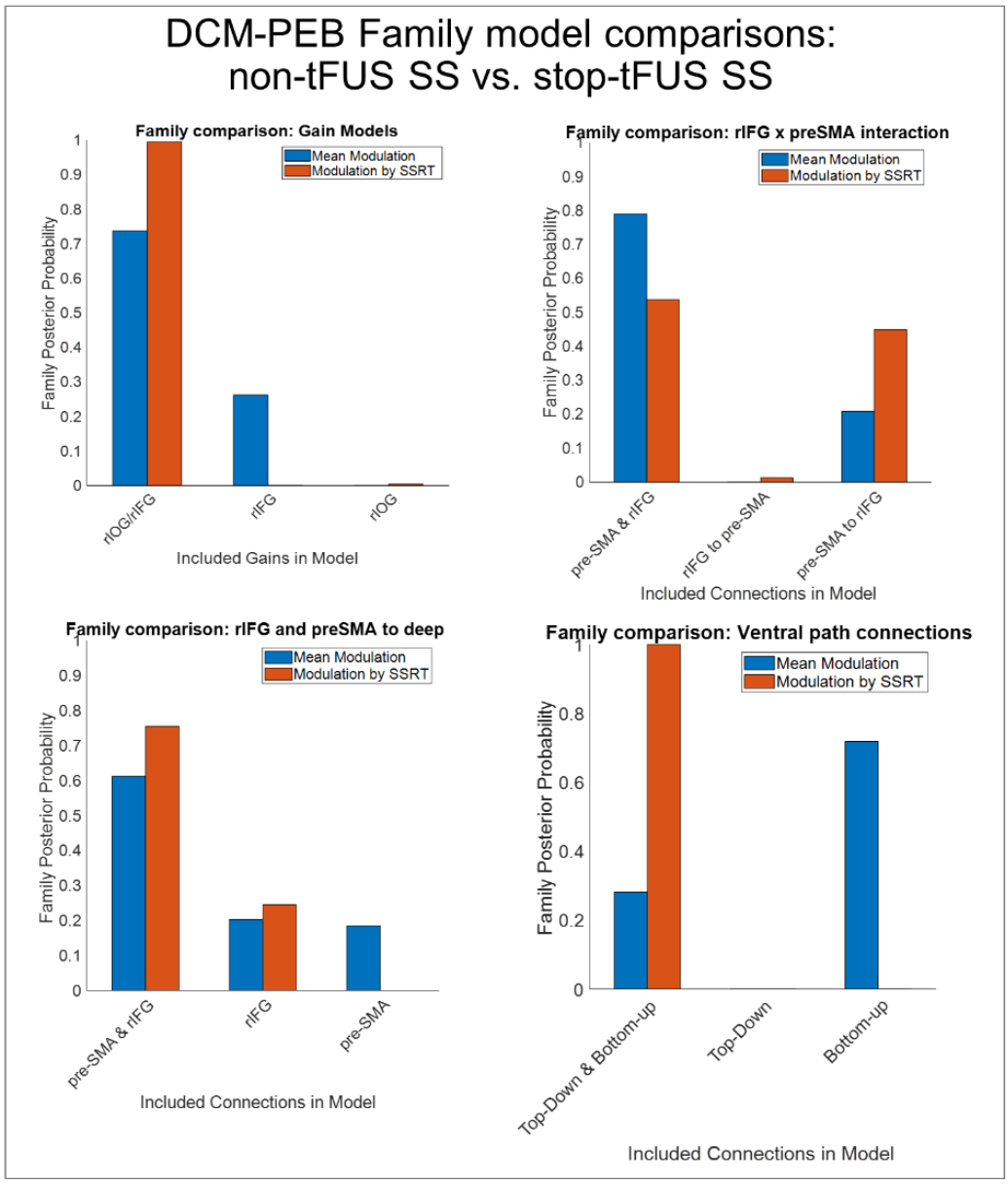

Figure S12. DCM-PEM Family model comparisons: non-tFUS SS vs. stop-tFUS SS
Each bar plot shows the marginal probability of each family marginalized separately for changes in the mean connectivity (blue bars) and connectivity changes predicted by tFUS induced changes in SSRT (orange bars). The Bayesian model averaged parameters are presented in the main text

SUPPLEMENTAL REFERENCES

Aron, A.R., Herz, D.M., Brown, P., Forstmann, B.U., and Zaghloul, K. (2016). Frontosubthalamic Circuits for Control of Action and Cognition. The Journal of Neuroscience 36, 11489-11495.

Aron, A.R., and Poldrack, R.A. (2006). Cortical and subcortical contributions to stop signal response inhibition: role of the subthalamic nucleus. Journal of Neuroscience 26, 2424-2433.

Bissett, P.G., and Logan, G.D. (2014). Selective stopping? Maybe not. Journal of Experimental Psychology: General 143, 455.

Boehler, C.N., Appelbaum, L.G., Krebs, R.M., Hopf, J.-M., and Woldorff, M.G. (2010). Pinning down response inhibition in the brain—conjunction analyses of the stop-signal task. Neuroimage 52, 1621-1632.

Boehler, C.N., Münte, T.F., Krebs, R.M., Heinze, H.-J., Schoenfeld, M.A., and Hopf, J.-M. (2009). Sensory MEG responses predict successful and failed inhibition in a stop-signal task. Cerebral Cortex 19, 134-145.

Gelman, A., and Hill, J. (2007). Data analysis using regression and multilevelhierarchical models, Vol 1 (Cambridge University Press New York, NY, USA).

Guo, H., Hamilton, M., Offutt, S.J., Gloeckner, C.D., Li, T., Kim, Y., Legon, W., Alford, J.K., and Lim, H.H. (2018). Ultrasound Produces Extensive Brain Activation via a Cochlear Pathway. Neuron 98, 1020-1030.e1024.

Lacouture, Y., and Cousineau, D. (2008). How to use MATLAB to fit the ex-Gaussian and other probability functions to a distribution of response times. Tutorials in quantitative methods for psychology 4, 35-45.

Logan, G.D., and Cowan, W.B. (1984). On the ability to inhibit thought and action: A theory of an act of control. Psychological review 91, 295.

Matzke, D., Love, J., Wiecki, T.V., Brown, S.D., Logan, G.D., and Wagenmakers, E.-J. (2013). Release the BEESTS: Bayesian estimation of ex-Gaussian stop-signal reaction time distributions. Frontiers in Psychology 4, 918.

Mayka, M.A., Corcos, D.M., Leurgans, S.E., and Vaillancourt, D.E. (2006). Three-dimensional locations and boundaries of motor and premotor cortices as defined by functional brain imaging: A meta-analysis. Neuroimage 31, 1453-1474.

Obeso, I., Robles, N., Muñoz-Marrón, E., and Redolar-Ripoll, D. (2013). Dissociating the role of the pre-SMA in response inhibition and switching: a combined online and offline TMS approach. Frontiers in human neuroscience 7, 150.

Penny, W.D. (2012). Comparing dynamic causal models using AIC, BIC and free energy. Neuroimage 59, 319-330.

Rademacher, J., Morosan, P., Schormann, T., Schleicher, A., Werner, C., Freund, H.-J., and Zilles, K. (2001). Probabilistic mapping and volume measurement of human primary auditory cortex. Neuroimage 13, 669-683.

Rae, C.L., Hughes, L.E., Anderson, M.C., and Rowe, J.B. (2015). The prefrontal cortex achieves inhibitory control by facilitating subcortical motor pathway connectivity. Journal of neuroscience 35, 786-794.

Schmittmann, V.D., Jahfari, S., Borsboom, D., Savi, A.O., and Waldorp, L.J. (2015). Making Large-Scale Networks from fMRI Data. PLOS ONE 10, e0129074.

Verbruggen, F., and Logan, G.D. (2008). Response inhibition in the stop-signal paradigm. Trends in cognitive sciences 12, 418-424.

Wessel, J.R., and Aron, A.R. (2015). It's not too late: The onset of the frontocentral P3 indexes successful response inhibition in the stop - signal paradigm. Psychophysiology 52, 472-480.

Xu, K.Z., Anderson, B.A., Emeric, E.E., Sali, A.W., Stuphorn, V., Yantis, S., and Courtney, S.M. (2017). Neural basis of cognitive control over movement inhibition: human fMRI and primate electrophysiology evidence. Neuron 96, 1447-1458. e1446.

APPENDIX E

IRB APPROVALS AND HUMAN SUBJECTS CONSENT FORMS

Chapters 3 and 4:

The first consent form included below is titled: "Modulation of the Dorsal Attention and Default Mode Networks with Transcranial Focused Ultrasound (TFUS)". This form was used to collect the data analyzed in chapter 3 and 4 using ASU IRB approved study: IRB # STUDY00009449. The second included form is titled "Consent to transfer MRI scan". This consent form was used as an adjunct form for STUDY00009449 only for subjects in which MRI scans had been collected under a previous STUDY (IRB: STUDY00004362 or STUDY00006050), so that the MRI data could be used for STUDY00009449.

Chapters 5:

The third consent form included is titled: "Neural and behavioral basis of sensorimotor control and learning". This consent form was used for the data collected in Chapter 5, under ASU IRB # STUDY00006050.

SUBJECT CONSENT FORM

Modulation of the Dorsal Attention and Default Mode Networks with Transcranial Focused Ultrasound (TFUS)

SCHOOL OF BIOLOGICAL AND HEALTH SYSTEMS ENGINEERING:
ARIZONA STATE UNIVERSITY

INTRODUCTION

The purposes of this form is to provide you (as a prospective research participant) information that may affect your decision as to whether or not to participate in this research and to record the consent of those who agree to be involved in the study.

PRINCIPAL INVESTIGATOR & RESEARCH ASSOCIATES

William Tyler, Ph.D., (PI, Associate Professor, School of Biological and Health Systems Engineering); Maria Fini (graduate student, SBHSE), Nicholas Hool (graduate student, SBHSE), Taylor Hearn (graduate student), and Sarah Wyckoff, Ph.D. (research assistant professor).

Participant funding is supported by ASU internal WearTech program funds.

STUDY PURPOSE

This study is being conducted to evaluate how Transcranial Focused Ultrasound (TFUS) directed at specific brain areas can affect the resting state, as well as response to stimuli. We are interested in how TFUS applied to different areas of the brain can influence auditory, visual, and somatosensory processing, as well as attention and performance on simple reaction time tasks. Information gained from this research will be used to further our understanding of how TFUS can be used to modulate the brain.

DESCRIPTION OF RESEARCH STUDY

You will be one of approximately 80 able-bodied healthy individuals asked to participate in this project. You will be asked to perform the following procedures in the Tyler Laboratory in room 150 or 158C of Physical Education Building East.

Preparation stage (up to 30 minutes):

- ❑ You will have your head fitted with an electroencephalogram (EEG) cap (similar to a swim cap) that will measure non-invasively the activity of your brain. The EEG cap may be filled with gel to ensure good contact. In some cases up to 64 single EEG electrodes may be placed on your head instead of a cap.
- ❑ You will be connected to a heart rate monitor that is a strap or electrodes applied to the chest.
- ❑ You will have ultrasound gel and an ultrasound probe attached to your head and held in place with a net for the application of transcranial focused ultrasound (TFUS).
- ❑ You will be seated in front of a computer monitor that is connected to a computer.
- ❑ You may be asked to wear headphones in some parts of the experiment. Otherwise you will be asked to sit passively and follow the directions on the screen. Up to three optical sensors will monitor your facial temperature, your eye position and eye blinks, your pupil dilation, and your facial expressions.

- ❑ During the experiments your passive responses to various visual, auditory, and somatosensory stimuli will be monitored. In some cases you will be asked to view photos and numbers and respond with a button press. All specific instructions will be given on the computer
- ❑ You may see photographs ranging from faces to everyday objects and scenes, such furniture to landscapes, to extremely rare or exciting scenes, such as warzones.
- ❑ The images are categorized as pleasant (e.g. happy/excited face, nature landscapes), neutral (e.g. simple smile/straight face, roads/buildings), and unpleasant (e.g. sad/angry face, damaged/demolished buildings). If any of the media presented should make you feel too uncomfortable to continue with the study, you are free to immediately withdraw your participation and leave without giving up credit or payment.

Testing (up to 35 minutes):

- ❑ Once you have been fully connected to the hardware and situated in front of the monitor testing will begin.
- ❑ You will first become acquainted with the TFUS transducer and any auditory artifacts that you may experience during the testing period. These should be comfortable and at no point should cause you pain or distress. We will record a series of baseline responses to ensure that you are comfortable.
- ❑ You will be asked to follow the directions on the monitor once the testing begins.
- ❑ You will be presented with a series of auditory stimuli consisting of tones, visual stimuli consisting of objects, patterns, faces, images, and/or numbers presented on the monitor. We will record your brain's passive responses using EEG. You will be asked to remain relaxed throughout these recordings. We may also record changes in your heart rate, galvanic skin response, pupil dilation, eye motion, facial expression, facial temperature, and eye blinks in response to these auditory, visual, and somatosensory stimuli.
- ❑ At different time points throughout the presentation of auditory, visual, and somatosensory stimuli, we will deliver low intensity pulses of TFUS. The delivery of this pulse ultrasound is safe, below the FDA safety limits, should be comfortable, and should not cause you any pain or distress. If at any point during the study you should become uncomfortable or experience pain please notify the researcher.
- ❑ At the beginning, throughout the study, and at the end of the study you will be asked to complete a short questionnaire asking you to report importation about your mood and affect in that current moment. At the end of the study, you will be asked to complete a short questionnaire asking you to comment about your experience. All questionnaires will be administered using the REDCap survey platform.

MRI Imaging (Optional - up to 30 minutes):

- ❑ A small subset of participants will be asked to go off ASU campus to Barrow Neurologic Institute to obtain a structural MRI scan. In other cases, participants whom were already recruited and obtained MRI scans under STUDY00004362 (PI: Samuel McClure) and STUDY00006050 (PI Marco Santello) will be recruited. If recruited under this method, we will enroll the participant and utilize their MRI scans for our approved procedures.

Both consent for participation in our study and transfer of MRI data will be obtained from these participants before study enrollment. It is up to you to decide whether or not to participate.

- ❑ If you are a woman of childbearing potential, there may be unknown risks to the fetus from MRI. Therefore, before you can have the MRI, you must have a pregnancy test. If you are pregnant, you will not be allowed to participate in this study.
- ❑ Preparation (15 min) and scan time (15 min) will take about 30 minutes. You will be asked to lie down in the MRI scanner so that we can take a set of magnetic resonance (MR) images of your head. You will be provided with foam earplugs and headphones to protect your ears from the scanner noises. The MRI will be performed for the purpose of this study and is not to diagnose any disease. However, the images will be reviewed by a radiologic physician and you will be informed of an obvious abnormalities.

RISKS

There is a low-risk for some minor side-effects or adverse reactions that you may experience because of your participation in this study. These include side-effects of being from EEG, TFUS, viewing unpleasant images, and being in an MRI scanner.

Skin Irritation Risk:

The preparation of EEG electrodes involves injecting conductive gel with a plastic applicator and then moving it around the electrode well until acceptable impedance is achieved. This process has the potential to irritate the skin or cause a rash through light scraping of the scalp. The preparation of galvanic skin response and EKG electrodes involves the preparation of the skin with rubbing alcohol. Both of these procedures may irritate the skin and result in a mild rash. Minor skin irritation can occur if electrodes are placed over broken skin or wounds. We will avoid placing electrodes over these areas. Moreover, we will inspect the skin prior to electrode placement to further reduce the potential for minor irritation. Mild redness has been reported at the site of electrode placement, but this is an acute effect of vasodilation as opposed to inflammation and thus does not indicate damage.

Skin Discomfort Risk:

Ultrasonic stimulation can in rare cases feel slightly uncomfortable and result in a mild tingling or vibration sensation on the skin. This sensation only occurs while the stimulation is on and does not result in any lasting after effects. At high-intensities or stimulus events lasting for long durations, ultrasound can also lead to the heating of soft-tissue and bone. There have been no known adverse effects from TFUS used within the FDA safety limits in the literature, and it is commonly employed in fetal and cranial imaging.

Headache Risk:

A rare side effect of TFUS is the occurrence of a mild headache attributed to the net used to hold the transducer on the head. This is reported as being like wearing a hat that is too tight. This occurs in less than about 10% of subjects at incidence rates similar to sham procedures during both acute and repeated use procedures. Mild headaches typically resolve within a couple hours with no further complications. If a subject experiences a headache or discomfort, they may ask the researcher to reposition the net or discontinue use at any time.

MRI Risks:
MRI uses a strong magnetic field and can affect ferrous objects. Participants will be screened by questionnaire (and metal detector wand) for contraindications to MRI including implanted metal devices (e.g. plates, clips, pacemaker etc.) and current physical health (e.g. pregnancy). The bore of the MRI scanner is small and may be uncomfortable and somewhat claustrophobic. Participants are provided padding for the head and neck as well as a safety call button that if pressed will allow the participant to converse with the researchers. MRI scanning is quite loud and participants will be provided with ear protection.

Task Risks:
If you decide to take part in this study, you will be asked to view a variety of pictures that have been categorized to be pleasant, neutral, or unpleasant. If any of the media presented should make you feel too uncomfortable to continue with the study, you are free to immediately withdraw your participation and leave without giving up credit or payment. The content of the pictures may include unpleasant faces or scenes. To be clear: you may immediately end your participation if any aspect of the research procedure makes you too uncomfortable to continue.

There are no other known risks associated with this study. Participation is completely voluntary and participants are free to ask questions, ask for a break, or withdraw from the study without penalty.

INCULSION CITERIA

- ❑ Healthy male or females ages 18-55 years of age
- ❑ All adults will be able to give consent

EXCULSION CITERIA

- ❑ Please check each box acknowledging that you do NOT have this condition or exclusion criteria.
- ❑ I am NOT currently undergoing treatment or medication for neurological or psychological disorder, including addiction, epilepsy/seizure disorder, major depression (MD), attention deficit disorder (ADD), and attention deficit hyperactive disorder (ADHD)
- ❑ I do NOT have a medical implant (such as a pacemaker, cochlear implant, brain stimulation device)
- ❑ I do NOT have migraines or frequent headaches
- ❑ I do NOT have a history of panic attack or acute anxiety disorder
- ❑ I have NOT experienced frequent fainting or experienced vaso-vagal syncope or neurocardiogenic syncope even once.
- ❑ I do NOT have Temporomandibular joint (TMJ) disorder or other facial neuropathy
- ❑ I do NOT have history of concussions or brain injury
- ❑ I do NOT have history of significant face/head injury or if you have cranial or facial

metal plate or screw implants

- ❑ I do NOT have a history of claustrophobia
- ❑ I do NOT have a history of hospitalization for neurological or psychological disorder
- ❑ I have NOT had a recent hospitalization for surgery/illness
- ❑ I do NOT have vision or hearing that is uncorrectable (corrected vision or hearing is okay)
- ❑ I am NOT to my knowledge pregnant
- ❑ I have NOT had recent drug or alcohol treatment (within past 3 months)
- ❑ I do NOT have heart disease or diabetes

BENEFITS

While you will not directly benefit from participation, your participation may help investigators better understand how the brain learns, as well as how to enhance learning or training procedures.

NEW INFORMATION

If the researchers find new information during the study that would reasonably change your decision about participating, then they will provide this information to you.

CONFIDENTIALITY

Every effort will be made to maintain the confidentiality of your participation in this project. Each subject's name will be paired with a code number by the principal investigator. This code number will appear on all written materials. The list pairing the subject's name to the assigned code number will be kept separate from all research materials and will be available only to the principal investigator. Confidentiality will be maintained within legal limits.

WITHDRAWAL

You may choose to withdraw from the study at any time. If you do withdraw, then any data collected from you prior to your withdrawal will only be used under your verbal consent.

COMPENSATION

For this study, you (the participant) will be compensated $10 in cash per hour up to $20 for a 120 minute session.

COMPENSATION FOR ILLNESS AND INJURY

If you consent to participate in the study, then your consent does not waive any of your legal rights. However, no funds have been set aside to compensate you in the event of an injury.

VOLUNTARY CONSENT

1. I understand that informed consent is required of all persons participating in this project.
2. All procedures have been explained to me and all my questions have been answered to my satisfaction.

3. Any risks and/or discomforts have been explained to me.
4. Any benefits have been explained to me.
5. I understand that any questions that I have concerning the research study or my participation in the research study, before or after my consent, will be answered by William Tyler, Ph.D. or research associates, Tyler Laboratory, School of Biological and Health Systems Engineering, PEBE 158C and PEBE 170, at 480-965-9270.

   I also understand that if I have questions about my rights as a subject/participant in this research, or if I feel I have been placed at risk, I can contact the Chair of the Human subjects Institutional Review Board, through the ASU Research Compliance Office, at 480- 965-6788
6. I have been told that I may refuse to participate or to stop my participation in this project at any time before or during the project. I may also refuse to answer any question.
7. All information that is obtained in connection with this project and that can be identified with me will remain confidential as far as possible within legal limits.

   Information gained from this study that can be identified with me may be released to no one other than the principal investigator. The results may be published in scientific journals, professional publications, or educational presentations without identifying me by name.
8. This form explains the nature, demands, benefits and any risk of the project. By signing this form I agree knowingly to assume any risks involved. My participation is voluntary. I may choose not to participate or to withdraw my consent and discontinue participation at any time without penalty or loss of benefit. In signing this form, I am not waiving any legal claims, rights or remedies. A copy of this consent form will be offered to me.

AGREEMENT FOR THE USE OF VIDEO RECORDINGS

If you consent to participate in this study, please indicate whether you agree to be recorded on video during the study by checking the appropriate box below. If you agree, please also indicate whether the video clips can be used for publication/presentations. If you do not agree to be recorded in video, or for the video to be used in publications/presentations, you will still be eligible for participation in this study. Recording videos is useful to our study since we collect data about psychophysiological responses using multiple optical sensors.

- ❑ I agree to be recorded in video during the experiment.
- ❑ I agree that the video recordings can be used in publication/presentations.
- ❑ I do not agree to be recorded in video during the experiment.

My signature means that I agree to participate in the study.

_____	_____	_____
Subject's Signature	Printed Name	Date

INVESTIGATOR'S STATEMENT

"I certify that I have explained to the above individual the nature and purpose, the potential benefits and possible risks associated with participation in this research study, have answered any questions that have been raised, and have witnessed the above signature. These elements of Informed Consent conform to the Assurance given by Arizona State University to the Office for Research Integrity and Assurance to protect the rights of human subjects. I have provided (offered) the subject/participant a copy of this signed consent document"

Signature of Investigator _____ Date _____

CONSENT TO TRANSFER MRI SCAN

INTRODUCTION

The purpose of this form is to obtain your consent to transfer your MRI scan data ASU IRB # STUDY00009449 | Approval Period 1/10/2019 – 2/12/2020 obtained under a previous STUDY (IRB: STUDY00004362 and STUDY00006050). This scan information will only be used for data analysis purposes and the current study you are enrolled in (STUDY00009449).

RESEARCHER

Principle Investigator: William "Jamie" Tyler, Ph.D., School of Biological and Health Systems Engineering, Fulton College of Engineering

- ❑ I consent to have my T1 and T2 MRI scan data transferred to the above Principle Investigator
- ❑ I do not consent to have my MRI scan data transferred
- ❑ N/A; I do not have a previously collected MRI scan

Subject's Signature	Printed Name	Date

SUBJECT CONSENT FORM

Neural and behavioral basis of sensorimotor control and learning
SCHOOL OF BIOLOGICAL AND HEALTH SYSTEMS ENGINEERING:
ARIZONA STATE UNIVERSITY

INTRODUCTION

The purposes of this form are to provide you (as a prospective research study participant) information that may affect your decision as to whether or not to participate in this research and to record the consent of those who agree to be involved in the study.

RESEARCHERS

Principle Investigator: Marco Santello, Ph.D., School of Biological and Health Systems Engineering, Fulton College of Engineering

DESCRIPTION OF RESEARCH STUDY

These studies our focused on examining how the brain produces movements of the body, and how the brain manages the coordination of muscles through measurable electrical brain activity. We are examining these questions in people from ages 18-50. You will be tested on a series of tasks to examine your basic motor abilities. If you decide to participate in the experiment, you may be asked to participate in a version involving either transcranial magnetic stimulation (TMS), transcranial focused ultrasound (TFUS), and/ or electroencephalography (EEG). In the case that these methods will be employed, you maybe asked to also obtain an MRI of your brain. This will be done off campus and will require one of the researchers to bring you to the MRI facility. The MRI costs will be covered by the researchers. The combination of these methods will allow us to accurately track how the spatial and temporal dynamics of your brain activity changes during the course of an experiment. For any of the below experimental protocols, there is only one session. However, you may be invited to come back and participate in other experiments as sessions separate from the original. Therefore, any compensation for participation is for each individual session.

In some instances, you will be asked to lift objects up from the table, hold them, and replace them. The task and objects may include those encountered in activities of daily living (coffee mug, water bottle, etc), or instrumented object equipped with force sensors (ATI). We may also change object properties such as mass (usually less than 1000 g and up to 2000 g if two hands are used), center of mass, or texture of the graspable surfaces. Reflective markers will be attached to the object and/or hand using a tape to track the motion of the object and/or the hand while subjects perform various tasks. You will you're your right hand and/or left hand and grasp the object with 2, 3, or 5 digits. During lifting, you may be required to control the orientation of the objects, hold it for less than 5 seconds, and replace it on the table. Each experimental session consists of several blocks of trials. In some versions of this task, you will be asked to perform object lifting and manipulation together with another person. The total number of trials during one session would not exceed 250 (usually less than 40). During some portions of the task, you will either receive TMS or ultrasound, while in most cases we will record EEG from your scalp. If using any of these recording or

stimulation modalities, we will also record electromyographic activity from the surface of your muscles.

In some instances, you will interact with a virtual reality (VR) environment by applying forces with their thumb and index finger to levers attached to robotic devices. The robotic devices are motorized mechanical linkages that generate forces in response to forces exerted by the fingertips, thus generating the feeling of grasping a real object. To strengthen this feeling, the perceived object is displayed on a computer monitor placed in front of the subject. The maximum output of the device is limited to very small forces (up to a maximum of 6 Newtons). The VR environment contains virtual objects that participants need to grasp and manipulate through the robotic device. When not performing the task, participants can rest their hand and forearm on a foam pad. Each experimental session consists of several blocks of trials. The total number of trials during one session would not exceed 300 (usually less than 150). Participants may need to come back for subsequent sessions with the same or similar task requirements. The inter-session time varies between hours and days.We will collect EEG data during task performance, while simultaneously applying either TMS or TFUS.

In other instances, you will be asked to move a cursor on a screen using a mouse or a force transducer. The task requires you to respond as quick as possible to visual stimuli presented on a screen in front of you. The visual stimuli will consist of geometric shapes such as circles or triangles, or alphabetic characters from different languages. Each experimental session should not involve more than 600 trials. These sessions will also involve the collection of EEG data during task performance, while simultaneously applying either TMS or TFU.

When performing one of the above tasks, we may ask you to return to participate in other versions of the task to allow us comparison of your learning performance across several types of tasks.

If you say YES, then your participation in the study will last approximately two hours for any given session, at PEBE 174. Approximately 1200 people will be participating in the study.

RISKS

The current methods carry minimal safety risks. Some people report that their scalp muscles have discomfort, and/or a headache comes and goes after TMS, though both of these issues are less of a problem in the particular scalp areas we will be stimulating. Headaches from TMS can occur. Though, they are very uncommon, and most participants report these headaches as minor and being a 1-2 on a scale of 1-10 (10 being most severe). These headaches can last approximately 1 to 2 hours at most. Headaches have not been reported anywhere to last longer than this duration. TMS involves discharging brief magnetic pulses over the head. Possible effects on hearing have been described and so subjects and investigators will be asked to wear earplugs during any TMS to avoid this possibility. While no current evidence is available which suggests TMS may be damaging to fetus, pregnant females will not be included in the study. As with any electronic device or appliance, using it the wrong way could result in electric shock. While this is very, very unlikely, it cannot be completely excluded as a possibility. The risks of injury or discomfort in this research are minimal.

Recording of EEG is the most widely used method of neural data recording. It involves placing sensors in a cap, that is worn on the head. Because it is a passive recording system of electrical brain activity, it has no known or foreseeable risks.

The application of TFUS involves placing an ultrasonic transducer upon the head and discharging brief ultrasonic pulses. This process may produce a vibration/buzzing sensation upon the scalp and may also result in a warming sensation. If you feel discomfort at anytime during this application, please inform the research team and stimulation will be halted.

There is a possibility that the linkage system will move you at an uncomfortable speed, however, several safety precautions have been implemented to reduce this risk. Specifically, the maximal speed of the movement imposed by the linkage system is set below human physiological limits. If these speeds are exceeded the linkage system is designed to immediately shutdown. Although your fingers you will be attached to the device via Velcro-like straps, you will be able to remove your fingers from the device if you feel any discomfort to let go of the object to protect yourself from potential discomfort, pain, or injury. The metal cylindrical object is powered and connected to the USB port of a pc with proper shielding and grounding. The risk of getting static shock is no different than using metal objects in daily life. However, as with any research, there is some possibility that you may be subject to risks that have not yet been identified.

BENEFITS

Although you will not benefit individually from participation in the research, this study will help us to understand the relationship between the brain's capacity to change and sensorimotor learning. This information will be used to guide further studies in brain injured populations.

NEW INFORMATION

If the researchers find new information during the study that would reasonably change your decision about participating, then they will provide this information to you.

CONFIDENTIALITY

All information obtained in this study is strictly confidential unless disclosure is required by law. The results of this research study may be used in reports, presentations, and publications, but the researchers will not identify you. In order to maintain confidentiality of your records, Marco Santello or Justin Fine will code all of your information so your identity cannot be determined from any of the data. The key to the code is kept in a separate location from the data and the data are locked in a cabinet. Only Marco Santello or Justin Fine and the research assistant that enrolled you in the study will have access to both the codes and the code key.

WITHDRAWAL PRIVILEGE

It is ok for you to say no. Even if you say yes now, you are free to say no later, and withdraw from the study at any time. Your decision will not affect your relationship with Arizona State University or otherwise cause a loss of benefits to which you might otherwise be entitled.

COSTS AND PAYMENTS

The researchers want your decision about participating in the study to be absolutely voluntary. Yet they recognize that your participation may pose some inconvenience. You will be paid $20 for each session. All payments are made at the end of each phase.

COMPENSATION FOR ILLNESS AND INJURY

If you agree to participate in the study, then your consent does not waive any of your legal rights. However, no funds have been set aside to compensate you in the event of injury.

VOLUNTARY CONSENT

Any questions you have concerning the research study or your participation in the study, before or after your consent, will be answered by one of the following people: Dr. Marco Santello (480-965-8279), Justin Fine (480-965-8279), or Qiushi Fu (480-965-8279).

If you have questions about your rights as a subject/participant in this research, or if you feel you have been placed at risk; you can contact the Chair of the Human Subjects Institutional Review Board, through the ASU Office of Research Integrity and Assurance, at 480-965 6788.

This form explains the nature, demands, benefits and any risk of the project. By signing this form you agree knowingly to assume any risks involved. Remember, your participation is voluntary. You may choose not to participate or to withdraw your consent and discontinue participation at any time without penalty or loss of benefit. In signing this consent form, you are not waiving any legal claims, rights, or remedies. A copy of this consent form will be given (offered) to you.

Your signature below indicates that you consent to participate in the above study.

_____	_____	_____
Subject's Signature	Printed Name	Date

INVESTIGATOR'S STATEMENT

"I certify that I have explained to the above individual the nature and purpose, the potential benefits and possible risks associated with participation in this research study, have answered any questions that have been raised, and have witnessed the above signature. These elements of Informed Consent conform to the Assurance given by Arizona State University to the Office for Human Research Protections to protect the rights of human subjects. I have provided (offered) the subject/participant a copy of this signed consent document."

Signature of Investigator _____ Date_____

BIOGRAPHICAL SKETCH

Maria Elizabeth Fini was both in Manassas, Virginia in 1988, where she learned to treasure nature. In 2006, she completed her secondary education with an International Baccalaureate diploma. She attended the University of Virginia, and in 2010 received a Bachelor of Science in Biomedical Engineering with a double major in Studio Art. Following college, she earned a Certificate of Neural Intraoperative Monitoring (CNIM), and worked clinically as an electrophysiologist, mapping and monitoring brain and spine function in neurosurgery. Maria left the operating room in 2015 with a desire to develop her curiosity for consciousness and began graduate studies at Arizona State University researching ultrasound as a modality of noninvasive brain stimulation. Her education has been greatly deepened through practicing yoga, meditation, and delving into the many divergent fields that study consciousness, both academically and experientially. She aspires to explore beyond what is currently known about the mind, wellbeing, and the human capacity to heal and regenerate, interweaving knowledge of spirituality with science.